JOINT INSTITUTE FOR NUCLEAR RESEARCH
1956

JINR

INTRODUCTION TO EXPERIMENTAL NUCLEAR PHYSICS AND NUCLEAR ELECTRONICS

VOLUME 1

Introduction to Experimental Nuclear Physics

I. VANKOV
D. KAMANIN
YU. PANEBRATTSEV

JOINT INSTITUTE FOR NUCLEAR RESEARCH
University Centre

I. Vankov, D. Kamanin, Yu. Panebrattsev

Introduction to Experimental Nuclear Physics and Nuclear Electronics

Volume 1
Introduction to Experimental Nuclear Physics

Textbook

Edited by I. Vankov

Dubna 2021

The authors express their sincere gratitude to M. Krmar, K. Klygina, L. Kostov, N. Mkhaza, S. Pakuliak, G. Rainovski, C. Rossouw, A. Strekalovsky and S. Wyngaardt for their help with the preparation of this book.

Vankov I.

V26 Introduction to Experimental Nuclear Physics and Nuclear Electronics: In 2 vol. Vol. 1: Introduction to Experimental Nuclear Physics: Textbook for the Virtual Laboratory for the Study of Nuclear Physics project / I. Vankov, D. Kamanin, Yu. Panebrattsev; Ed. by I. Vankov. — Dubna: JINR, 2021. — XII, 299 p.

ISBN 978-5-9530-0564-7

The textbook represents a course on experimental nuclear physics for students of physics and engineering gaining practical experience at the Joint Institute for Nuclear Research. The course introduces the basic concepts needed to study experimental nuclear physics.

The course was developed as part of the Virtual Laboratory project (https://edu.jinr.ru/vlabs) for students of various fields of study in areas related to nuclear physics research. It will allow students to actively participate in various research activities that are being carried out at JINR.

ISBN 978-5-9530-0564-7

FOREWORD

At JINR, together with the JINR Member States and Associated Members, the project "Virtual laboratory for the study of nuclear physics" is being developed. The project is being developed in two directions – virtual labs and hands-on practicum. The results of the project are already being used at universities around the world, both as an Internet resource and as a local version in computer classes. During project's implementation a significant number of student practices and masterclasses were organized in Dubna. The experience gained because of using the "Virtual Laboratory" showed that, for the effective use of the project, it is necessary to have a study guide that contains basic knowledge of experimental nuclear physics and nuclear electronics in addition to digital resources.

The first volume of the textbook "Introduction to Experimental Nuclear Physics" consists of the following parts:

1. Basic Concepts
2. Radioactive Decay
3. Radiation Sources
4. Interaction of Radiation with Matter
5. Radiation Detectors

The second volume of the textbook "Introduction to Nuclear Electronics", which should be prepared for publication in 2022, will consist of the following parts:

1. Introduction to Detector Signal Processing
2. Preamplifiers
3. Radiation Energy Measurement
4. Timing Measurements
5. Detector Signal Counting and Current Measurements
6. Pulse Shape Discrimination
7. Position Sensitive Detection
8. Digital Signal and Systems
9. Digital Radiation Measuring

The authors of the textbook took part in various physical experiments and organized a variety of practicums for students. This course is a summary of their experience in experimental physics.

The following labels are used in the course materials:

 – important definitions;

 – important formulas;

 – example of problem-solving;

 – animations that can be viewed by QR code;

– QR code by which you can watch animations on the Internet.

Good luck! We hope this textbook will help you take the first steps towards understanding the processes and phenomena occurring in a nuclear physics experiment.

CONTENTS

PART 1. BASIC CONCEPTS

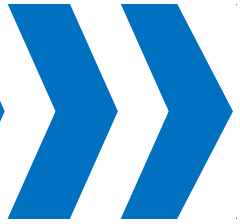

1.0. Introduction

The end of the 19th century and the beginning of the 20th century are marked by a series of remarkable discoveries in Physics. They not only cardinally changed the existing image of the world but also initiated technical progress.

Among these discoveries are the discovery of **X-rays** by **Röntgen** (1895), **Becquerel's** discovery of **radioactivity** (1896), **Thompson's** discovery of the electron (1897), **Planck's** hypothesis about the **quantum nature of light** (1900), **Rutherford's** discovery of the **atomic nucleus** (1911), and **Bohr's quantum model** of the atom (1913).

Later, the particles forming the atomic nucleus were discovered – the **proton** by **Rutherford** in 1919 and Chadwick's neutron in 1932. Based on that, Soviet scientists **Gapon** and **Ivanenko** and German physicist **Heisenberg** suggested the **neutron-proton** model of the atomic nucleus.

All of these discoveries have led physicists to understand the atomic structure. It was evident that classical physics laws do not work for microcosm objects that are subject to other laws – the laws of quantum mechanics. These laws were discovered and interpreted by a group of talented physicists, among which were **Heisenberg**, **Schrödinger**, **Pauli**, **Dirac**, **Landau**, **Fock** and many others.

In Part 1, we will introduce you to the smallest building blocks of matter – the so-called **elementary particles**, the **structure of the atom** and **atomic nucleus**, as well as the **fundamental laws** governing their properties and interactions.

1.1. World of the atom

1.1.1. Electron discovery

In 1869, the German physicist **Johann Hittorf** studied electrical conductivity in rarefied gases.

Fig. 1.1.1. Cathode rays cause fluorescence on the walls of the glass tube. A solid object placed in the path of the cathode rays casts a shadow on the wall of the tube across from the cathode

He discovered a glow emitted from the cathode, the size of which depended on the gas pressure. In 1876, the German physicist **Eugen Goldstein** called these rays **cathode rays.**

In 1896, the British physicist **Joseph John Thomson** and his colleagues performed experiments indicating that cathode rays were actually made up of unique particles (Fig. 1.1.1) rather than waves, atoms or molecules as previously believed.

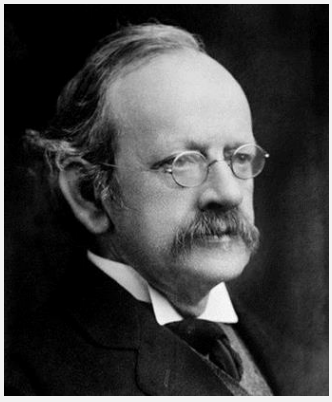

Joseph J. Thomson

Thomson called these particles corpuscles and estimated their mass-to-charge ratio, finding that it was about 1800 times smaller than the ratio for hydrogen, the smallest atom. He also showed that the negatively charged particles

emitted by radioactive-, heated-, and illuminated materials are all the same. Finally, the Irish physicist **George Fitzgerald** proposed that these particles be named **electrons**. Nevertheless, it is believed that Thomson discovered the electron in 1897.

Electron mass	$9.1094 \cdot 10^{-31}$ kg
	0.511 MeV/c^2
	$5.4858 \cdot 10^{-4}$ u
Electron charge	$-1.6022 \cdot 10^{-19}$ C
	$-1q_e$ (elementary charge)

Table 1.1.1. Electron mass and charge

Unified atomic mass unit (u or Da – from Dalton)

A unified atomic mass unit is a unit that is equal to one-twelfth of the mass of a carbon-12 atom:

$$1 \text{ u} = 1.66 \cdot 10^{-27} \text{ kg}.$$

Electronvolt

In atomic and nuclear physics, the **electronvolt** is used as a unit of energy and mass. One electronvolt is the energy that an electron gains while moving across an electric potential difference of one volt. The electron charge is $q_e = 1.6 \cdot 10^{-19}$ C, thus

$$1 \text{ eV} = 1.6 \cdot 10^{-19} \text{ J}. \qquad (1.1.1)$$

According to Einstein's mass-energy equation $E_0 = mc^2$, the mass can be estimated by its energy equivalent $m = E_0/c^2$. So

$$1 \text{ u} = 931.494 \text{ MeV}/c^2, \qquad (1.1.2)$$

$$1 \text{ kg} = 5.6 \cdot 10^{35} \text{ eV}/c^2.$$

Here c is the velocity of light.

Because of his investigations, Thomson suggested that atoms were divisible and that the electrons were their building blocks. To explain the overall neutral charge of the atom, he proposed that the electrons were distributed in a uniform sea of positive charge (Fig. 1.1.2), creating the so-called **plum**

pudding model [1] of the atom in which the electrons are embedded in the positive charge, like plums in a plum pudding.

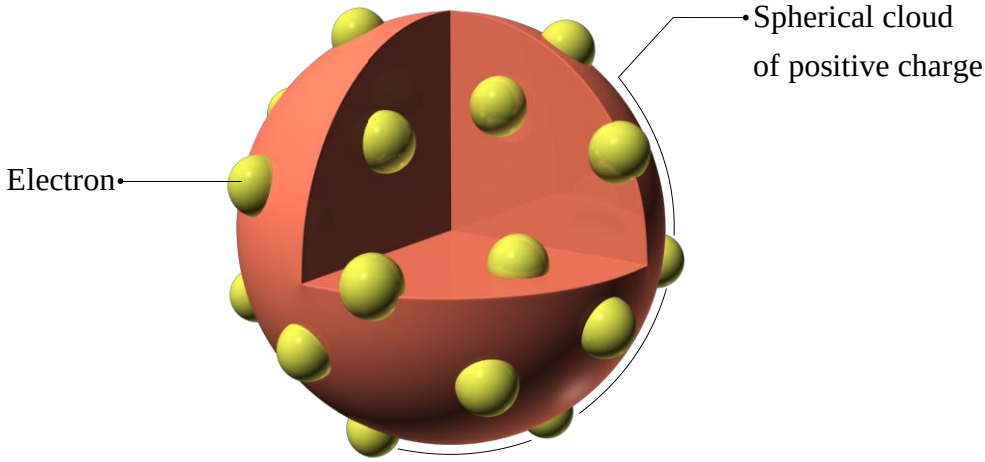

Fig. 1.1.2. Thomson's plum pudding model of the atom

The actual atomic structure was later discovered in Rutherford's experiments.

1.1.2. Rutherford's atomic model

In 1911, after the mathematical processing of the results of an experiment in which high energy streams of alpha particles were directed at a thin gold foil, **Ernest Rutherford** concluded that an atom is similar to the solar system, which means that there is a nucleus in the center of an atom with orbiting electrons around it [1].

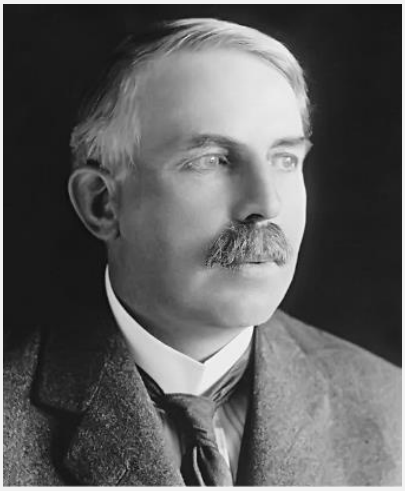

Ernest Rutherford

QR Scheme of Rutherford's experiment

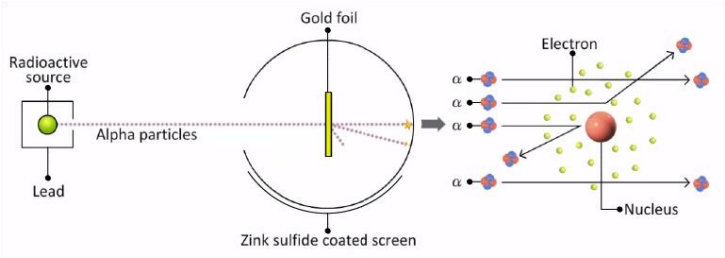

SCAN ME

The essence of the **planetary model** can be described by the following statements:

1. There is a positively charged nucleus in the center of an atom. In addition, it occupies a negligibly small space inside the atom.
2. Almost all of the atom's mass is concentrated in its nucleus, along with all of its positive charge.
3. Electrons orbit the nucleus. The number of electrons is equal to the value of the nucleus's positive charge (measured in elementary charges). Thus, the whole atom is neutral.

QR Size of the atom and its nucleus

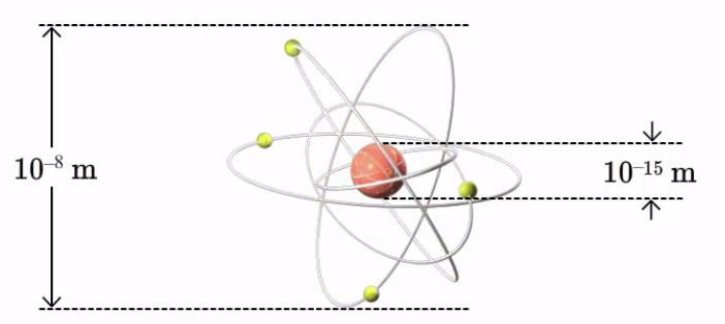

SCAN ME

It is obvious that the Solar system and the planetary model of the atom are physically different in nature. The motion of the Solar system's planets is determined by gravitational interactions and the law of universal gravitation. The orbits of the electrons, rotating around the positively charged nucleus, are determined by electromagnetic interactions. Electrons move in the nucleus' Coulomb field, but this motion cannot be explained within the framework of classical electrodynamics. Firstly, under accelerated motion, charged particles are emitting and losing energy. Thus, the orbiting electrons should collapse into the nucleus; this process should take about 10^{-8} seconds.

Secondly, within the framework of classical physics, the line character of the emission/absorption spectra of the atom cannot be explained.

In coming up with the theory of nuclear atomic structure, Rutherford knew that there are conflicting arguments with classical electrodynamics when it comes to how the electrons should collapse into the nucleus. But physics is considered an experimental science. Therefore, once experiments showed that the atom consisted of a nucleus with electrons orbiting around it, an explanation had to be found.

To explain Rutherford's experiments, scientists needed to radically change their understanding of the physical laws acting within the atom.

1.1.3. Bohr's atomic model

In 1913 Danish physicist **Niels Bohr** solved the above-mentioned problem. Bohr sincerely believed in the nuclear atomic model, which was discovered after the scattering experiments of Rutherford, and tried to understand how the electrons are located in the atom to obtain the definite atomic spectra.

Niels Bohr

His success was based on the inclusion of entirely new concepts in his theory [1, 2]. He introduced the idea of the **quantum of action**, which was unknown in classical physics at the time. His idea was based on the fact that the electron can orbit around the nucleus without emitting radiation. He knew that according to classical physics, electrons should collapse into the nucleus when orbiting around it. He then postulated that this does not happen for some unknown reason. Based on this assumption, he managed to explain the origin of the line spectra.

Planck Formula

In 1896, studying the blackbody radiation spectrum, the German physicist **Max Planck** introduced the idea of a **radiation quantum** and derived the following famous formula [3]:

$$E = \omega \frac{h}{2\pi} = \omega\hbar \qquad (1.1.3)$$

where

E is the thermal radiation energy of the blackbody,

ω – the angular frequency,

h – the Planck constant (quantum of action) – $h \approx 6.63 \cdot 10^{-34}$ J·s,

$\hbar$ (h-bar) – the reduced Planck constant (also named the "Dirac constant") – $\hbar = h/2\pi$.

Bohr suggested the first **quantum-mechanical atomic model**, which included a procedure where the atomic energy levels are quantized. He determined the electron motion structure in an atom: electrons can only exist by moving along firmly fixed orbits around the atom. In fact, he introduced the concept of **energy quantization**.

In his quantization rules, Bohr studied **the quantum of action** or **Planck constant** – *h*. Note that the Planck constant h and the angular momentum of the electron L have the same physical dimension: Joule × second.

Angular momentum of orbital motion

When describing a body's angular motion, a physical quantity that plays a significant role is the so-called **angular momentum**. For example, let us study the simplest case of particle motion – the point particle motion along a circular orbit of radius $\vec{\mathbf{r}}$ with a constant velocity $\vec{\mathbf{v}}$. In this case, the angular momentum of the orbital motion $\vec{\mathbf{L}}$, by definition, is equal to the vector cross product of the particle momentum $\vec{\mathbf{p}}$ ($\vec{\mathbf{p}} = m\vec{\mathbf{v}}$) and the radius vector $\vec{\mathbf{r}}$:

$$\vec{\mathbf{L}} = \vec{\mathbf{p}} \times \vec{\mathbf{r}} = \boldsymbol{m}\vec{\mathbf{v}} \times \vec{\mathbf{r}}, \qquad (1.1.4)$$

where m is the mass of the particle.

Angular momentum is an important quantity because it is a **conserved quantity** – the total angular momentum of a system remains constant until an external impact influences it. It means that

over time the direction of vectors $\vec{\mathbf{r}}$ and $\vec{\mathbf{p}}$ can change, but the vector $\vec{\mathbf{L}}$ remains constant (see Fig. 1.1.3).

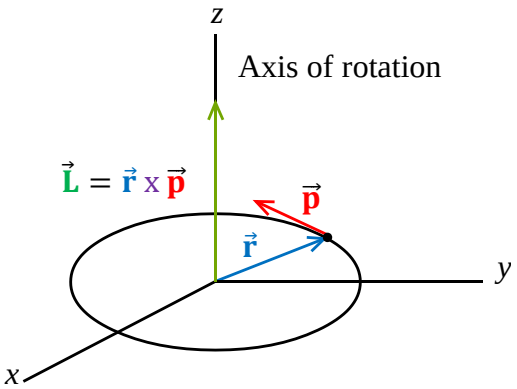

Fig. 1.1.3. Particle undergoing uniform circular motion in the (x, y) plane

Niels Bohr had an extraordinary intuition in physics. He further introduced the condition that the angular momentum of electrons orbiting around the nucleus is quantized as part of his atomic model.

Now let us consider the simplest atom that Bohr's atomic model explained very well, the hydrogen atom. In this case, Bohr suggested that the electron orbits around a stationary nucleus. The nucleus consists of one proton, which is positively charged and assumed to be slightly heavier than the electron. Therefore, the electron orbits in the Coulomb field of the nucleus.

1.1.4. Bohr's postulates

Niels Bohr's atomic model was based on three postulates.

Postulate 1

The atom can exist in specific steady (quantum) states, each of which corresponds to a definite energy E_n (where n is a state number). In these steady states, atoms do not emit or absorb energy.

Postulate 2

In a steady atomic state, the electrons move along stationary orbits, which are governed by the following quantum equation:

$$L = pr = \frac{nh}{2\pi} = n\hbar, \tag{1.1.5}$$

where

L is the magnitude of the angular momentum vector,

n – the state number (1, 2, 3, …),

p – the magnitude of the particle linear momentum vector,

r – the magnitude of the orbit radius vector.

Postulate 3

When an atom transits from one steady state to another, a quantum of electromagnetic radiation is emitted or absorbed (Fig. 1.1.4). The quantum energy is equal to the difference between the energies of the atom in these two steady states:

$$h\nu = E_m - E_n, \qquad (1.1.6)$$

where $h\nu$ is a quantum energy. Later, this quantum was named a **photon**.

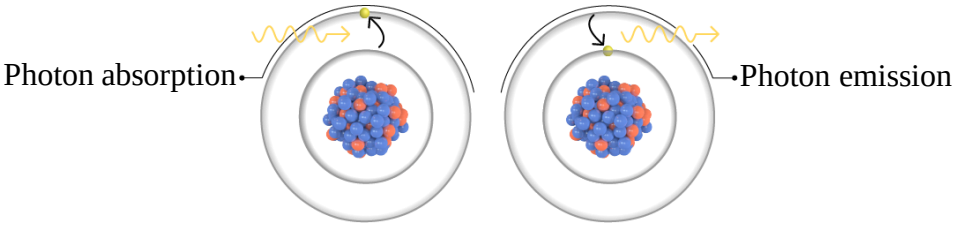

Fig. 1.1.4. Electron transitions in an atom

A group of brilliant physicists had to work hard for about 15 years to understand the physical content of Bohr's postulates and to complete the quantum mechanics.

1.1.5. Louis de Broglie's hypothesis

Louis de Broglie

In 1924, the French physicist **Louis de Broglie** suggested a hypothesis stating that photon emission quanta have particle-like and wave-like properties (wave-particle dualism) and that massive particles, such as electrons, protons

and atoms, also manifest such a wave-particle dualism [4]. If a particle has energy E and momentum $\vec{\mathbf{p}}$, then it can be represented by a wave with the length:

$$\lambda = h/\vec{\mathbf{p}}, \tag{1.1.7}$$

where h is the Planck constant.

In this way, De Broglie's hypothesis explained the existence of steady electron orbits in Bohr's atom: only the orbits which contain an integer number n of electron wavelengths are steady. As an example, electron orbits with $n = 4$ are shown in Fig. 1.1.5.

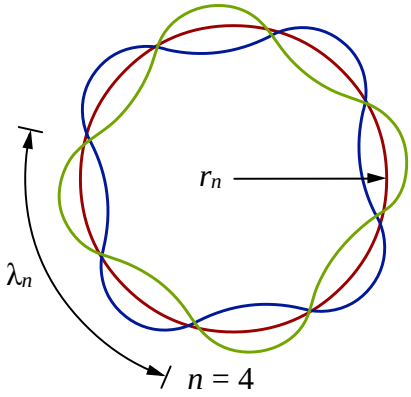

Fig. 1.1.5. Two stationary electron orbits in Bohr's atom with n= 4

We shall show now how the electron's angular momentum quantization condition in Bohr's theory of the hydrogen atom can be formulated in accordance with Louis de Broglie's hypothesis, which postulates that the electron has wave-like properties.

The equation of Bohr's second postulate (see Eq. (1.1.5)) can be transformed into

$$2\pi r = n\frac{h}{p} = n\frac{2\pi\hbar}{p}. \tag{1.1.5a}$$

According to Louis de Broglie's hypothesis (see Eq. (1.1.7)), the electron's motion is governed by a wave that has the following length:

$$\lambda_B = \frac{h}{p} = \frac{2\pi\hbar}{p}. \tag{1.1.7a}$$

Thus, the condition of Bohr's quantization can be written as

$$2\pi r = n\lambda_B, \; n = 1, 2, 3, \ldots \tag{1.1.8}$$

This equation postulates that only the orbits along the length of which an integer number of the electron's wavelength can be set will be stationary electron orbits.

Louis de Broglie's hypothesis was experimentally verified in 1927 when **C. Davisson** and **L. Germer** performed experiments showing electron diffraction on nickel crystals [5]. With this, they confirmed the wave character of the electrons.

1.1.6. Heisenberg's uncertainty principle

Werner Heisenberg

In 1927, the German physicist **Werner Heisenberg** discovered another fundamental law of quantum physics known as the **uncertainty principle** [6]. The main idea of this principle is that the position (x coordinate) and momentum ($\vec{\mathbf{p}}$) of a particle (for example of an electron in the atom) cannot be measured simultaneously with unlimited precision. This is not connected with a lower instrumental resolution or a poor experimental technique, but it reflects a fundamental law of nature [7].

According to the uncertainty principle, the measuring precision of the position (x) and momentum ($\vec{\mathbf{p}}$) of a particle is limited by the following equation:

$$\sigma_x \cdot \sigma_p \geq \hbar/2, \tag{1.1.9}$$

where σ_x and σ_p are the standard deviations [8] of the measurement of the respective quantity.

1.1.7. The wave function and the Schrödinger equation

Keep in mind that, at the beginning of the 20th century, experimental evidence suggested that photons, as well as atomic particles, have wave-like and particle-like behavior. However, the acceptance of light as being composed of particles led to a shocking realization. For example, if a beam of light shines on an imperfectly transparent sheet of glass, 95 % of the light may transmit through the glass, while 5 % is reflected back. This makes perfect sense if light is a wave (the wave simply splits and a smaller wave is reflected back). However, if it is considered as a stream of identical particles, then all we can say is that each photon arriving at the glass has a 95 % chance of being transmitted and a 5 % chance of being reflected [9].

Thus, it is not possible to predict a single definite result based on one observation, only a number of different possible outcomes, each with a particular probability. Moreover, this conclusion is valid not only for the photons but also for all microcosmic objects. Physics had therefore changed overnight from a state of absolute certainty to the one of merely predicting the odds! This was the start of quantum mechanics.

Erwin Schrödinger

In light of the new situation, the main problem was determining the probability of an object being at a particular point in space at a given moment. The solution was found [10] by the Austrian physicist Erwin Schrödinger, who, in 1925, showed an abstract mathematical wave called a **probability wave** (or **wave function**), which could give us the requested information. He proposed a groundbreaking wave equation analogous to the known equations for other wave motions in nature.

Schrödinger equation

Simply put, the Schrödinger equation describes the evolution of a nonrelativistic quantum system (in space and time) by a **wave function Ψ**, satisfying the so-called time-dependent Schrödinger equation [10]:

$$i\hbar \frac{\partial}{\partial t}[\Psi(\vec{\mathbf{r}}, t)] = \hat{\mathrm{H}}[\Psi(\vec{\mathbf{r}}, t)], \tag{1.1.10}$$

where

i is the imaginary unit,

$\hbar$ – the reduced Planck constant,

$\vec{\mathbf{r}}$ – the position vector,

t – the time,

$\hat{\mathrm{H}}$ – the Hamiltonian operator (which characterizes the sum of the potential and kinetic energy of the system under consideration).

This equation is considered a central result in the study of quantum systems. Its exceptional significance is conditioned by its extensive application – for analysis and description of the behavior of most different systems – from elementary particles to macro objects.

The Schrödinger equation determines how wave functions evolve over time. These wave functions behave qualitatively like other waves, such as water waves or waves on a string, because the Schrödinger equation is mathematically a type of wave function. This explains the name "wave function" and gives rise to the wave-particle duality. However, the wave function in quantum mechanics describes a kind of physical phenomenon, which fundamentally differs from that of classical mechanical waves.

The German physicist Max Born proposed a statistical interpretation of Schrödinger's wave function [11]: the squared modulus of the wave function $|\Psi|^2$ is a real number interpreted as the probability of finding a particle at any point (x, y, z) at any time (t), i.e. its **probability density ρ** (x, y, z, t) is:

$$\rho = |\Psi|^2 = \Psi \cdot \Psi^*, \tag{1.1.11}$$

where Ψ^* is the complex conjugate wave function of Ψ.

Like the common wave function, which describes the propagation of ripples on the water's surface, the Schrödinger equation describes the propagation of probability waves of the particle location in space and time. Peaks of this

wave (points of the maximum probability ρ) show what place in space is the most probable for the particle's appearance at a given moment.

The integral of this quantity ρ, over all the system's degrees of freedom (*x*, *y*, *z*, *t*), must be one because it covers all possible probabilities. This general requirement, which a wave function must satisfy, is called the **normalization condition**.

As an example, here is the so-called "one-dimensional stationary Schrödinger equation":

$$\frac{\partial^2 \Psi}{\partial x^2} + \frac{8\pi^2 m}{h^2}(E - U)\Psi = 0 \qquad (1.1.12)$$

where

x is the particle position,

h – the Planck constant,

m – the particle mass,

E – the total particle energy,

U – the potential energy of the particle.

This equation is widely used to study various objects in chemistry, biology, semiconductor materials, and more.

1.1.8. Quantum numbers

Microcosm objects – atoms and atomic nuclei – are all quantum systems. It means that physical values, which define these microsystems, must possess discrete values. These discrete values (integer or fractional numbers) are called **quantum numbers**.

The Bohr model was a one-dimensional model that used one quantum number to describe the distribution of electrons in the atom. The only information that was important was the size of the orbit, which was described by the **principal quantum number *n*** (***n*-quantum number**). Schrödinger's model allowed the electron to occupy three-dimensional space. It, therefore, required three coordinates, or three quantum numbers, to describe the orbitals in which electrons can be found.

The three coordinates that come from Schrödinger's wave equations are the **principal** (***n***), the **angular momentum** (***l***), and the **magnetic** (***m*$_l$**) quantum numbers [12]. These quantum numbers describe the size, shape, and orientation in the space of the electron orbitals in an atom [13].

The **principal quantum number** (***n***) describes the size of the orbital. Orbitals for which $n = 2$ are larger than those for which $n = 1$. Because protons and

electrons have opposite electrical charges, electrons are attracted to the nucleus of the atom. Therefore, in order to transfer an electron from one orbital, which is closer to the nucleus (n = 1), into another one, which is further from the nucleus (n = 2), the electron needs extra energy. Thus, the principal quantum number indirectly describes the electron energy corresponding to each orbital.

The sets of orbitals with the same n value are often referred to as **electron shells** or **energy levels.** In the notation of the Periodic (Mendeleev's) table of elements, the main shells of the electron are labeled as K (n = 1), L (n = 2), M (n = 3), etc.

The **angular momentum quantum number** (also known as the **azimuthal quantum number**) (***l***) describes the shape of the orbital. Orbitals have shapes that are best described as **spherical** (l = 0), **polar** (l = 1), or **cloverleaf** (l = 2) – see Fig. 1.1.6. They can even take on more complex shapes when the value of the angular quantum number becomes larger.

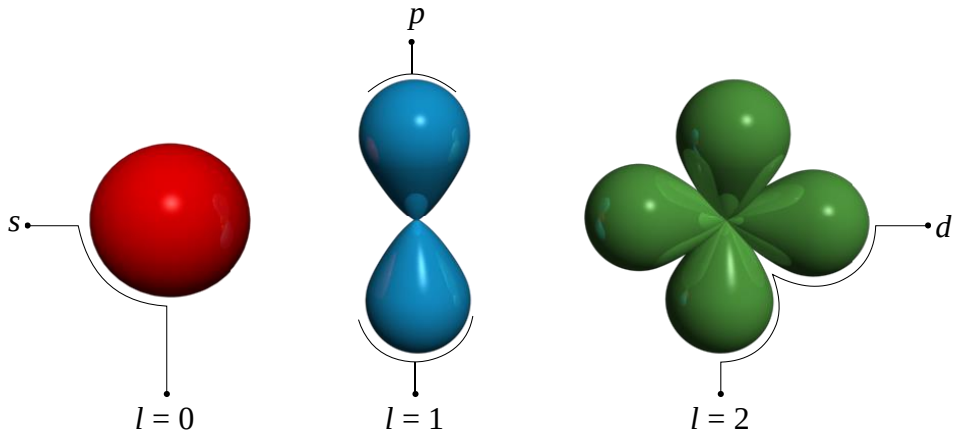

Fig. 1.1.6. Spherical, polar and cloverleaf shapes of orbitals

There is only one way a sphere (l = 0) can be oriented in space. Orbitals that have polar (l = 1) or cloverleaf (l = 2) shapes, however, can be pointed in different directions (Fig. 1.1.7).

Therefore, we need a third quantum number. That is the magnetic quantum number (m_l), which describes a particular orbital orientation in space. (It is called the magnetic quantum number because the effect of different orientations of the orbitals was first observed in the presence of a magnetic field.)

Rules governing the allowed combinations of quantum numbers

- The three quantum numbers (n, l, and m_l) that describe an orbital are integers: 0, 1, 2, 3, and so on.

- The principal quantum number (n) cannot be zero. The allowed values of n are therefore 1, 2, 3, 4, and so on.
- The angular quantum number (l) can be any integer between 0 and n – 1. If n = 3, for example, l can be either 0, 1, or 2.
- The magnetic quantum number (m_l) can be any integer between $-l$ and $+l$. If l = 2, m_l can be either –2, –1, 0, +1, or +2.

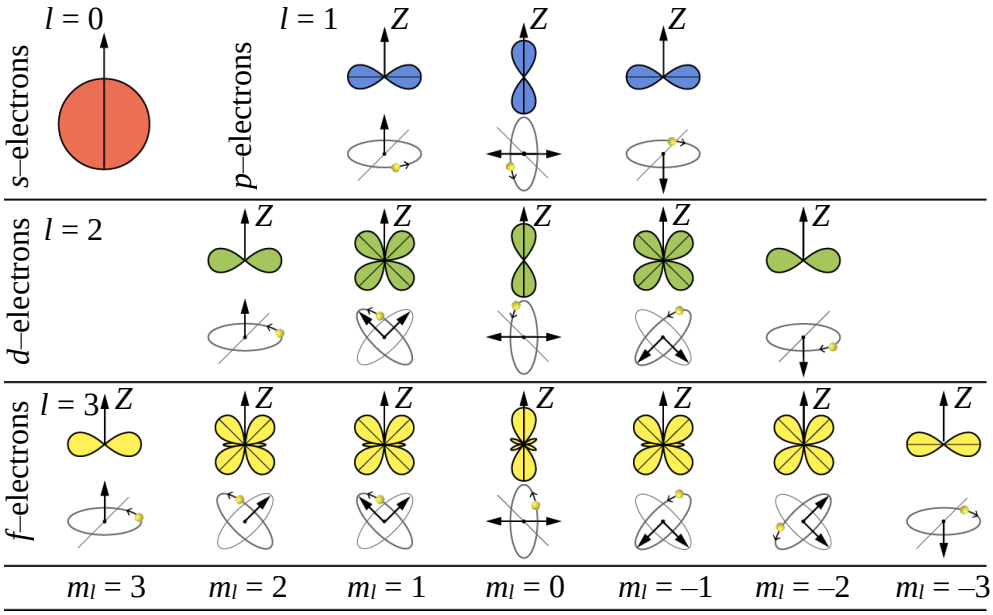

Fig. 1.1.7. The spatial orientation of atomic orbitals

However, to distinguish between two electrons of the orbital, we need a fourth quantum number. It is called the **spin quantum number** (S, m_s).

1.1.9. Electron spin and the Pauli Exclusion Principle

Let's compare the atom with a planetary system. Planets revolve around the Sun as well as around their axes. In the same way, electrons revolve around the nucleus and around their axes. Electron orbiting is described by the orbital angular momentum $\vec{\mathbf{L}}_{orb}$. The rotation of the electron around its axis is determined by the intrinsic angular momentum $\vec{\mathbf{L}}_{intr}$, which is described by the electron **spin quantum number** (or **spin**) – $\boldsymbol{S}$.

The spin characterizes the intrinsic angular momentum not only of the electron but also of all particles and atomic nuclei. According to the laws of quantum mechanics, the intrinsic angular momentum, as well as the spin, can take only certain quantized values [14, 15]. Therefore, the allowed values for spin are non-negative integers or half-integers – $S = a/2$, where a can be any non-negative integer. **Fermions** (such as the electron, proton or neutron) have

half-integer spin values (1/2, 3/2, 5/2, etc.), whereas **bosons** (e.g. photons, mesons) have integer spin values (0, 1, 2, etc.). In our case, the electron spin quantum number is $S = 1/2$.

The value of S for an elementary particle depends only on the type of particle and cannot be altered in any known way.

The spin direction is also quantized and limited by the relation

$$S_z = m_s \hbar, \tag{1.1.13}$$

where

S_z is the spin projection on an arbitrary axis Z,

m_s – the so-called **secondary** (or **magnetic**) **spin quantum number**,

m_s ranges from $-S$ to $+S$ in steps of one. So m_s has $(2S + 1)$ different values. Because, for the electron $S = ½$, thus $m_s = \pm 1/2$ (Fig. 1.1.8).

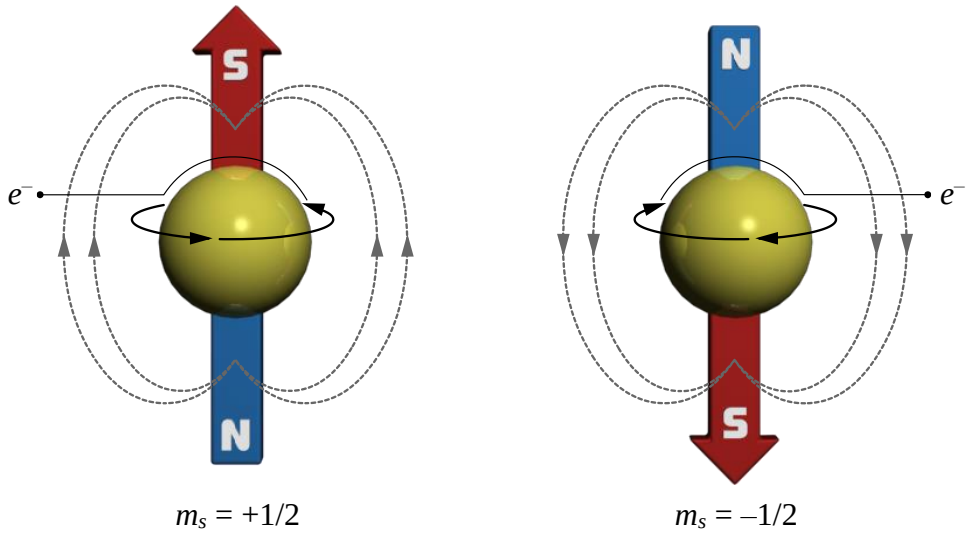

$m_s = +1/2$ $m_s = -1/2$

Fig. 1.1.8. Electrons behave in certain respects as if they were tiny charged spheres spinning around their axes. This spin gives rise to a tiny magnetic field and to a fourth quantum number m_s

The SI unit of spin is J·s (joule·second), just like classical angular momentum. In practice, spin is given as a dimensionless quantity by dividing it by the reduced Planck constant $\hbar$, which has the same units as the angular momentum (see Eq. (1.1.3)):

$$S = L_{intr}/\hbar, \tag{1.1.14}$$

The spin plays a key role in the occupation of electron orbitals of multi-electron atoms. In fact, two electrons that are spinning in the same direction

cannot simultaneously occupy one orbital with the definite values of n and l. It is forbidden by the **Pauli Exclusion Principle**, which was formulated by the Austrian physicist **Wolfgang Pauli** in 1925.

Wolfgang Pauli

The Pauli exclusion principle [16, 17] restricts the number of electrons that can occupy one orbital. According to this principle, no more than two electrons can occupy any orbital on the condition that they have opposite spins ($m_{s1} = 1/2$, $m_{s2} = -1/2$). That is why, in the atom, two electrons with four identical quantum numbers (n, l, m_l, m_s) can't exist. The exclusion principle has subsequently been generalized to include a whole class of particles (the fermions), of which the electron is only one representative.

1.1.10. Electron magnetic dipole momentum

The **electron magnetic dipole momentum** [18] is the magnetic momentum of an electron created by the intrinsic properties of its electric charge and spin. According to classical mechanics, the magnetic dipole momentum $\vec{\boldsymbol{\mu}}_e$ of an electron is

$$\vec{\boldsymbol{\mu}}_e = \frac{-q_e}{2m_e c}\vec{\mathbf{L}}, \tag{1.1.15}$$

where

m_e is the electron rest mass,

$\vec{\mathbf{L}}$ – its angular momentum,

c – the speed of light.

This angular momentum $\vec{\mathbf{L}}$ can be the electron spin angular momentum, its orbital angular momentum, or its total orbital momentum. The Eq. (1.1.15) remains valid according to quantum mechanics and only gets multiplied by a correction factor *g*, known as the ***g*-factor**:

$$\vec{\boldsymbol{\mu}}_e = g\frac{-q_e}{2m_e c}\vec{\mathbf{L}}. \tag{1.1.16}$$

Usually, the electron magnetic momentum is expressed in the **Bohr magneton** μ_B [19]. It is a physical constant, which in SI units is defined as

$$\mu_B = \frac{q_e \hbar}{2m_e}, \tag{1.1.17}$$

and in Gaussian CGS units as

$$\mu_B = \frac{q_e \hbar}{2m_e c}, \tag{1.1.18}$$

where

q_e is the elementary charge,

$\hbar$ – the reduced Planck constant,

m_e – the electron rest mass,

c – the light velocity.

The values of the Bohr magneton in different systems of units are given in Table 1.1.2 below:

System of units	Value	Units
SI	$9.274 \cdot 10^{-24}$	J/T
CGS	$9.274 \cdot 10^{-21}$	erg/G
eV	$5.788 \cdot 10^{-5}$	eV/T
Atomic units	1/2	$e\hbar/m_\mathrm{e}$

Table 1.1.2. The values of the Bohr magneton

Using the Bohr magneton and the reduced Planck constant, the electron magnetic momentum can be expressed as

$$\mu_{eS} = -g\mu_B \frac{\vec{\mathbf{L}}}{\hbar}. \tag{1.1.19}$$

Only the intrinsic spin magnetic moment of an electron is

$$\mu_{eS} = -g\mu_B \frac{L_{intr}}{\hbar}. \qquad (1.1.20)$$

Here, L_{intr} is the electron intrinsic (spin) angular momentum. Because the magnitude of the electron spin is $S = 1/2$, L_{intr} magnitude is $L_{intr} = S\hbar = \hbar/2$ (see Eq. (1.1.14)). The spin g-factor is approximately $g_s \approx 2$. Thus, the electron spin magnetic momentum is approximately equal to 1 Bohr magneton ($\mu_{eS} = 1\mu_B$).

1.1.11. Modern theory of the atom structure

The modern theory of atomic structure is based on the following statements [20, 21]:

1. The electron has a wave-corpuscle duality nature. It can act as a particle or as a wave. As a particle, the electron has a definite mass and charge. At the same time, a moving electron shows wave properties; for example, it has the ability to diffract. The electron wavelength λ and its velocity υ are connected by the **Louis de Broglie ratio** (see Eq. (1.1.7)):

$$\lambda = h/m_e\upsilon, \qquad (1.1.7b)$$

   where
   m_e is the electron rest mass,
   υ – the magnitude of its velocity.

2. According to the uncertainty principle of Heisenberg (see Section 1.1.6), it is not possible to measure the position of an electron (for example, its x-coordinate) and its velocity ($\vec{\mathbf{v}}$) simultaneously with limitless accuracy. Changing the particle momentum in Eq. (1.1.9) according to equation (1.1.4) – $\vec{\mathbf{p}} = m\vec{\mathbf{v}}$, we can obtain the precision limiting condition for the electron:

$$\Delta x \cdot m_e \cdot \Delta\upsilon \geq \hbar/2, \qquad (1.1.9a)$$

   where
   Δx is the uncertainty in position,
   $\Delta\upsilon$ – the measurement error of velocity.

3. An electron in the atom does not move along definite trajectories. It can appear in any part of the near-nuclear space. However, the probability of it being in different parts of this space is not the same. The space around the atomic nucleus, where the probability of the electron's positioning is pretty high, is called an **atomic orbital**.

4. Atomic nuclei are made of **protons** and **neutrons** (joint name – **nucleons**). The number of protons equals the atomic number of an element. The sum of protons and neutrons equals the atomic mass number (see Section 1.2.5).

Models of the atoms: a) Bohr's model; b) Quantum mechanical model

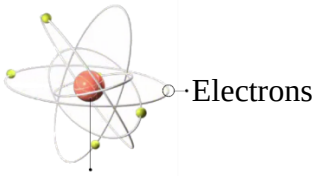

a

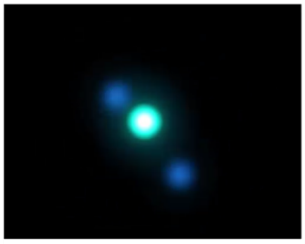

b

SCAN ME

The animation above shows the difference between Bohr's atom model and the Quantum mechanical atom model. In the second picture, two electrons are shown in their most probable positions.

References

[1] Early Atomic Models – From Mechanical to Quantum (1904-1913). https://arxiv.org/ftp/arxiv/papers/1208/1208.5262.pdf

[2] Bohr Model. https://en.wikipedia.org/wiki/Bohr_model

[3] Planck-Einstein Relation. https://en.wikipedia.org/wiki/Planck%E2%80%93Einstein_relation

[4] Matter wave. https://en.wikipedia.org/wiki/Matter_wave

[5] Davisson–Germer experiment: diffraction of electrons by a nickel crystal. https://en.wikipedia.org/wiki/Davisson%E2%80%93Germer_experiment

[6] Uncertainty principle. http://hyperphysics.phy-astr.gsu.edu/hbase/uncer.html

[7] Uncertainty principle. https://en.wikipedia.org/wiki/Uncertainty_principle

[8] Standard deviation.
https://en.wikipedia.org/wiki/Standard_deviation

[9] Probability waves and complementarity.
https://www.physicsoftheuniverse.com/topics_quantum_probability.html

[10] Schrödinger equation.
https://en.wikipedia.org/wiki/Schr%C3%B6dinger_equation

[11] Probability amplitude.
https://en.wikipedia.org/wiki/Schr%C3%B6dinger_equation

[12] Quantum number.
https://en.wikipedia.org/wiki/Quantum_number

[13] Quantum numbers and electron configurations.
http://chemed.chem.purdue.edu/genchem/topicreview/bp/ch6/quantum.html

[14] Spin quantum number.
https://en.wikipedia.org/wiki/Spin_quantum_number

[15] Spin quantum number. https://physics.tutorvista.com/modern-physics/spin-quantum-number.html

[16] Pauli Exclusion Principle.
https://en.wikipedia.org/wiki/Pauli_exclusion_principle

[17] Pauli Exclusion Principle.
https://www.britannica.com/science/Pauli-exclusion-principle

[18] Electron magnetic moment.
https://en.wikipedia.org/wiki/Electron_magnetic_moment

[19] Bohr magneton. https://en.wikipedia.org/wiki/Bohr_magneton

[20] Atomic theory. https://en.wikipedia.org/wiki/Atomic_theory

[21] Formation of the atomic theory.
http://www.t.soka.ac.jp/chem/iwanami/intorduct/ch01atomic.pdf

1.2. Atomic nucleus

1.2.1. Proton discovery

Rutherford's experiment on alpha particle[1] scattering by thin gold foils carried out in 1911, and other experiments showed that atomic nuclei, as well as atoms, have a complex structure.

In 1913, **Rutherford** suggested a hypothesis that there is a particle called the **proton** in the nucleus of the hydrogen atom, which is also a part of the nuclei of all chemical elements. Later, in 1919, he carried out a series of experiments that confirmed this hypothesis [1]. In those experiments, nitrogen atoms were bombarded by alpha particles. As a result, the nitrogen atom split into two parts – the oxygen atom and the hydrogen one containing the nucleus with only one proton (Fig. 1.2.1).

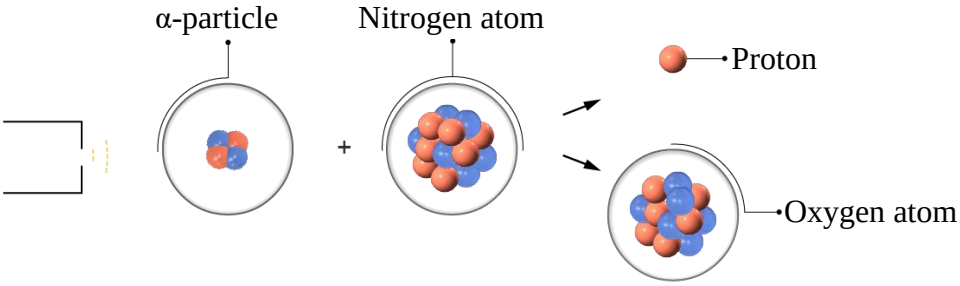

Fig. 1.2.1. Proton discovery experiment: $^{14}_{7}N + {}^{4}_{2}He \rightarrow {}^{17}_{8}O + {}^{1}_{1}H$

The proton's positive charge was found to be equal to the negative charge of the electron, but its mass was found to be about 1800 times greater than that of the electron.

Proton mass	$1.6726 \cdot 10^{-27}$ kg
	938.272 MeV/c^2
	1.0073 u
Proton charge	$1.6022 \cdot 10^{-19}$ C
	+ 1 q_e (elementary charge)

Table 1.2.1. Proton mass and charge

1.2.2. Neutron discovery

After the discovery of the proton, it was believed that atomic nuclei consisted only of protons. However, this belief was not confirmed because the ratio of nuclear charge to its mass did not stay constant for different nuclei, as it

[1] An alpha particle is a helium nucleus consisting of 2 protons and 2 neutrons (see Section 2.1).

should have been if the nuclei only consisted of protons. For heavier nuclei, this ratio is lower than it is for light nuclei.

James Chadwick

In 1920, Rutherford proposed a new hypothesis: that an uncharged particle with a mass approximately equal to the proton mass is present in the nuclear structure. He called it a **neutron** [2]. Over the next few years, physicists could not find this particle despite carrying out many experiments. In the early 1930s, many studies on the interaction between alpha particles and beryllium found that beryllium produced intense radiation, which was thought to be gamma radiation because an electrical field did not influence it. In 1931, French scientists **Irene Curie** and **Frederic Joliot** showed that if this unknown radiation fell on paraffin wax, it ejected protons with very high energy. In 1932, the English scientist **James Chadwick**, who was also looking very actively for the neutron, performed a similar experiment (Fig. 1.2.2) and measured all of the reaction's parameters much more precisely. As a result, he proved that the "beryllium radiation" consists of neutral particles with a mass very near to the proton mass [3]. In this manner, the neutron was discovered experimentally twelve years after Rutherford's hypothesis.

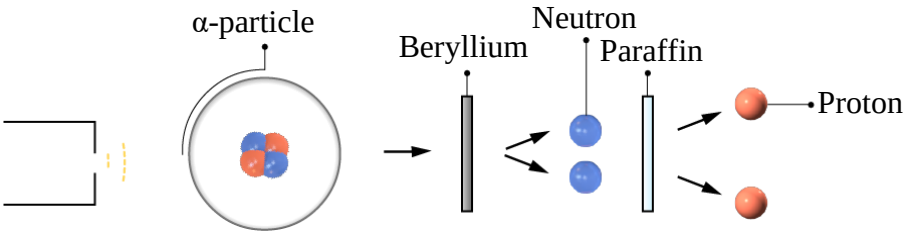

Fig. 1.2.2. Neutron discovery experiment: $^{9}_{4}Be + {}^{4}_{2}He \rightarrow {}^{12}_{8}C + {}^{1}_{0}n$

Neutron mass	$1.6749 \cdot 10^{-27}$ kg
	1.0086 u
	939.565 MeV/c^2
Neutron charge	0

Table 1.2.2. Neutron mass and charge

1.2.3. Neutron-proton model of the atomic nucleus

Heisenberg [4, 5] came up with the neutron-proton model for the atomic nucleus (Fig. 1.2.3). According to this model, all nuclei consist of two types of particles, namely, protons and neutrons. From this model, the protons and neutrons were called **nucleons**, and atomic nuclei were called **nuclides**.

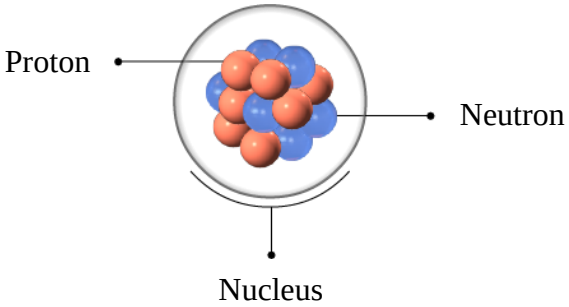

Fig. 1.2.3. Neutron-proton model of the atomic nucleus

1.2.4. Nuclear charge

The number of protons in the atomic nucleus is equal to the number of electrons in the atomic shell. That is why the atom is electrically neutral. The positive electrical charge of the nucleus Q_N is proportional to the absolute value of the electron charge [6]:

$$Q_N = Z|q_e|. \qquad (1.2.1)$$

The integer number Z is equal to the number of protons in the nucleus and coincides with the atomic number in the Mendeleev periodic table. The number Z is called the **charge** (or the **atomic**) **number**.

The first person who managed to measure the nuclear charge through an indirect method was the English physicist **Henry Moseley** in 1913. He performed a series of experiments and determined the relation between the frequency of characteristic X-ray radiation ν and the charge Z:

$$\sqrt{\nu} = aZ - b. \qquad (1.2.2)$$

Moseley also determined that the values of constants *a* and *b* did not depend on the type of chemical element for the fixed line of the X-ray spectrum. This result, known as **Moseley's law** [7], served as an important confirmation of the Mendeleev periodic table – it showed that the element arrangement is based on a physical regularity.

J. Chadwick measured the nuclear charge directly for the first time in 1920. He studied the scattering of alpha particles on metal films, essentially repeating the experiments that had led Rutherford to create the nuclear model of the atom. Measuring the angular dependence of scattered alpha particles and using the Rutherford equation between this dependence and the nuclear charge $Z\,|q_e|$, he determined the charges of the nuclei of platinum, silver and copper. He experimentally found that the measured charges were the same as $Q_N = Z\,|q_e|$ within an error margin of less than 1.5 % [8].

In terms of the properties of the whole **atom**, there is another quantity that is most important – the so-called **effective nuclear charge**. It is defined as the **net positive charge** experienced by the valence-shell electrons of an atom due to the shielding effect of electrons in the inner shells. Because of the positive nuclear charge, the repulsive force exerted by inner shell electrons lessens the attraction on the outermost electrons [9]. The effective charge Q_{eff} can roughly be calculated by the equation:

$$Q_{eff} = Q_N - n_{SE}q_e = (Z - n_{SE})q_e, \qquad (1.2.3)$$

where n_{SE} is the number of inner-shell electrons. Only in the hydrogen atom is there no screening effect because it has only one electron.

1.2.5. Mass number

The total number of nucleons in a nucleus is called the **mass number** and is denoted by the letter *A*. The mass number is usually expressed in atomic mass units but is rounded to the nearest integer number. The difference between the mass number and charge number is equal to the number of neutrons *N*:

$$N = A - Z. \qquad (1.2.4)$$

Nuclei of chemical elements are denoted by the symbol ${}^{A}_{Z}\mathrm{X}$ (Fig. 1.2.4).

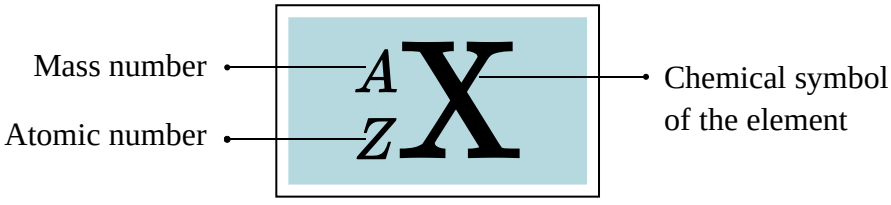

Fig. 1.2.4. Chemical element notation

For example, the symbol $^{252}_{98}$Cf corresponds to the californium nucleus with the total number of nucleons 252 – the number of protons is 98 and the number of neutrons: $N = 252 - 98 = 154$.

By analogy, $^{4}_{2}$He describes the helium nucleus, which consists of 2 protons and 2 neutrons. For this nucleus, there is one more designation – the **α-particle** (see Section 2.1):

$$\alpha \equiv {}^{4}_{2}\mathrm{He}.$$

1.2.6. Isotopes, isotones, isobars

Nuclei with the same Z and different A are called **isotopes** (Fig. 1.2.5). For example, uranium ($Z = 92$) has isotopes $^{235}_{92}$U and $^{238}_{92}$U, having 143 and 146 neutrons, respectively.

Nuclei with the same A and different Z are called **isobars**.

Nuclei with the same N and different Z are called **isotones**.

Some examples are given below:

Isotopes: hydrogen has three isotopes – protium, deuterium and tritium (Fig. 1.2.5).

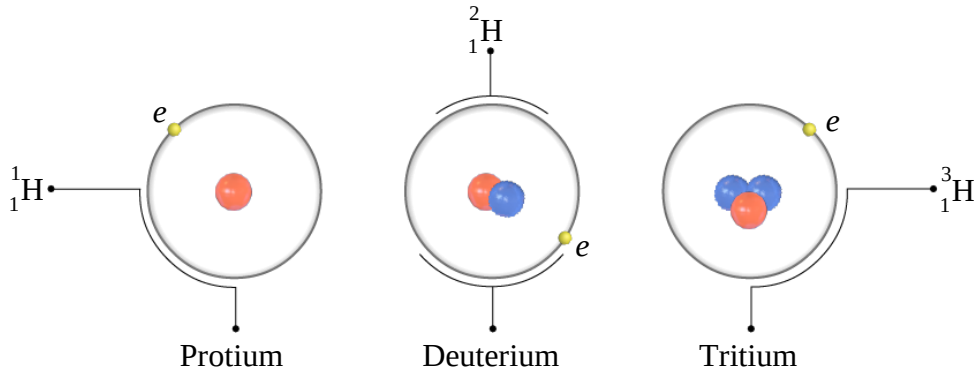

Fig. 1.2.5. Hydrogen isotopes

Isobars: beryllium-10 ($^{10}_{4}$Be), boron-10 ($^{10}_{5}$B) and carbon-10 ($^{10}_{6}$C).

Isotones: carbon-14 ($^{14}_{6}$C), nitrogen-15 ($^{15}_{7}$N) and oxygen-16 ($^{16}_{8}$O).

1.2.7. Nuclear mass

The mass number A determines the **nuclear mass**. Because the masses of the proton and the neutron are approximately equal, the mass of a nucleus (m_N) will be:

$$m_N = Am_n - E_B/c^2, \qquad (1.2.5)$$

where

m_n is the mass of one nucleon,

E_B – the binding energy (see Section 1.3.4),

c – the light velocity.

Devices that are used for the measurement of the atom or nuclear masses are called **mass spectrometers**. The operation principle of such devices was first suggested by the English physicist **Joseph John Thomson** [10] in 1907. In the mass spectrometer, the nucleus mass is determined by observing the motion of an ion of this element in an electric and magnetic field.

Let's see how the mass spectrometer works [11].

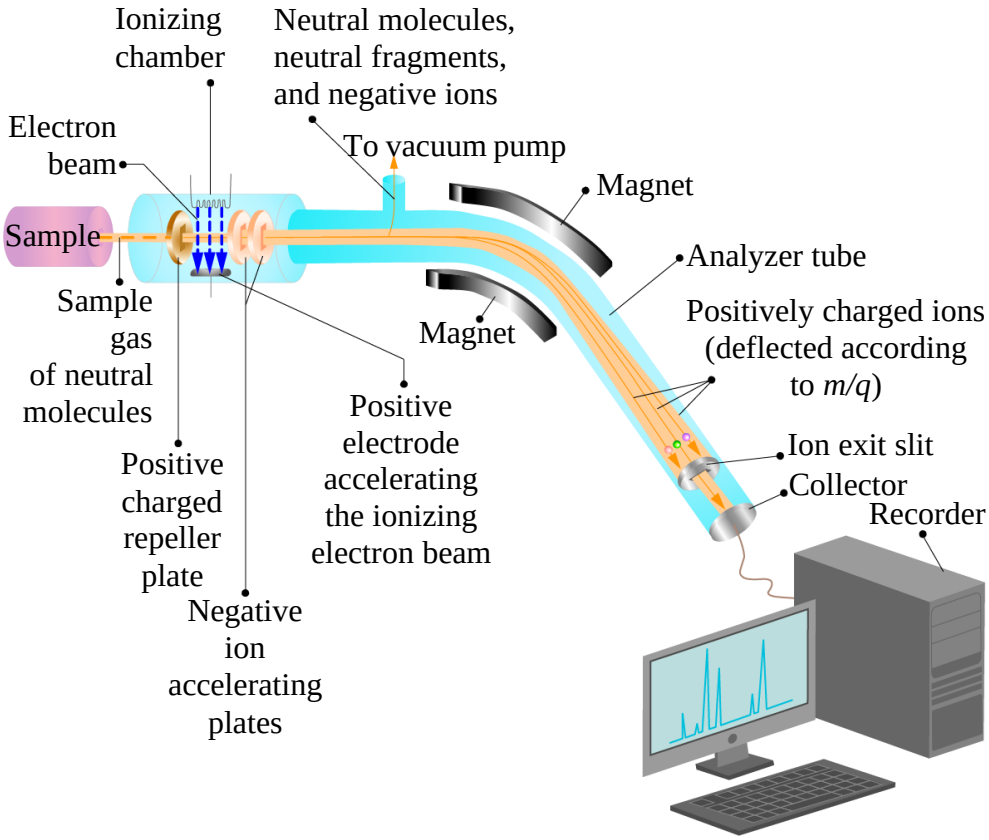

Fig. 1.2.6. Principle of operation of a mass spectrometer

The sample of the object under investigation is placed into a chamber (Fig. 1.2.6) in a gas form. From this chamber, the neutral gas enters the ionizing chamber where its atoms are ionized (in this case, by electron beam irradiation). The ions are then accelerated in an electric field with an

accelerating voltage U. As a result, each ion with a mass m and a charge q_e (usually, single-charged ions are created) gains kinetic energy:

$$\frac{mv^2}{2} = q_e U, \tag{1.2.6}$$

where v is the ion velocity.

After acceleration, the ions go into part of a toroidal tube with a homogeneous magnetic field inside, perpendicular to the toroid plane. It deflects the ions and makes them move in a circular path. Depending on the magnetic field strength $\vec{\mathbf{H}}$, the velocity, and the mass of the ion, it can either hit the walls of the tube, or it can go through it to its opposite side where an ion collector is located. From the equality of the Lorentz force and the centrifugal force, it appears that

$$\frac{q_e v H}{c} = \frac{mv^2}{r}, \tag{1.2.7}$$

where

H is the magnitude of the magnetic field vector $\vec{\mathbf{H}}$,

r – the radius of the ion trajectory (equal to the mean toroid radius).

Combining equations (1.2.6) and (1.2.7), the following equation for the ion mass is derived:

$$m = \frac{q_e r^2 H^2}{2Uc^2}. \tag{1.2.8}$$

This result basically yields the nuclear mass because the mass of the atom's electrons is negligible.

1.2.8. Nuclear radius

According to quantum mechanics, the surface of a nucleus is "indistinct", and the atomic nucleus does not have a well-defined boundary. That is why it is not easy to get an idea of the size of the nucleus.

Postulations about the atomic nucleus's actual size first appeared after Rutherford's experiments on alpha particle scattering. **Rutherford** determined that the nucleus has the shape of a ball with a radius of 10 femtometers (fm) – 1 fm = 10^{-15} m.

Later on, the nuclear radius was measured by different methods, amongst which were: the measurement of the energy of alpha particles emitted from radioactive nuclei; studying of neutron and electron scattering by nuclei; looking at the binding energy of the nucleus, etc.

The American physicist **Robert Hofstadter** [12] carried out the first experiments of electron scattering by atomic nuclei in 1956. In quantum mechanics, any particle can be characterized by the **de Broglie** wavelength (see Eq. (1.1.7a)):

$$\lambda = \frac{h}{p} \approx \frac{hc}{E_e} = \frac{1240}{E_e\ [\text{MeV}]}\ \text{fm}, \qquad (1.1.7c)$$

where E_e is the energy of the electron in MeV.

At a specific energy level of about 100 MeV, an electron's de Broglie wavelength (λ = 12.4 fm) becomes comparable with the nuclear size and nuclei diffraction appears. Hypothetically, the nucleus is a ball made of nuclear matter with a constant density. Using the results of the calculation of the electron diffraction pattern, radii of different nuclei were determined. Thus, the following dependence of the nuclear radius on the number of nucleons in the nucleus was found (Fig. 1.2.7):

$$R = r_0 A^{1/3}, \qquad (1.2.9)$$

where r_0 = 1.2–1.3 fm.

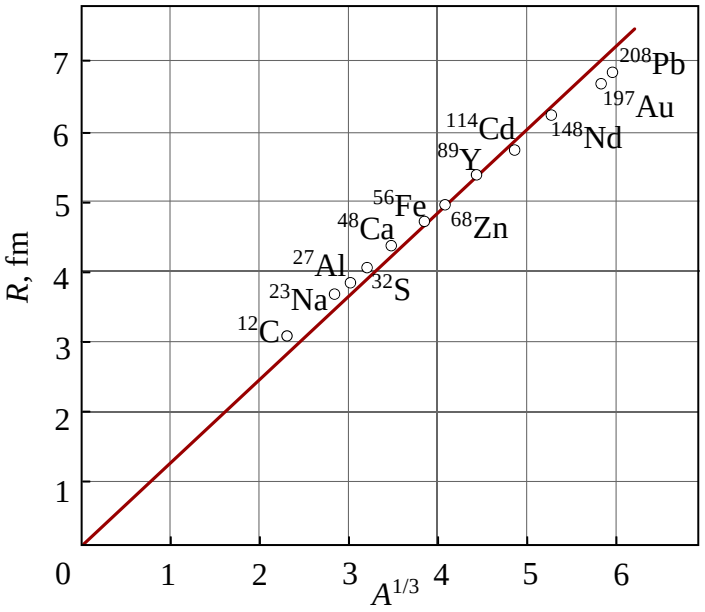

Fig. 1.2.7. Radii of atomic nuclei obtained in the experiments on the electron scattering by the nuclei

A similar dependence was observed using another method: the study of fast neutron scattering – when they pass through a layer of material – confirmed the equation given above, but with slightly different values of r_0: r_0 = 1.3–1.4 fm.

These results lead to the consideration that the nucleus could have two radii:

– an **electromagnetic radius** with the parameter r_0 = 1.2–1.3 fm, which characterizes the proton charge distribution in the nucleus;
– a **nuclear radius** having the parameter r_0 = 1.3–1.4 fm, which characterizes the radius of the zone of nuclear interaction or the radius of the action of nuclear force (see Section 1.3.1).

1.2.9. Nuclear shape

Until 1950, it was believed that the shape of the atomic nucleus was spherical. But then, the American physicist **James Rainwater** (in 1950) and Danish physicists **Aage N. Bohr** and **Ben R. Mottelson** (in 1951) suggested and justified the hypothesis that the shape of many nuclei differs from the ball-shape. After that, many other investigations confirmed and developed their concept further. It was shown [13] that the nuclei can be spherical, rugby ball-shaped (prolate deformation), discus-shaped (oblate deformation), and triaxial (a combination of oblate and prolate deformation). The form strongly depends on the rate of the neutrons and protons in the nuclei. Even the isotope nuclei of the same nuclide may have different shapes.

Within the last few years, three strange, pear-shaped nuclei were discovered – radium-226 ($^{226}_{88}$Ra) – 1993, radium-224 ($^{224}_{88}$Ra) – 2013, and barium-144 ($^{144}_{56}$Ba) – 2016. In them, the symmetry of the charge distribution is violated, and physicists hope to find an explanation for the lack of antimatter in the universe by studying them [14].

1.2.10. Nuclear charge distribution

For a description of the electrical charge density distribution in the nucleus, different models were applied. In some of the **nuclear shell models** (see Section 1.4.3B), it is described by the so-called Wood-Saxon shape [15] (Fig. 1.2.8), giving good results for the spherical nuclei:

$$\rho = \frac{\rho_0}{1 + \exp\left[\frac{r - R_0}{\delta}\right]}, \qquad (1.2.10)$$

where

ρ_0 is the charge density in the center of the nucleus,

r – the distance from the center of the nucleus,

$R_0 = 1.08 \cdot A^{1/3}$ fm – the nuclear radius at which the charge density decreases twice over,

δ – determines the shape slope – at a distance of 4.4δ, the relative charge density ρ/ρ_0 falls from 0.9 to 0.1 (see Fig. 1.2.8); for all nuclei with $A > 40$, $\delta \approx 0.55$ fm.

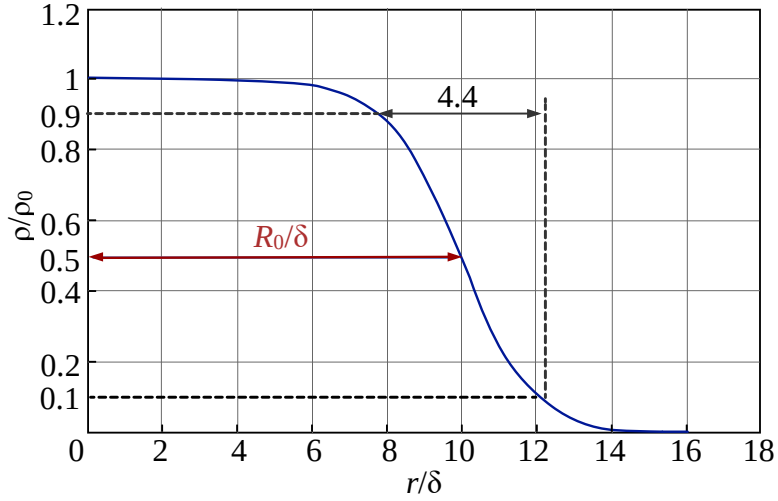

Fig. 1.2.8. Charge density distribution in a nucleus with A = 132 (R_0 = 5.5 fm)

In the central region of the nucleus, protons are distributed evenly, which provides nearly the same charge density. At a certain distance from the nuclear center (around $0{,}6R_0/\delta$), the number of protons and the charge density begins to decrease (Fig. 1.2.8).

1.2.11. Nuclear spin

Each proton and neutron has its own angular momentum, which is the sum of its intrinsic (spin) angular momentum $\vec{\mathbf{S}}$, with a magnitude of $S = 1/2$ ($m_S = \pm 1/2$ – see Section 1.1.9), and the orbital momentum $\vec{\mathbf{L}}$, caused by the motion relative to the general center of nuclear inertia:

$$\vec{\mathbf{J}} = \vec{\mathbf{S}} + \vec{\mathbf{L}}. \qquad (1.2.11)$$

The total angular momentum of the nucleus $\vec{\mathbf{L}}_N$ is equal to the sum of the angular momenta of the protons and neutrons, which contains:

$$\vec{\mathbf{M}}_N = \sum_1^Z \vec{\mathbf{J}}_P + \sum_1^N \vec{\mathbf{J}}_N, \qquad (1.2.12)$$

where

$\vec{\mathbf{J}}_P$ is the total angular momentum of a proton,

$\vec{\mathbf{J}}_N$ – the total angular momentum of a neutron [16].

As with the elementary particles (see Section 1.1.9), the nuclear spin $\vec{\mathbf{S}}_N$ describes the nuclear angular momentum:

$$S_N = M_N/\hbar, \tag{1.2.13}$$

where

S_N is the nuclear spin magnitude,

M_N – the magnitude of the nuclear angular momentum $\overrightarrow{\mathbf{M}}_N$.

Because different elements have a different number of protons, *Z*, and neutrons *N*, the nuclear spin alters widely. Nevertheless, there are some rules that limit its variation [17]:

– all nuclei containing an **even number of protons** and an **even number** of neutrons have no spin (their spin is 0); this phenomenon can be explained by the fact that the nucleons form pairs with oppositely oriented momenta, and therefore, the total angular momentum is zero.

– the spin of all nuclei with an **even mass number** (excluding the case above) is always an integer (1, 2, 3, etc.).

– the spin of all nuclei with an **odd mass number** is always a half-integer (1/2, 3/2, 5/2, etc.).

These rules are illustrated in Table 1.2.3.

Mass number	**Number of protons**	**Number of neutrons**	**Spin**	**Example**
Even	Even	Even	0	$^{16}_{8}$O
Even	Odd	Odd	Integer (1, 2, …)	$^{2}_{1}$H
Odd	Even	Odd	Half-integer (1/2, 3/2, …)	$^{13}_{6}$C
Odd	Odd	Even	Half-integer (1/2, 3/2, …)	$^{15}_{7}$N

Table 1.2.3. Rules limiting the nuclear spin values

Another limitation is that the spins of all stable nuclei do not exceed 9/2. This suggests that most of the nucleons are bound in closed "nuclear shells", which have a total momentum of zero.

Some examples of the nuclear spin of different elements and their isotopes are shown in Table 1.2.4.

Isotope	Spin	Isotope	Spin
$^{1}_{1}\mathrm{H}$	1/2	$^{12}_{6}\mathrm{C}$	0
$^{2}_{1}\mathrm{H}$	1	$^{14}_{7}\mathrm{N}$	1
$^{3}_{1}\mathrm{H}$	1/2	$^{39}_{19}\mathrm{K}$	3/2
$^{3}_{2}\mathrm{He}$	1/2	$^{40}_{20}\mathrm{Ca}$	0
$^{4}_{2}\mathrm{He}$	0	$^{208}_{82}\mathrm{Pb}$	0
$^{7}_{3}\mathrm{Li}$	3/2	$^{235}_{92}\mathrm{U}$	7/2

Table 1.2.4. Spins of some nuclei

Like the electron spin, the number of nuclear spin projections (S_Z) on an arbitrary axis Z (see Eq. (1.1.13)) is limited to $m_s = 2S + 1$. For example, a nucleus with a spin of 9/2 will have 10 projections – from −9/2 to 9/2 by a step of 1.

1.2.12. Magnetic dipole momentum of the nucleus

Just like the electron, the protons and neutrons also create their own magnetic dipole momenta, which is a direct consequence of their spin. Since the nucleus is composed of protons and neutrons condensed into a single region, the nucleus as a whole also has its own magnetic dipole momentum.

The magnetic dipole momenta of the nucleons are measured in another type of magneton, called nuclear magneton μ_N [18]:

$$\mu_N = \frac{q_e \hbar}{2m_p}, \tag{1.2.14}$$

and in the Gaussian CGS units:

$$\mu_N = \frac{q_e \hbar}{2m_p c}, \tag{1.2.15}$$

where

q_e is the elementary charge,

$\hbar$ – the reduced Planck constant,

m_p – the mass of the proton,

c – the light velocity.

The nuclear magneton differs from the Bohr magneton by the sign of the elementary charge and the use of the proton mass instead of the electron mass (see Eqs. (1.1.15) and (1.1.16)). The values of μ_N are given in Table 1.2.5. They are m_p:$m_e \approx 1836$ times smaller than the values of the Bohr magneton.

System of units	Value	Units
SI	$5.051 \cdot 10^{-27}$	J/T
CGS	$5.051 \cdot 10^{-24}$	erg/G
eV	$3.153 \cdot 10^{-8}$	eV/T
Atomic units	1/2	

Table 1.2.5. The values of the nuclear magneton

The magnetic momentum of the nucleus is closely related to its spin. As mentioned above, the protons and neutrons in the nucleus form pairs of opposite total angular momentum, the spin of which is zero. Therefore, the magnetic momentum of a nucleus with even numbers of both protons and neutrons, just like its spin, is zero. The magnetic momentum of a nucleus with an odd number of protons and an even number of neutrons (or vice versa) will be that of the remaining unpaired nucleon. For a nucleus with odd numbers of both protons and neutrons, the total magnetic momentum will be some combination of the magnetic momenta of both of the "last" unpaired proton and neutron.

The magnetic dipole momentum of the nucleus $\vec{\boldsymbol{\mu}}$ is proportional [19] to the angular momentum $\vec{\mathbf{M}}_N$ and respectively to the spin $\vec{\mathbf{S}}_N$:

$$\vec{\boldsymbol{\mu}} = g \frac{q_e}{2m_p} \vec{\mathbf{S}}_N. \tag{1.2.16}$$

Accordingly, for the magnetic dipole momentum projection μ_Z on an arbitrary axis Z, the following equation can be obtained:

$$\mu_Z = g \frac{q_e \hbar}{2m_p} m_S = g m_N m_S, \tag{1.2.17}$$

(expressed by the nuclear magneton). The g-factor has different values for different nuclei. Because the nuclear spin (m_s) can have different signs, the

nuclear magnetic momentum can be positive or negative. The positive value means that the directions of the spin and that of the magnetic momentum coincide. The negative value shows that they are opposites.

The Z-projection of the nuclear magnetic momentum is important because when the nucleus is interacting with an external magnetic field, the axis Z can be selected to be parallel to the magnetic field vector $\vec{\mathbf{H}}$. In this way, the quantitative analysis of their interaction is simplified.

1.2.13. Electrical quadrupole momentum of the nucleus

Besides magnetic momenta, atomic nuclei also have electric momenta, which is dependent on the charge distribution in the nucleus. The quadrupole momentum appears because of the violation of the spherical symmetry of the charge distribution. The quadrupole momentum in the nucleus is equal to zero if the charge distribution is spherically symmetric.

By convention, the positive value of the quadrupole momentum means that the nucleus is elongated along the spin axis (prolate form). Its negative value means that the nucleus is stretched in the plane perpendicular to the spin axis (oblate form) [20].

Most of the heavy nuclei have quite an elongated shape. However, all the nuclei with an equal number of protons and neutrons ($Z = N$) are spherically symmetric.

1.2.14. Parity

The wave function (see Section 1.1.7) of a system of particles, or that of a nucleus, thoroughly describes its behavior as a function of space and time. **Parity** is a quantum number that characterizes the symmetry of the wave function of a particle or of a particle system with respect to some discrete transformations.

P-parity (space parity) characterizes the behavior of the wave function under a mirror inversion of the axes in the rectangular coordinate system (coordinates x, y, z change into $-x$, $-y$, $-z$, i.e. a right-handed coordinate system changes into a left-handed one or vice versa) [21]).

C-parity is a quantum number that characterizes the wave function of a particle or system of particles under the charge conjugation (a particle changes into the corresponding antiparticle).

T-parity is a quantum number that characterizes the wave function of a particle or system of particles under time reversal (the direction of time flow changes to the opposite: $t \rightarrow -t$).

P-parity (often referred to only as **parity**) is the most frequently used of these quantum numbers. It can take only two values: +1 (for an even wave function,

which does not change its sign under a mirror coordinate inversion) or −1 (for an odd wave function). The atomic nucleus can be presented as a set of independently moving nucleons. Then the nuclear P-parity will be equal to the product of the intrinsic parities of each nucleon and have the value $(-1)^{\sum l_i}$:

$$P_N = P_1 P_2 \ldots P_n (-1)^{\sum l_i}, \qquad (1.2.18)$$

where

l_i is the orbital number defining the motion characteristics of the i-th nucleon,

n – the number of nucleons in the nucleus.

(Since the nucleon number does not change during nuclear interactions, the parity of the individual nucleons does not affect the nucleus parity. It depends only on their relative motions, i.e. on their orbital numbers l_i.)

For example, in the nucleus $^{7}_{3}$Li, 4 nucleons (2 protons and 2 neutrons) are at the s-level with $l = 0$ and 3 nucleons – at the p-level with $l = 1$. Therefore $P_{\mathrm{Li}} = (-1)^3 = -1$.

According to the **parity conservation law**, the parity of a closed system in the initial state is conserved in the consequent instants of time. However, the parity conservation law is not applicable to weak interaction [22].

References

[1] *Cottingham, W. N., D. A. Greenwood*. An Introduction to Nuclear Physics. Cambridge University Press, 1986. ISBN 9780521657334.

[2] Neutron. https://en.wikipedia.org/wiki/Neutron#Discovery

[3] Neutron – to the fiftieth anniversary of its discovery (in Russian). Moscow, Nauka, 1983. http://elib.biblioatom.ru/text/neytron-k-pyatidesyatiletiyu-otkrytiya_1983/go,226/

[4] *Heisenberg, W*. Über den Bau der Atomkerne I. Z. Phys. **77,** 1932, p.p. 1-11.

[5] *Heisenberg, W*. Über den Bau der Atomkerne II. *Z. Phys*. **78,** 1932, p.p. 156–164.

[6] Nuclear charge (in Russian). http://ru.solverbook.com/spravochnik/fizika/zaryad-yadra-atoma/

[7] Henry Moseley's law. https:///en.wikipedia.org/wiki/Moseley%27s_law

[8] James Chadwick. https://en.wikipedia.org/wiki/James_Chadwick

[9] The shielding effect and effective nuclear charge. https://courses.lumenlearning.com/introchem/chapter/the-shielding-effect-and-effective-nuclear-charge/

[10] J. J. Thomson. https://en.wikipedia.org/wiki/J._J._Thomson

[11] Mass spectrometry. https://www2.chemistry.msu.edu/faculty/reusch/virttxtjml/spectrpy/massspec/masspec1.htm

[12] Robert Hofstadter. https://en.wikipedia.org/wiki/Robert_Hofstadter

[13] Atomic nucleus. https://en.wikipedia.org/wiki/Atomic_nucleus

[14] How pear-shaped nuclei may help search for antimatter? https://cosmosmagazine.com/physics/how-pear-shaped-nuclei-may-help-search-for-antimatter (Orig. art.: *Bucher, B. et al*. Direct evidence of octupole deformation in neutron rich ^{144}Ba. Phys. Rev. Lett., **116**, 112503, 2016.)

[15] Woods-Saxon shape. https://nukephysik101.wordpress.com/2011/02/16/woods-saxon-shape/

[16] Nucleon and nuclear angular momentum. http://www.physics.valpo.edu/courses/p430/ppt/Krane_ch3_4.pdf

[17] Nuclear spin. https://physics.tutorvista.com/modern-physics/nuclear-spin.html

[18] Nuclear magneton. https://en.wikipedia.org/wiki/Nuclear_magneton

[19] Nuclear magnetic moment. http://hyperphysics.phy-astr.gsu.edu/hbase/Nuclear/nspin.html#c2

[20] Electrical quadrupole moments of nuclei. http://hyperphysics.phy-astr.gsu.edu/hbase/Nuclear/elequad.html

[21] Parity. ttp://hyperphysichs.phy-astr.gsu.edu/hbase/quantum/parity.html

[22] Fundamental interaction. https://en.wikipedia.org/wiki/Fundamental_interaction

1.3. Mass and energy

1.3.1. Nuclear force

Atomic nuclei are stable structures despite the fact that they contain particles of the same charge – protons. This means that among the nucleons in the nucleus, there should exist a special force. Moreover, this force is radically different from gravitational and electromagnetic forces. This special force is referred to as the **nuclear force** (also known as the **strong force**). It exceeds the electromagnetic force by around 100 times and the gravitational force between the nucleons by about 38 orders of magnitude [1].

The nuclear force determines the **strong interaction** – one of the fundamental interactions in the universe. However, it has a short-range character. The range of its action is a few fm, which is slightly greater than the size of the nucleons of about 1 fm. However, its action rapidly decreases and becomes insignificant at distances beyond about 2.5 fm. This property is known as the **saturation of nuclear force**.

At distances less than 0.7 fm, the nuclear force becomes repulsive. This repulsive component is responsible for the physical size of nuclei since the nucleons can come no closer than the force allows. The characteristic time[1] of the strong force is $\sim 10^{-23}$ s (the shortest of all fundamental forces).

1.3.2. Nuclear energy

In 1905 the great physicist Albert Einstein derived his famous equation:

$$E_0 = mc^2, \tag{1.3.1}$$

which actually became a symbol of the XX century.

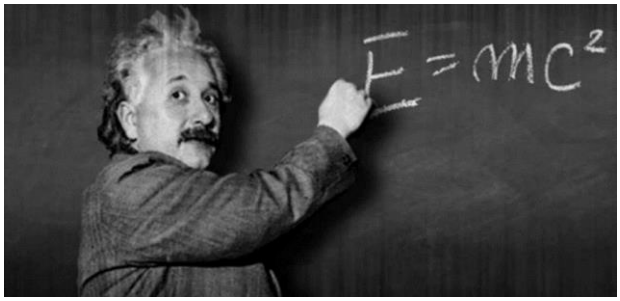

Fig. 1.3.1. Albert Einstein is writing down his famous energy-mass equivalence equation

[1] The **characteristic time** is the measure of how long the force needs to act in order to produce an effect.

This equation shows that the total energy of a rest-isolated system (a proton, a neutron, an atomic nucleus, a molecule) is bound with its mass. This equation describes the equivalence of mass and energy. For example, if we know the mass of a proton (m_p) and the speed of light (c), then we can calculate the proton's total energy E_0 in its rest system by using Einstein's equation:

$$E_0 = m_p c^2 = 1.6726 \cdot 10^{-27} \text{ kg} \cdot 9 \cdot 10^{16} \text{ m}^2/c^2 \approx \approx 1.5 \cdot 10^{-10} \text{ J} \approx 938 \text{ MeV}. \quad (1.3.2)$$

1.3.3. Mass defect

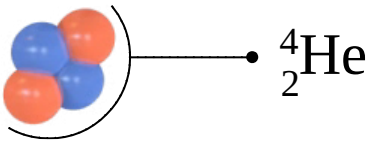

Fig. 1.3.2. The Helium nucleus

Consider the following example. Let us examine the rest mass (m_{He}) of the helium nucleus ($^4_2$He).

The helium nucleus consists of 2 protons and 2 neutrons (Fig. 1.3.2) with:

- mass of the proton $m_p = 1.007276$ u;
- mass of the neutron $m_n = 1.008665$ u.

The total mass of the nucleons of the helium nucleus should be

$$m_\Sigma = 2m_p + 2m_n = 4.0319 \text{ u}. \quad (1.3.3)$$

However, the actual measured mass of the helium nucleus is

$$m_{\text{He}} = 4.0026 \text{ u},$$

which shows that

$$m_{\text{He}} < 2m_p + 2m_n. \quad (1.3.4)$$

This example proves that the rest mass of an atomic nucleus is usually less than the sum of the individual masses of the constituent protons and neutrons when separated!

The difference between the sum of the rest masses of the nucleons that form an atomic nucleus and the rest mass of the same atomic nucleus is called the **nucleus mass defect**:

$$\Delta m_N = Z \cdot m_p + N \cdot m_n - m_N, \quad (1.3.5)$$

where

Δm_N is the nucleus mass defect,

m_N – the mass of the nucleus,

Z – atomic number (number of protons),

N – number of neutrons ($N = A - Z$).

1.3.4. Binding Energy

Nuclear binding energy

Nuclear binding energy $E_B(A, Z)$ is the minimum energy required to separate a nucleus into its components – protons and neutrons, and it can be calculated from the mass defect:

$$E_B(A, Z) = \Delta mc^2 = [Z \cdot m_p + (A - Z) \cdot m_n - m_N(A, Z)] \cdot c^2. \qquad (1.3.6)$$

When a nucleus is formed by the fusion of free protons and neutrons, the released energy is equal to the binding energy.

The values of the binding energies for some nuclei are as follows:

$$E_B(^4_2\mathrm{He}) \approx 28 \text{ MeV};$$
$$E_B(^{12}_6\mathrm{C}) \approx 92 \text{ MeV};$$
$$E_B(^{16}_8\mathrm{O}) \approx 128 \text{ MeV};$$
$$E_B(^{32}_{16}\mathrm{S}) \approx 272 \text{ MeV}.$$

Such large values of the binding energies of nucleons indicate the immense forces that firmly hold protons and neutrons within the nucleus despite the large electromagnetic repulsion between positively charged protons.

1.3.5. Specific binding energy

For comparison with nuclear stability, specific binding energy is introduced.

Specific binding energy

The specific binding energy ε_B is defined as the binding energy per nucleon:

$$\varepsilon_B = \frac{E_B}{A}. \qquad (1.3.7)$$

In other words, the specific binding energy is the energy that is required to remove one nucleon from the nucleus.

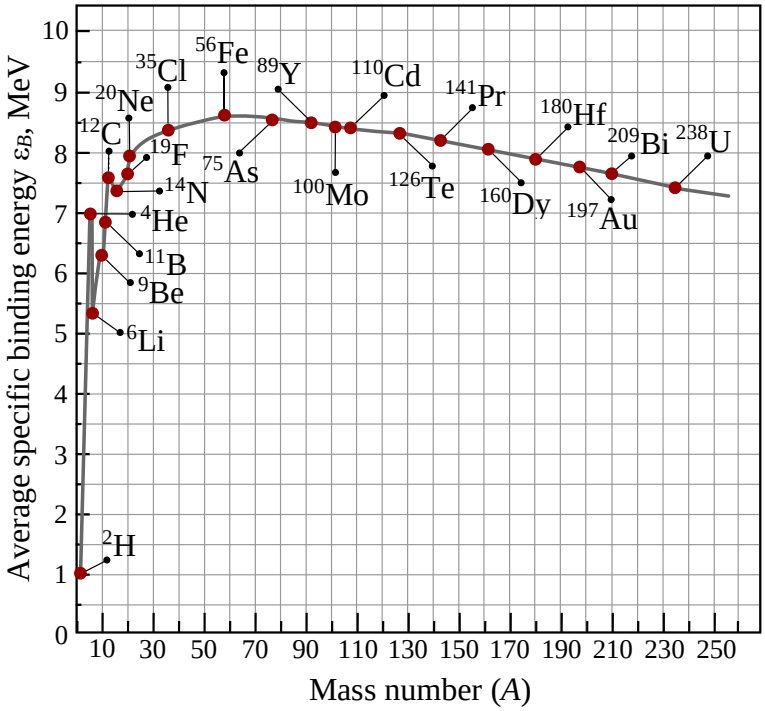

Fig. 1.3.3. The average specific binding energy as a function of the mass number (A)

The greater the value of the specific binding energy, the more stable the nucleus is. Fig. 1.3.3 shows that the nuclei with the strongest binding energy are in the area of iron ($A \sim 55$–60). This means that for **light nuclei**, **nuclear fusion** is the process that produces energy (due to the increase in specific binding energy). Conversely, the **fission** of **heavy nuclei** is the process that releases energy.

Generally, Fig. 1.3.3 shows that the binding energy is relatively low depending on the number of nucleons in the nuclei. The reason is that because of the nuclear force saturation, each nucleon interacts only with its nearest neighbors and nothing beyond them. Thus, an increase in the number of nucleons cannot increase the specific binding energy. Only the lowest ε_B of the lightest nuclei can be attributed to the limited number of neighboring nucleons. Therefore, it rapidly increases with an increase in the number of nucleons.

1.3.6. *N*–*Z* diagram of the atomic nuclei

At present, about 3500 atomic nuclei have been discovered. They have different combinations of Z (number of protons) and N (number of neutrons). It is estimated that the total number of atomic nuclei should be about 6500. Only about 250 of these nuclei are stable.

Fig. 1.3.4 depicts the so-called *N*–*Z* diagram of atomic nuclei. The black cells represent stable nuclei. The area of stable nuclei is usually called the valley of stability [2]. The following equation between the number of neutrons and the number of protons characterizes the nuclei of the valley of stability:

$$N/Z = 0.98 + 0.015A^{2/3}, \qquad (1.3.8)$$

where A is the mass number. The line of stable nuclides running down the center of the valley of stability is known as the line of beta stability.

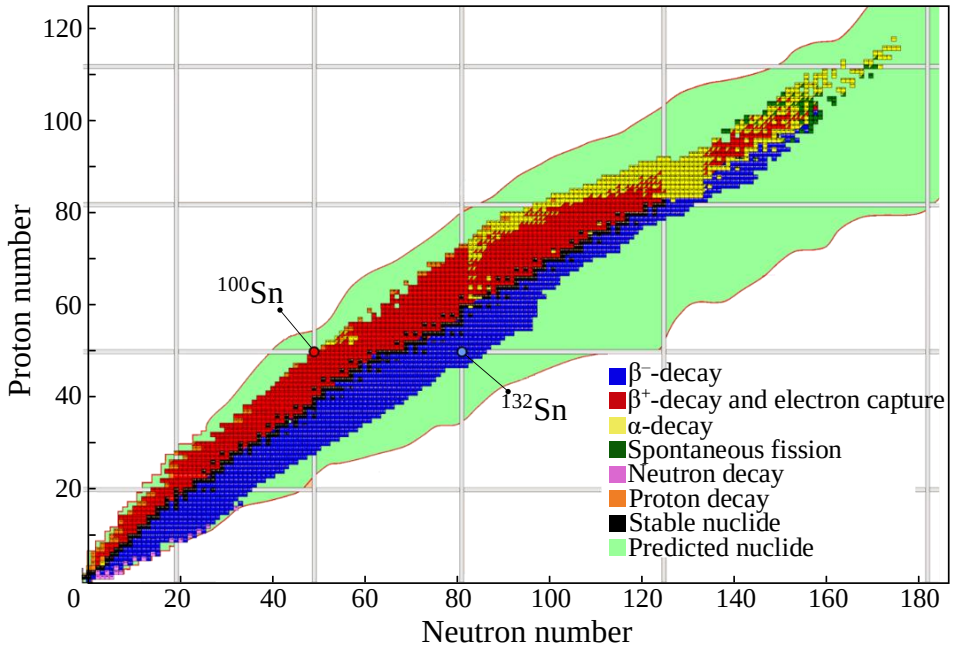

Fig. 1.3.4. (N–Z) diagram of atomic nuclei

To the right side of the valley of stability, the so-called **neutron-rich** nuclei are located where the number of neutrons is greater than the number of protons. They usually undergo β^--decay (see Section 2.2). To its left side are the **proton-rich** nuclei, where the number of protons exceeds the number of neutrons. These nuclei undergo β^+-decay and electron capture (see Section 2.2).

Light stable nuclei ($A < 40$) have approximately equal numbers of neutrons and protons. In the area of large A, the ratio between the neutron and the proton numbers increases, reaching a value of 1.6 for $A \sim 250$. These nuclei undergo α-decay (see Section 2.1) and spontaneous fission since, with the increase in the number of nucleons, short-range nuclear force compensates less for the long-range Coulomb repulsion of protons in the nucleus.

Heavy nuclei are energetically more stable if they contain a greater number of neutrons *N* compared to the number of protons *Z*. The heaviest stable nuclei are the nuclides of lead ($Z = 82$) and bismuth ($Z = 83$).

The red lines outline the green area of the probable existence of atomic nuclei.

Today the region of superheavy atomic nuclei (in the top right corner of the diagram, $Z > 105$) is actively being explored. Until now, all elements up to $Z = 118$ have been laboratory synthesized. All of them are unstable (radioactive) with a very short half-life. Theoretical calculations and experimental data have enabled the postulation of the existence of a so-called **island of stability** [3] containing even heavier nuclei ($A \sim 120$ and $Z \sim 300$) with a much longer half-life – from days to millions of years. However, it is not yet possible to reach them.

References

[1] Fundamental interaction. https://en.wikipedia.org/wiki/Fundamental_interaction

[2] Committee on Nuclear Physics of the National Research Council. Nuclear physics. Nat. Acad. Press., Washington, D. C., 1999. https://www.nap.edu/read/6288/chapter/5#50

[3] Island of stability. https://en.wikipedia.org/wiki/Island_of_stability

1.4. Nuclear models

1.4.1. Necessity of nuclear models

There are two main obstacles opposing nuclear theory [1]. The first is that the nucleon-nucleon force is quite complex and its form is still not explicitly known. The major reason for this is that, in fact, the actual interactions are between quarks of which the nucleons are made up: to this day, no analytical description of these interactions at low energies exists. The second difficulty is that the nucleus is a quantum system of many strongly interacting particles (protons and neutrons), which does not allow one to find an analytical quantum-mechanical solution – the many-body Schrödinger equation cannot be solved definitively.

These two obstacles imply the use of models relying on the systems of simplifying approximations (physical and mathematical), by means of which one can calculate the characteristics of the nuclei structures, as well as their interactions with other systems. The models are designed to describe all main characteristics of the nucleus: spin, parity, magnetic dipole moments, and electric quadrupole moments; and to explain more properties of the excited nuclear states and to describe various interaction processes of the nuclei with different particles or other nuclei. The number of parameters and the ability to predict new properties of the nuclei while explaining the existing ones determines the effectiveness of the model. However, any model has limited capabilities and cannot give a complete description of all properties of the nucleus. As a result, one has to resort to a large number of models adapted to describe a limited range of phenomena, but which together correspond to the modern level of knowledge about the nucleus.

The basis of every nuclear model assumes that any set of degrees of freedom has some autonomy for each selected object. The degrees of freedom can be classified as **collective**, corresponding to the coherent movement of a large number of particles, and **monoparticles** – corresponding to the independent movement of individual nucleons. They determine two main directions of nuclear model development.

In the first one, the nucleus is considered as an ensemble of strongly interacting nucleons that creates collective (coherent) motion, i.e. as a single quantum mechanical particle. In this manner, the many-body problem can be reduced to a one-body problem. The nucleons in the nucleus interact with their nearest neighbors, and they practically do not move – their mean free path is much smaller than the nuclear radius. These models form a group of **collective nuclear models**.

In the second concept, the nucleons move almost independently (without interacting with each other) in an averaged potential field in the nucleus created by the nucleons. In this case, a product of single-particle wave functions can replace the many-body wave function. As a result, their mean free path is of the order of the nuclear radius. These models form the group of so-called **independent particle models**.

The most popular and often used models of both groups, as well as some combined models, will briefly be described below.

1.4.2. Collective models

A. Liquid-drop model

The **Liquid-drop model** is the first and most used collective model. It was suggested in 1929 by the Russian-born American physicists **G. Gamow** and further developed by **N. Bohr**, **Y. Frenkel** and **J.A. Wheeler** in 1936 [2]. The drop model is based on an analogy between the behavior of nucleons in the nucleus and the behavior of the molecules in a droplet of liquid. So, the forces acting between the constituent molecule-particles in the liquid and the nucleons in the nucleus are short-range, and therefore saturation is peculiar to them. A liquid drop under specific external conditions has a characteristic substance. The nuclei are characterized by a practically constant specific binding energy and a constant density independent of the number of nucleons in the nucleus. Thus, the volume of the drop, as well as the volume of the nucleus, is proportional to the number of particles, i.e. to the mass number A. Respectively, the nuclear density is independent of A, and the nucleus is incompressible as a liquid drop.

The nucleons in the nucleus behave like the molecules in a drop of liquid – the nuclear force on the nucleons on the surface is different from those on nucleons in the interior of the nucleus (the internal nucleons are completely surrounded by other attracting nucleons), which is an analogy with the force that forms a drop of liquid. In the droplet model, the nucleus is considered as a continuous medium consisting of neutron and proton fluids and is described by the equations of classical hydrodynamics.

The essential difference between a nucleus and a drop of liquid lies in the fact that the model treats the nucleus as a drop of an electrically charged incompressible fluid (with a density equal to a nuclear one), obeying the laws of quantum mechanics. Due to the high density of nucleons in the nucleus and the powerful interaction between them, collisions are very frequent, and therefore the independent motion of individual nucleons is impossible. As in a drop of ordinary liquid, the surface in the core can fluctuate. If the amplitude

of the oscillations increases spontaneously, the drop will disintegrate; that is, the nucleus will split.

The droplet model explains many important features of nuclei very well:

- the spherical shape of most nuclei;
- the dependence of the nuclear radius on the mass number ($R = r_0 A^{1/3}$, see Section 1.2.8);
- the reasons for nuclear fission and its mechanism: the model calculates an energy barrier to fission as a sum of the repulsive Coulomb force between the protons of the nucleus and the attractive surface tension of the skin of the "liquid-drop" nucleus; if the barrier is low enough, the nucleus might undergo spontaneous fission; for higher barriers, it takes a nuclear reaction (e. g. with a neutron) to induce fission;
- the saturation properties, i.e. the binding energy E_B of a nucleus with Z protons and N neutrons, which is determined by the semi-empirical formula of **K. Weizsäcker** [3]:

$$E_B(A, Z) = a_V A - a_S A^{2/3} - a_C Z^2/A^{1/3} - a_A (A - 2Z)^2/A + \delta(A, Z), \quad (1.4.1)$$

where $A = Z + N$ is the mass number.

The first term (called the **volume term**) is proportional to A (i.e. to the nuclear radius R raised to the third power – see equation (1.2.9)) and represents the binding energy of the nucleons in the volume of the nucleus.

The second term (called the **surface term**) is proportional to $A^{2/3}$ (i.e. to R^2) and represents a decrease in the binding energy of the nucleus at the drop surface (because these nucleons have fewer neighbors to provide full attraction).

The next term, proportional to Z^2, is known as the **Coulomb term**. It represents the repulsive electrostatic energy decreasing the binding energy. The model assumes that the electric charge of protons is uniformly distributed inside the whole nucleus – a sphere with a radius of $R = r_0 A^{1/3}$. The Coulomb forces are not saturated, and each of the Z protons interacts with all the other $Z - 1$. Thus, the term is proportional to $Z(Z - 1) \approx Z^2$.

The fourth term, proportional to $(A-2Z)^2$, is known as the **asymmetry term**. Its theoretical justification is more complex. If we confine ourselves only to the first three terms, which follow from the droplet model, the stability of the nucleus should increase with an increase in the number of neutrons in the nucleus for a given number of protons. However, experimental data point to a different trend – towards the higher stability of nuclei with $N = Z$.

This term – an amendment to the energy of symmetry, does not follow from the liquid drop model and reflects the tendency, as observed in nature, toward

symmetry in the structure of nuclei. In the absence of Coulomb forces, the maximum of the specific binding energy at a fixed A would correspond to all nuclei with an equal number of protons Z and neutrons N (symmetry effect), i.e. $Z = N = A/2$. This is due to the charge independence of the nuclear force and the implementation of the Pauli Exclusion Principle (see Section 1.1.9). The equal number of protons and neutrons in light nuclei lying on the line of beta stability (see Section 1.3.6), in which the energy of the Coulomb repulsion is small, confirms this concept.

However, as the number of protons increases (from $Z > 20$), Coulomb forces begin to play an increasingly prominent role, and the compensation for their repulsive action (whose magnitude is $\sim Z^2$) is achieved by increasing the number of neutrons that enlarge the nuclear attraction force. For this reason, in stable nuclei with $Z > 20$, the number of neutrons must be greater than the number of protons. Because of the Pauli principle, however, the number of particle quantum states with the same energy level is limited, and when more particles are "added" to the nucleus, they have to occupy a higher energy level. Thus, they increase the total energy of the nucleus by decreasing the binding energy. As a result, the deviation from the equality $Z = N = A/2$ in any direction leads to a decrease in the specific energy of the nucleus bond and the fourth term in the formula must be negative. It is proportional to the square of the difference between N and Z and because $N = A - Z$ – to $(A - 2Z)^2$.

The last term (called the **pairing term**) represents the increased stability of the ground state of the nuclei with an even number of protons and/or neutrons. The reason is the tendency of two protons or two neutrons with opposite spin (and with all other quantum numbers being equal) to create pairs with a higher strong force. For example, the nuclei with even numbers N and Z (even-even nuclei) have a specific binding energy of about 1 MeV greater than the neighboring nuclei, in which either N or Z is odd, and consequently, A is odd (even-odd or odd-even nuclei). Nuclei with an odd number of both protons and neutrons (odd-odd nuclei) have the lowest specific binding energy among neighboring nuclei. Only four stable nuclei of the latter type are known.

Therefore, the function $\delta(A, Z)$ of the last term takes three different values:

$$\delta = \begin{cases} -\delta_0 - \text{for even-even nuclei,} \\ 0 - \text{for nuclei with } A \text{ odd,} \\ +\delta_0 - \text{for odd-odd nuclei } (A \text{ is even}) \end{cases} \qquad (1.4.2)$$

where δ_0 is found empirically to have a value of about 1 MeV, slowly decreasing with the mass number A. According to modern experimental data,

the dependence on the mass number A can be expressed as

$$\delta_0 = a_P A^{-1/2}. \quad (1.4.3)$$

The formula of K. Weizsäcker is widely used to calculate different nuclear quantities. For example, the mass of the nuclei for different values of A and Z can be determined by the equation

$$m(A,Z) = Zm_P + (A-Z)m_N - E_B(A,Z), \quad (1.4.4)$$

where the binding energy $E_B(A, Z)$ is calculated from the equation in (1.4.1).

The liquid-drop model naturally has limited potentialities. It cannot precisely describe some terms in Eq. (1.4.1), such as the symmetrical and the pairing energies. It also does not explain the existence and the particular stability of **magic nuclei**[1] [4], or the asymmetry of fission – why the splitting of the heavy nucleus produces two **asymmetrical pieces** (see Section 2.4.1). Additionally, the drop model is not suitable for the quantitative description of the energy spectra of excited nuclear states [5].

The drop model is a macroscopic theory because it does not take into account the microscopic structure of the nucleus, for example, the distribution of nuclear shells. It is also a semi-classical model – it contains some quantum-mechanical approaches, such as taking into account the influence of the Pauli Exclusion Principle, pairing effects, and others.

B. Vibrational model

The **vibrational nuclear model** is an extension of the liquid drop model using quantum mechanical principles. It is based on an analogy with the classical theory of small oscillations of a liquid drop. In it, the nucleus is considered as a liquid drop that is vibrating at a high frequency. Thus, the nucleus' average shape is spherical, but the instantaneous shape is not since it oscillates. The model shows that any excited state of the nucleus can be interpreted as a quantized state of a nuclear vibration [6].

C. Rotational model

According to experimental data in the range of mass numbers $150 < A < 190$ and $A > 200$, the quadrupole moments of the nuclei are extremely large and differ from the values predicted by the shell model (see below) by tens of

[1] A **magic number** is such a specific number of nucleons (either protons or neutrons separately) that they are arranged into complete shells within the atomic nuclei. The most widely recognized magic numbers are **2, 8, 20, 28, 50, 82,** and **126** [3]. It has been found that nuclei, whose number of protons or neutrons is equal to any of the magical numbers, are much more stable than the others are. They are called **magic nuclei** where one nucleon type or the other is at a magic number and **doubly magic nuclei** when both are.

times. In the same range of values of A, the energy dependence of the nuclei's lower excited states on the nuclear spin is similar to the dependence of the energy of a rotating top on its angular momentum.

On the basis of this analogy, in 1950, **A. Bohr** and **B. Mottelson** proposed the **rotational nuclear model**, which proposed to consider the nucleus as a rigid body with no spherical form and a fixed center of mass [7]. The conglomerate of individual nucleons forms a compact entity, like the top or a rugby ball. The only possible motion of such an object is rotation.

An essential feature of the rotational model is the combination of rotation of the whole nucleus as an object with the individual nucleons' motion in a non-spherical potential field. It is assumed here that the entire nucleus' rotation occurs slowly enough for the intrinsic structure to be very little perturbed by this motion.

The rotational model makes it possible to describe a number of essential properties of a large group of nuclei. In a sense, it complements the shell model (see below) since it works very well with nuclei that have a number of neutrons and protons that are far from magic numbers. However, the very appearance of a rotational spectrum (the fact of rotation of the nucleus as a whole) remains unexplained.

1.4.3. Independent particle models

A. Fermi Gas Model

The **Fermi gas model** is a semi-classical model of this group built on an analogy between the nucleus and an ideal Fermi gas [8]. According to the model, the nucleons as fermions (neutrons and protons, having spin 1/2, are fermions), following the Pauli Exclusion Principle (see Section 1.1.9), are moving freely (without interaction) within the nucleus volume. The binding potential, generated by all nuclei, is described as an infinite well of potential. The model gives accurate estimates of the mean-field potential and the average kinetic energy of the nucleons. The Fermi gas model also makes it possible to explain qualitatively why in light and middle heavy stable nuclei, the number of protons and neutrons are roughly equal ($N \approx Z$).

The application of the Fermi gas model is limited since it completely ignores the individual characteristics of the nuclei, in particular, their shell structure.

B. Shell Model

Soviet physicist **D. Ivanenko** (together with **E. Gapon**) proposed the first shell model in 1932. It was developed in 1949 in several physicists' independent works, most notably **E. P. Wigner**, **M. Mayer** and **J. H. Jensen**.

The ascertainment of the "magic numbers" of the protons and neutrons in the nuclei (2, 8, 20, 28, 50, 82, and 126) led to the idea that the nucleons in the nuclei are also distributed in shells, similar to the electrons in atoms. However, with the incredibly strong force acting between them and with so many nucleons to collide with, how can nucleons possibly complete the entire orbit without any interaction? The reason for this is [9] the Pauli Exclusion Principle (see Section 1.1.9). It prohibits energy loss since only one nuclear particle can occupy a given energy state (two fermions cannot occupy one quantum state). In densely packed nuclear matter, all low-energy states are filled; therefore, particles cannot take part in interactions that will lower their energy since no low-energy states are available to which they could go. Scattering at the expense of an external particle, which increases the energy of a nucleon, is possible, but scattering, which reduces the energy of a particle, is excluded by the Pauli principle. This is a fundamental quantum idea – if there is no available "hole" for a collision to knock a nucleon into, then the collision will not occur. (There is no classical analogue for this situation.) Therefore, the average free path of a nucleon turns out to be larger than the size of the nucleus, which makes it possible to identify individual nucleon orbits.

The model assumes nucleon distribution in the nucleus at discrete energy levels (shells) and that the nucleus is filled with nucleons (according to the Pauli Exclusion Principle) with a large energy gap between each shell. The stability of the nucleus depends on the filling of the individual shells – the nuclei with fully filled shells are the most stable. The shells for protons and neutrons are independent of each other. Therefore, one can have "magic nuclei" where one nucleon type or the other is at a magic number, and "doubly magic" nuclei where both are. Due to some variations in the orbital filling, the uppermost magic numbers are 126 and, speculatively, 184 for neutrons but only 114 for protons, which plays a role in the search for the so-called "island of stability" (see Section 1.3.6).

The shell model is based on the concept of the nucleus as a system of nucleons independently moving in a **mean potential field** of the nucleus. The field is created by the force action between all of the nucleons (self-aligned field) and keeps it bound to the nucleus. In contrast to the liquid drop model, which almost immediately appeared in its final form, the shell model has undergone a long period of searching for the optimal shape of the mean-field potential to ensure the correct values of "magic numbers" and other nuclear parameters.

There are two approaches in the attempts to define the mean-field potential.

- The **phenomenological[1] approach** is a parameterization [11] of the nuclear potential by an appropriate mathematical function. One of the first successful attempts of parametrization was by a three-dimensional harmonic oscillator [12], whose Schrödinger equation can be solved explicitly. In addition, a spin-orbit interaction [13] had to be included therein to receive the actual values of the "magic numbers" and other experimentally determined parameters.

  The most recent parameterizations are based on more realistic functions, which account for the experimental data more accurately. The realistic potentials have to include the spin-orbit interaction. This makes it possible to obtain the correct description of the energy levels with spin and parity of the states, the magic numbers of protons and neutrons in nuclei, the magnetic moments, the quadrupole moments, and others.

  In particular, excellent results are obtained by applying the Woods-Saxon potential [14], a modification of which was used for the nuclear charge distribution (see Section 1.2.10):

$$E(r) = -\frac{E_0}{\left[1 + \exp\left(\frac{r - R}{a}\right)\right]}, \tag{1.4.5}$$

  where

  E_0 (having a dimension of energy) represents the potential well depth,

  R – the nuclear radius,

  r – the distance from the center of the nucleus.

  The Woods-Saxon potential has a few important properties corresponding to the actual properties of the nuclei (Fig. 1.4.1):

  – the potential increases monotonically with the particle distance to the center of the nucleus (r), i.e. attracting;

  – for large A, it is approximately flat around the nucleus center;

  – nucleons near the surface of the nucleus experience a larger force towards the center;

[1] The **phenomenological model** [10] is a scientific model that describes the empirical relationship of phenomena to each other in a way which is consistent with fundamental theory but is not directly derived from theory. A phenomenological model foregoes any attempt to explain why the variables interact the way they do, and simply attempts to describe the relationship with the assumption that the relationship extends past the measured values.

– the potential rapidly approaches zero as r moves toward infinity, reflecting the short distance action of the strong nuclear force.

A particular disadvantage is that the Schrödinger equation, used to find the nucleons' energy levels, cannot be solved analytically and has to be treated numerically.

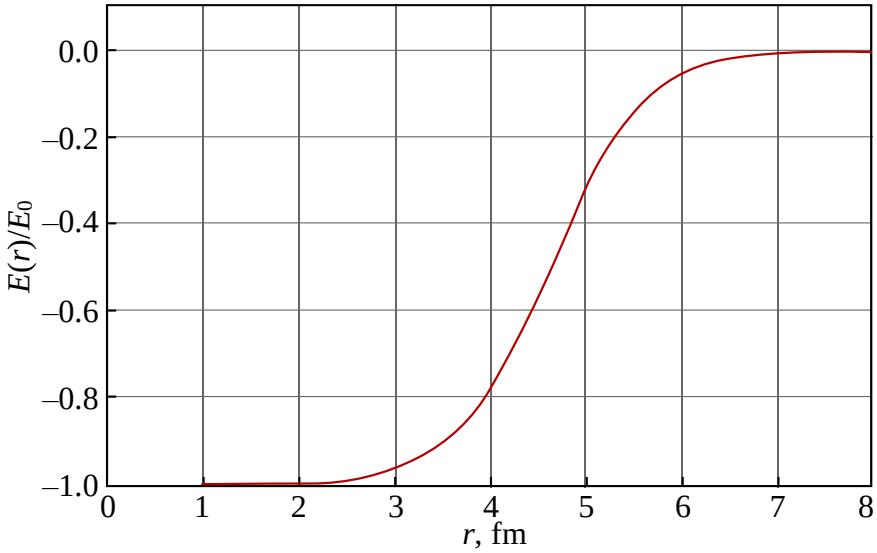

Fig. 1.4.1. Wood-Saxon potential relative to E_0 for $R \approx 4.6$ fm ($A = 50$) and $a = 0.5$ fm

- The **self-consistent approach** aims to deduce the nuclear potential mathematically from an effective nucleon-nucleon interaction. For this purpose, the so-called **Hartree-Fock** method [15] was applied. It implies a resolution of the Schrödinger equation in an iterative fashion, using the so-called **Variational method** [16]. The method consists of choosing a "trial wave function" depending on one or more parameters and finding the values of these parameters for which the expectation value of the energy is the lowest possible. This method leads to a system of equations with local (Hartree) [17] and non-local (Fock) [18] contributions to the mean-field potential.

  This approach is continuously being developed, creating new mathematical relationships that reflect the nucleus' processes more accurately.

The shell model of the nucleus explained the spins and magnetic moments of the nuclei, the different levels of stability of the atomic nuclei, as well as the periodicity of changes in their properties. This model is well applicable to the description of light and medium nuclei, as well as for nuclei that are in the ground (unexcited) state. In addition, by explaining the nature of magic numbers and correct reproduction of their values, the shell model

qualitatively describes other characteristics of odd nuclei: the spins of ground states, magnetic moments, probabilities of beta transitions and magnetic gamma transitions, etc. It plays an important role in describing the properties of deformed nuclei in which the average field is deformed (mainly quadrupole). The shell model of the nucleus and its subsequent modifications explain a wide range of experimental data on the excitation spectra of nuclei, with energies of up to 3–5 MeV. The shell structure is also manifested at higher excitation energies – up to 30–50 MeV, corresponding to the excitation of the inner shells' nucleons.

1.4.4. Other nuclear models

A. The unified nuclear model

The shell model cannot explain two experimentally found features:

- the nuclei that are very close to the "magic nuclei" have static and dynamic quadrupole moments much larger than those estimated by the shell model, and they exhibit vibrational spectra;
- for the nuclei far from the "magic nuclei", the enhancement in the quadrupole moments is very pronounced, and the nuclei in the region exhibit rotational spectra; the presence of such spectra clearly indicates that the nuclear potential is no longer spherical.

These and some other experimental results show that, besides their independent motions, the nucleons have to also participate in some collective (coherent) motions. This concept was developed by **A. Bohr** and **B. Mottelson**, who in 1953 proposed their **Unified (Collective) nuclear model** [19]. This model incorporates aspects of both the shell model and the liquid-drop model and thus can explain specific magnetic and electric properties of the nuclei that neither of the two can do separately [20].

As seen in the shell model, the nuclear energy levels are calculated on the basis of a single nucleon (proton or neutron) moving in a potential field produced by all the other nucleons. The nuclear structure and behavior are explained by considering single nucleons beyond a passive nuclear core composed of paired protons and paired neutrons that fill groups of energy levels (namely the shells). In the liquid-drop model, the nuclear structure and behavior are explained based on all the nucleons' statistical contributions (much as the molecules in spherical drops of water contribute to the overall energy and surface tension).

According to the unified model, the nucleus consists of a stable internal part – the core is formed by the filled nucleon shells and external nucleons moving in the field created by the core's nucleons. The core can change its shape according to the interaction with these external nucleons:

- When the number of external nucleons is small (as in the nuclei very close to the "magic nuclei"), the average shape of the core (as well as that of the nucleus) remains spherical, but the instantaneous shape is not – the shape vibrates. This process explains why the corresponding nuclei have varied and closely layered energy levels.
- When the number of external nucleons is larger, they strongly deform the core, and it becomes non-spherical – an elongated or oblate ellipsoid. The deformed nucleus can rotate (around the axis, perpendicular to the deformation axis), which explains the experimentally observed rotational energy levels of these nuclei.

What can be observed in this model is, in a sense, a further development of the Vibrational and Rotational models described in Section 1.4.2.

The increase in nuclear deformation that occurs with the increase in the number of unpaired nucleons accounts for the measured electric quadrupole moments, which may be considered a measure of how much the distribution of electric charges in the nucleus deviates from spherical symmetry.

The unified model led to the introduction of the concept of single-particle (related to the excitation of external nucleons) and collective (rotational and vibrational, associated with the excitation of the core) energy levels of the nucleus and the ascertainment of their values, spin, parity, etc.

B. The pair correlation model

The unified model encountered difficulties explaining the experimental data, especially in those nuclei in which several nucleons move outside the core. The natural way to improve the generalized model is to take into account their interaction. This interaction is significantly different from the interaction between a pair of free nucleons and is called a residual interaction: only a part of the nucleon-nucleon force that remains after the separation of the self-consistent field (the shell model excludes the residual interaction). The residual interaction leads to the fact that the motion of the external nucleons in the field of the core is no longer independent but correlated. The corresponding modifications of the shell model are called models of pair correlations, the most well-known of which is the superfluidity nuclear model. It was developed by **N.N. Bogolyubov**, **A. Bor**, **B. Mottelson**, and **D. Pines**, and was presented in 1958 [21]. The basis of this model is the assumption that pairs of protons and neutrons with equal and opposite angular momenta form a type of bound state in the nucleus. In order to break this bond (to separate one pair), it is necessary to expend energy of up to 1–2 MeV. Therefore, the excitation energy of the even-even nuclei, in which all nucleons form coupled pairs, should be 2 MeV. In contrast, the neighboring odd nuclei should have an excitation energy level of about 10 times less (150–

200 keV), which is actually observed in the experiment. With the help of the models of pair correlations, it is possible to clearly describe the spins and the quadrupole moments of the nuclei's ground states, as well as the energies, spins, quadrupole moments, and transition probabilities of excited one-nucleon and collective (rotational and vibrational) nuclei states of up to 3–6 MeV. The model clearly describes the density of the energy levels and the properties of neutron resonances, which allows one to calculate the equilibrium deformations of nuclei both in the ground and in the excited state.

The nuclear models examined here are basic, covering the properties of most nuclei. However, they are not able to describe many properties of different nuclei observed experimentally. For e. g., as is proved strongly by Jaminon et al.[22], the Hartree-Fock method is generally unable to correctly describe two basic nuclear characteristics simultaneously, namely the density and momentum distributions. The main reason for this is that its ground state nuclear wave function includes Pauli correlations but does not account for the important part of the short-range, tensor, and other nucleon-nucleon correlations that are related to peculiarities of the nucleon-nucleon force at short distances (the repulsive force at $r \sim 0.4$ fm, the non-central character of the nucleon-nucleon force, etc.). All of this led to the development of different **theoretical correlation methods**: the Brueckner theory [23], exp(S) –method (or coupled-cluster many-body theory) [24], the Jastrow method [25] and its extensions, the generator coordinate method [26], the coherent density fluctuation model [27], the natural orbital method [28, 29], and others. (A detailed review of the correlation methods and the correlation effects on the nuclear structure and reactions can be found in [27]).

1.4.5. Tendency of modern nuclear theory development

The development of nuclear theory is closely related to nuclear physics experiments. On the one hand, the theory seeks to explain the experimental results obtained. On the other hand, the created models predict new possible properties in nuclei whose experimental confirmation or rejection directs the next steps of the theory.

Nowadays, the search for a consistent explanation of nuclei's most essential properties with a solid basis of general physical principles and experimental data continues non-stop. Primary efforts aim to comprehensively analyze and clarify the determinant role of quarks and their interactions over the properties of the nuclei. For example, it was recently experimentally found [29] that the two-nucleon pairs (mentioned above in 1.4.4.B) are far more reliant on the interactions between their quarks than between the whole nucleons.

Other modern research directions include investigating the so-called **exotic nuclei** with their increased sizes that deviate substantially from the $R \sim A^{1/3}$

rule; and studying the interaction between neutrinos and nuclei, which are expected to reveal new properties and regularities of the nuclei.

References

[1] *Heyde, K.* Basic Ideas and Concepts in Nuclear Physics, 2 edn. Institute of Physics Publishing, Bristol and Philadelphia, 1999.

[2] *Bohr, N., F. Kalckar.* On the Transmutation of Atomic Nuclei by Impact of Material Particles, Part I: General Theoretical Remarks. Mat.-Fys. Medd. Dan. Vidensk, Selsk. **14**, 1937, p.p. 10-40.

[3] *Von Weizsäcker, C. F. Zu*r. Theorie der Kernmassen. Zeitschrift für Physis (in German), **96**, 7–8, 1935, p.p. 431–458.

[4] Magic number. https://en.wikipedia.org/wiki/Magic_number_(physics)

[5] *Beckman, I. N.* Models of the atomic nucleus structure. (In Russian). https://studfiles.net/preview/4049740/

[6] *Rowe, D. J.* Nuclear Collective Motion. Models and Theory. Methuen and Co. Ltd., 1970. Part 1, Ch. 2. p. 16. http://wwwucjf.troja.mff.cuni.cz/~knapp/work/Rowe/02-%20The%20collective%20vibrational%20model.pdf

[7] Rotational model. https://www.kth.se/social/upload/5176d9b0f276543c2c2bd4db/CH5.pdf

[8] Fermi gas model. (Introduction to Nuclear Science). Simon Fraser University, 2011. https://web-docs.gsi.de/~wolle/TELEKOLLEG/KERN/LECTURE/Fraser/L10.pdf

[9] Shell model of nucleus. http://hyperphysics.phy-astr.gsu.edu/hbase/Nuclear/shell.html

[10] Phenomenological model. https://en.wikipedia.org/wiki/Phenomenological_model

[11] Parametrization. https://en.wikipedia.org/wiki/Parametrization

[12] Quantum harmonic oscilator. https://en.wikipedia.org/wiki/Quantum_harmonic_oscillator#Example:_3D_isotropi

[13] Orbite interaction. https://en.wikipedia.org/wiki/Spin%E2%80%93orbit_interaction

[14] Wood-Saxon potential. https://en.wikipedia.org/wiki/Woods–Saxon_potential

[15] Hartree-Fock method. https://en.wikipedia.org/wiki/Hartree–Fock_method

[16] Variational method. https://en.wikipedia.org/wiki/Variational_method_(quantum_mechanics)

[17] *Hartree, D. R.* The wave mechanics of an atom with a non-Coulomb central field. Proc. Camb. Phil. Soc. **24**, 1928, p.p. 89-110. https://elib.bsu.by/bitstream/123456789/154382/1/1928-024%20PCPS%20Hartree%20-%20The%20wave%20mechanics%20of%20an%20atom%20with%20a%20non-Coulomb%20central%20field%201.pdf

[18] *Fock, V. A.* Näherungsmethode zur Lösung des quantenmechanischen Mehrkörper Problems. Zeitschr. Phys. **61**, 1930, p. 126. https://link.springer.com/article/10.1007/BF01340294

[19] *Bohr, A., B. R. Mottelson*. Collective nuclear motion and the unified model. http://cds.cern.ch/record/212241/files/cern-55-07.pdf

[20] [Collective model. https://www.britannica.com/science/collective-model

[21] *Bohr, A., B. R. Mottelson, D. Pines*. Possible analogy between the excitation spectra of nuclei and those of the superconducting metallic state. Phys. Rev. **110**, 1958, p. 936. https://journals.aps.org/pr/abstract/10.1103/PhysRev.110.936

[22] *Jaminon, M., C. Mahaux, H. Ngo*. Inability of any Hartree-Fock approximation to reproduce simultaneously the density and momentum distribution of nuclei. Phys. Lett. **158B**, 1985, p. 103. https://www.sciencedirect.com/science/article/abs/pii/0370269385913723

[23] *Brueckner, K. A., R. J. Eden, N.C. Francis*. High-energy reactions and the evidence for correlations in the nuclear ground state wave

function. Phys. Rev. **98**, 1955, p. 1445. https://journals.aps.org/pr/abstract/10.1103/PhysRev.98.1445

[24] *Zabolitzky, J. G., W. Ey*. Momentum distributions of nucleons in nuclei. Phys. Lett. **76B**, 1978, p. 527 (and references therein). https://www.sciencedirect.com/science/article/abs/pii/0370269378908468

[25] *Jastrow, R*. Many-body problem with strong forces. Phys. Rev. **98**, 1955, p. 1479. https://journals.aps.org/pr/abstract/10.1103/PhysRev.98.1479

[26] *J. J. Griffin, J. A. Wheeler.* Collective motions in nuclei by the method of generator coordinates. Phys. Rev. **108,** 1957, p. 311. https://journals.aps.org/pr/abstract/10.1103/PhysRev.108.311

[27] *Antonov, N., P. E. Hodgson, I. Zh. Petkov*. Nucleon Correlations in Nuclei. Springer-Verlag, Berlin, Heidelberg, New York, 1993. Nucleon Momentum and Density Distributions in Nuclei. Clarendon Press, Oxford, 1988.

[28] *Löwdin, P. O.* Quantum theory of many-particle systems, Part 1. Phys. Rev. **97**, 1955, p. 1474. https://journals.aps.org/pr/abstract/10.1103/PhysRev.97.1474

[29] *Hen, O., G. A. Miller, E. Piasetzky, L.B. Weinstein*. Nucleon-nucleon correlations, short-lived excitations, and the quarks within. 2017. https://arxiv.org/pdf/1611.09748.pdf

PART 2. RADIOACTIVE DECAY

2.0. Introduction

As is mentioned in Section 1.3, a relatively small part of all nuclei are stable, i.e. they remain unchanged indefinitely. The others are unstable, generally because they possess an excess of internal energy. **Radioactive decay**, or **radioactivity**, is the process by which the nucleus of an unstable atom loses energy either by emitting radiation – alpha particle, beta particle, gamma-ray – or by fission and fusion. The term **decay** is used to show that, during this process, the quantity of the initially unstable isotopes decreases because it is most often converted into another isotope by emitting radiation. Any material that spontaneously emits such radiation is considered **radioactive**.

These emissions are collectively called **ionizing radiation** since the result of their interactions with matter is its ionization (see Part 4).

Henry Becquerel

Marie Curie

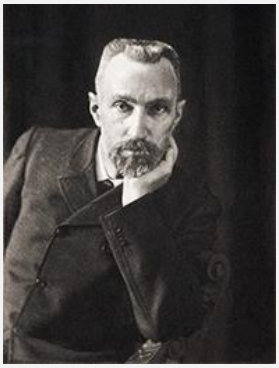

Pierre Curie

Firstly, radioactivity can be observed in natural heavy elements like uranium, thorium and radium. French physicist **Henry Becquerel** discovered this in 1896 [1] by observing that a phosphorescent uranium salt caused a photo plate to blacken. Two years later, in 1898, **Marie** and **Pierre Curie** isolated the first natural radioactive elements – polonium and radium [2]. Later, many lighter, naturally radioactive isotopes were found – potassium-40 ($^{40}_{19}\mathrm{K}$), rubidium-87 ($^{87}_{37}\mathrm{Rb}$), samarium-157 ($^{157}_{62}\mathrm{Sm}$), etc. [3]. Now, besides natural radioactive isotopes, a large number of so-called **synthetic radioactive isotopes** are being produced as the result of the irradiation of stable isotopes with different radiations – protons, neutrons and others [4, 5].

The basic characteristics of the different types of radiation will be described in this part.

References

[1] Henri Becquerel – Biography, Facts and Pictures. http://science-story-telling.eu/files/Biographies/Biographoy_Becquerel_ENG.pdf

[2] The Discovery of the Radioactivity. http://www2.lbl.gov/abc/wallchart/chapters/03/4.html

[3] Radioactivity in Nature. http://www2.lbl.gov/abc/wallchart/chapters/03/5.html

[4] Manual for Reactor produced Isotopes. IAEA, Wien. https://www-pub.iaea.org/books/IAEABooks/6407/Manual-for-Reactor-Produced-Radioisotopes

[5] Cyclotron Produced Radionuclides: Physical Characteristics and Production Methods. IAEA, Wien. https://www-pub.iaea.org/books/iaeabooks/7892/Cyclotron-Produced-Radionuclides-Physical-Characteristics-and-Production-Methods

2.1. Alpha decay

2.1.1. Alpha particles

Alpha decay (**α-decay**) is a radioactive process in which a particle consisting of two neutrons and two protons, called an **alpha particle**, is ejected from a radioactive atom's nucleus (see the animation). The alpha particle is identical to the nucleus of a helium atom, and its protons and neutrons are held together by a powerful nuclear force. The charge of a single alpha particle is $+2e$ due to the fact that it does not contain electrons.

QR Alpha decay

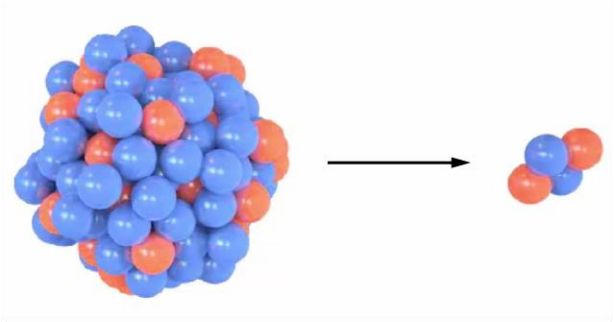

SCAN ME

Ernest Rutherford first described alpha particles in 1899 during his investigations of radioactivity [1]. In 1907, they were identified as helium nuclei. In 1928, the Russian-American physicist George Gamow proposed the theory of alpha decay via tunneling [2, 3].

2.1.2. Alpha decay mechanism

The fundamental reason for the alpha decay is the short range of the nuclear force – about 1 fm (see Section 1.3.1). Thus, the strength of the nuclear force, which keeps the nucleus together, is proportional to the number of its nucleons (i.e. to its mass number). At the same time, the total repulsive electromagnetic force, which is trying to break the nucleus apart, is roughly proportional to the square of its atomic number. For this reason, a large nucleus (with $Z > 50$ and $A > 105$) will become unstable – the repulsive electromagnetic force exceeds the nuclear force, and alpha decay occurs as a means of increasing the nucleus' stability by reducing its size.

One important question is why this nucleus stabilization is done by ejecting namely an alpha particle and not a single proton, neutron, or a lighter nucleus. Part of the reason is the very high binding energy of the alpha particle itself.

The other part comes from the balance of energies. We can use the Law of Conservation of Energy to write an equation for disintegration energy:

$$m_{par}c^2 = (m_d + m_\alpha)c^2 + Q, \quad (2.1.1)$$

or

$$Q = (m_{par} - m_d - m_\alpha)c^2, \quad (2.1.2)$$

where

Q is the disintegration energy (so-called Q-value – total energy released),

m_{par} – the mass of the parent nucleus,

m_d – the mass of the daughter nucleus,

m_α – the mass of the alpha particle.

The calculations show that alpha particle emission will usually be possible ($Q > 0$) with just the parent nucleus' energy, while other decay modes will require additional energy.

For example, alpha particle emission from uranium-232 would need only 5.4 MeV, while a single proton emission would require 6.1 MeV.

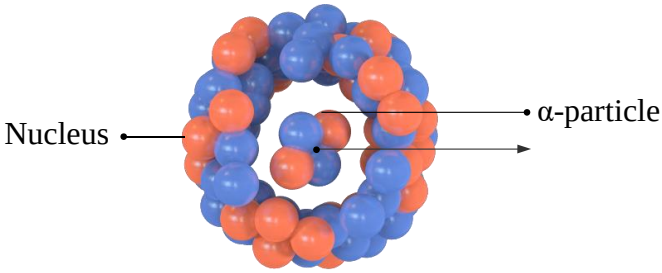

Fig. 2.1.1. Alpha particle ejection

However, these disintegration energies are substantially smaller than the potential barrier provided by the nuclear force, which prevents the alpha particle from escaping. The energy needed is generally in the range of about 25 MeV, while the real disintegration energy varies between 4 and 9 MeV. In classic physics, alpha particles could not escape from the nucleus. However, the quantum tunneling effect allows them to escape even though they do not have enough energy to overcome the nuclear force (Fig. 2.1.1). This is possible because of the wave nature of matter, which allows the alpha particle to spend some of its time in a region so far from the nucleus centrum that the repulsive electromagnetic force fully compensates for the attraction of the nuclear force. From this point, alpha particles can escape, and in quantum mechanics, after a certain time, they do so.

This mechanism of alpha decay explains the very long half-life of some radioactive isotopes, like uranium-238 ($^{238}_{92}$U), with, for example, $T_{1/2} = 4.5 \times 10^{21}$ years: escaping through the potential barrier by tunneling is

a random and relatively rare process depending on the individual characteristics of the isotope's nuclei.

2.1.3. Alpha particles' energy

Most of the disintegration energy becomes kinetic energy of the alpha particle itself, but to preserve the Law of the Conservation of Momentum, part of this energy determines the recoil of the nucleus. However, since the mass numbers of most alpha-emitting radioisotopes exceed 210, which is far greater than the mass number of the alpha particle (Z_α = 4), this difference is generally relatively small. For this reason, the emmited alpha particles have almost **equal** amounts of **energy**, i.e. the alpha radiation is, in practice, **mono-energetic**. The corresponding distribution of energy (called energy spectra) for four isotopes (polonium-209 and 210, plutonium-239 and americium-241) are shown in Fig. 2.1.2.

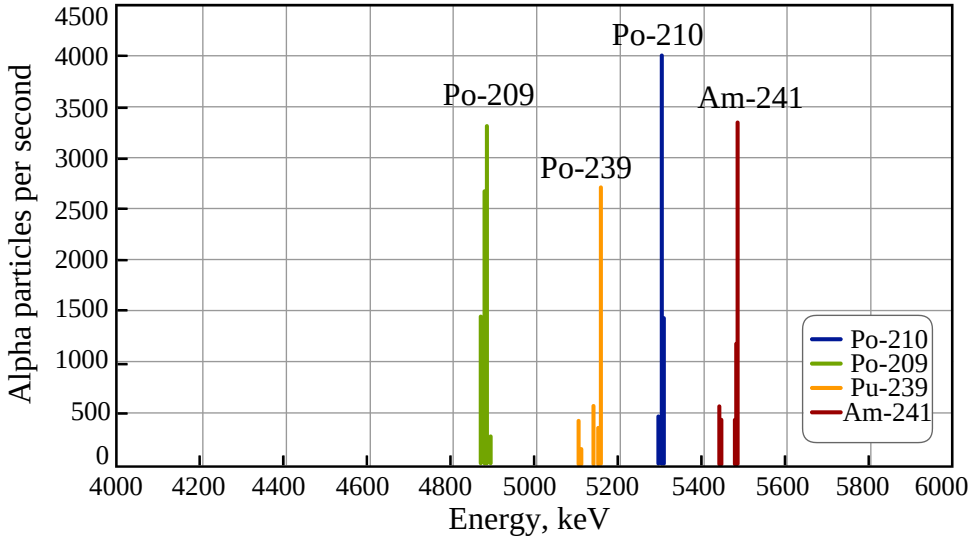

Fig. 2.1.2. Examples of the alpha particle energy spectra

As can be seen, plutonium and americium, besides alpha particles with definite energies, also emit particles with slightly different energies. This is due to the fact that certain nuclei have numerous energy states, and their *Q*-value depends on particular states of the parent and daughter nuclei, between which an alpha decay takes place. After the decay, the nuclei are not in their basic states and the remaining energy is usually emitted by a gamma quantum (see Section 2.3).

The alpha particles have relatively high energy – 3-7 MeV, with higher energy alpha particles being emitted from the larger nuclei. Nevertheless, their speed is lower because of their high mass: with a typical kinetic energy of 5 MeV, alpha particles are easily absorbed by other materials (see

Section 4.2). For example, they can pass only a few centimeters in the air or be stopped by a thick sheet of paper.

2.1.4. General form (generic equation) of alpha decay

When a less stable element transforms into a more stable one due to alpha decay, the new (daughter) isotope's atomic number will be decreased by two units and its mass number by four. However, the sum of the protons, as well as of the neutrons of the new products (daughter nucleus and alpha particle), remain equal to those of the parent nucleus:

$$ {}^{A}_{Z}\mathrm{X} \rightarrow {}^{A-4}_{Z-2}\mathrm{X}' + {}^{4}_{2}\alpha, \qquad (2.1.3) $$

where

X is the parent nucleus (less stable),

X′ – the daughter nucleus (more stable),

α – the alpha particle (helium nucleus).

As an example, consider polonium-210 – ${}^{210}_{84}\mathrm{Po}$ (the first radioactive isotope discovered by **Maria** and **Pierre Curie** in 1898). Inside this nucleus, there are 84 protons and 126 neutrons. After the emission of an alpha particle, the daughter nucleus will have 82 protons and 124 neutrons, which corresponds to a stable isotope of lead – lead-206 (${}^{206}_{82}\mathrm{Pb}$).

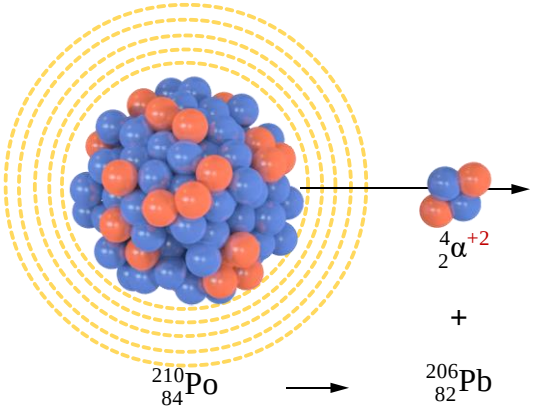

Fig. 2.1.3. Alpha-decay of polonium-210

In this example, the parent radioactive isotope, emitting the alpha particle, is converted directly into a stable isotope. However, most often in nature, the radioactive process is a series of successive alpha and beta decays (see Section 2.2), ending with a stable isotope. As an example, here one can see the decay chain of thorium-232, which is a primordial radioisotope:

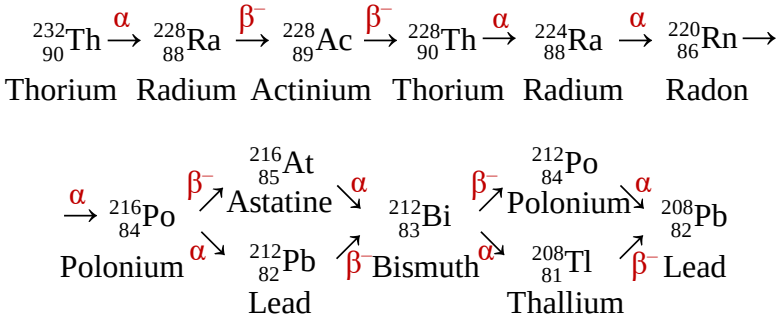

Fig. 2.1.4. Decay chain of thorium-232

References

[1] Ernest Rutherford. Biographical. https://www.nobelprize.org/prizes/chemistry/1908/rutherford/biographical/

[2] *Gamow, G.* Zur Quantentheorie des Atomkernes. (On the quantum theory of the atomic nucleus). Zeitschrift für Physik, **51**, 3, 1928, p.p. 204–212.

[3] Gamow theory of alpha decay. https://web.archive.org/web/20090224200050/http://www.phy.uct.ac.za/courses/phy300w/np/ch1/node38.html

2.2. Beta decay

2.2.1. Beta particles

Beta-decay (**β-decay**) is a radioactive process in which an **electron** or **positron** is emitted from the nucleus of a radioactive atom, along with an unusual particle called an **electron antineutrino** $\bar{\nu}_e$ or **electron neutrino** ν_e, respectively (see the animation). The neutrino and antineutrino are almost massless particles that carry away some of the decay process energy.

QR Beta minus decay

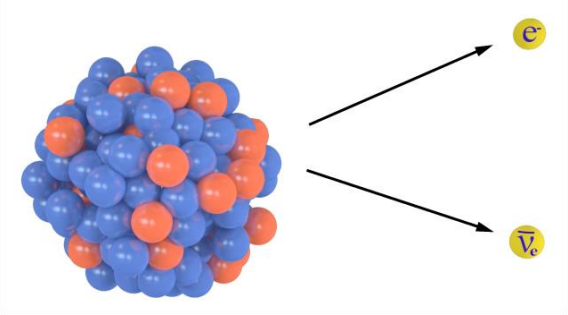

SCAN ME

Soon after the discovery of radioactivity in 1899, **Rutherford** [1, 2] separated radioactive emissions into two types: alpha and beta (now beta minus). This division is based on the difference in their penetration ability: a thick sheet of paper could stop alpha particles, while beta emissions could penetrate several millimeters of aluminum. A few months later, **Becquerel** measured the mass-to-charge ratio for beta particles and found that it is the same for the electron [2, 3]. Therefore, he suggested that the beta particle is, in fact, an electron. Nevertheless, the name **beta particle** remains to distinguish it from the electrons, which orbit the atom.

2.2.2. Beta particles' energy

Further study of beta emission has found a strange phenomenon: while the energy of alpha particles has a narrow distribution (see Fig. 2.1.2)), the energy spectrum of beta particles is continuous – the nuclei emit beta particles with different energies, from 0 to a maximum value (E_{max}, Fig. 2.2.1) [4].

This fact seemingly contradicted the Law of Energy Conservation since, at each beta decay, the nucleus loses a fixed amount of energy, corresponding to the maximum value in the beta spectrum. Only in 1930, after many speculations, did **Wolfgang Pauli** [5] suppose that, in addition to the electron, a second particle is being ejected by the nucleus, which carries the rest of the energy. In 1931, **Enrico Fermi** named it the **neutrino** and proposed the beta

decay theory in 1934 [6, 7]. However, neutrino interaction with matter was so weak that detecting it proved a severe experimental challenge. Neutrinos were finally detected in 1956 by **Cl. Cowan** and **Fr. Reines**, who had indirectly measured the antineutrinos created in a nuclear reactor by beta-decay [7].

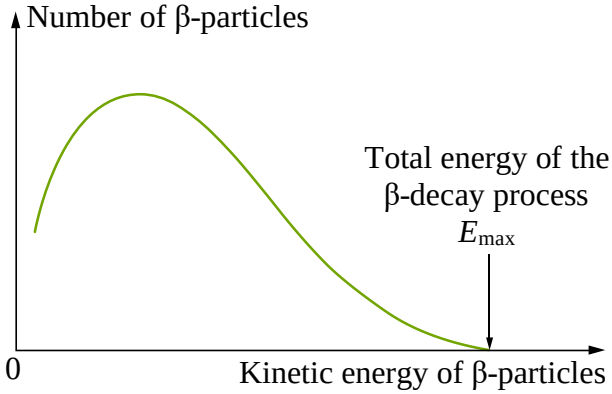

Fig. 2.2.1. Typical beta particle's energy spectrum

2.2.3. Beta-decay mechanism

There are two types of beta decay, known as **beta minus** and **beta plus**. In beta minus (β^-) decay, a neutron is transmuted into a proton in the nucleus, and an electron is emitted together with an electron antineutrino. In beta plus (β^+) decay, a proton converts into a neutron, and the process creates a positron and an electron neutrino.

The reason for both processes is the instability of the nucleus. Generally, unstable nuclei are of two types: neutron-rich and proton-rich (see Section 1.3.6). In the nucleus of the first type, when the number of neutrons significantly exceeds the number of protons ($A/Z > 5$), the quantity of exchanged virtual mesons between the nucleons (see Section 1.3.1) is not sufficient to support the stability of all neutrons. As a result, one neutron decays and the newly created electron is emitted outside the nucleus together with an electron antineutrino:

$$n \rightarrow p^+ + e^- + \bar{\nu}_e. \qquad (2.2.1)$$

With the new proton, the rate A/Z of the nucleus decreases and the stability increases. A typical example is the nucleus of hydrogen: its nucleus consists of only one proton ($A = Z = 1$); if a neutron is added, it results in the isotope hydrogen-2 ($^2_1$H), called deuterium ($^2_1$D), which is also stable; if another neutron is added to the same nucleus, the new isotope hydrogen-3 ($^3_1$H), also called tritium ($^3_1$T), is created, which is radioactive; through a β^- decay it

transforms into helium-3 ($^3_2$He), whose nucleus consists of 2 protons and 1 neutron and is stable.

The reason for the instability of the proton-rich nuclei is the higher rate of protons in comparison to neutrons. Then the repulsive electromagnetic force becomes too large and cannot be countered by the nuclear force. The result is a β^+ decay during which a proton transmutes into a neutron, and a positron (e^+) together with an electron neutrino are emitted from the nucleus:

$$p^+ = n + e^+ + \nu_e \tag{2.2.2}$$

Thus, the number of protons decreases and the stability of the nucleus increases.

2.2.4. Generic equations of beta decay

- In **β^- decay**, where a neutron is converted into a proton, the mass number *A* remains constant, but the number of protons increases by 1. As a result, the initial isotope with an atomic number *Z* is transformed into an isotope of another chemical element with atomic number *Z* + 1:

$$^A_Z\mathrm{X} \xrightarrow{\beta^-} {}^A_{Z+1}\mathrm{X}' + e^- + \bar{\nu}_e. \tag{2.2.3}$$

  A typical example is the beta decay of cobalt-60, which is transformed into nickel-60:

$$^{60}_{27}\mathrm{Co} \xrightarrow{\beta^-} {}^{60}_{28}\mathrm{Ni} + e^- + \bar{\nu}_e. \tag{2.2.4}$$

- In **β^+ decay**, conversely, a proton is transformed into a neutron and the atomic number *Z* decreases by 1, while the mass number *A* remains unchanged:

$$^A_Z\mathrm{X} \xrightarrow{\beta^+} {}^A_{Z-1}\mathrm{X}' + e^+ + \nu_e. \tag{2.2.5}$$

  In this manner, for example, the isotope sodium-22 decays and transforms into neon-22:

$$^{22}_{11}\mathrm{Na} \xrightarrow{\beta^+} {}^{22}_{10}\mathrm{Ne} + e^+ + \nu_e. \tag{2.2.6}$$

- Another process is observed in proton-rich nuclei that also refers to beta radioactive decay – the so-called **electron capture**. This is a process during which a nucleus captures one of its atomic electrons, and one proton transforms into a neutron, resulting in the emission of an electron neutrino:

$$^A_Z\mathrm{X} + e^+ \rightarrow {}^A_{Z-1}\mathrm{X}' + \nu_e. \tag{2.2.7}$$

If the captured electron comes from the innermost shell of the atom – the K-shell, which has the highest probability to interact with the nucleus – the process is called K-capture. If it comes from the L-shell, the process is called L-capture, etc.

An example of K-capture is the decay of potassium-40, by which it transforms into argon-40:

$$^{40}_{19}\mathrm{K} + e^{+} \rightarrow {}^{40}_{18}\mathrm{Ar} + \nu_e. \tag{2.2.8}$$

2.2.5. Energy relations of beta decay

The *Q*-value (the total energy released) for beta decay is the sum of the kinetic energies of the emitted beta particle, neutrino and recoiling nucleus. Because of the large mass of the nucleus compared to that of the beta particle and neutrino, the kinetic energy of the recoiling nucleus is insignificant and can therefore be overlooked. Thus, the total energy is distributed randomly between the beta particle and the corresponding neutrino. Beta particles can therefore be emitted with any amount of kinetic energy ranging from 0 to *Q*. The typical values of *Q* are around 1 MeV, but they can range from a few keV to a few tens of MeV [2]. Since the rest mass of the beta particles is too small (511 keV/c^2), the most energetic ones are ultra-relativistic – with speeds very close to the speed of light.

- **β^- decay**

  Following the generic equation for this decay, we can write:

$$Q = [m_N({}^{A}_{Z}\mathrm{X}) - m_N({}^{A}_{Z+1}\mathrm{X}') - m_\mathrm{e} - m_{\bar{\nu}_e}]c^2, \tag{2.2.9}$$

  where

  $m_N({}^{A}_{Z}\mathrm{X})$ is the mass of the nucleus of the ${}^{A}_{Z}\mathrm{X}$ atom,

  $m_N({}^{A}_{Z+1}\mathrm{X}')$ – the mass of the nucleus of the ${}^{A}_{Z+1}\mathrm{X}'$ atom,

  m_e – the mass of the electron,

  $m_{\bar{\nu}_e}$ – the mass of the electron antineutrino.

  In other words, the total energy released is the mass energy of the initial nucleus, minus the mass energy of the final nucleus, electron and antineutrino. The mass of each nucleus m_N is related to the standard atomic mass *m* by

$$m({}^{A}_{Z}\mathrm{X})c^2 = m_N({}^{A}_{Z}\mathrm{X})c^2 + Zm_e c^2 - \sum_{i=1}^{Z} E_{B_i}. \tag{2.2.10}$$

  And that of each nucleus m_{N+1} is related to its standard atomic mass by

$$m({}_{Z+1}^{A}\mathrm{X})c^2 = m_N({}_{Z+1}^{A}\mathrm{X})c^2 + (Z+1)m_e c^2 - \sum_{i=1}^{Z+1} E_{B_i}. \qquad (2.2.10a)$$

That is, the energy corresponding to the standard atomic mass is equal to the nucleus energy, plus the energy of the atomic electrons, minus the sum of the binding energy E_{B_i} of each electron. Determining $m_N({}_{Z}^{A}\mathrm{X})$ and $m_N({}_{Z+1}^{A}\mathrm{X}')$ from these two equations and substituting them into (2.2.9), we obtain

$$Q = m({}_{Z}^{A}\mathrm{X})c^2 - Zm_e c^2 + \sum_{i=1}^{Z} E_{B_i} - [m({}_{Z+1}^{A}\mathrm{X})c^2 -$$

$$- (Z+1)m_e c^2 + \sum_{i=1}^{Z+1} E_{B_i}] - m_e c^2 - m_{\bar{\nu}_e} c^2.$$

The nearly-zero antineutrino mass and the difference between both the sum of the electron binding energies, which is very small for high-Z atoms, can be ignored in this equation. Then the final results are

$$Q \approx [m({}_{Z}^{A}\mathrm{X}) - m({}_{Z+1}^{A}\mathrm{X}')]c^2. \qquad (2.2.11)$$

(because the sum of all electron masses is zero: $-Zm_e + (Z+1)\,m_e - m_e = 0$).

This energy is carried away as kinetic energy by the electron and antineutrino.

Because the reaction will proceed only when the Q is positive, β^- decay can occur when the mass of the parent atom is greater than the mass of the daughter one. For example, the mass of cobalt-60 (the parent isotope) is 59.934 u, while the mass of nickel-60 (the daughter isotope) is 59.931u.

- **β^+ decay**

The calculation of the Q-value, in this case, is similar:

$$Q = [m_N({}_{Z}^{A}\mathrm{X}) - m_N({}_{Z-1}^{A}\mathrm{X}') - m_e - m_{\nu_e}]c^2,$$

taking into account that the mass of the positron is equal to that of the electron ($m_p = m_e$), and an electron neutrino (m_{ν_e}) is emitted instead of an antineutrino.

However, now equation 2.2.10a is replaced by

$$m({}_{Z-1}^{A}\mathrm{X})c^2 = m_N({}_{Z-1}^{A}\mathrm{X})c^2 + (Z-1)m_e c^2 - \sum_{i=1}^{Z-1} E_{B_i}. \qquad (2.2.10b)$$

Therefore the result is

$$Q \approx [m(^{A}_{Z}\mathrm{X}) - m(_{Z-1}{}^{A}\mathrm{X}') - 2m_e]c^2 \qquad (2.2.12)$$

(because the sum of all electron masses is $-2m_e$). As can be seen, the total released energy has decreased by $2m_ec^2$ in this case. Because the reaction will proceed only when the Q is positive, β^+ decay can occur when the parent atom's mass exceeds that of the daughter's by at least twice the mass of the electron. In the example above (see Eq. 2.2.6), the mass of sodium-22 is 21.9944 u, and that of neon-22 is 21.2213 u, while m_e = $5.4858 \cdot 10^{-4}$ u.

- **Electron capture**

  The analogous calculation for electron capture must take into account the binding energy of the electrons. This is because the atom will be left in an excited state after capturing the electron, and the binding energy of the innermost captured electron is significant. Using the generic equation for electron capture, we obtain

$$Q = [m_N(^{A}_{Z}\mathrm{X}) + m_e - m_N(_{Z-1}{}^{A}\mathrm{X}') - m_{\nu_e}]c^2. \qquad (2.2.13)$$

  In the same way, it can be simplified to

$$Q = [m(^{A}_{Z}\mathrm{X}) - m(_{Z-1}{}^{A}\mathrm{X}')]c^2 - E_{be}, \qquad (2.2.14)$$

  where E_{be} is the binding energy of the captured electron.

  Because the electron's binding energy is much less than its own energy (m_ec^2), nuclei that can undergo β^+ decay can always undergo an electron capture too, but the reverse is not true.

References

[1] Ernest Rutherford. Biographical. https://www.nobelprize.org/prizes/chemistry/1908/rutherford/biographical/

[2] Beta decay. https://en.wikipedia.org/wiki/Beta_decay#Discovery_and_initial_ characterization

[3] Henri Becquerel – Biography, Facts and Pictures. https://www.famousscientists.org/henri-becquerel/

[4] Chadwick, J. "Intensitätsverteilung im magnetischen Spektren der β-Strahlen von Radium B + C". Verhandlungen der

Deutschen Physikalischen Gesellschaft (in German). **16,** 1914, 383–391.

[5] Wolfgang Pauli. https://en.wikipedia.org/wiki/Wolfgang_Pauli

[6] *Fermi, E. Versuch einer Theorie der β-Strahlen I.* Zeitschrift für Physik A, ***88,*** *3–4, 1934, p.p. 161–177.*

[7] Neutrino. https://en.wikipedia.org/wiki/Neutrino#

2.3. Gamma decay

2.3.1. Gamma radiation

Gamma decay (γ-decay) is a process in which an excited nucleus emits a pulse of electromagnetic radiation called a **gamma-ray**, thereby releasing its excess energy (see the animation). Gamma rays (or **gamma radiation**) consist of **photons** and are identical in nature to light or micro waves but of very high frequency and energy.

QR Gamma decay

gamma ray (γ)

SCAN ME

A French scientist, **Paul Villard** [1], discovered gamma radiation in the year 1900 while studying the radiation emitted from radium. He found that this radiation had a very high penetrating power. Sometime later, gamma radiation was recognized as being of a type fundamentally different from alpha and beta particles. In 1903, **Ernest Rutherford** named it "**gamma**" by analogy with the alpha and beta rays that he had differentiated in 1899. (The order of the Greek letters corresponds to their penetrating power – alpha being the lowest).

Gamma rays typically have frequencies above 10 exahertz (1 exahertz = 10^{18} Hz), and therefore have energies above 100 keV and wavelengths less than 10 picometers (10^{-11} m), which is less than the diameter of an atom. Their frequency range overlaps with that of the X-ray. Therefore, the term "gamma rays" is generally used for photons emitted by atomic nuclei, while electrons outside the nuclei emit X-rays. They differ in terms of their energy – in contrast to orbital electron transitions, which generally release photons of low energy (about 1 eV), nuclei tend to release photons of very high energy (keV –MeV).

2.3.2. Gamma decay mechanism

As is known, a quantum mechanical system of bound particles can only take on certain discrete values of energy, called **energy levels**. Most famous are

the energy levels of the orbital electrons in atoms, which are bound by the electric field of the nucleus. Still, they are also typical for the nuclei as a system of nucleons that are bound by nuclear force (see Section 1.4.3).

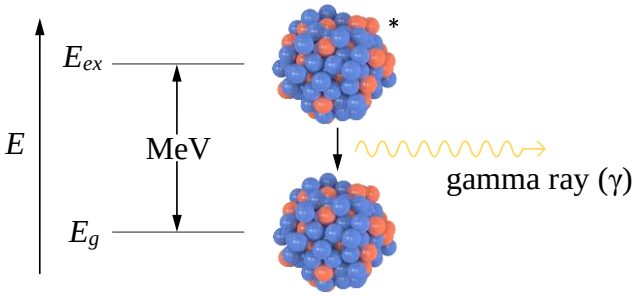

Fig. 2.3.1. Gamma transitions in the nucleus

Each nucleus has a stable energy level, known as the **ground level** (E_g, Fig. 2.3.1), and one or more states with higher energies (E_{ex}) corresponding to its **excited states**. When a nucleus has been excited, it passes to a lower energy level due to gamma decay, i.e. emitting gamma quantum.

Most often, the nucleus remains in an excited state after an alpha or beta decay. Then it can go to the ground state directly by only one gamma decay or by a few decays, passing through lower energy levels. The process is typical for each different isotope and depends on its specific structure.

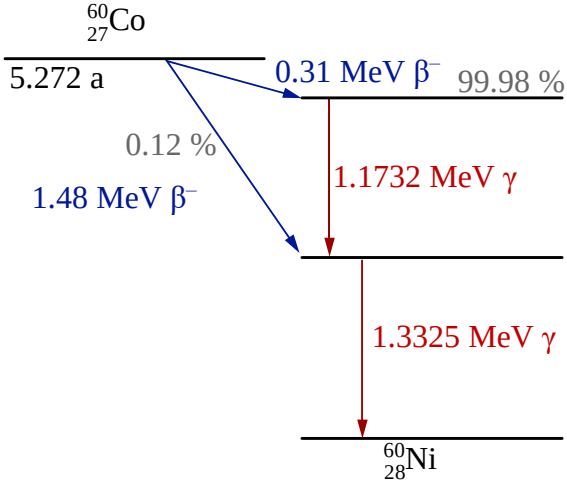

Fig. 2.3.2. Gamma decay of cobalt-60

As an example, the radioactive decay of the isotope cobalt-60 is shown in Fig. 2.3.2: 99.88 % of the parent nuclei $^{60}_{27}$Co first undergoes a β^--decay in which a decrease of 0.31 MeV takes place in its own energy level. The daughter nucleus $^{60}_{28}$Ni is excited and undergoes two successive gamma decays, emitting gamma rays with two different energies: 1.1732 MeV at the

first transition and 1.3325 MeV at the second. Only 0.12 % of the parent nuclei, emitting β^- particles, decreases their energy level by 1.48 MeV, after which they pass to the ground state having undergone only one gamma decay.

2.3.3. Generic equation of gamma decay

Gamma emission changes neither the atomic number nor the atomic mass. It only decreases the energy level of the nucleus:

$$ {}^{A}_{Z}\mathrm{X}^{*} \rightarrow {}^{A}_{Z}\mathrm{X} + \gamma, \tag{2.3.1} $$

where ${}^{A}_{Z}\mathrm{X}^{*}$ is the excited nucleus.

When the excited state of the nucleus is a result of another radioactive decay (alpha or beta), a combined equation could be written for both decays:

$$ {}^{A}_{Z}\mathrm{X} \xrightarrow{\alpha} {}^{A-4}_{Z-2}\mathrm{X}'^{*} + {}^{4}_{2}\alpha \xrightarrow{\gamma} {}^{A-4}_{Z-2}\mathrm{X}' + \gamma, \tag{2.3.2} $$

or

$$ {}^{A}_{Z}\mathrm{X} \xrightarrow{\beta} {}^{A}_{Z+1}\mathrm{X}'^{*} + e^{-} + \bar{\nu}_{e} \xrightarrow{\gamma} {}^{A}_{Z+1}\mathrm{X}' + \gamma. \tag{2.3.3} $$

2.3.4. Gamma radiation energy

The energy of gamma radiation strictly corresponds to the difference between the two energy levels of the nucleus. Therefore, gamma rays are **mono-energetic**. It means that each radioactive gamma isotope emits gamma rays with one or several (depending on the number of its energy states and transitions) definite energies. For this reason, the gamma radionuclides can easily be identified by the energy of their gamma radiation.

Usually, the energy of gamma radiation is between 100 keV and 10 MeV. A specific example is an annihilation between a positron and an electron when two gamma photons with an energy of 511 keV are produced. For example, during β^+-decay, the released positron collides with an electron orbiting the atom, thus annihilating each other and resulting in the creation of two gamma rays.

Gamma radiation has a relatively high penetration power. This is due to the absence of an electrical charge – there are no electromagnetic interactions with matter (see Section 4.4).

References

[1] *Gerward, L.* Paul Villard and his Discovery of Gamma Rays, Physics in Perspective 1, 1999, p.p. 367-383. https://web.archive.org/web/20050316204556/http://www.blis.canberra.edu.au/irps/Archives/vol14no1/Gerward.html

2.4. Fission and fusion

Nuclear reactions release energy when the total mass of the products is less than the sum of the masses of the initial nuclei. The "lost mass" (Δm) appears as kinetic energy of the products ($E_0 = \Delta mc^2$).

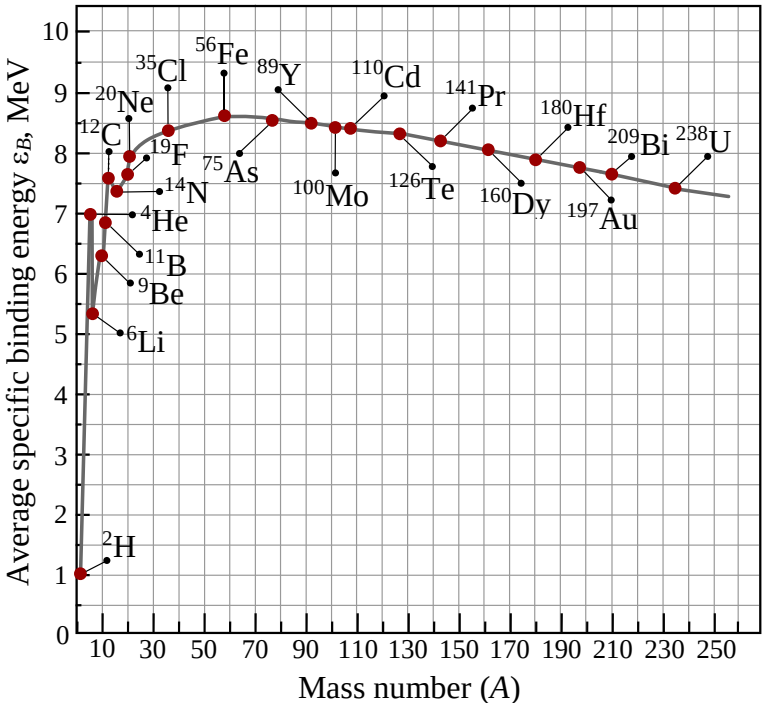

Fig. 2.4.1. Specific binding energy of the nuclei as a function of their mass

Looking at the specific binding energy diagram (Fig. 2.4.1), it is obvious that there are two possible types of exothermic nuclear reactions: the split of a very heavy nucleus into two lighter nuclei or the joining of two light nuclei into one heavier nucleus. The first reaction is called **nuclear fission,** and the second – **nuclear fusion**.

2.4.1. Nuclear Fission

Nuclear fission is a process [1] in which the nucleus of an atom splits into smaller parts – lighter nuclei called fragments. The fission process also produces free neutrons and gamma photons and releases a considerable amount of energy. It can start either without an external influence – **spontaneous fission** (a form of radioactive decay) or after a **nuclear reaction** (an interaction with an elementary particle or another nucleus) – **induced fission**.

German physicists **Otto Hahn** and **Fritz Strassman** [2] discovered induced nuclear fission in 1938 by bombarding uranium-235 with neutrons

(Fig. 2.4.2). In 1939, the Austrian physicist **Lise Meitner** and her nephew **Otto Frisch** provided a theoretical explanation of this phenomenon [3]. After that, many physicists of different countries worked on its practical application for military and civil aims.

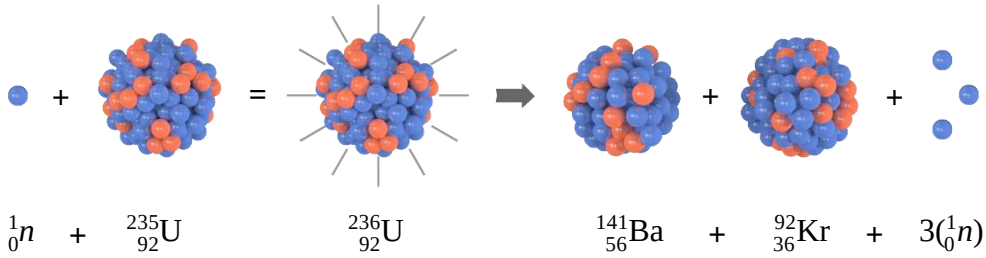

Fig. 2.4.2. The process of nucleus fission

Because of the presence of neutrons in cosmic rays, the discovery of spontaneous fission (without any interaction with neutrons) was more difficult. It was observed in uranium-238 for the first time by the Russian physicists **G. Flerov** and **P. Petrzhak** in 1940: they did the experiments in a Moscow metro station about 60 m underground, where cosmic neutrons could not penetrate at all [4].

Fission mechanism

Induced nuclear fission is explained by the **liquid drop model** of the nucleus (see Section 1.4.2.A). According to this model, the atomic nucleus behaves like the molecules in a drop of liquid; however, the fluid consists of nucleons instead (protons and neutrons). In the frame of this model, the fission process is explained based on the competition between the attractive nuclear force that ties together all nucleons and the repulsive Coulomb force between the protons [5].

QR Induced nuclear fission

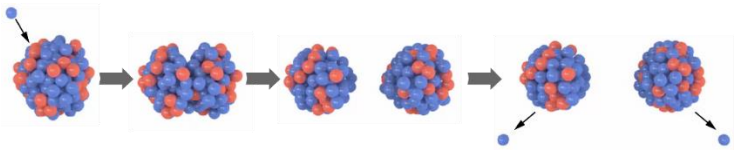

SCAN ME

In the ground state, the nucleus is spherical. If a sufficient amount of kinetic energy is added, this spherical nucleus may be distorted into a dumbbell shape, and then it may be split into two fragments (see the animation).

In our case, the neutron is absorbed into the nucleus along with the energy that it carries. The increment of energy elongates the entire nucleus and increases the distance between its nucleons. Since a powerful nuclear force

acts only over short distances (see Section 1.3.1), the nucleus elongation weakens the attraction between the nucleons. As a result, the repulsive electromagnetic force between the protons overpowers the nuclear force, and the nucleus splits into lighter, more stable nuclei, much like a liquid molecular drop.

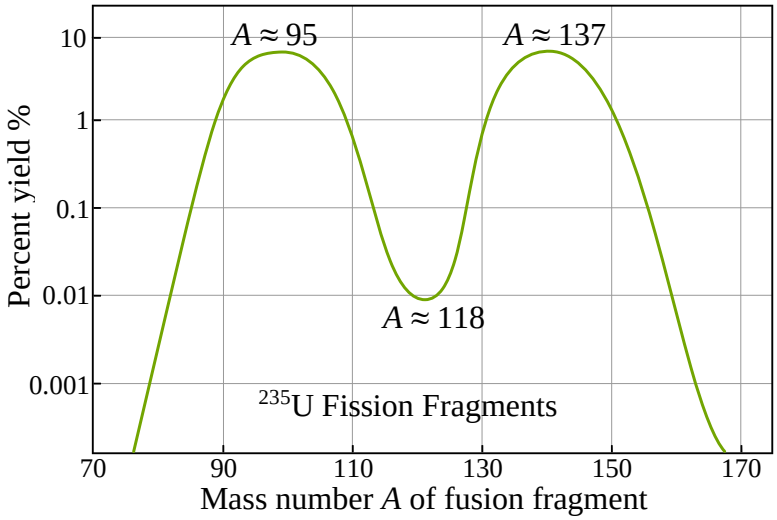

Fig. 2.4.3. Fission fragment yield

This model predicts the symmetric division of the original nucleus, i.e. the fission fragments have to have identical masses, which is yet to be confirmed by experiments. They showed that the masses of the fragments are different and that both peaks in their mass number (*A*) distribution (Fig. 2.4.3) are around 95 ± 15 u and 137 ± 15 u. Despite multiple theoretical attempts, this phenomenon could not be explained within the Liquid drop model.

The nuclear **Shell model** has provided a better explanation (see Section 1.4.3.B). The positions of the peaks in the fragment mass distribution correlated very well with the magic numbers. For example, the preference for the formation of nuclei with neutron numbers close to 82 would favor the formation of nuclides near the peak in the heavier group. It was also shown that the process in which one fission product is smaller than the other gives a more energetically favorable outcome.

Spontaneous fission is a form of radioactive decay. It becomes energetically possible (theoretically) for nuclei with atomic masses greater than 92 u, but it has never been observed in elements lighter than 232 u. Naturally occurring thorium-232, uranium-235 and uranium-238 undergo spontaneous fission, but in the vast majority of radioactive decays, alpha decay or beta decay occurs instead.

Synthetic elements with a high atomic number of A > 100 are more susceptible to spontaneous fission. For example, californium-252 ($^{252}_{98}$Cf), with a half-life of 2.65 years, undergoes alpha decay 96.9 % of the time to form curium-248 ($^{248}_{96}$Cm) but the remaining 3.1 % of decays are spontaneous fission. For this reason, it is widely used as a source of neutrons (see Section 3.4.1).

Regardless of its type, the fission process splits the particle into fragments and always produces neutrons, releases gamma radiation and a relatively high quantity of energy – about 200 MeV for uranium-235. This amount of energy is a result of the difference in the binding energy between the initial heavy isotope and both fragments (see Fig. 2.4.1).

Compared with the energy released at chemical oxidation (a few eV per event when burning coal), nuclear fuel contains at least ten million times more usable energy per unit mass than chemical fuel. This finding marks the starting point of the research and development devoted to the practical use of the fission process.

Chain reaction

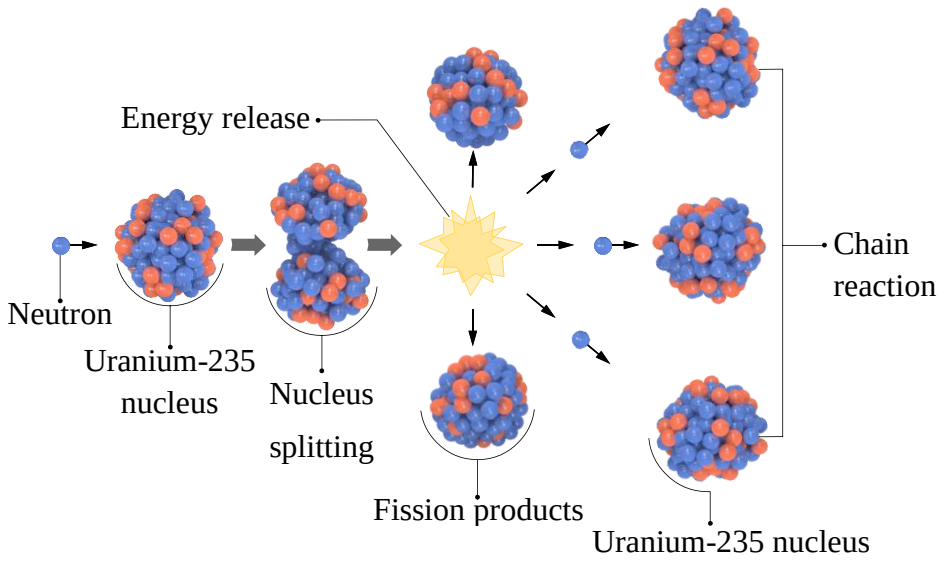

Fig. 2.4.4. Chain reaction of nuclei fission

The release of more than one neutron in each act of fission can activate a chain reaction: neutrons from the first fission reaction can cause an average of one or more subsequent nuclear fissions, thus leading to the possibility of a self-sustained fission process (Fig. 2.4.4). A necessary condition for maintaining such a chain reaction is that the nuclei of the original isotope can absorb the released neutrons. From this perspective, the most suitable isotopes

for nuclear fuel are uranium-235 and plutonium-239, which absorb neutrons with relatively low energy. The most commonly occurring isotope in nature is the isotope uranium-238, which undergoes induced fission only when impacted by a neutron with over 1 MeV of kinetic energy. However, too few of the neutrons produced by ^{238}U fission are energetic enough to induce further fissions in ^{238}U, so no chain reaction is possible with this isotope. This problem is solved by its enrichment with ^{235}U.

A second condition for a self-sustaining chain reaction is that at least one neutron must be absorbed after each fission by a fuel nucleus. The problem is that if the quantity of the fuel nuclei is small, large amounts of the released free neutrons dissipate without any impact on a nucleus. Therefore, a chain reaction can start only in a minimal quantity of nuclei called the **critical mass**. The actual value of this critical mass strongly depends on the properties of the fissionable material (nuclear properties, density, shape, purity, temperature, etc.) and its surroundings.

The concept of a nuclear chain reaction via neutrons was first reported by Hungarian scientist **Leo Szilard** in 1933 [6], soon after the discovery of the neutron (1932). Seven years later, in 1939, **Szilard** and **Enrico Fermi** [7] discovered the neutron multiplication in uranium, proving the possibility of a chain reaction. In 1942, a team led by Fermi produced the first artificial self-sustaining nuclear chain reaction using an experimental reactor at the University of Chicago.

Since then, research and development on the use of nuclear fission have been conducted in two fundamentally different directions:

- The creation of **weapons of mass destruction** – the first fission bomb was produced and tested in 1945 by an international team of physicists led by **Oppenheimer** in the USA.
- The production of **electricity** via a nuclear reactor – the first **nuclear power plants** were constructed in the USA, USSR and England between 1948 and 1956.

2.4.2. Nuclear Fusion

Nuclear fusion is a process in which two or more atomic nuclei come close enough to form one or more different atomic nuclei and subatomic particles (neutrons and/or protons). The difference in mass between the products and initial constituents provides the release of large amounts of energy. In the early stages of the stellar evolution of the Sun and other stars, hydrogen fused to form helium, releasing energy in the form of photons (light) and neutrinos. During the later stages of stellar evolution, heavier nuclei (up to iron) were synthesized through fusion.

In 1929, **R. Atkinson** and **Fr. Houtermans**, using Gamow's quantum tunneling theory, showed that fusing light nuclei could create energy in accordance with Einstein's formula of mass-energy equivalence and that those heavy nuclei could be built up by a successive series of fusions [8]. In 1932, the Australian physicist, **M. Oliphant**, using a particle accelerator to fire heavy hydrogen nuclei (deuterons), was the first to accomplish the fusion process in a laboratory: he discovered the nuclei of tritium and helium-3 [9].

Again, this process's military application was the first unique utilization of the vast amount of energy released from the fusion – the thermonuclear bomb – which was tested successfully in 1951. From that time up to now, a lot of research has been conducted in an effort to find a safe and profitable method to produce and use "fusion" energy.

Fusion Mechanism

A fusion reaction occurs when two (or more) atomic nuclei come close enough to each other for a predetermined period of time, allowing a strong nuclear force to overcome the electromagnetic force that is pushing them apart and fuses them into a single heavier nucleus instead. A typical example is the fusion of a deuterium (^{2}H) nucleus with a tritium (^{3}H) nucleus (see the animation). The result is a helium-4 (^{4}He) nucleus, a neutron and a total of 17.6 MeV released energy.

QR Typical fusion reaction

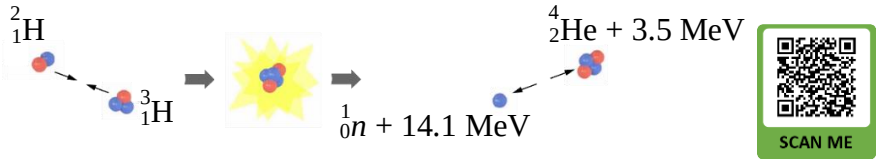

A big problem of the fusion realization in practice is the large amount of energy necessary to bring both nuclei close enough to one another – this requires even more energy than the energy released upon fusion. Ways of bringing nuclei together include speeding up atoms in a particle accelerator or heating them to high temperatures.

When an atom is heated above its ionization energy, its electrons are stripped away, leaving just the bare nucleus as an ion. The result is a hot cloud made up of ions (known as **a plasma**) and the electrons formerly attached to the nuclei. Because the charges are separated, plasmas are electrically conductive and magnetically controllable, which creates the possibility to control the entire process. Project ITER (which means "The way" in Latin) is the last attempt in which 35 nations are collaborating to build the world's largest

magnetic fusion device (in France) in order to prove the feasibility of fusion as a large-scale source of energy [10].

References

[1] Nuclear fission. https://en.wikipedia.org/wiki/Nuclear_fission

[2] *Hahn, O., F. Strassmann. Über den Nachweis und das Verhalten der bei der Bestrahlung des Urans mittels Neutronen entstehenden Erdalkalimetalle (On the detection and characteristics of the alkaline earth metals formed by irradiation of uranium with neutrons). Naturwissenschaften,* ***27,*** *1, 1939, p.p. 11-15.*

[3] *Meitner, L., O. R. Frisch*. Disintegration of Uranium by Neutrons: a New Type of Nuclear Reaction. Nature, **143,** 3615, 1939, p.p. 239.

[4] *Petrzhak, K. A., G. N. Flerov*. Spontaneous fission of nuclei. Usp. Fiz. Nauk 73, 1961, p.p. 655-683.

[5] Nuclear fission theory. https://www.britannica.com/science/nuclear-fission/Fission-theory#ref496491

[6] *Szilard, L*. Improvement in or relating to the Transmutation of Chemical Elements. Patent GB630726 (A) – 1936-03-30. https://worldwide.espacenet.com/publicationDetails/originalDocument?locale=en_EP&FT=D&CC=GB&DB=&NR=630726A&date=19360330&ND=&KC=A

[7] *Anderson, H., E. Fermi, H. Hanstein*. "Production of Neutrons in Uranium Bombarded by Neutrons". Physical Review. **55,** 8, 1939. p.p. 797–798.

[8] *Atkinson, R., F. Houtermans*. Aufbaumöglichkeit in Sternen (Development in Stars), Z. für Physik **54**, 1929, p.p. 656-665.

[9] *Oliphant, M. L. E., A. R. Kempton, Rutherford, Lord*. The Accurate Determination of the Energy Released in Certain Nuclear Transformations. Proc. of the Royal Society A, **149,** 867, 1935, p.p. 406–416.

[10] ITER&Beyond. https://web.archive.org/web/20120922162049/http://www.iter.org/proj/iterandbeyond

2.5. Radioactive decay regularities

2.5.1. The law of radioactive decay

A very important feature of radioactive decay is its spontaneous character – it is an intrinsic process of the nucleus depending only on its internal state. Many experiments were carried out to determine the influence of outside factors on the radioactive process: radioactive substances were heated up to temperatures of 1000 °C; they were put under the pressure of many gigapascals; they were exposed to very strong magnetic fields. All of the tests yielded the same result – the rate of the radioactive decay remained unchanged.

All these studies led to the conclusion that a radionuclide nucleus has no "memory" or way of translating its history into its present behavior. A nucleus does not "age" with the passage of time. Thus, the probability of its breaking down does not increase with time but stays constant no matter how long the nucleus has been in existence. This probability may vary greatly between different types of nuclei, leading to many different observed decay rates. However, the probability remains unchanged over time.

On the other hand, the probability that at least one nucleus will decay in a "large number of nuclei" increases with the passage of time.

What does a "large number of nuclei" mean?

The atomic mass of a radium-226 nucleus is

$$A_{\mathrm{Ra}} = 226.02 \text{ g/mole}.$$

The Avogadro number is

$$N_A = 6.02 \cdot 10^{23} \text{ mole}^{-1}.$$

Then 1 g of radium-226 contains

$$\frac{N_A}{A_{\mathrm{Ra}}} = \frac{6.02 \cdot 10^{23}}{226.02} \approx 3 \cdot 10^{21} \text{ nuclei},$$

which is a really large number.

These two assumptions led **Rutherford** and **Soddy** to conclude that the number of decayed nuclei dN in a certain time interval dt is only proportional to the number of nuclei N and the duration of this interval:

$$dN = -\lambda N dt, \tag{2.5.1}$$

where λ is a coefficient of proportionality, called the **constant of the radioactive decay**. The minus sign corresponds to the decrease in the quantity of the initial nuclei during the radioactive decay process.

The solution of this differential equation gives

$$N = N_0 e^{-\lambda t}, \tag{2.5.2}$$

where N_0 is the initial number of radioactive nuclei (at the moment $t = 0$).

This is called the **Law of Radioactive Decay** [1, 2] and shows that, during the decay, the number of the radioactive nuclei decreases exponentially (Fig. 2.5.1). This law does not depend on the origin of the radioactive element – whether it is natural or synthetically produced.

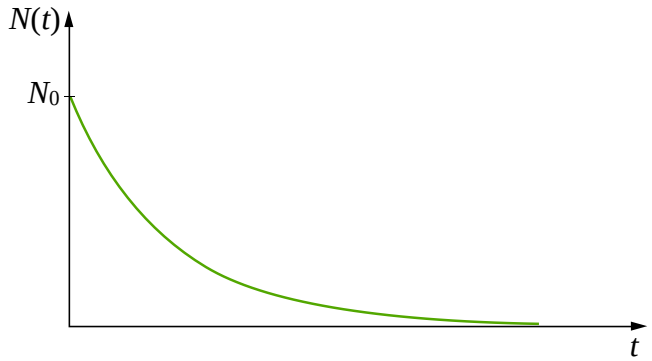

Fig. 2.5.1. Graph of the radioactive decay law

The rate of the process depends on the constant λ, but it is most often evaluated by the so-called **half-life** ($T_{1/2}$) of the isotope. That refers to the time during which half of the initial number of nuclei decayed:

$$N = N_0/2. \tag{2.5.3}$$

By combining this equation with the Law of Radioactive Decay equation, we obtain

$$T_{1/2} = \ln 2/\lambda = 0.693/\lambda. \tag{2.5.4}$$

The half-life of different isotopes varies greatly. To date, the measured half-life values are in a range of about 55 orders – from $2.3 \cdot 10^{-23}$ s (for hydrogen-7) to $6.9 \cdot 10^{31}$ s (for tellurium-128).

During radioactive decay, the nuclei of the first isotope N_A decay to become the nuclei of a new isotope N_B. However, the total number of nuclei of both isotopes remains constant and equal to the number of nuclei of the initial isotope A (N_{A0}):

$$N_A + N_B = N_{A0}. \tag{2.5.5}$$

Replacing N_A from the radioactive decay law, we obtain

$$N_B = N_{A0} - N_A = N_{A0} - N_{A0}e^{-\lambda t} = N_{A0}(1 - e^{-\lambda t}). \tag{2.5.6}$$

This equation shows that the number of the new isotope's nuclei increases exponentially during the radioactive process.

2.5.2. Activity

The rate of the decay (i.e. the number of nuclei of the initial isotope decaying in a unit of time) is a basic parameter of each radioactive source, called **activity**:

$$R = \left|\frac{dN}{dt}\right| = \lambda N_0 e^{-\lambda t} = \lambda N. \tag{2.5.7}$$

As can be seen in (2.5.7), the activity is proportional to the radioactive constant λ, i.e. it is inversely proportional to the half-life. That means that **the shorter the half-life of an isotope is, the higher its activity will be**. The initial isotope activity decreases exponentially over time, which corresponds to the decrease in the number of its nuclei.

The SI-unit used to measure the activity is **Becquerel** (**Bq**), which is equal to 1 decay per second, i.e. its dimension is s^{-1}. The non-SI unit of activity **Curie** (**Ci**) is still in use. The rate between them is

$$\begin{aligned} 1\ \text{Ci} &= 3.7 \cdot 10^{10}\ \text{Bq} = 37\ \text{GBq and} \\ 1\ \text{Bq} &= 2.703 \cdot 10^{-11}\ \text{Ci} \approx 27\ \text{pCi}. \end{aligned} \tag{2.5.8}$$

Example 1

It was determined that 1 gram of radium-226 undergoes $3.7 \cdot 10^{10}$ decays in 1 second, which leads to the question of how to calculate the half-life of radium-226 nuclei.

Solution:

$$R = \lambda N \Longrightarrow \lambda = \frac{R}{N} \Longrightarrow \lambda = \frac{R}{N_A/A_{\text{Ra}}} = R\frac{A_{\text{Ra}}}{N_A},$$

where R is the material activity, A_{Ra} – the atomic mass of radium, and N_A – the Avogadro constant.

$$T_{1/2} = \frac{\ln 2}{\lambda} = \frac{0.693}{R} \cdot \frac{N_A}{A_{\text{Ra}}} = \frac{0.693}{3.7 \cdot 10^{10}} \cdot \frac{6.02 \cdot 10^{23}}{226} \approx$$
$$\approx 5 \cdot 10^{10}\ \text{s} \approx 1600\ \text{years}.$$

Answer: The half-life of radium-226 nuclei is approximately 1600 years.

2.5.3. Stochastic character[1] of radioactive processes

The spontaneous nature of radioactive decay determines the stochastic (i.e. random) character of the radioactive processes. As was mentioned above, it is impossible to predict when a radioactive nucleus will decay. Moreover, it is also impossible to predict exactly how many nuclei will decay within a specific time interval. In other words, it is not possible to find a fixed mathematical equation to determine either the number of decayed nuclei in a sequence of equal time intervals or the intervals between every two decays.

Nevertheless, if we intermittently measure the number of decays during a fixed time interval, it will become clear that despite a large number of varying results, some of them repeat more often than others. The resulting conclusion is that the probability of receiving each one of the possible numbers of decays (0, 1, ..., ∞) during equal time intervals varies. The equation that shows the dependence between the values of a random quantity and the probability of receiving each of these values is called the Distribution Law of this random quantity [3]. In our case, the number of decays in many equal time intervals follows the so-called **Poisson distribution** [4, 5]:

$$p_k = \frac{(\bar{k})^k}{k!} e^{-\bar{k}} = \frac{(nt)^k}{k!} e^{-nt}, \tag{2.5.9}$$

where

p_k is the probability to have k events (in our case – decays) in the interval t,

$\bar{k}$ – the mean value of k, determined by a great number of measurements,

$n = \bar{k}/t$ – the mean number of events in unit time, i.e. the activity of the isotope.

For example, the probability of having no decays in an interval t is

$$p_0 = \frac{(nt)^0}{0!} e^{-nt} = e^{-nt} \text{ (because } 0! = 1), \tag{2.5.10}$$

or to have only one decay:

$$p_1 = nte^{-nt}. \tag{2.5.11}$$

[1] The whole analysis of the stochastic character of radioactive processes is carried out considering that the half-life of radioactive isotopes is much longer than the duration of the experiments, i.e. that the activity of the isotopes remains constant all the time.

The sum of the probability to receive all possible results of the number of decays (from 0 to ∞) in a fixed time interval t obviously has to be 1 because in such a case, all possible results are included:

$$\sum_{k=0}^{\infty} p_k = \sum_{k=0}^{\infty} \frac{(\bar{k})^k}{k!} e^{-\bar{k}} = e^{-\bar{k}} \sum_{k=0}^{\infty} \frac{(\bar{k})^k}{k!} = e^{-\bar{k}} e^{\bar{k}} = 1 \qquad (2.5.12)$$

(the last sum is an exact derivative of the function $e^{\bar{k}}$ in a power series).

The Poisson distribution is a discrete distribution where k can take only integer values (decays based on non-integers do not exist). In the graph (Fig. 2.5.2), a line connects the discrete points for the purpose of better visibility only. The highest probabilities have the results equal to $\bar{k} - 1$ and to $\bar{k}$ because these two probabilities are equal:

$$p_{\bar{k}} = \frac{\bar{k}^{\bar{k}} e^{-\bar{k}}}{\bar{k}!} = \frac{\bar{k}\bar{k}^{\bar{k}-1} e^{-\bar{k}}}{\bar{k}(\bar{k}-1)!} = \frac{\bar{k}^{-\bar{k}-1} e^{\bar{k}}}{(\bar{k}-1)!} = p_{\bar{k}-1}. \qquad (2.5.13)$$

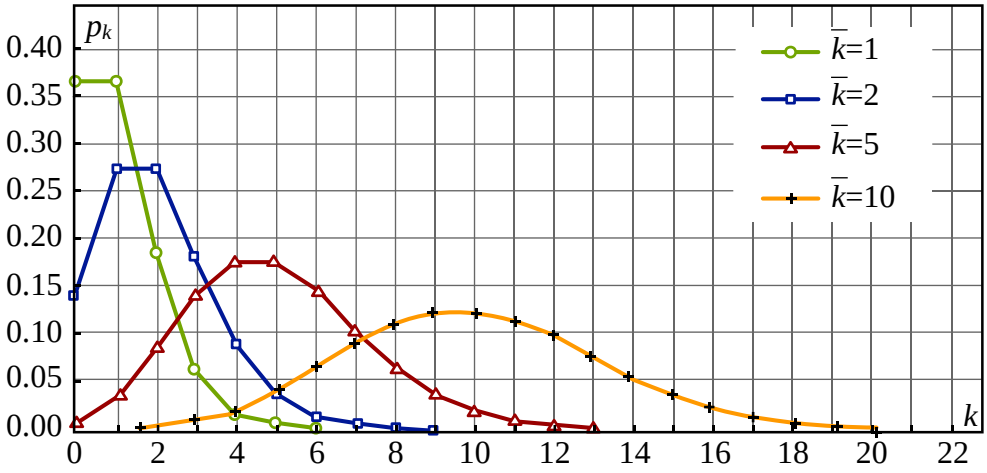

Fig. 2.5.2. Poisson distributions with different average values

At low $\bar{k}$ values, the distribution is highly asymmetric because k can only be positive. However, with the increase of $\bar{k}$, the distribution becomes more and more symmetric.

Most often, the purpose of the measurement is to determine the mean value $\bar{k}$, and from it – the rate of the decay $\bar{n} = \bar{k}/t$. In fact, each result is a value of k, which we accept as $\bar{k}$. To find the error, which has been made in this case (the difference between the actual value of $\bar{k}$ and the measured value k), it is necessary to evaluate the deviation of the results from the mean value. The quantity **variance** (also sometimes referred to as **dispersion**)

$$Var = \overline{(k - \bar{k})^2} \qquad (2.5.14)$$

(which is the mean value of the square of all possible deviations of *k* towards $\bar{k}$) is used for this purpose.

A characteristic feature of the Poisson distribution is that the variance and the average value $\bar{k}$ are equal:

$$Var = \bar{k}. \qquad (2.5.15)$$

The quantity

$$\sigma = \sqrt{Var} = \sqrt{\bar{k}}, \qquad (2.5.16)$$

is called a **standard deviation**. It best evaluates the difference in the measured results *k* from their mean value $\bar{k}$. At $\bar{k} >> 1$, i.e. at a symmetric Poisson distribution, 68 % of all results fall within the zone $\bar{k} \pm \sigma$ (with a sufficiently large number of measurements), 95.4 % of the results fall in the zone $\bar{k} \pm 2\sigma$, and 99.7 % (Fig. 2.5.3) fall in the zone $\bar{k} \pm 3\sigma$.

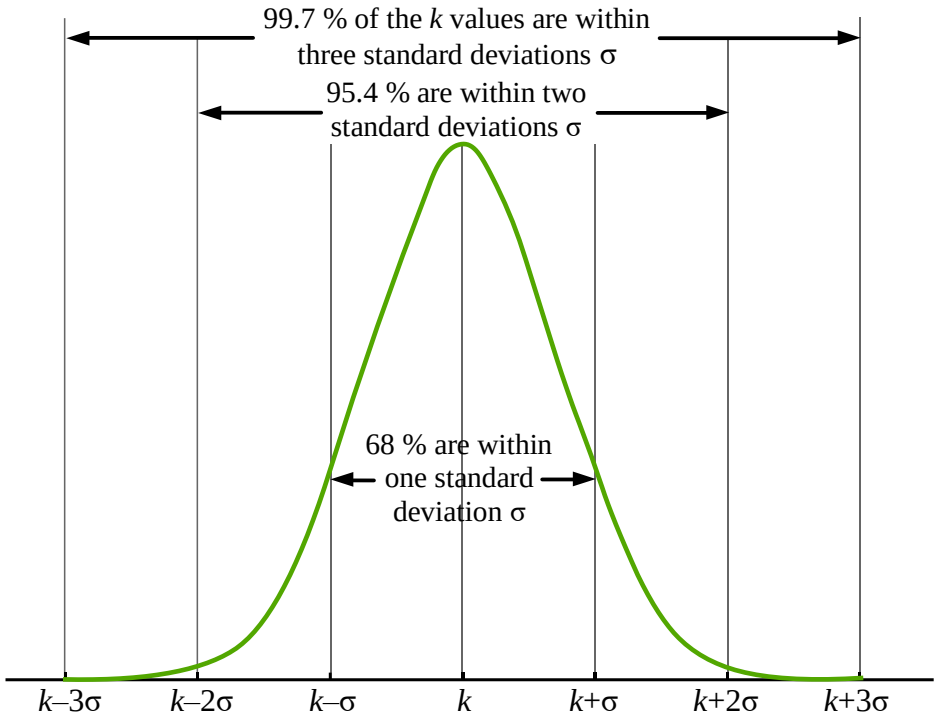

Fig. 2.5.3. Distribution of the k values around the mean value $\bar{k}$

For this reason, the possible maximum absolute error is actually ± 3σ, but in practice, it is acceptable to evaluate the absolute error by ± σ. Therefore, the relative error (relative standard deviation) is

$$\delta = \pm\sigma/\bar{k}, \tag{2.5.17}$$

or replacing σ from equation (2.5.16):

$$\delta = \pm\frac{1}{\sqrt{\bar{k}}} = \frac{1}{\sqrt{nt}}. \tag{2.5.18}$$

The last equation shows that, in order to increase the precision when measuring the activity of an isotope (*n* is set), the measurement time *t* should increase.

When the result of a study is the difference between two random quantities with Poisson distribution, the variance of the result is equal to the sum of the variances of these quantities (because there is usually no correlation between these two quantities). Respectively, the standard deviation of the result is the root mean square (*rms*) of the standard deviations of these quantities:

$$\sigma = \sqrt{\sigma_1^2 + \sigma_2^2}\,. \tag{2.5.19}$$

At sufficiently high values of $\bar{k}$ ($\bar{k} \geq 20$) the discrete distribution of Poisson can be replaced by the continuous **Normal or Gaussian distribution** [6]:

$$f(k) = \frac{1}{\sigma\sqrt{2\pi}} e^{-(k-\bar{k})^2/2\sigma^2} = \frac{1}{\sqrt{2\pi\bar{k}}} e^{-(k-\bar{k})^2/2\bar{k}}, \tag{2.5.20}$$

the variance of which has to be equal to the mean value (see eq. (2.5.15) and (2.5.16)) as it is in the Poisson distribution.

The function *f*(*k*) is called the **probability density function** (**PDF**). It is shown in Fig. 2.5.4 for $\bar{k}$ = 100. The corresponding values of the Poisson distribution are marked by crosses and show a very good match to the PDF (the difference is in the limit of ± 1.5 %). The probability of receiving results between the two values of *k* (k_1 and k_2) is equal to the area under the function *f*(*k*) between these two values:

$$p_{k_1-k_2} = \int_{k_1}^{k_2} f(k)dk. \tag{2.5.21}$$

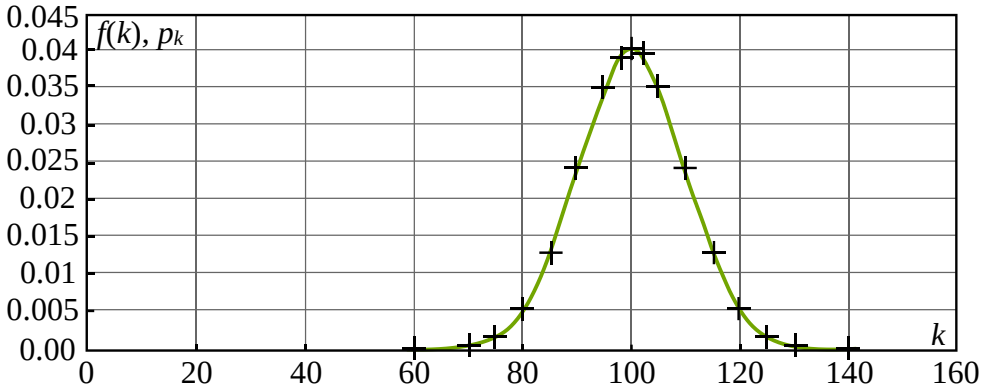

Fig. 2.5.4. A normal distribution with $\bar{k}$ = 100 (the green line) and the values of a corresponding Poisson distribution (the crosses)

2.5.4. Distribution of the time intervals between successive decays

For electronic devices used in nuclear research, another random quantity is significant – the distribution of the time intervals between the successive decays. Their dead time has to be short enough so that a minimum number of decays is lost.

The probability density function of this distribution can be found when taking into account some considerations. The following two conditions must be fulfilled simultaneously to obtain an interval *t* between two consecutive decays: there should not be a single decay throughout this interval *t*, and there should be one decay during an infinitely short interval *dt*, after that. The probability of the first event is $p_0 = e^{-nt}$ and of the second is $p_1 = ndte^{-ndt} \approx ndt$ (taking into account that $ndt \ll 1$ and $e^{-ndt} \approx 1$. Because these two probabilities are independent, the likelihood of both events happening simultaneously is equal to the product of their probabilities:

$$p(t)dt = e^{-nt}ndt, \tag{2.5.22}$$

or the **probability density function of the time intervals** will be

$$p(t) = ne^{-nt}. \tag{2.5.23}$$

This equation (Fig. 2.5.5) shows a very important difference between the random distributions of the number of the decays in a fixed time interval and that of the time intervals between the decays. The number of decays has a mean value, and the results with the highest probability will be close to the average value. The intervals have no mean value, and therefore the shortest of them have the highest probability (see Fig. 2.5.5.). Another conclusion from the time interval distribution is that any electronic device will miss some decays since there are no devices with zero dead time.

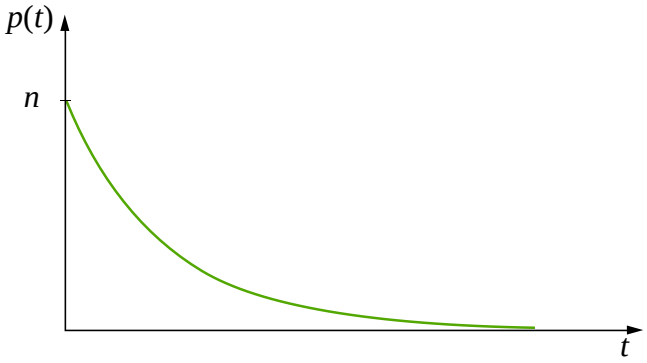

Fig. 2.5.5. Exponential probability density function of the time intervals between the decays

References

[1] *Rutherford, E., F. Soddy*. The Cause and Nature of Radioactivity I, II. Philosophical Magazine IV, 1902, p.p. 370–396, 569–585.

[2] *Weinert F*. Radioactive Decay Law (Rutherford-Soddy). https://link.springer.com/chapter/10.1007/978-3-540-70626-7_183

[3] *V.I. Goldansky, A.V. Kutsenko, M.I. Podgoretsky*. Counting statistics of nuclear particles. Delhi: Hindustan Pub. Corp., 1962.

[4] *Poisson, S. D*. Probabilité des jugements en matière criminelle et en matière civile, précédées des règles générales du calcul des probabilités. Bachelier, Paris, 1837.

[5] Poisson distribution. https://en.wikipedia.org/wiki/Poisson_distribution

[6] Normal (Gaussian) distribution. https://en.wikipedia.org/wiki/Normal_distribution

PART 3. RADIATION SOURCES

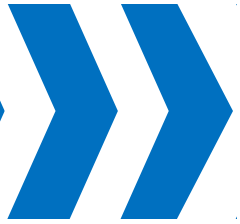

3.0. Introduction

Radiation, the sources of which will be described in part 3, can be categorized into four types [1]:

1. heavy charged particles,
2. fast electrons,
3. electromagnetic radiation,
4. neutrons.

The first two types form the group of **charged particulate radiation,** and the last two types – the group of **uncharged radiation**.

The group of **charged particulate radiation** includes all energetic ions with a mass of one atomic mass unit or greater, such as protons, alpha particles, fission products or products of different nuclear reactions.

Fast electrons include beta particles (positive or negative) emitted during nuclear decay, as well as high energy electrons produced by any other process – cathode emissions, accelerator beams and so forth.

Gamma rays – a product of nuclear decay and **X-rays** (Roentgen rays), which is emitted by electrons moving between their atom's shells, are the most used type of **electromagnetic radiation**.

The **last category** includes **neutrons** generated by different processes like fission, nuclear reactions and others.

For research and practical applications, sources of radiation with different energy are required – the energy range spans over six decades (from 10 eV to 20 MeV). The lowest energy level corresponds to the amount of energy necessary to produce ionization in matter. The upper limit is reached in particle accelerators.

From the history of nuclear physics, we know that the first radioactive sources of alpha and beta particles and gamma rays contained natural radioactive nuclei. Later, many methods for the creation of various new radioactive isotopes (called **synthetic** isotopes) and technologies for the production of powerful sources of neutrons, gamma quanta, protons and nuclei were developed. For these purposes, reactors and accelerators are used to irradiate the corresponding target.

Another natural source of radiation is the so-called **cosmic rays** – fluxes of different particles and photons coming from the Cosmos. They originate from different cosmic processes, such as burning (e.g., our Sun) or exploding (for example, Supernova stars). These bodies produce immense amounts of radiation with very high energy, some of which reach the Earth. They have

no practical application but create background radiation that decreases the precision of radioactivity measurements.

For many practical applications and different physical investigations, the main source of radiation is nuclear reactors and particle accelerators. They may produce different types of radiation with varying levels of energy.

Thanks to Dr. S. N. Ahmed, from whose book [2] the data in the Tables are taken.

References

[1] *Knoll, G. F.* Radiation detection and measurement. Third ed. John Valley & Sons Inc., New York, 2000. https://phyusdb.files.wordpress.com/2013/03/radiationdetectionanddmeasurementbyknoll.pdf

[2] *Ahmed, S. N.* Physics and engineering of radiation detectors. Elsevier, Amsterdam, 2007. https://www.elsevier.com/books/physics-and-engineering-of-radiation-detection/ahmed/978-0-12-045581-2

3.1. Heavy charged particle sources

3.1.1. Proton sources

The effective application of proton beams in several fields, such as radiography, imaging, and fundamental physics research, has led to the development of different types of proton production facilities.

Most used are particle accelerators in which protons can be accelerated up to very high energies. For example, the most powerful accelerator in the world – the Large Hadron Collider at CERN, Geneva [1] – accelerates two proton beams up to 7 TeV each. However, such accelerators are enormous and costly machines. Recently, a new type of very compact laser-ion accelerators [2] is being used for the production of protons intended for medical applications. In order to accelerate protons up to several MeV, a highly intense laser ($> 10^{19}$ W/cm^2) with ultra-short pulses is focused on a solid-, or gaseous target. This results in a collimated beam of high-energy protons that can be used, for example, to destroy cancerous tissues.

There are no natural radioactive isotopes emitting protons. However, they can be produced by nuclear reactions – by irradiating specific targets with high-energy particles. This process excites the nuclei of the target, and they become unstable. The excited nuclei then decay by emitting protons, alpha particles and other components. Some of the proton emitting isotopes and their half-life periods of $T_{1/2}$ are shown in Table 3.1.1.

Element	**Isotope**	$T_{1/2}$
Cesium	$^{113}_{55}$Cs	17 μs
Bismuth	$^{185m}_{83}$Bi	44 μs
Indium	$^{109}_{53}$I	103 μs
Thulium	$^{147m}_{69}$Tm	360 μs
Rhenium	$^{157}_{75}$Re	370 μs
Lutetium	$^{151}_{71}$Lu	120 ms
Tantalum	$^{157}_{73}$Ta	300 ms

Table 3.1.1. Sources of protons

3.1.2. Alpha particle sources

There are a few natural radioactive isotopes that emit alpha particles – mainly unstable heavy elements (see Section 2.1.3). Other alpha radioactive isotopes, necessary for different practical applications, are synthetically produced by nuclear reactions.

As was explained in Section 2.1.3, the alpha radionuclides emit one, or a few, mono-energetic beams of alpha particles with closely related energy values. The exact amount of energy depends on the type of isotope and is limited by its half-life period, which varies greatly. Most radioactive isotopes emit alpha particles in the range of 4–6 MeV.

The energy and the half-life period of the most commonly used alpha radioisotopes can be viewed in Table 3.1.2.

Element	**Isotope**	$T_{1/2}$	**Energy, MeV**
Bismuth	$^{213}_{83}$Bi	45.6 minutes	5.549 (7 %), 5.869 (93 %)
Radium	$^{223}_{88}$Ra	11.435 days	5.607 (25.7 %), 5.716 (52.6 %)
Polonium	$^{210}_{84}$Po	138.376 days	5.304 (100 %)
Californium	$^{252}_{98}$Cf	2.645 years	6.076 (15.7 %), 6.118 (82.2 %)
Curium	$^{244}_{96}$Cm	18.1 years	5.763 (23.6%), 5.805 (76.4 %)
Americium	$^{241}_{95}$Am	432.2 years	5.443 (13 %), 5.486 (85,5 %)
Thorium	$^{229}_{90}$Th	7340 years	4.845 (56.2 %), 4.901 (10.2 %)
Plutonium	$^{239}_{94}$Pu	24110 years	5.144 (15.1 %), 5.156 (73.3 %)

Table 3.1.2. Sources of alpha particles

For different scientific research purposes, alpha particles can be accelerated up to very high energies.

3.1.3. Spontaneous fission

The fission process (see Section 2.4.) is the only spontaneous source of energetic heavy charged particles with a mass greater than that of the alpha particle – so-called **fission fragments**. All heavy nuclei are, in principle, unstable against spontaneous fission, but for most of them, this process is energetically inhibited. It is intrinsic only for some transuranic elements of very large mass numbers. A typical example is the californium isotope $^{252}_{98}$Cf that undergoes spontaneous fission in 3.1 % of its decays (the remaining 96.9 % being alpha decays) [3]. The actual half-life for this isotope is 2.65 years, and a sample of 1 microgram of $^{252}_{98}$Cf will emit $1.92 \cdot 10^7$ alpha particles and undergo $6.14 \cdot 10^5$ spontaneous fissions per second. Each fission process also produces neutrons, and therefore the same isotopes are used as neutron sources (see Section 3.4).

The fragments themselves are stripped of their electrons and represent multi charged ions. During their motion, they catch electrons from the surrounding matter and lose their charge relatively fast.

The main application of fission fragments is for the testing and calibration of the detectors used in heavy ion measurements.

In some super heavy elements, a special fission process called **ternary fission** produces three fragments instead of two [4]. Most often (in more than 90% of the ternary fissions), the third fragment is an alpha particle with a very high energy level – around 16 MeV. This type of fission can be both spontaneous – as that of californium-252, and thermal-neutron-induced – as that of uranium-235. The process is relatively rare – 1 ternary fission per 1-2 million binary fissions, but nevertheless, it is used as the only source of alpha particles with very high energy.

References

[1] The Large Hadron Collider. https://home.cern/topics/large-hadron-collider

[2] *Dunne, M.* Laser driven particle accelerators. Science **312**, 5772, 2006, p.p. 374-376. http://science.sciencemag.org/content/312/5772/374.full

[3] Isotopes of californium. https://en.wikipedia.org/wiki/Isotopes_of_californium

[4] *Muga, M. L.* Ternary Fission. IAEA, INIS, RN: 45008544. https://inis.iaea.org/search/search.aspx?orig_q=RN:45008544

3.2. Electron and positron sources

3.2.1. Beta-minus radioactive decay

The most often used sources of fast electrons are radioactive isotopes decaying by beta-minus emission. They are produced relatively easily through irradiating stable isotopes with neutrons at nuclear reactors. As was clarified above (see Sections 2.2 and 2.3), after a radioactive nucleus undergoes beta decay, the resulting (daughter) nucleus is usually left in an excited energy state. In this case, it additionally emits one or more gamma photons to return to its basic energy state.

The most popular sources of fast electrons are shown in Table 3.2.1 below, where the pure beta-emitters are marked with (p). The energy spectrum of the electrons emitted by these isotopes is continuous (because of the simultaneous irradiation of antineutrinos). Therefore, the maximum value of the kinetic energy of electrons (E_{max}) is also provided in Table 3.2.1.

Element	**Isotope**	$T_{1/2}$	**Energy (E_{max})**
Cooper	$^{64}_{29}$Cu	12.7 hours	578.7 keV
Sodium	$^{24}_{11}$Na	14.952 hours	1.393 MeV
Yttrium (p)	$^{90}_{39}$Y	64.0 hours	2.280 MeV
Phosphorus (p)	$^{32}_{15}$P	14.262 days	1.710 MeV
Chromium	$^{51}_{24}$Cr	27.702 days	752.73 keV
Iodine	$^{125}_{53}$I	59.408 days	150.61 keV
Thallium (p)	$^{204}_{81}$Tl	3.78 years	763.40 keV
Cobalt	$^{60}_{27}$Co	5.271 years	318.13 keV
Strontium (p)	$^{90}_{38}$Sr	28.79 years	546.0 keV
Cesium	$^{137}_{55}$Cs	30.07 years	513.97 keV

Table 3.2.1. Most popular sources of fast electrons

3.2.2. Internal conversion

The continuous energy spectrum of beta particles is unsuitable for some applications. A typical example is the energy calibration of a radiation detector. In this case, it is necessary to use a flux of mono-energetic electrons.

There is a nuclear process called "**internal conversion**" that could result in the emission of mono-energetic electrons.

This process starts with an excited nucleus, the state of which is usually a result of a preceding radioactive decay. The standard method of de-excitation is through the emission of a gamma photon. However, for some excited nuclei, gamma decay may be prohibited. Then the nuclear excitation energy E_{ex} is transferred directly to one of the orbital electrons of the atom, which will be emitted with an energy of

$$E_e = E_{ex} - E_b, \tag{3.2.1}$$

where E_b is the binding energy in the original electron shell.

Since the conversion electron can originate from any one of the different electron shells within the atom, a single nuclear excitation level generally leads to several groups of electrons with different energies in each group. The spectrum may be further complicated in cases where more than one excited state within the nucleus is generated. Furthermore, the converted electron energy spectrum may also be superimposed on the continuous energy spectrum of the beta radiation produced by the parent nucleus. (Very often, only such a beta emission leads to the excited state of the nucleus). Despite these disadvantages, the conversion electron sources are the only practical laboratory-scale sources of mono-energetic electron groups in the high keV to MeV energy range. Several useful radioisotope sources of conversion electrons [1] are shown in Table 3.2.2.

Parent element	Tin	Cerium	Cadmium	Cesium	Bismuth
Parent isotope	$^{113}_{50}$Sn	$^{139}_{58}$Ce	$^{109}_{48}$Cd	$^{137}_{55}$Cs	$^{207}_{83}$Bi
Parent $T_{1/2}$	115 days	137 days	453 days	30.2 years	38 years
Daughter element	Indium	Lanthanum	Silver	Barium	Lead
Daughter isotope	$^{113m}_{49}$In	$^{139m}_{57}$La	$^{109m}_{47}$Ag	$^{137m}_{55}$Ba	$^{207}_{82}$Pb
Transition Energy (keV)	393	166	88	662	570, 1064
Conversion electron energy (keV)	365, 389	126, 159	62,84	624, 656	482, 554, 967, 1048

Table 3.2.2. Sources of mono-energetic electrons generated by internal conversion

3.2.3. Beta-plus radioactive decay

The only laboratory-scale sources of positrons are beta-plus radioactive isotopes (see Table 3.2.3). A significant disadvantage is the short life of a positron, which is annihilated immediately (see Section 3.3.6) upon collision with an electron.

Element	**Isotope**	$T_{1/2}$	**Energy (E_{max})**
Oxygen	$^{15}_{8}O$	122.24 sec.	1.732 MeV
Nitrogen	$^{13}_{7}N$	9.97 min.	1.200 MeV
Carbon	$^{11}_{6}C$	20.39 min.	96 keV
Fluorine	$^{18}_{9}F$	109.77 min.	6.366 MeV
Sodium	$^{22}_{11}Na$	2.6 years	0.546 MeV

Table 3.2.3. Most popular sources of fast positrons

A commonly used positron source is ^{22}Na because of its long half-life. The energy spectrum of the emitted positrons has a maximum of about 240 keV (Fig. 3.2.1).

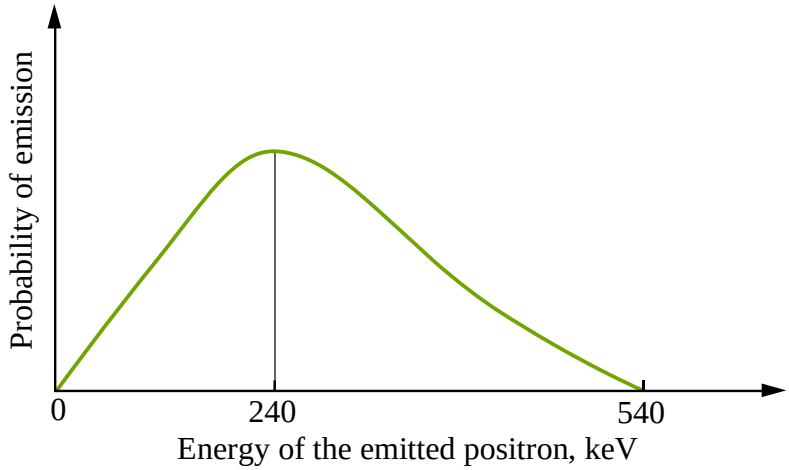

Fig. 3.2.1. Positron energy spectrum of ^{22}Na

3.2.4. Other electron sources

One commonly used device to produce a collimated electron beam with precise energy is the **electron gun** [2]. In it, the primary source of electrons is a heated cathode. The produced free electrons are then accelerated to an anode. The bias voltage between the anode and cathode U_B defines the energy E_e of the thus formed electron beam:

$$E_e = U_B[\text{eV}]. \tag{3.2.2}$$

In addition to its widespread use in electron beam displays, it is often utilized in laboratory-scale experiments.

For specific applications and for high-energy physics investigations, electron (or positron) accelerators are used to receive mono-energetic beams of these particles. The most powerful accelerator of this type was the LEP (Large Positron-Electron) collider at the European Laboratory of Particle Physics at CERN near Geneva. It operated from 1989 until 2000 and accelerated electrons and positrons (in opposite directions in a common tube) up to 209 GeV in the center of mass [3].

References

[1] *Knoll, G. F.* Radiation detection and measurement. Third ed. John Valley & Sons Inc., New York, 2000. https://phyusdb.files.wordpress.com/2013/03/radiationdetectionandmeasurementbyknoll.pdf

[2] Electron gun. https://en.wikipedia.org/wiki/Electron_gun

[3] The Large Electron-Positron collider (LEP). https://en.wikipedia.org/wiki/Large_Electron%E2%80%93Positron_Collider

3.3. Sources of electromagnetic radiation

3.3.1. Electromagnetic radiation

Each electromagnetic radiation is characterized by its frequency ν or respectively by its wavelength λ ($\nu\lambda = c$), where c is the radiation (light) velocity in vacuum. In other media, the velocity of the electromagnetic radiation can be found through the equation $c' = c/n = \nu\lambda/n$, where n is the refractive index of the medium. There is a wide variety of electromagnetic radiation in the universe, which finds different applications, as is shown in Fig. 3.3.1. In this course, attention will be paid mainly to gamma- and X-rays, the origin of which is closely connected with nuclear processes and the interaction of radiation with matter.

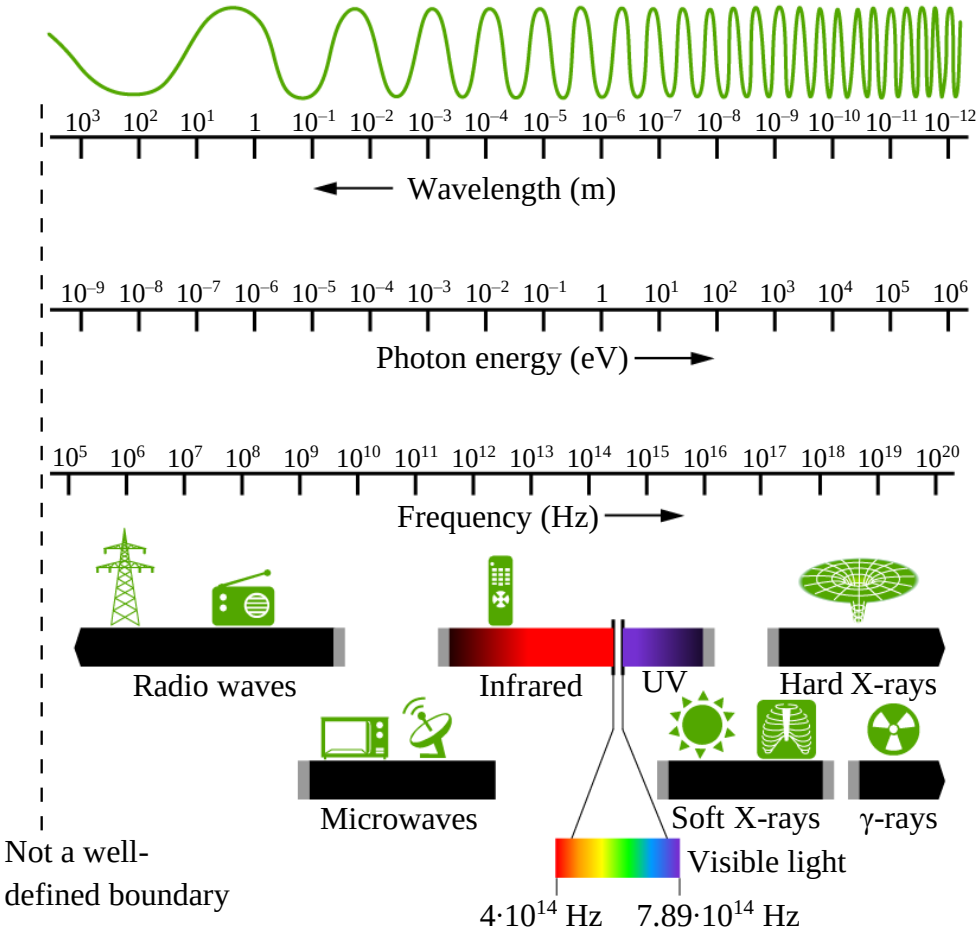

Fig. 3.3.1. Basic characteristics of the electromagnetic radiations in the universe

Electromagnetic radiation propagates as small packets of electromagnetic waves, called **photons**. A photon is one quantum of electromagnetic energy E_{PH}, which can be calculated by the Max Plank equation:

$$E_{PH} = h\nu = \frac{hc}{\lambda}. \tag{3.3.1}$$

Here, h is the Max Plank constant $h = 6.626 \cdot 10^{-34}$ J·s, which is now considered to be a universal constant.

In the Standard Model of particle physics, the photon is considered as a fundamental particle without a rest mass. Nevertheless, an important property of photons is that they carry a momentum P_{PH}, which, for a photon with energy E_{PH}, frequency ν, and wavelength λ, is

$$P_{PH} = \frac{E_{PH}}{c} = \frac{h\nu}{c} = \frac{h}{\lambda}. \tag{3.3.2}$$

When travelling through a medium, the photons interact with the nuclei and electrons of the medium, losing their energy in different ways. These processes will be analyzed in the next Part 4 (see Section 4.3).

The most important processes leading to the emission of electromagnetic radiation are described below.

3.3.2. Radioactive sources of electromagnetic radiation

As was explained in Section 2.3, a nucleus, excited by a previous alpha or beta decay, releases its excess energy through gamma decay, i.e. emitting gamma radiation with very high frequencies – above 10^{19} Hz (see Fig. 3.3.1). There is a large number of gamma radioactive isotopes. Some of them are natural, but most of them are synthetic – produced at nuclear reactors or accelerators. The most commonly used radioactive gamma sources with their energies and half-lives are shown in Table 3.3.1.

The gamma rays from any single nucleus transition are practically mono-energetic with very well defined energies since the energies of nuclear states are predetermined. Common gamma ray sources, based on beta decay, are limited to energy levels below 2.8 MeV. Nuclear reactions can produce gamma sources with higher energy levels, but they have extremely short half-lives. One nuclide that can be useful as a potential source of gamma rays of higher energy is ^{56}Co. This isotope's decay scheme, which includes both electron capture and beta-plus decay, provides a complex spectrum of gamma rays whose energy levels extend to 3.55 MeV [1].

Element	Isotope	$T_{1/2}$	Energy
Sodium	$^{24}_{11}$Na	14.959 hours	1.368 MeV, 2.754 MeV
Strontium	$^{85}_{38}$Sr	64.84 days	514.005 keV
Yttrium	$^{88}_{39}$Y	106.65 days	898.036 keV, 1.836 MeV
Magnesium	$^{54}_{25}$Mg	312.3 days	834.838 keV
Cadmium	$^{109}_{48}$Cd	462.86 days	88.034 keV
Cobalt	$^{60}_{27}$Co	5,271 years	1.173 MeV, 1.332 MeV
Lead	$^{210}_{82}$Pb	22.3 years	46.539 keV
Cesium	$^{137}_{55}$Cs	30.07 years	661.657 keV
Americium	$^{241}_{95}$Am	432.2 years	59.541 keV
Niobium	$^{94}_{41}$Nb	$2.03 \cdot 10^4$ years	765.803 keV

Table 3.3.1. Most commonly used radioactive gamma sources

3.3.3. Bremsstrahlung

When a charged particle is decelerated (receiving a negative acceleration and thereby losing speed) by a Coulomb field, it emits electromagnetic radiation that is called **Bremsstrahlung** (from German: *bremsen* – "to brake", and *Strahlung* – "radiation", i.e., "braking radiation" or "deceleration radiation"). This process is typical for fast electrons moving through a medium where they are decelerated by the electrical field of the atomic nuclei of the medium (Fig. 3.3.2).

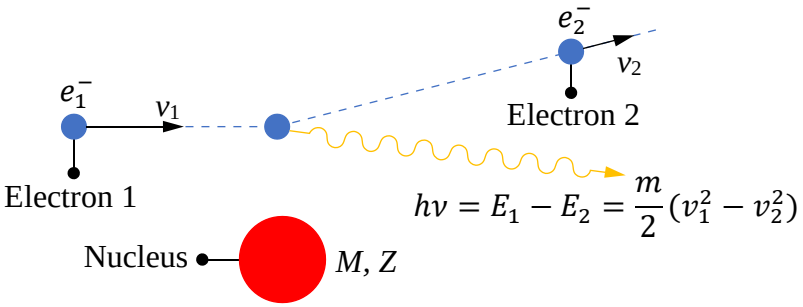

Fig. 3.3.2. Bremsstrahlung emission

In a nonrelativistic case (when the velocity of the electrons is sufficiently lower than the velocity of light so that their mass is not changed), the Bremsstrahlung radiation power P_{BS} can be calculated by

$$P_{BS} = \frac{2q_e^2 Z^2}{3c^3}|\vec{\mathbf{a}}|^2, \tag{3.3.3}$$

where

q_e is the charge of the electron,

Z – the atomic number of the medium (see Section 1.2.4),

c – the light velocity,

$\vec{\mathbf{a}}$ – the deceleration (or acceleration) of the particle.

According to Newton's Law where $\vec{\mathbf{F}} = m\vec{\mathbf{a}}$ (i.e. $\vec{\mathbf{a}} = \vec{\mathbf{F}}/m$), the power of the radiation, and the radiation losses of the particle, respectively, are inversely proportional to the square of its mass ($P_{BS} \sim 1/m^2$). For this reason, Bremsstrahlung is quite significant to light particles like electrons and can be ignored when it comes to heavily charged particles. This equation also shows that the Bremsstrahlung increases with the increase of the medium's atomic number Z.

The Bremsstrahlung consists of X-ray photons with a continuous energy spectrum since there are no quantized energy transitions involved in this process compared to that of the characteristic X-ray (see Fig. 3.3.3 in the next Section).

3.3.4. Characteristic X-rays

When the typical configuration of an atom's orbital electrons is disturbed by an excitation process, the atom may exist in this excited state for a short time only. There is a natural tendency in the electrons to rearrange themselves in order to return the atom to its lowest energy (ground) state. During this transition to the ground state, the excess energy is ejected, emitting an X-ray photon whose energy is equal to the energy difference between the initial and final shells of this electron. For example, if the electron gap is in the K shell, then a characteristic K X-ray is emitted. If the electron comes from the L shell, the emitted photon is marked as K_α, and its energy will be equal to the difference between the binding energies of the L and K shells. Similarly, if the electron comes from the M shell, the energy of the emitted K_β photon will be equal to the difference between the binding energy of the M and K shells, and so on.

One important feature is that all photons of one group have the same energy, and they are therefore called **characteristic X-rays**. The corresponding peaks

(see Fig. 3.3.3) in the energy spectrum are also marked as K_α, K_β and so on. A supplementary feature is that the energy of the characteristic X-ray does not depend on the energy of the exiting source (e.g. of the energy of the incident electrons).

The *K*-series X-rays generally have the most practical significance because their energies are the highest. Their energies regularly increase together with the atomic number of the element and are, for example, about 1 keV for sodium with $Z = 11$, 10 keV for gallium with $Z = 31$, and 100 keV for radium with $Z = 88$. The L-series X-rays do not reach 1 keV until $Z = 28$ and 10 keV at $Z = 74$. Detailed tables containing the precise energies of characteristic X-rays can be found in Ref. [1]. Because the energy of the characteristic X-ray is unique to each individual chemical element, they are commonly used in the elemental analysis of unknown samples – the so-called **Roentgen-Fluorescent Analysis** (**RFA**).

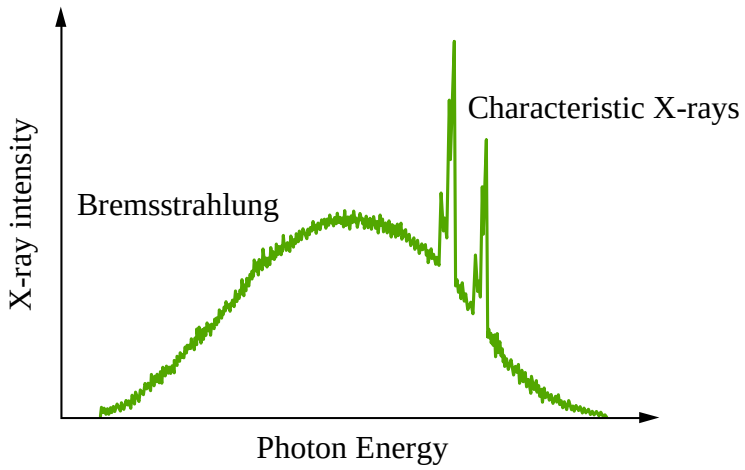

Fig. 3.3.3. A typical spectrum showing Bremsstrahlung continuum and the peaks corresponding to the characteristic X-rays

Very often, both processes – Bremsstrahlung and atom excitation – take place simultaneously. A typical example is the interaction of a target with fast electrons. They have enough energy to generate Bremsstrahlung and knock out the orbital electrons, leaving the atom in an excited state. The result is mixed electromagnetic radiation whose energy spectrum is a superposition of the Bremsstrahlung continuum and the characteristic X-ray peaks (Fig. 3.3.3).

A similar process is used in the Roentgen tubes, where the electrons are emitted from a heated cathode and accelerated to the anode at a very high voltage – 30–50 kV. The anode produces X-rays as a result of both processes – Bremsstrahlung and characteristic X-ray generation. However,

the process has a very low efficiency – only about 1 % of the consumed energy is converted into X-ray energy.

3.3.5. Synchrotron radiation

Another form of radiation is emitted when an electron beam is accelerated in a circular orbit at relativistic velocity. The process is very similar to the Bremsstrahlung emission – both are a result of charged particle acceleration, but under different conditions: Bremsstrahlung is a product of tangential acceleration while synchrotron radiation is produced by centripetal acceleration.

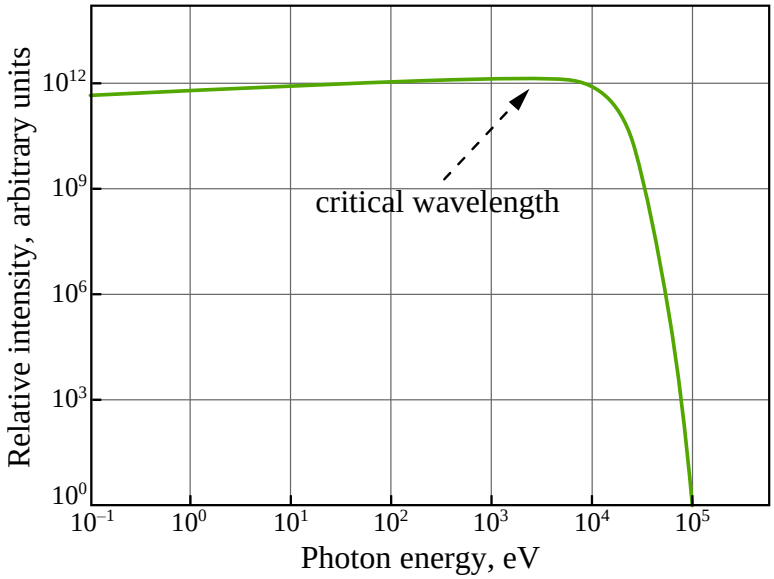

Fig. 3.3.4. An energy spectrum of synchrotron radiation

Over the last few decades, the quality of synchrotron radiation has come to be highly appreciated. When extracted from the accelerator in a tangential direction to the beam orbit, it appears as an intense and highly convergent beam of photons. The spectrum of synchrotron radiation is continuous and extends over a broad energy range – from infrared to hard X-rays. In general, the spectral distribution is smooth with a maximum near the so-called **critical wavelength** (Fig. 3.3.4), which divides the energy carried by the synchrotron radiation into two halves. The only limiting factor of the broad application of synchrotron radiation is the relatively high price of accelerators. Nevertheless, a number of high-energy accelerators, which are dedicated to the production of synchrotron radiation (with a typical electron energy of 500 MeV or more), have since been built.

3.3.6. Annihilation radiation

When a particle interacts with its antiparticle, it results in the **destruction** (**disappearance**) of both particles while simultaneously generating other particles. The most common occurrence of this is the interaction between positrons, resulting from a beta-plus decay, with electrons from the surrounding medium. When the positron energy is very low – towards the end of its range – the positron and an electron destroy one another and are replaced by two oppositely directed 0.511 MeV electromagnetic photons (Fig. 3.3.5.), known as **annihilation radiation**.

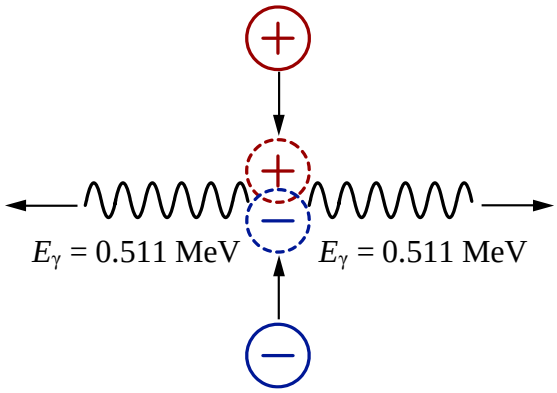

Fig. 3.3.5. Electron-positron annihilation

The minimum number of photons is two, and they move in opposite directions because of the Momentum Conservation Law. According to this law, the emitted photons' total momentum must be equal to that of the total combined momentum of the electron and positron. As was mentioned above, their energies, prior to the annihilation, are very low, and their total momentum is zero. One single photon cannot have momentum equal to zero – a minimum of two is necessary.

The energy of the photons is determined by the Law of the Conservation of Energy. Because the kinetic energies of the positron and the electron are negligible before the annihilation, their common energy is equal to the sum of the rest energies, each of which (following Einstein's famous formula) is $m_e c^2$ = 0.511 MeV. Here, m_e is the rest mass of the electron (equal to that of the positron), and c is the light velocity in a vacuum.

The annihilation radiation is usually superimposed on the gamma radiation, which may be emitted by the subsequent decay of the daughter isotope. For example, during the decay of ^{22}Na, photons of 0.511 MeV as well as of 1.274 MeV energy are emitted from the encapsulated source (annihilation occurs upon interaction with the electrons of the capsule).

The electron-positron annihilation process at low energies is used in a particular type of medical imaging called Positron Emission Tomography or PET. This method produces images by detecting photons that are emitted as a result of the annihilation.

When the positrons and electrons annihilate at very high kinetic energy, other elementary particles can be produced. For example, at the previous CERN collider LEP, the positrons and electrons collided with an energy of about 100 GeV, and another particle besides photons – the so-called *Z*-boson was produced.

3.3.7. Cherenkov radiation

As is mentioned in Section 3.3.1., the velocity of the electromagnetic radiation in any other medium (c') is lower than that in a vacuum (c): $c'=c/n$ where n is the refractive index of the medium. This fact leads to the possibility that a charged high-energy particle, such as an electron, can move at a speed higher than the speed of light in that medium. For example, the speed of light in water is 225 000 km/sec (n = 1.33), and each electron with an energy of more than 290 keV (like most of the beta particles) would have a speed higher than this value.

The most important fact is that such a movement creates a special kind of electromagnetic radiation, and the wavelengths of these photons lie in and around the visible region of the electromagnetic spectrum. This radiation was first observed by Soviet physicist **Pavel Cherenkov** in 1934 and was named after him. Later, this effect was explained by two other Soviet physicists – **Igor Tamm** and **Ilya Frank**. For this discovery and its explanation, the three shared the 1958 Nobel Prize.

The mechanism of Cherenkov radiation is based on the polarization of the atoms in the medium [2]: under the influence of the moving particle's electromagnetic field, the electrons' orbit of the outer atom shells are drawn out, and the electrical balance in the atoms is lost; they are transformed into dipoles (Fig. 3.3.6). After the particle transition, the medium atoms go back to their ground state, emitting electromagnetic radiation. It is important to note that the source of Cherenkov radiation is not the moving particles themselves but the atoms of the medium that were excited by the motion of the particles and then returned to their ground state. At the same time, the energy of the Cherenkov radiation is taken from the particles – they spend it on the polarization of the medium atoms.

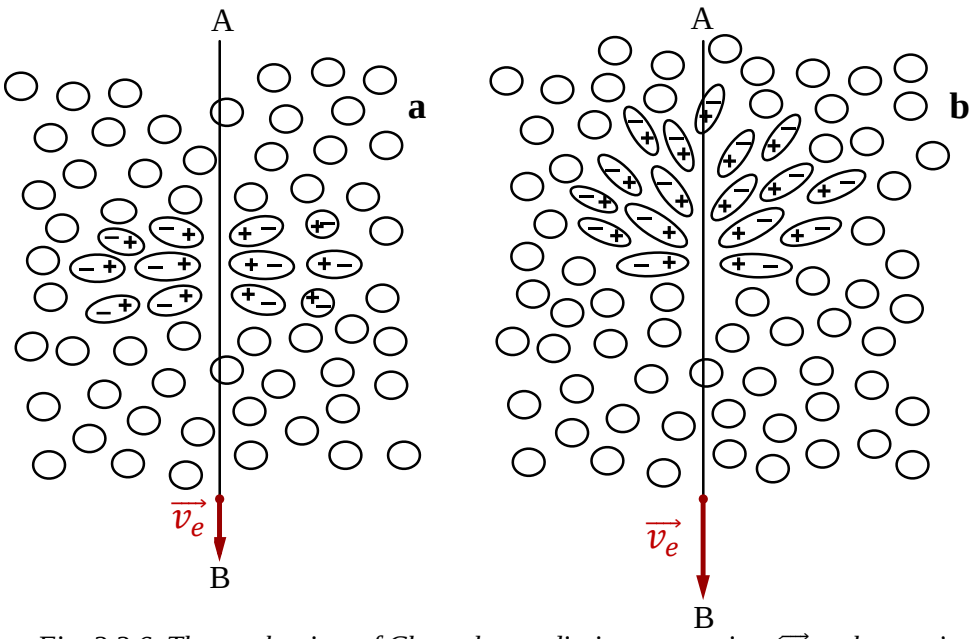

Fig. 3.3.6. The mechanism of Cherenkov radiation generation ($\overrightarrow{v_e}$ – electron's velocity)

What is the role of the particle's speed? When its speed is lower than c', the created polarization has a spherical symmetry (Fig. 3.3.6a) in each moment of time because the particle's electric field polarizes all neighbouring atoms at the same stage (the speed of the electromagnetic momentum transfer in the medium is also equal to c'). As a result, the combined electrical field outside all dipoles will be zero, and the photon emissions of the individual atoms will cancel each other out.

When $|\overrightarrow{v_e}| > c'$, the atom's polarization is delayed, and more of the dipoles are oriented in the direction of the particle's movement (Fig. 3.3.6b). In this case, the combined electrical field outside the dipoles is not zero, and the individual atom radiations are directed forward. Thus, they form a conical wavefront, which is observed as Cherenkov radiation.

The front of the Cherenkov radiation propagation can be found using the Huygens principle [3] – it is the envelope of the spherical waves emitted by individual dipoles at each point of the particle trajectory. Fig. 3.3.7A shows an instance where $\upsilon < c'$ ($\beta = \upsilon/c$), in which case the spherical light waves emitted by the electron along its trajectory do not catch up and intersect with one another. Therefore, no Cherenkov radiation is generated. Conversely, when $\upsilon > c'$, these waves will cross each other, and their common tangent shell forms the conical wavefront of the Cherenkov radiation (Fig. 3.3.7B).

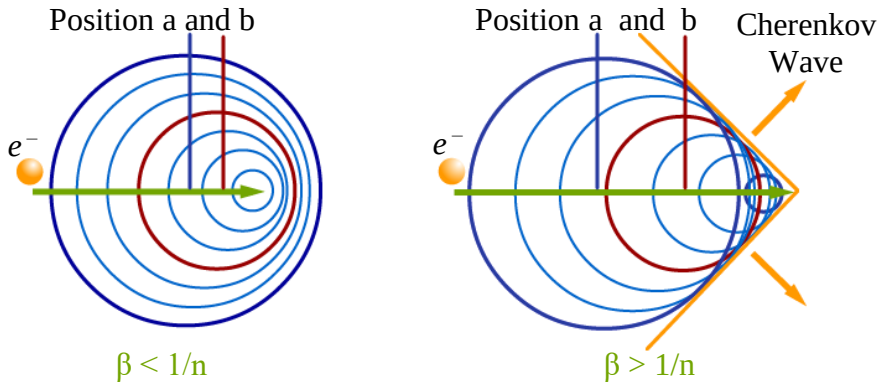

A. Electron slower than light B. Electron faster than light

Fig. 3.3.7. When the electrons move slower than the speed of light (Fig. A), the spherical light wave emitted in position (b) does not catch up with the one emitted previously in position (a). When the electron moves faster than the speed of light (Fig. B), the spherical waves catch up, generating a conical wavefront, which follows the electron

The angle of the radiation propagation (θ, Fig. 3.3.8) can be calculated using the fact that $AB = \upsilon t$, $AC = c't$ (t is the duration of the particle propagation). Therefore, the corresponding geometric equation is

$$\cos\theta = \sin\varphi = AC/AB. \tag{3.3.4}$$

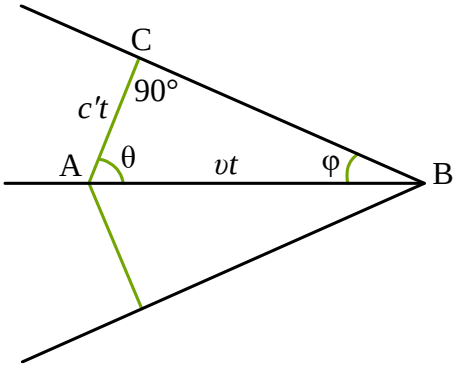

Fig. 3.3.8. Propagation angle of Cherenkov radiation

The result is

$$\cos\theta = \frac{c't}{\upsilon t} = \frac{c/v}{n} = \frac{1}{n\beta}, \tag{3.3.5}$$

where $\beta = \upsilon/c$ is the relative velocity of the particle. Because $\cos\theta \leq 1$ in the cone, the threshold of the particle's relative speed, under which there will be

no Cherenkov radiation, is $\beta_{min} = 1/n$, i.e. $\upsilon_{min} = c'$. This result confirms the origin of Cherenkov radiation.

The minimum particle energy necessary to create Cherenkov radiation can be calculated using the relativistic equation for kinetic energy [4]

$$E_{P_{\min}} = m_0 c^2 \left(\frac{1}{\sqrt{1 - \beta_{\min}^2}} - 1 \right), \tag{3.3.6}$$

where m_0c^2 is the rest energy of the particle.

For example, in water (n = 1.33, β_{min} = 0.75), the minimum energy of electrons and positrons (with m_0c^2 = 0.511 MeV) is relatively low – only 289 keV. At the same time, the minimum energy of protons (with m_0c^2 = 938 MeV) is much higher – 539 MeV.

The energy loss of the charged particles due to the Cherenkov radiation is relatively low. However, this radiation is very important for registering fast particles and determining their movement velocities and directions.

References

[1] *Knoll, G. F.* Radiation detection and measurement. Third ed. John Valley & Sons Inc., New York, 2000. https://phyusdb.files.wordpress.com/2013/03/radiationdetectionandmeasurementbyknoll.pdf

[2] Cherenkov Effect. http://www.radioactivity.eu.com/site/pages/Cherenkov_Effect.htm

[3] Huygens Principle. http://hyperphysics.phy-astr.gsu.edu/hbase/phyopt/huygen.html

[4] The Large Electron-Positron collider (LEP). https://en.wikipedia.org/wiki/Large_Electron%E2%80%93Positron_Collider

3.4. Sources of neutrons

As will be made clear further on, neutrons have many important and useful applications. However, there are no natural sources of neutrons since no neutron emissions take place during the most common radioactive decays (alpha, beta, and gamma). For this reason, other more complex and more expensive neutron sources have been created and are in use.

3.4.1. Spontaneous fission

Many transuranic heavy elements have isotopes with a considerably high probability of spontaneous fission (see Section 2.4.1). They can be used as the simplest neutron source since several fast neutrons are emitted during each instance of spontaneous fission. However, other products are emitted along with the neutrons: fission fragments, prompt gamma rays, as well as beta and gamma radiation from the fragments. For this reason, the isotope used as a neutron source has to be very well encapsulated in a thick container in order to emit only neutrons and gamma photons.

The most commonly used neutron source of this type is californium-252 ($^{252}_{98}$Cf). Its half-life is 2.65 years, which is very convenient for such a source, and it is one of the most widely produced of all transuranic elements. Californium-252 undergoes alpha decay 96.9% of the time to form curium-248 ($^{248}_{96}$Cm) while the remaining 3.1 % of decays are spontaneous fission.

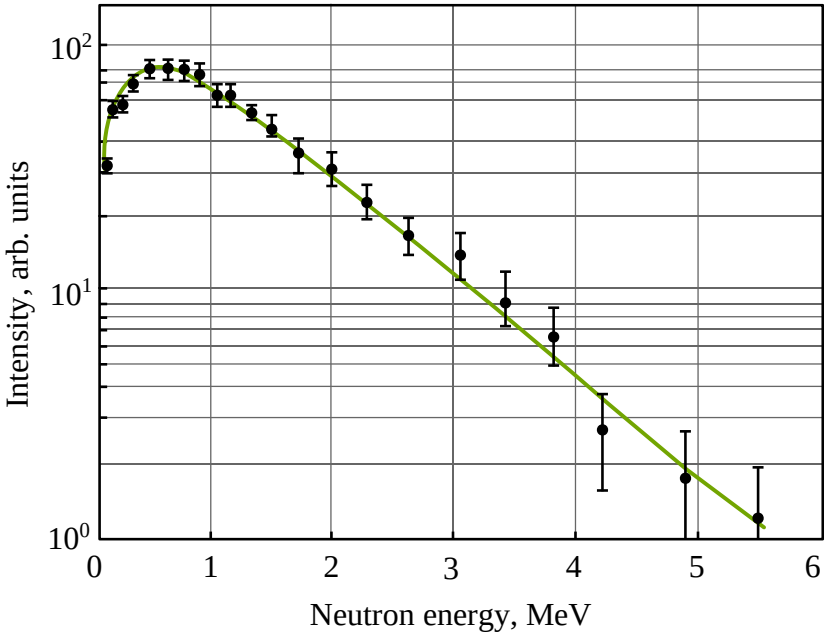

Fig. 3.4.1. The neutron energy spectrum of californium-252

The latter produces about 4 neutrons per fission, or 0.116 n/s per 1 Bq of total activity (alpha and spontaneous fission decays). One microgram of californium-252 emits $2.3 \cdot 10^6$ n/s, which creates the possibility to produce very compact neutron sources – the dimensions are limited only by the container used. The emitted neutrons' energy spectrum ranges from zero to several MeV, with a peak between 0.5 and 1 MeV (Fig. 3.4.1) and an average energy level of 2.1 MeV. At each instance of fission, excluding the neutron emissions, an average of 9.7 gamma photons are also emitted. Fortunately, their intensity is an order of magnitude lower than that of the neutrons. Therefore, they will not cause significant problems for applications requiring a moderately clean neutron flux.

No practical applications have been found for the other transuranic isotopes that also undergo spontaneous fission because of their short half-life or due to very rare instances of fission.

3.4.2. Radioisotope α,n-sources

This type of neutron source utilizes the so-called α,n-nuclear reaction – emission of neutrons resulting from alpha-particle irradiation. Because there are many alpha sources, mixing one of them with a suitable target gives rise to the possibility of fabricating composite neutron sources that are compact and very convenient for laboratory experiments and many other applications. Several different materials can be used as a target, but the maximum neutron yield is achieved with a beryllium target irradiated by alpha particles:

$$^{4}_{2}\alpha + {}^{9}_{4}\mathrm{Be} \rightarrow {}^{12}_{6}\mathrm{C} + {}^{1}_{0}n + 5.71\ \mathrm{MeV}. \qquad (3.4.1)$$

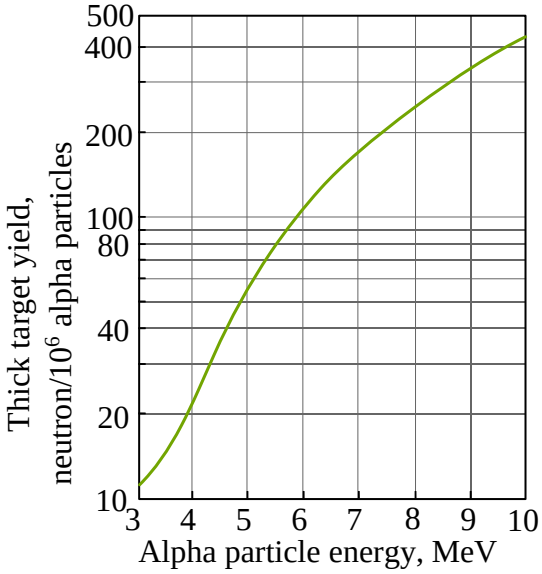

Fig. 3.4.2. The neutron yield of a thick beryllium target

The neutron yield of this reaction depends on the alpha particle energy (Fig. 3.4.2) [1]. Most of the alpha particles stop in the beryllium, and only 1 of about 10^4 particles interacts with a target nucleus.

The most suitable alpha sources are actinide metals. Besides their relatively high specific activity, another important feature is the possibility to form a stable alloy with beryllium. Therefore, neutron sources, which are prepared in this form, have high mechanical stability. In addition, each alpha particle can interact directly with the beryllium nuclei without any intermediate energy loss.

The most commonly used alpha sources combined with a beryllium target are shown in Table (3.4.1) [1]. In the beginning, the preferred neutron source was radium-226 ($^{226}_{88}$Ra/Be) because of radium availability. However, currently, the most commonly used source is plutonium-239 ($^{239}_{94}$Pu/Be) because radium-226 has a long chain of daughter isotopes that increases the gamma background.

Source	$T_{1/2}$	E_α **MeV**	**Neutron yield per 10^6 primary α-particles**		**Percent yield with E_n < 1,5 MeV**	
			Calculated	**Experimental**	**Calculated**	**Experimental**
$^{210}_{84}$Po/Be	138 d	5.30	73	69	13	12
$^{242}_{96}$Cm/Be	162 d	6.10	118	106	22	26
$^{244}_{96}$Cm/Be	18 y	5.79	100	–	18	29
$^{238}_{94}$Pu/Be	87.4 y	5.48	79	–	–	–
$^{241}_{95}$Am/Be	433 y	5.48	82	70	14	15–23
$^{226}_{88}$Ra/Be + daughters	1602 years	Mul-tiple	502	–	26	33–38
$^{239}_{94}$Pu/Be	24000 years	5.14	65	57	11	9–33

Table 3.4.1. Neutron sources using beryllium irradiated by an alpha source

A disadvantage of plutonium-239 is its very long half-life (low specific activity). For this reason, the neutron sources using it are bigger – a source in a corpus with a volume of 1 cm^3 and has a maximum neutron flux[1] of around

[1] In this course, the quantity **flux** is defined as the transfer rate of particles or photons through a unit area [number of particles·m^{-2}s^{-1}].

10^7 n/s. For higher neutron yield, sources with americium-241 or plutonium-238 are also widely used. A very convenient alpha source is curium ($^{244}_{96}$Cm) but its production is very limited.

The neutron energy spectra of all these alpha-neutron sources are similar. They cover a range of between a few hundred keV to 10 MeV with decreasing intensity. The spectra are irregular (they contain many peaks and valleys) because of the different alpha particle energy losses before the start of the α,*n* reaction and the neutron scattering in the beryllium.

Relatively large quantities of the radioactive isotope are involved in these neutron sources. Therefore, special precautions have to be taken to ensure that the material will remain safely encapsulated. Usually, the actinide-beryllium alloy is sealed into two individually welded stainless steel cylinders (Fig. 3.4.3). A small amount of free volume has to be left in the inner cylinder to accommodate the slow evolution of helium gas when alpha particles are neutralized at the end of their range in the beryllium.

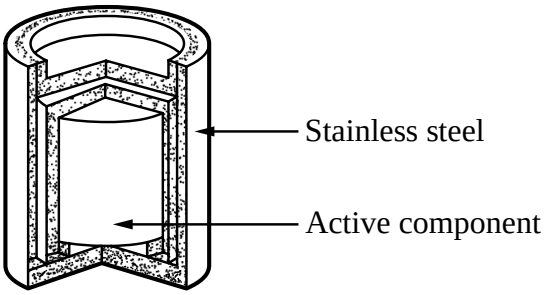

Fig. 3.4.3. A typical double-walled construction of an alpha/beryllium neutron source

3.4.3. Photo-neutron sources

A gamma-ray emitting radioisotope in combination with an appropriate target material can also be used to produce neutrons. Such a photo-neutron source uses a γ,*n* reaction in which a gamma-ray photon is absorbed by a target nucleus, supplying it with enough excitation energy for the emission of one free neutron. Only two target materials – beryllium-9 and deuterium – are practically suitable for this type of neutron source. The corresponding reactions are

$$h\gamma + {}^{9}_{4}\mathrm{Be} \rightarrow {}^{8}_{4}\mathrm{Be} + {}^{1}_{0}n - 1.666\ \mathrm{MeV}, \qquad (3.4.2)$$

$$h\gamma + {}^{2}_{1}\mathrm{H} \rightarrow {}^{1}_{1}\mathrm{H} + {}^{1}_{0}n - 1.226\ \mathrm{MeV}. \qquad (3.4.3)$$

Because both reactions need supplementary energy, only relatively high-energy gamma-ray isotopes can be used.

An essential advantage of photo-neutron sources is that if the gamma rays are mono-energetic, the emitted neutrons are also nearly mono-energetic. For large sources, the spectrum can be somewhat degraded by the scattering of some neutrons in the target before their emission.

A considerable disadvantage of these sources is that gamma-ray radioisotopes of very high activity are necessary to create moderate-intensity neutron sources. Normally, one of 10^5 to 10^6 gamma photons enters in a γ,n reaction. Therefore, the used gamma-ray sources have short half-lives, and the neutron emission appears in a high gamma-ray background.

3.4.4. Nuclear reactors

Nuclear reactors are the largest producer of neutrons. Their source is neutron-induced fission reactions:

$$^{235}_{92}\mathrm{U} + n \rightarrow FF_1 + FF_2 + (2-3)n, \qquad (3.4.4)$$

where FF_i indicates the fission fragments (see Section 2.4). Although most of these neutrons are used to induce further fission reactions, a sufficient number of them escapes the active reactor zone and can be used for different purposes. Their most common application is to irradiate different materials in order to create synthetic radioactive isotopes.

3.4.5. Spallation sources

Spallation [2] is a violent reaction in which very high energy particles bombard a target. The incident particle, such as a proton, disintegrates the nucleus through inelastic interactions (see Section 4.1.6). The result is an emission of protons, neutrons, α-particles, and other light and heavy particles. The neutrons produced in such a reaction can be separated and used in other experiments. A general spallation reaction with a proton as the incident particle can generally be written as

$$p + ST \rightarrow SF_1 + SF_2 + \ldots + SF_m + (k)n, \qquad (3.4.5)$$

where ST is the spallation target, and SF_i represents the spallation fragments. The number of neutrons produced in this reaction (k) depends on the type of target and the energy level of the incident particle.

The targets used in spallation sources are generally high Z materials, such as lead, tungsten, silver, or bismuth. However, it is also possible to generate neutrons by bombarding light elements with high energy protons. Two examples of such reactions are the production of neutrons by bombarding lithium-7 and beryllium-9 targets:

$$p + {}^{7}_{3}\mathrm{Li} \rightarrow {}^{7}_{4}\mathrm{Be} + n \quad \text{and} \quad p + {}^{9}_{4}\mathrm{Be} \rightarrow {}^{9}_{5}\mathrm{B} + n. \qquad (3.4.6)$$

These interactions are closer to nuclear reactions than to spallation ones since they do not involve the breakup of the target nuclei into several fragments.

A significant advantage of spallation sources is that they produce neutrons with a broad spectrum of energies ranging from a few eV to several GeV. Another advantage is their ability to generate neutrons continuously or in short pulses. The pulses could be as short as a nanosecond.

The most important problem is the necessity of a very expensive accelerator. Nevertheless, there are a few operating spallation accelerators in the world, such as SINQ [3] in Switzerland (1996), JSNS [4] in Japan (2008), and SNS [5] in the USA (2006). A European Spallation Source (ESS) [6] research facility is under construction in Sweden (expected to be operational in 2023).

References

[1] *Knoll, G. F.* Radiation detection and measurement. Third ed. John Valley & Sons Inc., New York, 2000. https://phyusdb.files.wordpress.com/2013/03/radiationdetectionandmeasurementbyknoll.pdf

[2] Spallation Neutron Source. https://en.wikipedia.org/wiki/Spallation_Neutron_Source

[3] SINQ: The Swiss Spallation Neutron Source. https://www.psi.ch/sinq/

[4] Japan Spallation Neutron Source (JSNS) of J-PARC. https://www.tandfonline.com/doi/abs/10.1080/10506890903405316

[5] Spallation Neutron Source (SNS). https://science.energy.gov/bes/suf/user-facilities/neutron-scattering-facilities/sns/

[6] European Spallation Source (ESS). https://europeanspallationsource.se/about

PART 4. INTERACTION OF RADIATION WITH MATTER

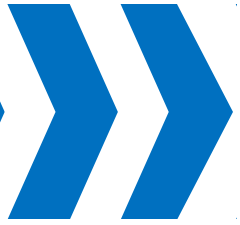

4.0. Introduction

In the previous part, the sources of the most important types of radiation were described. Knowledge about their interactions with different materials[1] is very important. The only way to detect and measure the properties of each type of radiation is to make it interact with some material and to study the resulting change in the system configuration. In fact, each radiation detector uses some form of radiation interaction to generate a measurable signal. This signal is then used to evaluate certain radiation properties.

Every type of radiation carries some energy with it and is, therefore, capable of exerting force on other particles through processes called **radiation interactions**. These interactions may or may not change the states and properties of the particles involved. The way radiation interacts with matter depends on the types of incidents and target objects as well as on their properties, such as charge, energy and momentum. The basic interaction process is clearly understood through quantum mechanics, quantum electrodynamics and quantum chromodynamics. However, in this course, we shall limit the description of the radiation interactions to their gross properties and basic physics relations.

To this end, it is necessary first to introduce some basic concepts, laws and definitions, which will be given in section 4.1.

For a detailed analysis of the interaction processes, the radiation types will be grouped in the same way as in part 2 – separated into four groups, as shown in Table 4.0.1 [1].

Charged Particle Radiation		**Uncharged Radiation**
Heavy charged particles	←	Neutrons
Fast electrons and positrons	←	X-rays and gamma rays

Table 4.0.1. Different radiation groups

The left column includes the radiation types that, due to each individual particle's electric charge, constantly interact through the Coulomb force with the electrons and nuclei present in every material they pass through.

The types of radiation in the right column are uncharged, and therefore they are not subject to the Coulomb force. However, each interaction of these particles or photons is catastrophic – it radically alters the properties of the incident object. In all instances, the interaction results in a full or partial

[1] In this course, the terms material, medium or absorber will be used for matter in which the radiation is propagating and interacting.

transfer of a particle's energy to the electron or nucleus of the constituent atom or to the charged particle products of the nuclear reaction. Another important feature of these types of radiation is that if such an interaction does not occur, the particle passes through the material without leaving a trace.

The horizontal arrows in the table show the result of such catastrophic interactions. An X- or gamma photon transfers all or part of its energy to the electrons within the material. The resulting secondary electron is very similar to the fast electrons of beta radiation. In contrast, the neutron interactions take place with the material nuclei and result in heavy charged particles, which then produce a detection signal.

The interaction processes of these four groups of radiation will be analyzed in sections 4.2 to 4.5.

References

[1] *Knoll, G.F*. Radiation detection and measurement. Third ed. John Valley & Sons Inc., New York, 2000. https://phyusdb.files.wordpress.com/2013/03/radiationdetectionandmeasurementbyknoll.pdf

4.1. Basic concepts, laws and definitions

4.1.1. Radiation flux and intensity

A **radiation flux** is defined [1] as the number of particles (or quanta) passing through a unit area within a unit of time. It is a basic parameter that characterizes the radiation's strength. The radiation is often isotropic, and its source can be considered as a point source (for example, like most of the radioactive sources). In such a case, at a distance r from the source, the surface S will be spherical, and the flux, namely –

$$\Phi = n/S = n/4\pi r^2 \, [s^{-1}m^{-2}], \tag{4.1.1}$$

where n is the number of particles irradiated by the source in a unit of time (i.e. the activity of the radioactive source). This relation is known as the **Inverse Square Law**, indicating that the strength of radiation decreases with the square of the distance to the source. The inverse square law plays an important role in radiation protection: it determines the minimum safe distance between the radiation source and the people working with it.

Although all actual radioactive sources are not necessarily point sources, this law can be used whenever the dimensions of the source can be overlooked compared to the distance r. When the radiation is anisotropic, a differential relation for the flux should be used:

$$\Phi = dn/dS. \tag{4.1.1a}$$

Another important consideration is that this law is valid only when the radiation passes through a medium in which there is no considerable absorption or scattering of the particles, such as in a vacuum or low-pressure gases. In other cases, the flux will decrease more rapidly than r^2.

A second important quantity characterizing the radiation flow (beam) is the flux of energy – the amount of energy transferred by the radiation per unit area per second at a certain distance r from the source, which is called **radiation intensity** (***J***). For mono-energetic radiation with an energy E:

$$J = \Phi E = nE/S = nE/4\pi r^2 \, [\text{Joule}\cdot s^{-1}m^{-1}]. \tag{4.1.2}$$

4.1.2. Cross-section

According to quantum mechanics, the interaction of radiation with matter is a random process. The cross-section is a quantity representing the probability of interaction. It shows how likely it is for a particle to interact with another one in a certain way. Mathematically, it is defined as per the below.

Suppose there is a beam of particles with a flux Φ flowing into a target. After interacting with the target, some of the beam particles get scattered. Suppose

a detector is able to count the average number of particles per unit of time (dn) that get scattered per unit of solid angle ($d\Omega$). This average quantity divided by the flux of incident particles is defined as the differential cross-section:

$$\frac{d\sigma}{d\Omega}(E,\Omega) = \frac{1}{\Phi}\frac{dn}{d\Omega}, \tag{4.1.3}$$

where σ is the cross-section and E is the energy of the incident particles.

The differential cross-section can be integrated to find the total cross-section at a specific energy E:

$$\sigma(E) = \int \frac{d\sigma}{d\Omega} d\Omega. \tag{4.1.4}$$

The conventional unit of the cross-section is **barn** (**b**), with 1 b = 10^{-24} cm^2.

4.1.3. Radiation length

Radiation length is a quantity that characterizes the overall energy losses of electrons and photons when passing through matter. It can be defined as the thickness of a material, passing through which an electron (or photon) loses $1 - 1/e$ (corresponding to about 63 %) of its energy by bremsstrahlung (or pair production). Radiation length is widely used because it relates the physical dimensions of the material (such as its depth) to a property of radiation (such as its rate of energy loss) and is usually represented by the symbol X_0.

The most commonly used semi-empirical equation to calculate the radiation length of electrons is [2]:

$$\frac{1}{X_0} = 4\alpha r_e^2 \frac{N_A}{A}\{Z^2[L_{rad} - f(Z)] + ZL'_{rad}\}. \tag{4.1.5}$$

Here, α = 1/137 is the electron fine-structure constant; r_e = 2.8179·10^{-13} cm is the classical electron radius; N_A = 6.022·10^{23} mole^{-1} is the Avogadro's number; Z and A are the atomic and mass numbers of the material element, respectively; and $f(Z)$ is a function which, for elements up to uranium, can be calculated using:

$$f(Z) = a^2[(1 + a^2)^{-1} + 0.20206 - -0.0369a^2 + \\ + 0.0083a^4 - 0.002a^6], \tag{4.1.6}$$

where $a = \alpha Z$. The values or functions of L_{rad} and L'_{rad} are given in Table 4.1.1.

Element	Z	L_{rad}	L'_{rad}
H	1	5.31	6.144
He	2	4.79	5.621
Li	3	4.74	5.805
Be	4	4.71	5.924
Others	> 4	ln (184.15$Z^{-1/3}$)	ln (1194$Z^{-2/3}$)

Table 4.1.1. Values or functions of L_{rad} and L'_{rad}

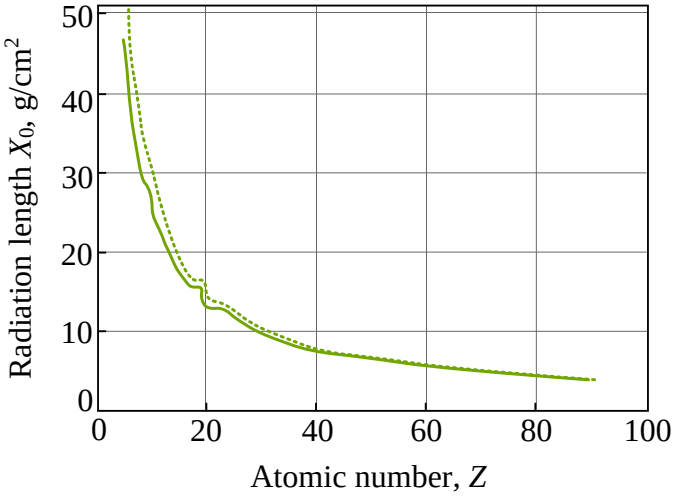

Fig. 4.1.1. Radiation length as a function of Z

The values of the radiation length as a function of Z calculated by the above equation are shown in Fig. 4.1.1 (the solid line). The values of X_0 are in units of g/cm^2, and they can be divided by the density of the material ρ [g/cm^3] to find the length in cm. The dashed line represents the X_0 values calculated with $L'_{\mathrm{rad}} = 0$. The results show that for $Z > 20$, the error, in this specific case, is lower than 5 % [2].

When the absorber is a mixture or compound, the effective radiation length can be calculated by taking the weighted mean

$$\frac{1}{X_0} = \sum \frac{w_i}{X_{0i}}, \tag{4.1.7}$$

where w_i and X_{0i} correspond to the fraction by weight and radiation length of the i^{th} material.

4.1.4. Conservation laws

Many of our readers are probably familiar with some of the conservation laws. Nevertheless, a few of them, which are important for interaction processes, will be considered here.

- **Conservation of Energy**

  This law states that the total energy of an isolated system always remains constant – it is said to be conserved over time. Here, the term isolated system means that external forces do not influence it. The last condition is relative and depends on the accuracy of the result desired. For example, one cannot escape the background electromagnetic field, which is present everywhere. However, its strength is so weak at the point of collision between two microscopic particles that it can safely be ignored for most practical purposes. At the fundamental level, the law of conservation of energy ensures that temporal translations do not violate the laws of nature. As mentioned in Part 1, mass and energy are bound up with Einstein's relation $E = mc^2$, which ensures that it is neither possible to destroy mass or energy nor is it possible to create them from nothing.

  Following this relation, each massive particle has an intrinsic energy content called **rest energy** to signify the amount of energy the particle contains when at rest. For particle interactions, it has been found that the sum of the rest energy and the kinetic energy of a closed system remains constant:

$$E_{rest} + E_{kin} = const. \tag{4.1.8}$$

  Here, E_{rest} is the total rest energy of all particles at any instant in time, and E_{kin} represents the total kinetic energy of these particles at the same instant in time.

- **Conservation of momentum**

  Both linear and angular momenta are conserved for any system not subject to external forces. For linear momentum, this law states that the total linear momentum of a closed system remains constant. It represents the fact that the laws of physics are the same at all locations in space. This law, together with the law of conservation of energy, is extensively used to determine the kinematic variables related to particle collisions.

  Linear momentum is a vector quantity, and a vector sum must be taken. In the case of a collision between particles, this law requires that

$$\sum \vec{\mathbf{P}}_i = \sum \vec{\mathbf{P}}_f, \tag{4.1.9}$$

where $\vec{\mathbf{P}}$ is the momentum. The subscripts *i* and *f* stand for the initial and final states of the system (such as before and after collision), and the vector sum is carried over all moving particles taking part in the collision.

Conservation of angular momentum ensures that there are no preferred directions; that is, the space is isotropic, and the laws of physics are the same in all directions.

- **Conservation of electrical charge**

The law of charge conservation states that the electrical charge can neither be created nor destroyed. It means that the change in charge in any volume of space is exactly equal to the amount of charge flowing into the volume minus the amount of charge flowing out of the volume. Mathematically, the law can be represented as a continuity equation

$$Q(t_1) = Q(t_2) + Q_{IN} - Q_{OUT}, \tag{4.1.10}$$

where $Q(t_i)$ is the quantity of electric charge in a specific volume at time t_i, Q_{IN} is the amount of charge flowing into the volume between time t_1 and t_2, and Q_{OUT} is the amount of charge flowing out of the volume during the same period of time.

For nuclear particles, this law also means that the unit charge can neither be created nor destroyed. But there is a fundamental difference between the negative unit charge carrier – the electron, and the positive unit charge carrier – the proton. The electron has no internal structure and therefore is an actual unit charge carrier. On the other hand, the proton is composed of three quarks, each carrying a fractional charge. The total charge is a unit charge, but internally the charge is divided between the proton constituents. A neutron is also composed of three quarks but in such a way that the fractional charges of these quarks cancel each-other out while the net charge on the neutron itself appears to be zero.

This law permits the elimination of some reactions. For example, the next beta-type decay is impossible:

$$n \rightarrow e + \gamma, \tag{4.1.11}$$

because it would imply the creation of a unit electrical charge. The correct reaction is

$$n \rightarrow p + e + \bar{\nu}, \tag{4.1.12}$$

where the sum of the charges on each side of the reaction is zero (*n* and *p* are a neutron and a proton, respectively).

4.1.5. Elastic interaction

Elastic interaction is a process in which an incident particle interacts with a target in such a way that the total kinetic energy of the system remains constant. It does not mean that there is no energy transfer between incident and target particles. Normally, the incident particle loses some of its kinetic energy and transfers it to the target. However, this energy only increases the kinetic energy of the target without changing its internal state, i.e. it does not start any target excitation process. The best practical model of an elastic interaction is the collision between two billiard balls – the incident ball transfers a part of its kinetic energy to the target ball without causing any deformation.

4.1.6. Inelastic interaction

In an inelastic interaction, a part of the energy that is transferred from the incident particle to the target is spent to change the internal state of the target, most often to cause an excitation process. For this reason, the sum of the kinetic energies of both objects after the interaction is smaller than it was before the interaction. However, the total energy of the system remains constant (in accordance with the energy conservation law).

References

[1] Flux vs Fluence. https://www.physicsforums.com/threads/flux-vs-fluence.196240/.

[2] *Ahmed, S. N.* Physics and Engineering of Radiation Detectors. Academic Press Inc., Elsevier, 2007. https://www.elsevier.com/books/physics-and-engineering-of-radiation-detection/ahmed/978-0-12-045581-2

4.2. Interaction of heavy charged particles with matter

While moving within matter, all particles interact with surrounding atoms (atomic nuclei and electrons). These interactions depend on the particle type, charge, and energy, as well as on the properties of the environment material. Nevertheless, the particle transfers a part of its energy to the medium at each interaction, which determines the so-called **particle energy loss**.

4.2.1. Ionization energy loss

When a charged particle passes through matter due to the Coulomb force, it interacts inelastically with the electrons of the atoms of the matter. The result is atom excitation or ionization. Excitation raises an electron to a higher energy shell, whereas ionization completely removes the electron from the atom. Ionization creates an ion pair, which consists of the (now) free electron and the positively charged atom from which this electron was removed. Some of the freed electrons may possess sufficient kinetic energy to cause further ionization events (such energetic electrons are called **delta electrons** or **delta rays**).

In both cases, the particle transfers part of its own energy to the electrons, and this energy loss is called **ionization loss**.

We have to find the relation between particle properties, environmental properties, and the value of the ionization loss. For this purpose, we will study the interaction between an atom's electron with a charge q_e and a mass m_e within the medium, and a particle with a charge zq_e and a mass $m_p >> m_e$. This particle moves in a straight line with a velocity v that is higher than the speed of rotation of the electron in the atom, and it passes at a minimum distance b from the electron (Fig. 4.2.1).

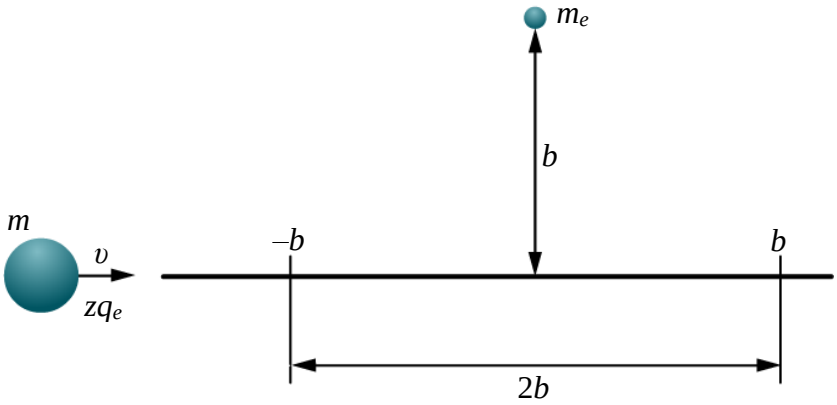

Fig. 4.2.1. Interaction of the passing particle with an atom's electron

The maximum force F_C of the Coulomb interaction between the particle and the electron at the moment of the closest approach is proportional to the product of both charges and inversely proportional to the distance square:

$$F_C \approx \frac{zq_e^2}{b^2}. \tag{4.2.1}$$

Taking into account that the particle interacts only at a small distance from the atom's electron (from $-b$ to b in Fig. 3.2.1), we can estimate the characteristic time of interaction:

$$\Delta t \approx \frac{2b}{v}. \tag{4.2.2}$$

Passing along the atom's electron, the particle transfers part of its own momentum to it:

$$\Delta p = F_C(b)\Delta t \approx \frac{2zq_e^2}{vb}, \tag{4.2.3}$$

and the kinetic energy of the electron becomes

$$\Delta E = \frac{\Delta p^2}{2m_e} \approx \frac{2z^2q_e^4}{m_e v^2 b^2}. \tag{4.2.4}$$

This energy is the exact energy loss of the charged particle at each act of interaction with an atom's electron.

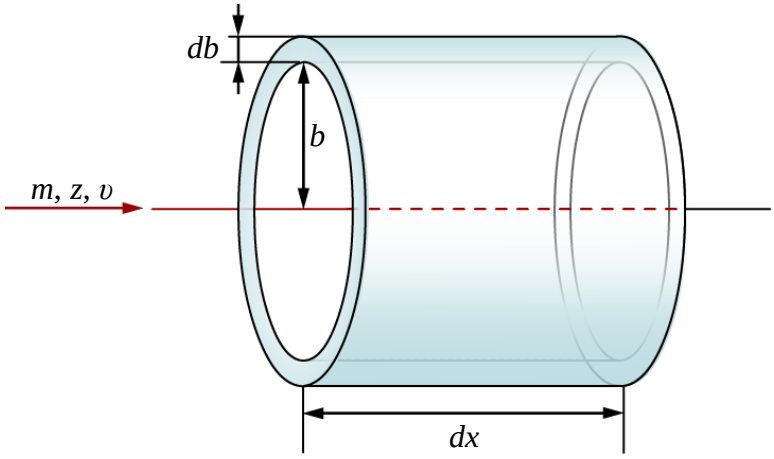

Fig. 4.2.2. Interaction of the passing particle with the atom's electrons of the environment

The environment consists of a large number of atoms, which can have different numbers of electrons. Let's study an environment layer with a radius *b*, a thickness *db*, and a length *dx* (Fig. 4.2.2). Its volume *V* is equal to

$$V = 2\pi b \cdot db \cdot dx. \tag{4.2.5}$$

The number of electrons in the chosen layer is

$$N = Vn_e. \tag{4.2.6}$$

where n_e is the electron density of the environment.

The total loss of energy in the layer is equal to the product of the energy loss ΔE and the number of electrons N:

$$dE = N\Delta E = -\frac{4\pi n_e z^2 q_e^4}{m_e v^2}\frac{db}{b}dx. \tag{4.2.7}$$

Then, the energy loss per unit distance in a db layer is

$$-\frac{dE}{dx}(b) = \frac{4\pi n_e z^2 q_e^4}{m_e v^2}\frac{db}{b} \tag{4.2.8}$$

(the minus sign shows that the particle energy decreases).

Integrating over b from $b_{\min}$ to $b_{\max}$, we will obtain the value of the total amount of energy lost by the particles at a distance of dx. It is called **specific ionization loss** or, more often – **stopping power**:

$$-\frac{dE}{dx} = \int_{b_{\min}}^{b_{\max}} \frac{dE}{dx}(b) = \frac{4\pi n_e z^2 q_e^4}{m_e v^2} \ln\frac{b_{\max}}{b_{\min}}. \tag{4.2.9}$$

Here, the integral is evaluated from minimum to maximum of the impact parameter b since integrating from 0 to ∞ would yield a divergent solution. But the transmitted kinetic energy is also limited to a certain range:

- the minimum transferred kinetic energy is approximately equal to the binding energy of an electron in an atom;
- the maximum value of the transferred kinetic energy can be determined by considering the kinematics of the scattering of a particle by an electron; it can be shown that in a non-relativistic case, it is

$$\frac{dE_{max}}{dx} = -2m_e v, \tag{4.2.10}$$

and in a relativistic case

$$\frac{dE_{max}}{dx} = -2m_e v\left(1 - \frac{v^2}{c^2}\right). \tag{4.2.10a}$$

Bethe-Bloch formula

The precise dependence of the heavy charged particles' energy loss, taking into account ionization at small energies and relativity, is known as the **Bethe-Bloch formula**:

$$\left|-\frac{dE}{dx}\right|_{ion} = \frac{4\pi n_e z^2 q_e^4}{m_e v^2} \cdot \cdot \left[\ln\left(\frac{2m_e v^2}{\bar{I}}\right) - \ln\left(1-\beta^2\right) - \beta^2\right], \tag{4.2.11}$$

where

m_e is the electron rest mass,

v – the particle velocity,

n_e – the electron density in matter,

$\bar{I}$ =13.6Z [eV] – the mean potential of atomic ionization,

$\beta = v/c$.

For electrons, the equation is

$$\left|-\frac{dE}{dx}\right|_{ion} = \frac{4\pi n_e z^2 q_e^4}{m_e v^2} \cdot \left[\ln\frac{E_e m_e v^2}{2\bar{I}(1-\beta^2)} - \right. \\ \left. - \ln 2\left(2\sqrt{1-\beta^2} - 1 + \beta^2\right) + 1 - \beta^2\right], \tag{4.2.11a}$$

where E_e is the kinetic energy of the electron.

A few deductions can be made from the Bethe-Bloch formula.

- The stopping power is a function of the particle velocity – $f(v)$. For non-relativistic particles ($v << c$, $\beta << 1$), only the first term in the angle bracket is important, and it fluctuates slowly with particle energy. Therefore, the specific energy loss of a given particle varies as $1/v^2$, or inversely, with particle energy. A heuristic explanation is that at a low velocity, the charged particle spends a greater amount of time in the vicinity of an electron and hence transfers more energy to it.
- When comparing differently charged particles with the same velocity, their stopping power is proportional to $(zq_e)^2$. Therefore, particles with the greatest charge will have the largest specific ionization loss. For example, alpha particles will have greater stopping power than the protons of the same velocity but less than fission fragments. This dependence helps to identify nuclei by measuring their specific ionization loss.

- Concerning the interacting material, the linear absorbing power is proportional to its electron density n_e. Therefore, the specific ionization loss increases with the growth of the atomic number and the volume density of the absorber.
- The stopping power does not depend on the mass of the particle:

$$\frac{dE}{dx} \approx \text{const} \cdot (zq_e)^2 n_e f(v). \qquad (4.2.12)$$

These relations are illustrated in Fig. 4.2.3, wherein the dependence of specific ionization loss in the air is shown as a function of the energy of different types of particles. As can be seen, the value *dE*/*dX* for all types of particles approaches a near-constant minimum limit value at energies above several hundred MeV, where their velocity nears the velocity of light. Fast electrons reach the same limit value but at a much lower energy level, at which they approach relativistic velocity due to their small mass.

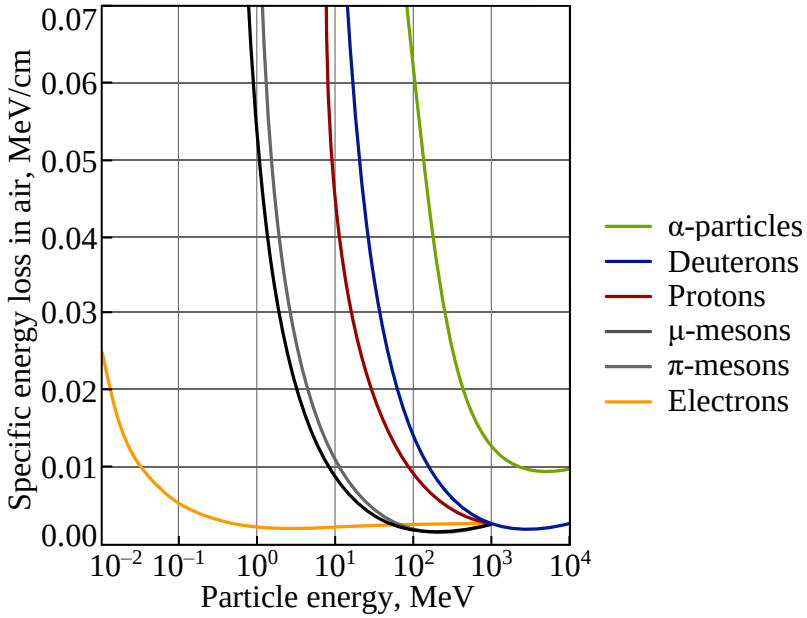

Fig. 4.2.3. Dependence of specific energy loss in the air on the particle energy for some types of particles

The Bethe-Bloch formula becomes inaccurate at low energies where the positively charged particles begin to pick up the electrons from the material atoms, which highly reduces the linear loss. Each positively charged nucleus absorbs *z* electrons at the end of its track, turning into a neutral atom while the positrons are annihilated (see section 3.3.6).

4.2.2. The Bragg curve

The changes in the incident particle's stopping power during its penetration in the material are known as the **Bragg curve**. Because in this case, the particle continuously loses energy (and velocity), while the stopping power increases almost to the end of its track (in correspondence with the Bethe-Bloch formula). There, the absorbed electrons reduce the particle charge, and the curve declines (Fig. 4.2.4).

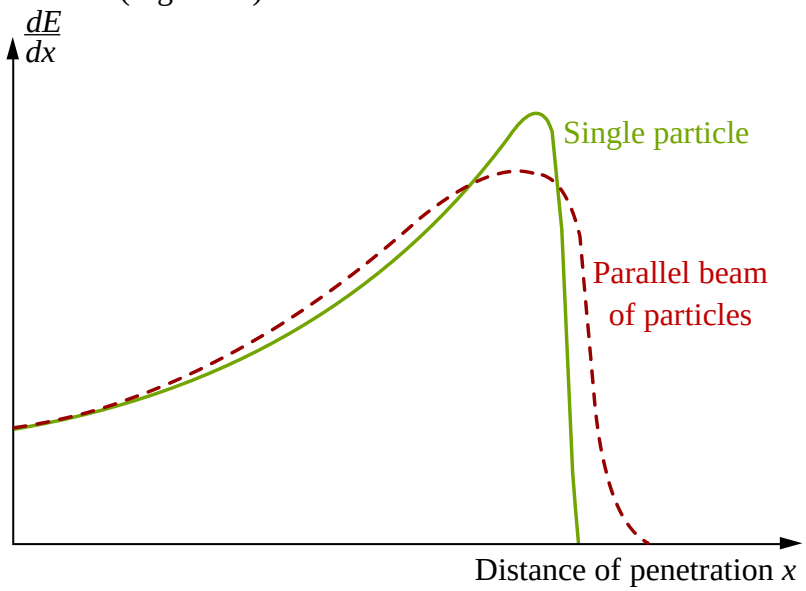

Fig. 4.2.4. Bragg curve of alpha particles

The difference between the curve of a single particle and that of a parallel beam of particles with equal initial energies is due to the random character of the ionization processes (see next section).

4.2.3. Energy straggling

The ionization of matter, as well as the interactions of the charged particles with matter, are stochastic. Therefore, the specific ionization energy loss of these particles in the matter is random in character. The Bethe-Bloch formula describes only the mean energy loss. The actual energy loss of each particle fluctuates around the mean value. This results in a particle's increased energy dispersion when a beam of particles with initially equal energy penetrates the material. This effect is called **energy straggling** and is illustrated in Fig. 4.2.5. As can be seen, the relative standard deviation (δ) of the particle energy spectrum increases during its penetration in the absorber. Only at the end of their range does δ decrease because of the very low energy level.

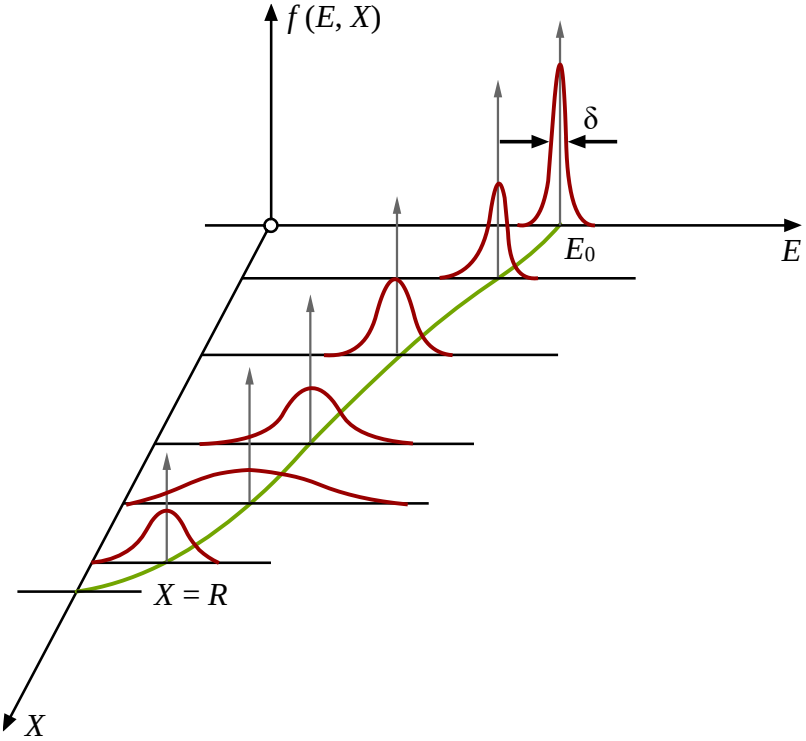

Fig. 4.2.5. Energy distribution in a beam of mono-energetically charged particles penetrating the material [1]

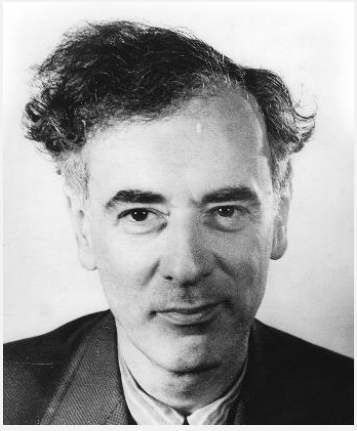

Lev Davidovich Landau

The first person who calculated the expected fluctuations of energy loss was the Soviet physicist, **L. D. Landau**. He derived the equation for the distribution function of energy loss – $\boldsymbol{P(\Delta E)}$ (**Landau distribution)** [2] and determined the expression for the most probable – ΔE_{prob} and mean – ΔE_{mean} energy loss (Fig. 4.2.6).

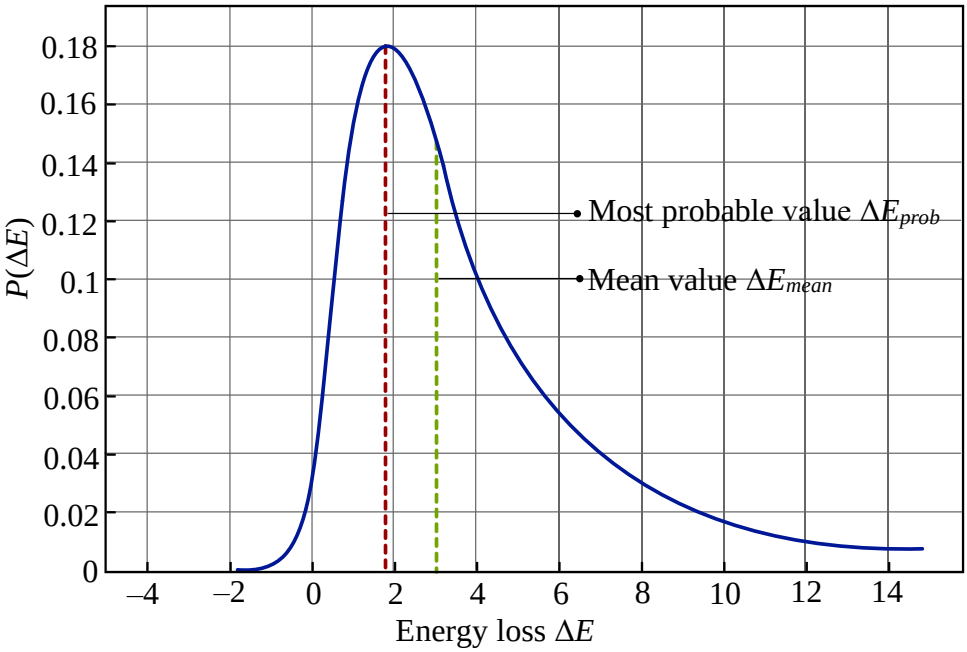

Fig. 4.2.6. Landau distribution

The increase in the thickness of the material layer causes the gradual transition from the Landau distribution to a Gaussian distribution in terms of energy loss. If the flow of particles passes through a thin material layer, then the distribution of ionizing loss takes the form of the Landau distribution. The thicker the material layer, the more the distribution will lean towards the normal one.

Later, other authors defined the required parameters of the experiment (particle characteristics, material, detector geometry etc.) that permits the use of the Landau or Gaussian distributions.

4.2.4. Mean ionization energy

When a particle stops in the material, all its energy (E_P) is spent on the excitation and ionization of the absorber atoms:

$$E_P = E_E + E_I, \tag{4.2.13}$$

where E_E is the energy expended on excitation, and E_I – such spent on ionization. If N_I is the number of ions created by the particle, then

$$\varepsilon = E_P / N_I \tag{4.2.14}$$

will be the mean energy consumed by the formation of a pair of ions, which is called **mean ionization energy**. It is typical for each material, and its value is necessary to calculate the particle energy by measuring the number of the

created ions (i.e. the current through the radiation detector) – a typical procedure in radiation energy spectroscopy.

The ε for gases is of the order of 25–35 eV, but it is much lower for solid states, 3.67 eV for silicon, and 2.96 eV for germanium (at a temperature of 77 K). In reality, the energy necessary for atom ionization (the so-called **ionization potential**) is significantly lower than ε because a big part of it is spent on atom excitations. For example, for nitrogen ε = 36 eV, while the ionization potential of nitrogen is only 15.5 eV. However, when the energy of a particle has to be measured, the current through the radiation detector is proportional only to the number of ions (the energy loss for excitation cannot be measured).

4.2.5. Multiple scattering by nuclei

When a charged particle passes in the immediate vicinity of an atom nucleus of the material, the Coulomb interaction occurs with this nucleus instead of with its electrons because the electrons do not shield the nucleus Coulomb field. In such a case, the particle will be diverted from its initial path due to the significant mass of the nucleus. This process is known as **Coulomb scattering**. It is an elastic scattering since the inner state of both participants (particle and nucleus) remain unchanged. Nevertheless, the interaction mechanism is similar to the ionization energy loss mentioned above.

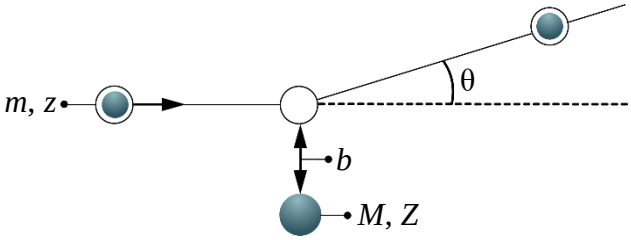

Fig. 4.2.7. Particle scattering in the Coulomb field of the nucleus

At each scattering, the particle deviates from its initial direction at an angle θ (Fig. 4.2.7). It can be calculated by the relation

$$\mathrm{tg}\theta = \Delta p/p, \tag{4.2.15}$$

where p is the momentum of the incident particle and Δp – its alteration by the scattering. Following a similar method as in section 4.2.1, we can find

$$\mathrm{tg}\theta = \frac{\Delta p}{p} = \frac{F\Delta \mathrm{t}}{p} = \frac{2Zzq_e^2}{mv^2}\frac{1}{b}, \tag{4.2.16}$$

where m and z are the mass and charge numbers of the particle, M, Z – the mass and atomic numbers of the nucleus, q_e – the charge of the electron, and b is the distance between the particle and the nucleus.

This relation shows that the scattering angle is inversely proportional to the particle mass m, the square of its velocity υ, and the distance to the nucleus b. For these reasons:

- the heavy particle is scattered at very small angles;
- scattering at small angles is predominant because the probability of interaction at a great distance is higher.

It is important to compare the specific energy loss of a particle (for example, an alpha particle) when it has an elastic scattering interaction with a nucleus – $(dE/dx)_N$, with a moment when it has an inelastic interaction with an atom's electron (the ionization loss) – $(dE/dx)_{ion}$:

$$\left(\frac{dE}{dx}\right)_N : \left(\frac{dE}{dx}\right)_{ion} = \frac{Zp^2}{2M} : \frac{p^2}{2m_e} = \frac{Zm_e}{Am_p} \approx \frac{1}{2}\frac{m_e}{m_p} \approx 0.025\ \%, \quad (4.2.17)$$

where Z and A are the mass number and the atomic number of the nucleus, respectively, and m_p – the mass of the proton.

This relation shows that the contribution of the elastic scattering to the particle energy loss is insignificant.

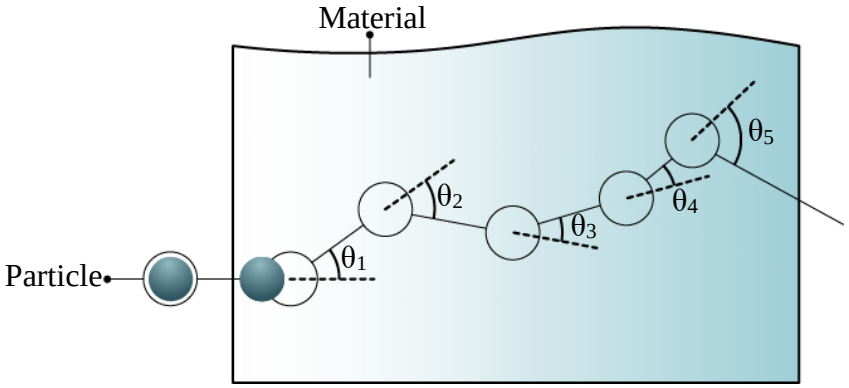

Fig. 4.2.8. Multiple scattering of the charged particle

However, what is much more important is the influence of the **multiple scattering** on the particle path in thick material. Despite the fact that each deflection angle is small, the sum of all their contributions adds a random component to the particle's path, which proceeds with a zig-zag trajectory (Fig. 4.2.8). As a result, the particle path becomes longer in comparison with the actual distance of the particle penetration in the material, and even backscattering of the incident particles can be observed (see section 4.3).

Because the deflection angle at each interaction is independent in terms of its value and direction, all possible values and directions have the same probability. As a result, the total deflection angle after a large enough number N of scatterings is zero:

$$\sum_{i=1}^{N} \theta_i = 0. \tag{4.2.18}$$

This compels the use of the **root mean square** (***rms***) **angle** θ_{rms} in the quantitative evaluation of the multiple scattering influence:

$$\theta_{rms} = \sqrt{\frac{1}{N}\sum_{i=1}^{N} \theta_i^2}. \tag{4.2.19}$$

For the *rms* angle (θ_{rms}) of multiple scattering with a distance of x, in an environment with a constant nuclear density n_N, the following dependency can be used:

$$\theta_{rms} \approx \frac{Zz}{mv^2}\sqrt{n_N x}. \tag{4.2.20}$$

4.2.6. Charged particle range

The best way to define the particle range is to analyze the variations in the flux Φ of mono-energetic particles when passing through a material (absorber) with increasing thickness D (Fig. 4.2.9).

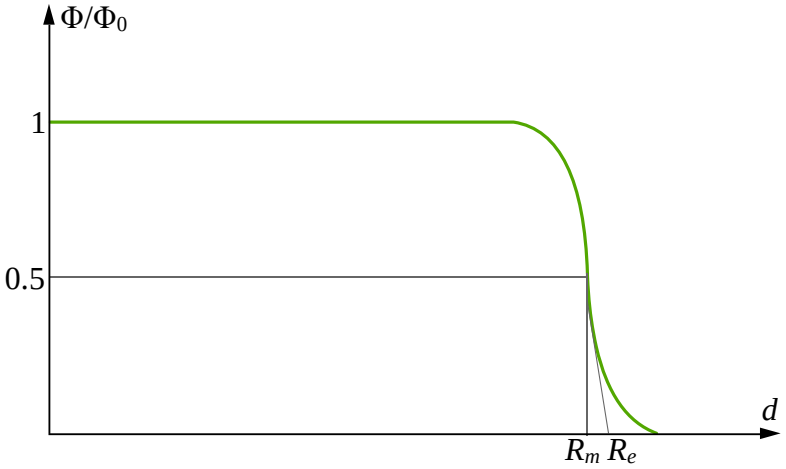

Fig. 4.2.9. The dependence of the relative particle flux on the thickness of the absorber material D

In the beginning, only the particles' energy will decrease (see Fig. 4.2.5), but the flux will stay the same. Due to the large mass of the particles, the interactions cannot change the particle direction; therefore, they move straight ahead. The flux will remain constant until the absorber thickness reaches the

shortest particle track in this material at the initial particle energy. Then, with the increase in thickness, more and more particles will lose all of their energy and will come to a stop.

The particle range is usually defined as the absorber thickness at which the initial particle flux decreases precisely 2 times ($\Phi/\Phi_0 = 0.5$). It is called the **mean particle range** (R_m). Some authors used the so-called **extrapolated range** (R_e), which can be found by extrapolating the linear portion of the end part of the curve to zero. The difference in the range of the particles with equal incident energy, called **range straggling**, is also due to the stochastic character of the ionization process and especially of the elastic scattering of the nuclei, which decreases their range.

Theoretically, an easier way to calculate the particle range is to integrate the function of stopping power into all values of E, from E_0 to 0:

$$R = \int_0^R dx = \int_{E_0}^0 \frac{dE}{-dE/dx}. \tag{4.2.21}$$

Taking into account that the particle energy is only kinetic, the following modification can be made:

$$\frac{dE}{dx} = \frac{d}{dx}\left(\frac{mv^2}{2}\right) = mv\frac{dv}{dx} \text{ or } dE = mvdv. \tag{4.2.22}$$

For the stopping power, equation (4.2.12) can be used in which non-relativistic charged particles $f(v)$ can be replaced by $1/v^2$:

$$-\frac{dE}{dx} \approx \text{const} \cdot \frac{(zq_e)^2 n_e}{v^2}. \tag{4.2.12a}$$

By placing the results of equations (4.2.22) and (4.2.12a) in (4.2.21), we obtain:

$$\begin{aligned} R = \int_0^R dx = \text{const} \int_0^v \frac{mvdv}{(zq_e)^2 n_e/v^2} = \\ = \text{const} \cdot \frac{mv^4}{n_e(zq_e)^2} \end{aligned} \tag{4.2.23}$$

Unfortunately, this equation does not indicate the range's actual results due to the elastic scattering and range straggling. Nevertheless, it can still be used as the basis for a few important conclusions:

- the range of particles with the same incident energy, charge and mass, is inversely proportional to the density of the material;

- at the same velocities, the ranges of charged particles in the matter are proportional to the particle masses and inversely proportional to the squares of their charges:

$$R_1 : R_2 = \frac{m_1}{z_1^2} : \frac{m_2}{z_2^2}; \qquad (4.2.24)$$

- at the same energies, the ranges of charged particles are inversely proportional to their masses:

$$R_1 : R_2 = \frac{m_2}{z_1^2} : \frac{m_1}{z_2^2} \qquad (4.2.25)$$

(by applying the following transformation – $mv^4/n_e(zq_e)^2 = m^2v^4/$ $/mn_e(zq_e)^2 = 4E^2/mn_e(zq_e)^2$).

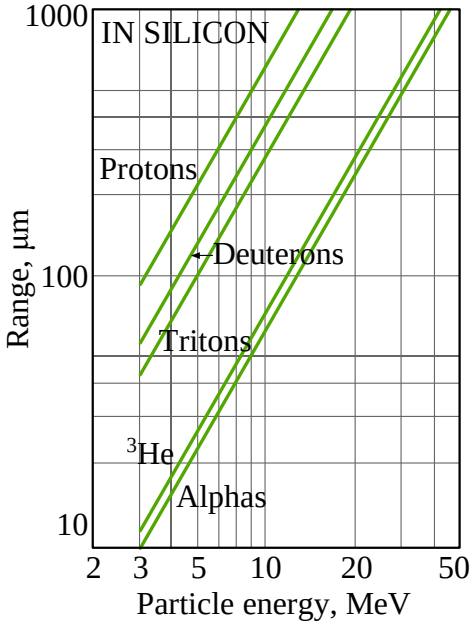

Fig. 4.2.10. Range-energy relation for different charge particles in silicon

The dependence of the charged particles range on their energy in different materials is an important piece of information. When it is necessary to measure their total incident energy, the active thickness of the detector has to be greater than their range in the detector material. The same also applies to the thickness of any radiation shielding. Therefore, there are many empirical formulas to calculate the mean range of different particle types in different materials and different energy regions. The special graphs showing the dependence of the range on the incident particle energy for different materials

and different types of particles are very useful. As an example, such a graph for silicon is shown in Fig. 4.2.10.

The mean range of alpha particles with an initial energy of 5–6 MeV in air is about 4–5 cm, but in more dense materials such as Plexiglas, glass and aluminum, it is about hundreds of μm. Despite the much higher stopping power of the fission fragments, their range is only two times smaller than that of alpha particles with 5 MeV of energy because their incident energy is much higher.

Evidently, the alpha particle's penetration ability is very low (Fig. 4.2.11). A sheet of paper, the surface layer of dead skin (the epidermis), or a few centimeters of air can easily stop them. For this reason, there is no problem shielding the alpha particles when they are outside of the human organism. What is much more dangerous is an alpha-emitting radionuclide deposited in the organism. In such a case, alpha particles are more damaging than most other types of radiation because a relatively large amount of energy is deposited within a tiny volume of tissue. For this reason, the minimum acceptable amounts of alpha radioactive isotopes in water and food are extremely low.

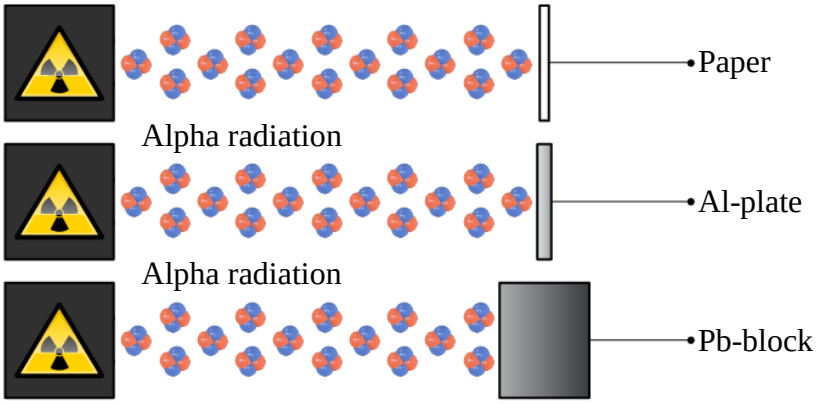

Fig. 4.2.11. Shielding of alpha particle

4.2.7. Behavior of fission fragments

As is mentioned in section 2.4.1, atom fragments are produced because of the fission of heavy nuclei. The main difference with lighter particles (alpha and protons) is that they are multi-charged ions – the new nuclei are stripped of many electrons. For this reason, the stopping power of an atom fragment has a specific dependence on the depth of penetration in the material – it continuously decreases for the duration of the penetration period. This dependence is due to the continuous reduction in the effective charge carried

by the fragment, which is neutralized by the electrons picked up from the absorber.

Another consequence is that their range is shorter than that of the alpha particle despite the very high fragment energy. For example, the range of a typical fission fragment is around two times shorter than that of a 5 MeV alpha particle.

References

[1] *Wilken, B., T. A. Fritz.* Energy distribution functions of low energy ions in silicon absorbers measured for large relative energy losses. Nucl. Instr. and Meth. **138**, 1976, p.p. 331-343. https://reader.elsevier.com/reader/sd/pii/0029554X76900434?token=75F1AD9DA69A991617DF49CFABF377036CB06C029F642C46D192ECE5073BA61D17A7C56117712BEC2E55E88FC545A067

[2] *Landau, L. On the Energy Loss of Fast Particles by Ionization. J. Phys. USSR, 8, 1944, p. 201.*

4.3. Interaction of electrons with matter

The behavior of electrons when moving through a material is very different from that of heavy charged particles. The primary reason is that they have far less mass, and therefore they lose much more energy and significantly change the direction of their movement at each interaction. Additionally, their dynamic mass increases with their energy. For example, the dynamic mass of an electron with an energy of 10 MeV is about 20 times greater than its rest mass. As a result, the electrons' paths in the medium are much more tortuous (Fig. 4.3.1) and their flux in the depth of the material decreases (see section 4.3.4).

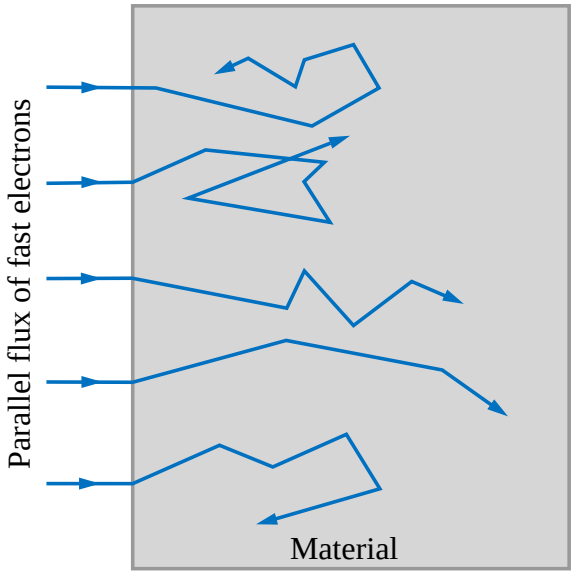

Fig. 4.3.1. Exemplary trajectories of fast electrons in matter

There are three types of interactions that are the most important for beta particles and for electron beams with low and moderate energy: **inelastic interactions** with the atoms' electrons (**loss of energy by ionization**); **elastic scattering** at atoms' electrons and nuclei; **inelastic interaction**s with an atoms' nuclei, producing bremsstrahlung (**radiative energy loss**). The electrons with very high energy (relativistic electrons) have specific interactions producing synchrotron radiation (see section 3.3.5) and Cherenkov radiation (see section 3.3.7).

4.3.1. Inelastic interaction with an atom's electron

In this process, the incident electrons transfer some of their own energy to that of the electrons of the atom shells, resulting in the excitation or ionization of the atoms. It is similar to the same type of interactions of heavy charged

particles (see section 4.2.1), and the specific energy loss (the stopping power) resulting from ionization can be calculated by the corresponding Bethe-Bloch formula (see Eq. (4.2.11a)):

$$\left|-\frac{dE}{dx}\right|_{ion} = \frac{4\pi n_e z^2 q_e^4}{m_e v^2}\left[\ln\frac{E_e m_e v^2}{2\bar{I}\left(1-\beta^2\right)} - \ln 2\left(2\sqrt{1-\beta^2}-1+\beta^2\right)+1-\beta^2\right],$$

where

m_e is the electron rest mass,

v – the electron velocity,

n_e – the electron density of the material,

q_e – the charge of the electron,

E_e – the electron's kinetic energy,

$\bar{I}$ =13.6Z [eV] – the mean potential of atomic ionization,

$\beta = v/c$.

When the transferred energy is not enough to ionize the atom (to separate the electron from the atom), the atom is only excited (the electron moves to an outer shell). Then, going back to its original shell, the electron irradiates the so-called **characteristic X-ray** (see section 3.3.4).

4.3.2. Elastic scattering

These interactions happen between the incident electrons and the electrons from the atoms' shells as well as between the incident electrons and the atoms' nuclei. Only an exchange of kinetic energy takes place at each interaction without any excitation, ionization or irradiation.

As is shown in section 4.2.5 (see Eq. (4.2.17)), the specific kinetic energy loss of the scattering at nuclei is negligible compared with the ionization loss:

$$\left(\frac{dE}{dx}\right)_N : \left(\frac{dE}{dx}\right)_{ion} \approx 0.025\ \%.$$

The energy loss of the scattering at the atom electron is also very low because a more significant transfer of energy will cause an inelastic interaction – the atoms' electron will be displaced from its shell.

However, multiple scattering of this type results in the drastic modification of the electrons' direction of movement, and consequently, their paths (see section 4.3.4).

The ratio between the cross-sections of both processes (σ_N of scattering at a nucleus and σ_e – at an electron) is roughly equal to the atomic number Z of the medium atoms:

$$\sigma_N/\sigma_e \approx Z. \qquad (4.3.1)$$

Thus, in a hydrogen medium ($Z = 1$), the probability of both types of scattering is equal, but in heavier materials, interactions predominate with the atom's nuclei. For example, in gold ($Z = 79$), only about 1 % of the scatterings are from the atom's electrons.

4.3.3. Inelastic interactions with nuclei

When light charged particles like electrons have higher energy levels, they can interact inelastically with nuclei, producing electromagnetic radiation called **bremsstrahlung** (see section 3.3.3). This type of energy loss is named radiative energy loss, and the linear specific loss through this process is:

$$\left|-\frac{dE}{dx}\right|_{rad} = \frac{n_e E_e (Z+1) q_e^4}{137 m_e^2 c^4}\left(4\ln\frac{2E_e}{m_e c^2} - \frac{4}{3}\right), \qquad (4.3.2)$$

where

n_e is the electron density in the material,

E_e – the electron energy,

Z – the atomic number of the material,

q_e – the charge of the electron,

m_e – the rest mass of the electron,

c – the light velocity.

Factors E_e and Z in the numerator of this equation show that radiative losses are more important for high electron energies and absorber materials with large atomic numbers. The ratio between specific energy losses due to the radiative- and ionization processes is approximately [1]

$$\frac{(dE/dx)_{rad}}{(dE/dx)_{ion}} \approx \frac{E_e Z}{700}, \qquad (4.3.3)$$

where E_e is in units of MeV. For beta particles whose typical maximum energies are less than a few MeV, the radiative losses are normally a small part of the energy losses due to the ionization and excitation of the atoms. They became significant only in absorbing materials with a high atomic number.

This fact is important for radiation shielding: the containers for beta sources normally have a double-layer construction – an inner cylinder of light material, which produces low bremsstrahlung, and an outer one made of heavy material – to absorb the bremsstrahlung.

4.3.4. Electron range

A. Absorption of mono-energetic electrons

When a beam of mono-energetic electrons passes through absorbers of increasing thickness while its output flux is being measured, it can be observed that even the smallest increase in the absorber thickness value leads to the loss of electrons. The flux decreases due to the scattering of some electrons, which are emitted from it. A plot of the relative flux (Φ/Φ_0) versus absorber thickness D (the so-called **transmission curve** – Fig. 4.3.2) shows that it begins to decrease immediately and gradually approaches zero for large absorber thickness. The electrons, whose direction is changed at least as they pass through the material, actually reach the greatest depth in it.

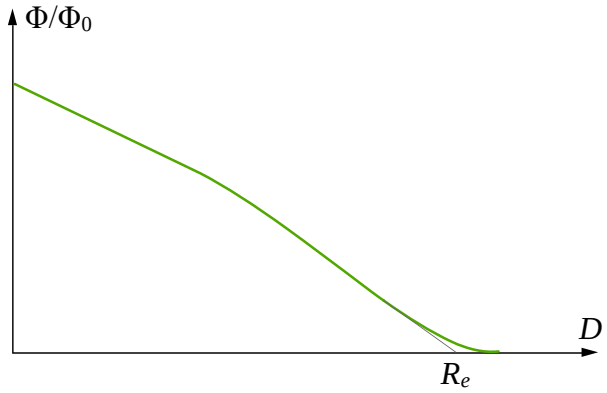

Fig. 4.3.2. Transmission curve for mono-energetic electrons. R_e is the extrapolated range

The conception of the range is relative because the path of the electrons is much longer than the penetrating thickness. Normally, it can be defined by extrapolating the linear part of the transmission curve to zero (R_e, Fig. 4.3.2), which shows the absorber thickness necessary to stop almost all electrons. The electron path length in a material is hundreds of times greater than that of heavy charged particles of equivalent energy because the specific energy loss of the electrons is much lower. A very crude estimation of the electron range is about 2 mm per MeV in light materials and about 1 mm per MeV in absorbers of moderate density [1].

B. Absorption of beta particles

The transmission curve for beta particles emitted by a radioactive source is very different from that mentioned above because of the continuous distribution of their energy (see section 2.2.2). Because of the faster absorption of the beta particles with low energy, the initial slope is much

steeper. It was experimentally found that the relative decrease of the beta particle flux is proportional to the thickness of the absorber layer *dD*:

$$d\Phi_\beta/\Phi_\beta = -\mu_\beta dD, \tag{4.3.4}$$

where μ_β is a coefficient of proportionality (the minus sign shows the decrease of the flux according to the depth of the material). The solution of this equation[1] is:

$$\Phi_\beta = \Phi_{\beta 0} e^{-\mu_\beta D}, \tag{4.3.5}$$

which shows that the flux decreases exponentially in relation to its depth in the material. Here, Φ_β is the flux at a depth D, $\Phi_{\beta 0}$ – the incident flux and μ_β is called the absorption coefficient. The μ_β value is typical for each material but also depends on the maximum energy of the beta particles.

For evaluation of the absorption capability of the material, another parameter is commonly used – **half-value thickness $D_{1/2}$**.This is the thickness of the material at which the incident flux of beta particles is reduced by one-half – $\Phi_\beta = \Phi_{\beta 0}/2$. The relation between $D_{1/2}$ and μ_β can be found from the equation for Φ_β, using this condition:

$$D_{1/2} = \ln 2/\mu_\beta = 0.693/\mu_\beta, \tag{4.3.6}$$

Data for the product of the half-value thickness and material density ($D_{1/2}\rho$), depending on the maximum beta particle energy, is depicted in Table 4.3.1. With it, the half-value thickness can be calculated for a given beta source (i.e. $E_{\beta max}$) and absorber material (i.e. ρ).

$E_{\beta max}$, MeV	$D_{1/2}\rho$, g/cm^2
0.15	0.027
0.50	0.176
1.00	0.530
2.00	1.400
3.00	2.100

Table 4.3.1. Dependence of the product $D_{1/2}\rho$ on the maximal energy of the beta particles

[1] By integrating both sides of this equation, we receive $\ln \Phi_\beta = -\mu_\beta D + \ln A$, where $\ln A$ is the integration constant. It can be determined by the condition $\Phi_\beta = \Phi_{\beta 0}$ at $D = 0$ – $\ln A = \Phi_{\beta 0}$.

In Fig. 4.3.3, different means of beta particle shielding are illustrated. In comparison with the alpha particle, the penetration ability of beta particles is much higher. The standard application of heavy metal shielding is not effective here because of the higher generation of bremsstrahlung. Aluminum is a suitable choice for beta particles of not very high energy. For sources with the highest energy levels, double shielding is normally used: light material (like aluminum or plastic) is placed nearest the source with a heavy metal layer around its outside to shield the bremsstrahlung. If heavy metal shielding is used on its own, then intense bremsstrahlung will be emitted from it.

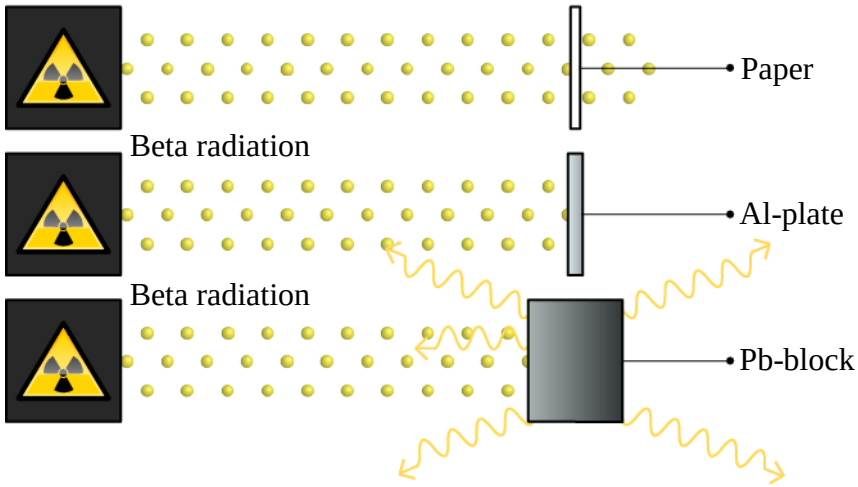

Fig. 4.3.3. Beta particle shielding

C. Backscattering

The fact that the electrons undergo large-angle deflections along their paths is the reason for the phenomenon of **backscattering** – an incident electron entering an absorber surface can undergo so many large deviations that it goes back out through the same surface. The rate between the flux of the backscattered electrons Φ_{BS} to the incident electron flux $\Phi_{\beta 0}$ is called the **backscattering coefficient** (η_{BS}):

$$\eta_{BS} = \Phi_{BS}/\Phi_{\beta 0}. \qquad (4.3.7)$$

The backscattering coefficient depends on the energy of the incident electrons as well as on the density (i.e. on the atomic number) of the absorber. It is highest for the electrons with low incident energy and increases with the increase of the atomic number of the absorber. The dependence of the backscattering coefficient on the incident electron energy for some absorber materials is shown in Fig. 4.3.4 [1].

The dependence of the backscattering coefficient on the atomic number is used for the quantitative analysis of the heavy elements content in a lighter element matrix. A typical example is the measuring of the precious metal coating thickness on lighter metals [2].

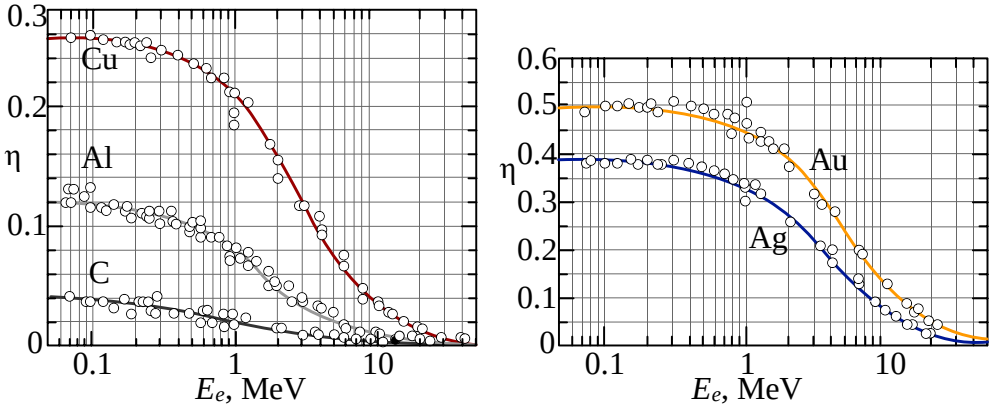

Fig. 4.3.4. Dependence of the backscattering coefficient on the incident electron energy for different absorber materials

4.3.5. Positron interactions

The Coulomb forces that determine all interactions between the charged particles and the matter are present for either positive or negative particle charge. Whether the interaction involves a repulsive or attractive force between the incident particle and atoms' electrons, the impulse and energy transfer for particles of equal mass are about the same. Therefore, the tracks of positrons in an absorber are similar to those of normal negative electrons, and their specific energy loss and range are about the same for equal initial energies.

The big difference is that each positron is annihilated when it comes into contact with an electron at the end of its track, resulting in two 0.511 MeV photons (see section 3.3.6). Because of the higher penetration of photons, this radiation reaches much farther from the original positron track and may disturb the operation of neighboring radiation detectors.

In summary, Fig. 4.3.5 shows the relative specific energy losses ($[dE/dx]/E_e$) per radiation length (X_0) due to the different types of electron and positron interactions and their dependence on the incident particle energy in an absorber of lead ($Z = 82$) [3]. As can be seen, ionization dominates at low to moderate energies, and there is a minimal difference between the curves of electrons and positrons.

The energy loss due to the bremsstrahlung process is relatively high because of the high atomic number of the absorber. It becomes dominant at moderate and high energy levels of incident particles.

The energy losses due to elastic scattering are very low, and it only takes place at low particle energy. The curve of positron annihilation represents the energy loss due to the interactions of incident positrons with the electrons of the absorber, the quantity of which is very low.

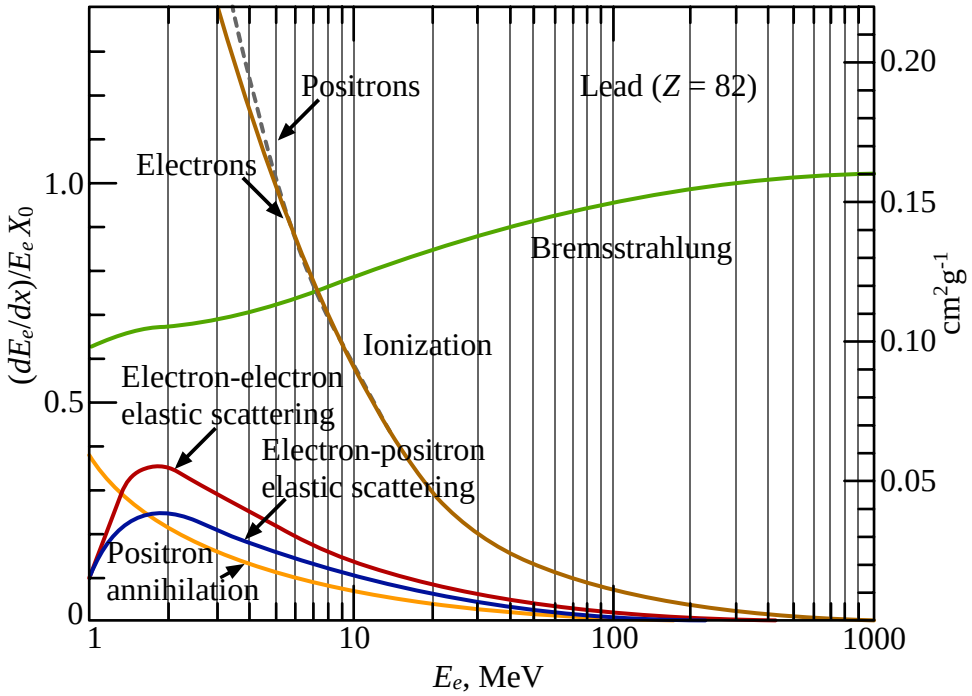

Fig. 4.3.5. Relative specific energy losses per radiation length of electrons and positrons due to different interaction processes depending on incident particle energy

References

[1] *Knoll, G.F.* Radiation detection and measurement. Third ed. John Valley & Sons Inc., New York, 2000. https://phyusdb.files.wordpress.com/2013/03/radiationdetectionandmeasurementbyknoll.pdf

[2] Metal plating processes and methods of measuring surface hardness and thickness of coatings. https://www.balseal.com/sites/default/files/tr105_020707140651.pdf

[3] *Ahmed, S. N.* Physics and Engineering of Radiation Detectors. Academic Press Inc., Elsevier, 2007. https://www.elsevier.com/books/physics-and-engineering-of-radiation-detection/ahmed/978-0-12-045581-2

4.4. Interaction of gamma radiation with matter

As is mentioned above, gamma rays are photons (quanta of light), and they have neither electric charge nor rest mass. Therefore, the interaction of gamma rays with matter is weak. Although a large number of different interaction processes between gamma rays and matter are known, only three of them play an important role in radiation measurements and protection: **photoelectric effect** (**photoelectric absorption**), **Compton scattering**, and **pair production**. Each of these processes provokes complete or partial loss of the gamma photon energy. As a result, the photon either disappears entirely or is scattered along a significant angle. This behavior is principally different from that of charged particles, which gradually slow down through their continuous and successive interactions with many absorber atoms.

4.4.1. Photoelectric effect

The **photoelectric effect** is an interactive process between a photon and an absorber atom in which the photon completely disappears (for this reason, the process is also called **photoelectric absorption**) and an electron (named a photoelectron) is ejected from the atom's shell (Fig. 4.4.1). It is important to note that the interaction is with the atom as a whole and is not possible with a free electron.

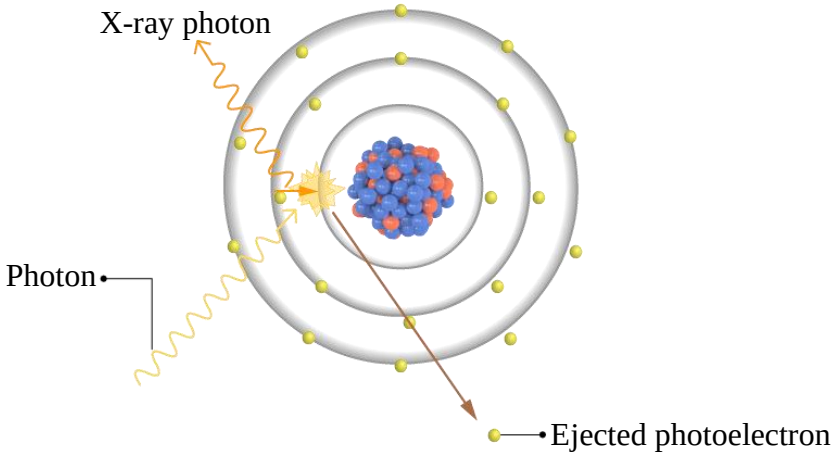

Fig. 4.4.1. Photon interaction due to the photoelectric effect in lead

The energy of the photoelectron E_{pe} is:

$$E_{pe} = E_{\gamma} - E_{bi}, \qquad (4.4.1)$$

where E_{γ} is the energy of the gamma-photon and E_{bi} – the binding energy of the corresponding i atom's shell. For gamma rays of sufficient energy, the most probable origin of the photoelectron is the most tightly bound (K) shell

of the atom. The electron then moves through the material and loses its energy as described for beta interactions. If the photon energy is insufficient to knock an electron from the *K*-shell, then the interaction occurs with an electron of the *L* or *M* shells.

After the interaction, the atom is ionized, having an electron vacancy in the corresponding shell. This vacancy is filled through the capture of a free electron from the absorber or by a rearrangement of the electrons from the other atom shells. Therefore, one or a few characteristic X-ray photons can be emitted too (Fig. 4.4.1). These normally have a lower energy level and are quickly absorbed by the medium. However, they have a negative influence on the precise measurement of gamma-ray energy.

An X-ray photon, emitted because of a photoelectric effect, can also knock out another orbital electron, provided that its energy is equal to the binding energy of that electron. Such an electron is called an **Auger electron**. The process is essentially without radiation because the excess energy of the atom is used and taken away by the Auger electron.

The cross-section of the interactions of the photoelectric effect increases rapidly with the atomic number *Z* of the absorber. In addition, it also has an inverse relationship with the energy of gamma (or X-) photon:

$$\sigma_{pe} \propto Z^n / E_\gamma^{3,5}, \tag{4.4.2}$$

where *n* is between 4 and 5 [1]. This strong dependence of the photoelectric absorption on the medium's atomic number is the main reason for the use of heavy material (such as lead) for gamma-ray shielding, and germanium for gamma spectroscopic detectors (see section 5.3)

4.4.2. Compton scattering

Compton scattering is an interaction between the incident gamma photons and the electrons of the outer shells of the medium's atoms. In this process, the incoming gamma photon transfers a part of its energy to an electron. As a result, the gamma-photon is deflected at an angle θ with respect to its original direction (Fig. 4.4.2). The electron, called a recoil electron, is ejected from its shell at an angle φ. Because all angles of scattering are possible, the energy transferred to the electron can vary from 0 to a large fraction of the gamma photon's energy. The relation between the energy of the scattered photon (E_γ) and its scattering angle can be derived using the laws of the conservation of energy and of momentum [1]:

$$E_\gamma = \frac{E_{\gamma 0}}{1 + \frac{E_{\gamma 0}}{m_e c^2}(1 - \cos\theta)}, \tag{4.4.3}$$

where $E_{\gamma 0}$ is the energy of the incident photon, and m_e is the rest mass of the electron (i.e. $m_e c^2$ is the rest energy of the electron, equal to 0.511 MeV).

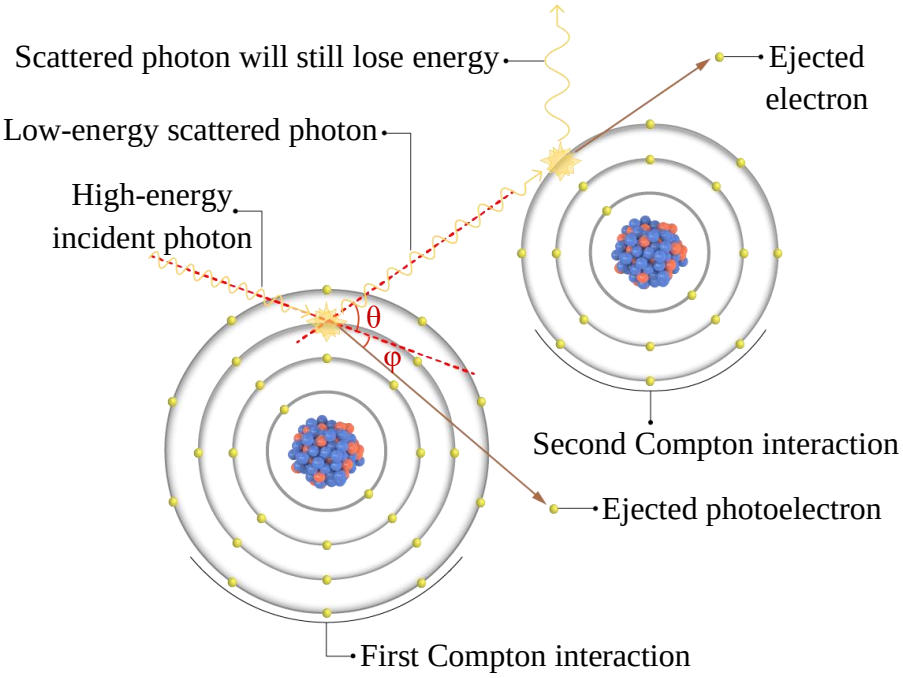

Fig. 4.4.2. Compton scattering

This relation shows that the energy of the scattered photon depends not only on the energy of the incident photon but also on the scattering angle θ, i.e. Compton scattering is not an isotropic process. At very small angles ($\theta \approx 0$) $\cos\theta \approx 1$ and $E_\gamma = E_\gamma^{\max} \approx E_{\gamma 0}$ because there is practically no scattering, i.e. no interaction. $E_\gamma^{\max}$ is the upper limit of energy transferred to the scattered photon.

An intermediary case is when $\theta = \pi/2$ (the photon is scattered at a right angle). Then $\cos\theta = 0$ and:

$$E_\gamma = \frac{E_{\gamma 0}}{1 + \frac{E_{\gamma 0}}{m_e c^2}}. \tag{4.4.4}$$

The other extreme case is where $\theta = \pi$, then $\cos\theta = -1$. Thus:

$$E_\gamma = E_\gamma^{\min} = \frac{E_{\gamma 0}}{1 + \frac{2E_{\gamma 0}}{m_e c^2}}. \qquad (4.4.5)$$

which is the minimum value of the scattered photon energy. This equation can be transformed into:

$$E_\gamma^{\min} = \frac{m_e c^2}{2} \cdot \frac{1}{1 + \frac{m_e c^2}{2E_{\gamma 0}}}. \qquad (4.4.6)$$

Here, $m_e c^2 = 0.511$ MeV is the rest energy of the electron once more. Assuming that it is much smaller than the incident photon energy ($m_e c^2 << E_{\gamma 0}$), the second term in the denominator can be neglected. Then:

$$E_\gamma^{\min} \approx \frac{m_e c^2}{2} = 0.255 \text{ MeV}. \qquad (4.4.7)$$

For gamma spectroscopy, the energy received by the recoil electron is the most important. Taking into account that a part of the transferred energy has to liberate the electron from the atom's shell, we can write:

$$E_e = E_{\gamma 0} - E_\gamma - E_b \approx E_{\gamma 0} - E_\gamma, \qquad (4.4.8)$$

where E_b is the binding energy of the electron, which can be neglected for atoms with low to moderate *Z*. This relation shows that the energy of the recoil electrons will vary from zero (for θ = 0) to $E_e^{\max} = E_{\gamma 0} - 0.255$ [MeV] (for θ = π). The distribution of the number of recoil electrons over their energy is shown in Fig. 4.4.3.

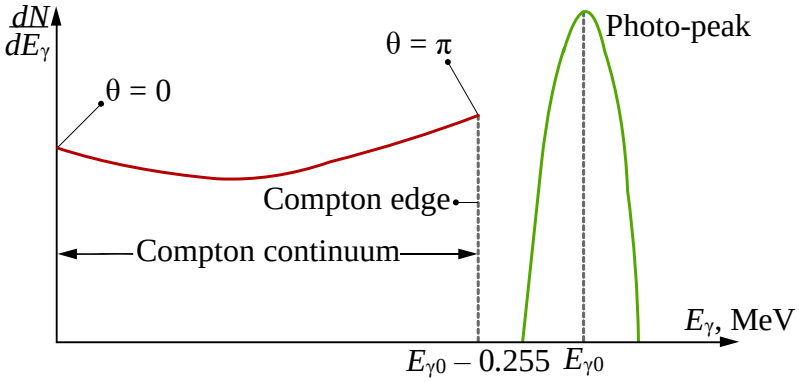

Fig. 4.4.3. Energy distribution of electrons ejected by photoelectric effect or Compton scattering

Their energy range is called the Compton continuum, and their highest energy – the Compton edge. For the sake of comparison, Fig. 4.4.3 also shows the photo-peak corresponding to the photoelectric effect of the gamma photons with the same energy. The problem arises when there is a mixture of radionuclides emitting gamma photons of different energies – then the Compton continuums of the isotopes with higher energy hide the gamma radiation photo-peaks of the lower energy.

Compton scattering is a predominant process of gamma radiation with intermediate energies. After one or several Compton scatterings, the energy of the scattered gamma photons becomes low enough to be absorbed by a photoelectric interaction.

4.4.3. Pair production

Pair production is an interaction between the incident gamma photon and the Coulomb field of a nucleus: when the energy of the gamma photon exceeds twice the rest-mass energy of the electron ($2 \times 0.511 = 1.022$ MeV), it may disappear, producing an electron-positron pair (Fig. 4.4.4). All the excess energy of the photon above the necessary 1.022 MeV goes into kinetic energy shared by the electron and the positron. The positron is annihilated when it loses its kinetic energy in the medium. For this reason, such an interaction is always followed by the irradiation of two gamma photons of 0.511 MeV that either escape or interact with matter through Compton scattering or the photoelectric effect.

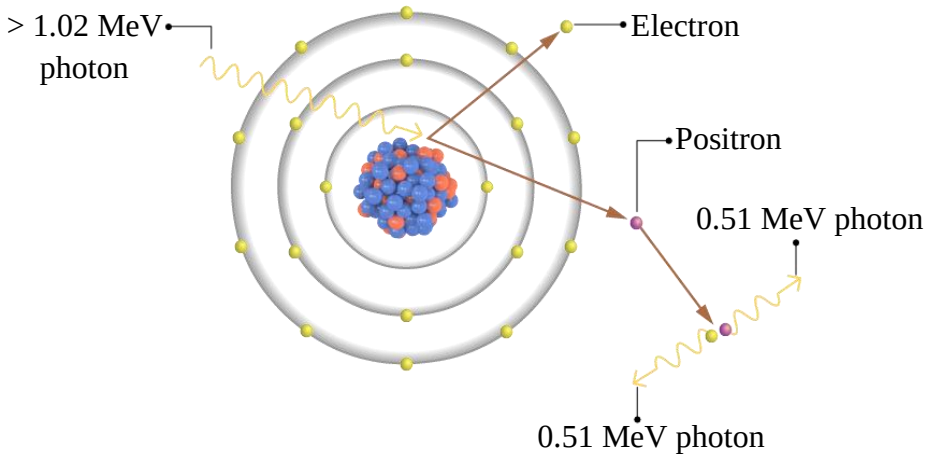

Fig. 4.4.4. Pair production

Pair production is a typical process for high-energy gamma rays and increases with the rise in their energy level.

The relative importance of the three essential types of interaction for different radiation energy and materials with different atomic numbers Z is presented in Fig. 4.4.5 [2]. As is mentioned above, the photoelectric effect predominates at low energy levels. Compton scattering is the most frequent interaction at intermediary energies, and pair production is most probable at the highest of energies. The green lines separating the three zones correspond to the equal probability of the adjacent types of interactions (for σ, τ and κ, see the next section).

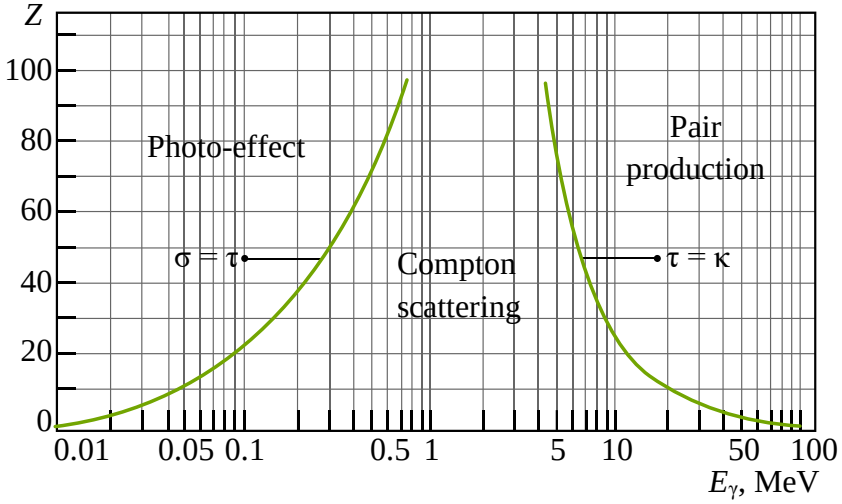

Fig. 4.4.5. Relative importance of the three essential types of gamma-ray interactions

4.4.4. Absorption of gamma radiation

When a beam of gamma rays moves through matter, each of the interaction processes removes gamma photons either by way of absorption or by scattering, decreasing their flux. As with the electrons, the relative reduction of the gamma-ray flux is proportional to the thickness of the absorber layer dD:

$$d\Phi_\gamma/\Phi_\gamma = \mu_\gamma dD \qquad (4.4.9)$$

or

$$\Phi_\gamma = \Phi_{\gamma 0} e^{-\mu_\gamma D}, \qquad (4.4.10)$$

where $\Phi_{\gamma 0}$ is the incident gamma-ray flux. The main difference is that here, the linear attenuation coefficient μ_γ is not a constant. It is the sum of three coefficients characterizing the probability of each type of interaction in a unit path through the material:

$$\mu_\gamma = \sigma + \tau + \kappa, \qquad (4.4.11)$$

where σ, τ and κ correspond to the photoelectric effect, Compton scattering and pair production. Since these coefficients depend on the gamma photons' energy and the atomic number of the absorption material, μ_γ also depends on these two factors. In Fig. 4.4.6, these relations are shown for a lead absorber. It is clear that with the increase of energy, σ decreases very fast, τ – slowly, while κ increases at high energies. The coefficient μ_γ is minimal at intermediary energies.

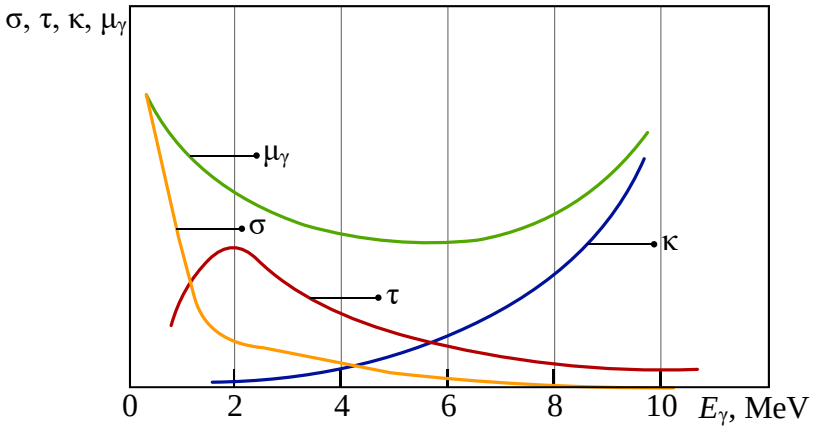

Fig. 4.4.6. Dependences of the linear attenuation coefficients on energy for lead

The gamma-ray photons can also be characterized by their mean free path λ, defined as the average distance traveled through the absorber before an interaction takes place. Its value can be obtained from:

$$\lambda_\gamma = \frac{\int_0^\infty x e^{-\mu_\gamma x} dx}{\int_0^\infty e^{-\mu_\gamma x}\, dx} = \frac{1}{\mu_\gamma}, \qquad (4.4.12)$$

and is the reciprocal value of the linear attenuation coefficient. For the commonly used gamma source energy, it varies from a few mm to a few cm.

The parameter μ_γ is not convenient for the evaluation of the gamma-ray absorption features of the different materials because it depends on their density. The so-called **mass attenuation coefficient** is used in its place:

$$\mu_{\gamma m} = \mu_\gamma/\rho \ \ [\mathrm{cm}^2/\mathrm{g}], \qquad (4.4.13)$$

where ρ is the mass density of the material. For a given gamma-ray energy, the mass attenuation coefficient does not change with the physical state of a given absorber. For example, it is the same for water, whether it is in a liquid

or vapor form. For a compound or a mixture of *n* elements, the coefficient can be calculated by:

$$\mu_{\gamma m} = \sum_{i}^{n} w_i \mu_{\gamma m i}, \qquad (4.4.14)$$

where the w_i factors represent the weight fraction of the element *i* in the compound or mixture, and $\mu_{\gamma mi}$ is the mass attenuation coefficient of the element *i*.

Fig. 4.4.7 illustrates the penetration ability of gamma rays. Because of the lack of mass and charge, it is very high. Only shielding in the form of heavy materials like lead is suitable for them.

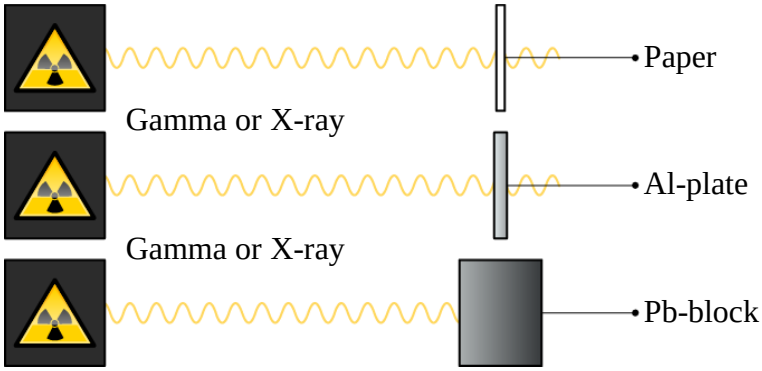

Fig. 4.4.7. Gamma radiation shielding

References

[1] *Ahmed, S. N.* Physics and Engineering of Radiation Detectors. Academic Press Inc., Elsevier, 2007. https://www.elsevier.com/books/physics-and-engineering-of-radiation-detection/ahmed/978-0-12-045581-2

[2] *Knoll, G.F.* Radiation detection and measurement. Third ed., John Valley & Sons Inc., New York, 2000. https://phyusdb.files.wordpress.com/2013/03/radiationdetectionandmeasurementbyknoll.pdf

4.5. Interaction of neutrons with matter

The interactions of neutrons strongly depend on their energy. For this purpose, they can be classified into three groups:

- slow neutrons – with energy up to 1 keV;
- intermediary neutrons – with energy between 1–100 keV;
- fast neutrons – with energy above 100 keV.

Neutrons don't carry an electrical charge, and therefore they are not affected by the electrical fields of the atoms. For this reason, they move freely through the large spaces between the atoms without interacting with them. However, when passing near the atomic nuclei, they are impacted by the strong nuclear force. In these cases, depending on their energy, they interact with nuclei in different ways:

- Elastic Scattering
- Inelastic Scattering
- Transmutation
- Radiative Capture
- Fission

4.5.1. Elastic scattering

Elastic scattering is the most frequent type of neutron interaction and takes place independently of their energy level. During the interaction, the neutron transfers a portion of its kinetic energy to the nuclei, which can be recoiled. The energy transfer from the neutron strongly depends on the atomic number of the nuclei. The maximum amount of energy is transferred to hydrogen nuclei (Fig. 4.5.1), which have the same mass as the neutron (the interaction is similar to that between billiard balls when one collides with another). With the increase in the atomic number, the quantity of transferred energy decreases. For example, to reduce the speed of a fast neutron and turn it into a very slow one (with about 0.025 eV energy, which is known as a thermal neutron), 18 interactions with hydrogen nuclei, 100 with carbon nuclei and more than 2000 with uranium nuclei are needed. For this reason, hydrogen-containing materials like water and paraffin are used for neutron shielding.

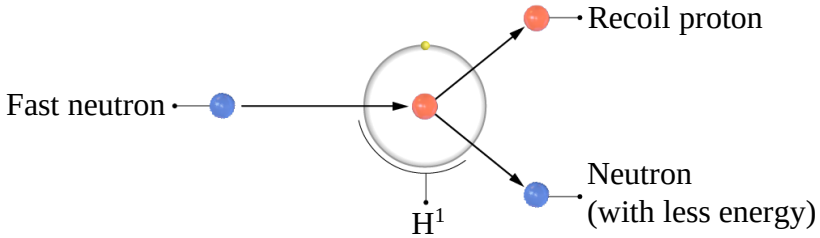

Fig. 4.5.1. Elastic neutron scattering by a hydrogen atom

The elastic scattering process of neutrons with nuclei can occur in two different modes: **potential elastic scattering** and **resonance elastic scattering**. Potential elastic scattering refers to the process in which the neutron is acted on by the short-range nuclear force of the nucleus and, as a result, ricochets off of it without touching the particles' inside. In the resonance mode, a neutron with the right amount of energy is absorbed by the nucleus leading to the subsequent emission of another neutron to converse the kinetic energy [1].

4.5.2. Inelastic scattering

During inelastic scattering, a part of the neutron energy is absorbed by the nucleus, and it passes over into an excited state. Its return to the base state is attended by the irradiation of one or a few gamma photons. This interaction is possible only for fast neutrons because their energy exceeds the amount of energy necessary to excite the nuclei – from 0.1 to several MeV.

4.5.3. Transmutation

Transmutation is an interaction after which an element transforms into another one. Neutrons of all energies are capable of provoking transmutations. A typical example is an interaction between a slow neutron and a boron-10 nucleus:

$$ {}^{1}_{0}n + {}^{10}_{5}\mathrm{B} \rightarrow {}^{7}_{3}\mathrm{Li} + {}^{4}_{2}\alpha, \qquad (4.5.1) $$

which results in a new isotope, lithium-7, and the emission of an alpha particle.

A similar reaction occurs with helium-3:

$$ {}^{1}_{0}n + {}^{3}_{2}\mathrm{He} \rightarrow {}^{3}_{1}\mathrm{p} + {}^{3}_{1}\mathrm{T}, \qquad (4.5.2) $$

during which a proton and a tritium nucleus are created. These two reactions are mostly used in gas-filled neutron detectors (see section 5.2).

4.5.4. Radiative capture

At the instance of a radiative capture, the neutron enters the nuclear structure and creates a new isotope of the same element, which is in an excited state, and returns to the base state by emitting a gamma photon:

$$ {}^{1}_{0}n + {}^{A}_{Z}\mathrm{X} \rightarrow {}^{A+1}_{Z}\mathrm{X} + {}^{0}_{0}\gamma. \qquad (4.5.3) $$

This interaction is called an *n*,γ reaction. It is typical for thermal neutrons and is commonly used for the production of synthetic radioactive isotopes in nuclear reactors where large fluxes of thermal neutrons are created. An example is the production of cobalt-60:

$$ {}_{0}^{1}n + {}_{27}^{59}\mathrm{Co} \rightarrow {}_{27}^{60}\mathrm{Co} + {}_{0}^{0}\gamma. \qquad (4.5.4) $$

4.5.5. Fission

During this process (see section 2.4.1), a heavy nucleus such as uranium-235 absorbs a neutron and then splits into smaller parts – lighter nuclei called **fragments**. The fission process also produces free neutrons and gamma photons and releases a very large amount of energy. The generation of more than one neutron at each act of fission gives rise to the possibility to establish a fission chain reaction. It is used in nuclear reactors, where its rate is strongly controlled, as well as in nuclear weapons, where it is uncontrolled.

4.5.6. Passage of neutrons throughout matter

As mentioned above, neutrons predominantly interact with the nuclei within the material (because of their absence of electrical charge). However, the strong force range is very short, and the neutrons draw very close to the nucleus. That creates the possibility to use them for structural analysis of the material without its disintegration. Today, this method is commonly used under the name **neutronography**.

As a result of the different interactions, the neutron flux also decreases exponentially with the increase in the material thickness:

$$ \Phi_n = \Phi_{n0} e^{-\mu_n D}, \qquad (4.5.5) $$

where μ_n is the attenuation coefficient of neutrons.

Different ways of neutron shielding are shown in Fig. 4.5.2. Typically, for the shielding of neutron sources used in research projects, the building of paraffin walls is enough. Water shielding is even more effective but needs vessels with suitable forms.

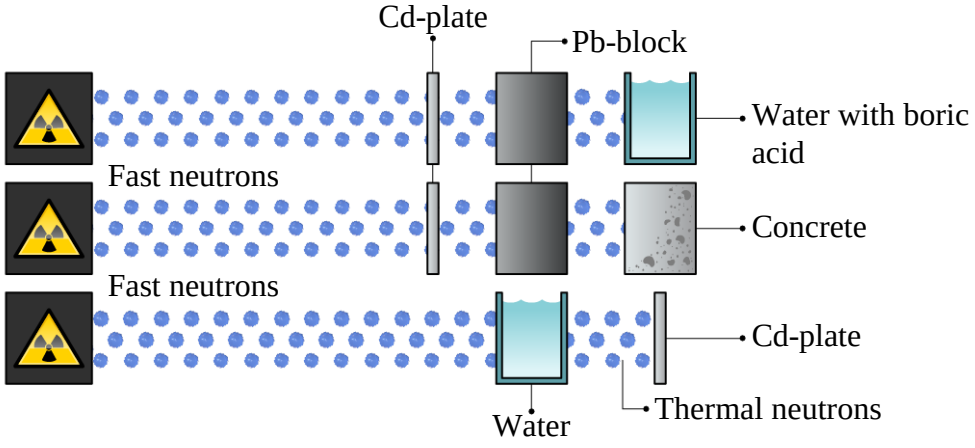

Fig. 4.5.2. Neutron shielding

Neutron absorption is widely used to regulate the power of nuclear reactors. For this purpose, two specific elements are used since they have very high cross-sections for neutrons. The first is boron-10, which absorbs the neutrons by way of the transmutation reaction described above. Its cross-section is maximal for thermal neutrons and decreases smoothly with the increase of the neutron's energy. It is most commonly used as boric acid, which is added to the cooling water in the first reactor circle, increasing its absorption of neutrons many times (see the upper drawing in Fig. 4.5.2).

The second element is cadmium-113, which also has a very high cross-section of neutron absorption, but only for neutrons with energy below 0.5 eV. The corresponding *n*,γ reaction is

$$ {}^{1}_{0}n + {}^{113}_{48}\mathrm{Cd} \rightarrow {}^{114}_{48}\mathrm{Cd} + \gamma. \qquad (4.5.6) $$

As a shield, cadmium may be used only after the thermalization of the neutrons (after their energy has been reduced below 0.5 eV), as is shown in the bottom drawing in Fig. 4.5.2. The middle drawing illustrates that cadmium and heavy metals cannot stop fast neutrons and that concrete is much better for this purpose.

References

[1] *Ahmed, S. N.* Physics and Engineering of Radiation Detectors. Academic Press Inc., Elsevier, 2007. https://www.elsevier.com/books/physics-and-engineering-of-radiation-detection/ahmed/978-0-12-045581-2

4.6. Radiation dose

Upon interacting with any medium, radiation deposits energy into it and inevitably causes changes in its state and properties. Some of them can be useful, but in most cases, the modifications are undesirable and are harmful and dangerous to the health of living organisms. For this reason, one important challenge is to quantify the effect provoked in the irradiated object by its interaction with ionizing radiation. Several physical quantities are used for this purpose, commonly referred to as a **radiation dose** or just **dose**.

4.6.1. Exposure dose

Historically, the first quantity used to evaluate the impact of irradiation was the **exposure dose** or only **exposure**. It evaluates the radiation's influence on the object by measuring the number of ions created in its material. Exposure is defined only for photons (gamma and X-rays) as the electric charge (Q) freed by such radiation in a specified volume of air divided by the mass of that air (m):

$$X = \frac{Q}{m} = \frac{lq_e}{m}, \tag{4.6.1}$$

where

l is the number of the ion pairs created,

q_e – the charge of the electron.

The first unit of the exposure dose was **Roentgen** (**R**). One Roentgen is defined as the exposure dose received from gamma or X-ray radiation, which produces ions with a charge of 1 esu (electrostatic unit) per polarity in 0.001293 g of air (mass of 1 cm^3 air at 0 °C and 760 mm Hg). Nowadays, it is largely replaced by the SI unit **Coulomb per kilogram** (**C/kg**). One Roentgen equals $2.58 \cdot 10^{-4}$ C/kg, and one Coulomb per kilogram is equivalent to 3876 R.

At present, the exposure is used mainly for the evaluation of the gamma-radiation background in the air. It is not suitable to estimate the radiation damage in the other mediums because it does not take into account the interaction specifics of the radiation other than that of the gamma-rays as well as the absorption characteristic of the target material.

4.6.2. Absorbed dose

An **absorbed dose** is a measure of the energy deposited in an irradiated medium. It is defined as the mean energy deposited by ionizing radiation in an elementary volume of the medium:

$$D = dE/dm. \quad (4.6.2)$$

For bodies with a final volume, under isotropic radiation, the absorbed dose is equal to the ratio of the total deposited energy to the mass of the object:

$$D = E/m. \quad (4.6.3)$$

The SI unit of the absorbed dose is **Joule per kilogram** (**J/kg**), which is named **Gray** (**Gy**) – in honor of the English physicist **Hal Gray**. Nevertheless, the older CGS unit **rad** (**r**adiation **a**bsorbed **d**ose) is still in use in certain countries (mainly outside of Europe). Both units are connected by the relation:

$$1\ \text{Gy} = 100\ \text{rad} \quad \text{or} \quad 1\ \text{rad} = 0.01\ \text{Gy}. \quad (4.6.4)$$

4.6.3. Dose rate

In many cases, it is important to be able to calculate what dose would be obtained by an object in a radiation field during a specific amount of time. For this purpose, it is necessary to know the dose that would be obtained per unit of time – a quantity called a **dose rate**.

The exposure dose rate can be calculated by the equation

$$P_X = X/t, \quad (4.6.5)$$

where *t* is the time of measurement.

The SI unit of the **exposure dose rate** is expressed as a **Coulomb per kilogram per second** (**C/kg·s**). Taking into account that one Coulomb per second is equal to one Ampere, the unit may also be referred to as **Ampere per kilogram**. In practice, the most commonly used unit is **Roentgen per hour** (**R/h**).

The **rate of the absorbed dose** is determined by the relation

$$P_D = D/t. \quad (4.6.6)$$

The base unit thereof in SI is **Gray per second** (**Gy/s**), but **Gray per hour** (**Gy/h**) is also accepted. It should be noted that 1 Gy = 1 J/kg and, respectively, 1 Gy/s = 1 J/kg·s. However, 1 J/s = 1 W and thus, a unit of absorbed dose rate can also be expressed as **Watt per kilogram** (**W/kg**).

4.6.4. Equivalent dose

The absorbed dose is widely used for the evaluation of the radiation effects in many different but inanimate objects such as electronic components and

devices, radiation detectors, seed materials etc. However, it is not precise enough to estimate the actual health risk for the irradiation of living organisms because:

- the same absorbed dose of different types of radiation causes a different biological effect;
- different tissues have different biological sensitivity to equal doses of the same type of radiation.

Therefore, the following specific doses have been introduced, and they are used to limit the radiation exposure time of living organisms.

1. Equivalent absorbed dose (*H*)

This quantity takes into account the type of radiation applied to the biological objects (the designation *H* comes from the word *harm*). It represents the absorbed dose D_R obtained from a given type of radiation *R*, multiplied by a corresponding **radiation weighting factor w_R**, defined by the harmful effect of this radiation:

$$H = w_R D_R. \tag{4.6.7}$$

Since w_R is a dimensionless factor, the equivalent absorbed dose should also be measured in J/kg. But to distinguish both doses and to highlight the specific relation of the equivalent dose to biological objects, the unit of equivalent absorbed dose is called a **Sievert** (**Sv**) in honor of the Swedish physician and physicist **Rolf Sievert** who worked in the field of ionizing radiation protection. In the USA, the unit **rem** (**r**oentgen **e**quivalent **m**en) is still widely used. The relation between both units is

$$1 \text{ rem} = 0.01 \text{ Sv}. \tag{4.6.8}$$

When the radiation field is produced by several types of ionizing radiation with different radiation weighting factors w_R, the equivalent absorbed dose is defined as the sum of its individual constituent components:

$$H = \sum_{(R)} w_R D_R. \tag{4.6.9}$$

Radiation weighting factors depend mainly on the ionizing action of the respective radiation per unit distance in the medium. For this reason, the most harmful are the heavy particles such as alpha particles and fission fragments. Respectively, the most harmless are the light particles (e.g. electrons) and photons. This is confirmed in Table 4.6.1, containing the values of the different weighting factors. The International Commission of Radiological Protection (ICRP) recommended them in 2007 [1, 2].

Radiation	Energy, E	w_R
Photons, electrons and muons	All	1
Neutrons	< 1 MeV 1 to 50 MeV > 50 MeV	$2.5 + 18.2 \cdot e^{-[\ln E]^2/6}$ $5.0 + 17.0 \cdot e^{-[\ln(2E)]^2/6}$ $2.5 + 3.25 \cdot e^{-[\ln(0.04E)]^2/6}$
Protons, charged pions	All	2
Alpha particles, fission fragments and heavy nuclei	All	20

Table 4.6.1. Radiation weighting factors

Evidently, the equivalent dose does not take into account the different radiation sensibility of the organs in the human body. For this reason, it is suitable only to estimate the radiation damage to an individual organ.

2. Effective equivalent dose (H_E)

This dose is used to estimate the radiation damage to the whole body. For this purpose, **tissue weighting factors** (w_T) are introduced, and the effective dose is calculated by the relation:

$$H_E = \sum_{(T)} w_T H_T = \sum_{(T)} w_T \sum_{(R)} w_R D_R \qquad (4.6.10)$$

(taking into account Eq. (4.6.9)). Here H_T is the equivalent dose absorbed by tissue T.

Tissue weighting factors are dimensionless, and therefore the unit of the effective equivalent dose is also Sievert (Sv). The w_T values (Table 4.6.2) reflect the specific sensitivity and respective damage to the organ or tissue when exposed to ionizing radiation. The table also shows the development of the estimation of the organ's radiation sensitivity over the years.

Organs	Tissue weighting factors, w_T		
	ICRP26 1977	**ICRP60 1990**	**ICRP103 2007** [2]
Gonads	0.25	0.20	0.08
Red Bone Marrow	0.12	0.12	0.12
Colon	–	0.12	0.12
Lung	0.12	0.12	0.12
Stomach	–	0.12	0.12
Breasts	0.15	0.05	0.12
Bladder	–	0.05	0.04
Liver	–	0.05	0.04
Oesophagus	–	0.05	0.04
Thyroid	0.03	0.05	0.04
Skin	–	0.01	0.01
Bone surface	0.03	0.01	0.01
Salivary glands	–	–	0.01
Brain	–	–	0.01
Remainder of body	0.30	0.05	0.12
Total	**1.00**	**1.00**	**1.00**

Table 4.6.2. Tissue weighting factors

References

[1] ICRP, 2007. The 2007 Recommendations of the International Commission on Radiological Protection. ICRP Publication 103. Ann. ICRP 37 (2-4).

[2] Source and effects of ionizing radiations. UNSCEAR-2008 Annex A, Table A1, p. 40. http://www.unscear.org/docs/publications/2008/UNSCEAR_2008_Annex-A-CORR.pdf

PART 5. RADIATION DETECTORS

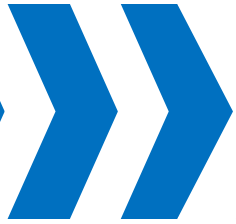

5.0. Introduction

It has been made clear up to this point that radiation is energy traveling in the form of particles or photons. Unfortunately, the human organism has no senses capable of perceiving these forms of energy without assistance. For this reason, we need instruments to indicate the presence of radiation and to measure some of its basic characteristics. These instruments are called **radiation detectors**. Within these detectors, the interaction of radiation with the detector material is used to transform specific radiation energy into another type, which can easily be observed and the quantitative parameters of which can be measured.

The classification of the type of radiation detector is based namely on the kind of interaction used. Considering the review of radiation interactions, as described in Part 4, it is evident that the most frequent final result is the ionization of the matter. For this reason, the first and largest group of detectors consists of the so-called **ionization detectors**. Since the ions have charges, these detectors have the important advantage of transforming the radiation characteristics directly into the parameters of electrical signals, the measuring of which has widely been developed. This course focuses on the following detectors that form part of the previously mentioned groups: **gas-filled detectors**, **semiconductor detectors** and **thermoluminescent detectors**, which are the most commonly used.

Another large group includes the so-called **scintillation detectors**. Within these detectors, the radiation energy is first transformed into visible light, and then the visible light is turned into electrical signals by means of a photodetector.

There are also many other types of radiation detectors – photo, chemical, thermos, etc., which have been excluded from this course.

Later, special detectors used mainly in particle physics research will be described separately.

Before elaborating on the description of detectors, it is necessary to give some information about their basic properties and characteristics, which will be done in the next Section.

5.1. Basic detector characteristics

5.1.1. Generation of electrical signals in ionization detectors[1]

The basic function of detectors is to transform the characteristics of the radiation – such as the flux, energy, etc. – into easily and precisely measurable electrical signals, the high precision measuring of which has been developed extensively.

Based on the detectors' operating principle, they can be divided into two groups: **discrete**, through which a current passes as separated pulses, and **analog**, through which the current passes continuously. This course will describe all types of detectors which belong in the first group. A typical representative of the second group is the so-called emission detector, in which the radiation (gamma or neutron) causes an **emission** of electrons whose flux (i.e. current) is proportional to the intensity of the radiation 0.

The passing of each individual particle or photon through the operating volume of a detector will be referred to as **an event** from this point forward. Each event creates a certain quantity of primary ion pairs (L_0) in the detector, which is usually proportional to its energy (E):

$$L_0 = E/\varepsilon. \tag{5.1.1}$$

Here, ε is the mean energy necessary to produce one pair of ions.

In some detectors, so-called **secondary processes** are also running simultaneously, resulting in an increase in the initial number of charge carriers, i.e. an internal amplification of the signal. Examples of this type are the proportional- (sect. 5.2.3) and Geiger-Mueller (sect. 5.2.4) counters. In such a case, the total number of events (and the number of ion pairs) will be:

$$L = k_D L_0 = k_D E/\varepsilon, \tag{5.1.1a}$$

where k_D is the intrinsic amplification factor (gain) of the detector.

The ionization time is very short – from a few picoseconds in semiconductor detectors to a few nanoseconds in gas-filled detectors. For this reason, it can be accepted that at the moment when $t = 0$ (usually, the time is measured from the moment of the ion charge appearance), a total charge (plus and minus) is created in the detector volume:

$$Q_D = q_e 2L = 2q_e k_D L_0 = 2q_e k_D E/\varepsilon, \tag{5.1.2}$$

where $q_e = 1.602 \cdot 10^{-19}$ C (Coulombs) is the charge of the electron.

[1] The electrical signals generated by the **scintillation detectors** are analyzed in Section 5.5.2.

Furthermore, this charge is accumulated on the detector's electrodes (D, Fig. 5.1.1), creating an electrical signal. For this purpose, a specific voltage (U_{BIAS}, Fig. 5.1.1) is fed to the electrodes, and the aroused electrical field causes the electrons and positive ions to move in opposite directions. The charge collection time t_C (i.e. the time needed for full charge accumulation) varies considerably – from a few nanoseconds for some semiconductor detectors (see Section 5.3.3) to several milliseconds for ionizing chambers (see Section 5.2.2.). It depends on the mobility of the charged particles as well as on the mean distance that they have to travel to reach the detector's electrodes.

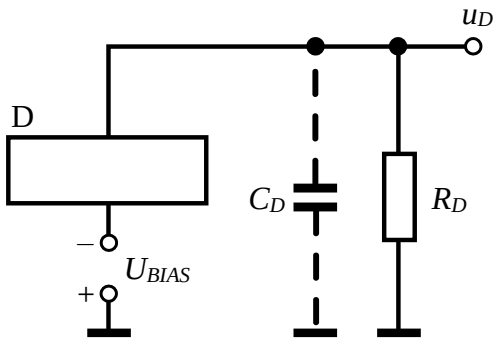

Fig. 5.1.1. A typical detector operating circuit

5.1.2. Amplitude and form of the detector signal

The directed movement of the charge carriers in the detector causes a current in the outer circuit. The only limiting condition about its value is

$$\int_0^{t_C} i(t)dt = Q_D, \qquad (5.1.3)$$

i.e. the integral of the current for the charge collection time (t_C) should be equal to the charge Q_D initially created in the detector. However, each type of detector has a different current time function $i(t)$. For gas-filled- and thin semiconductor detectors, the form of the current pulse, as shown in Fig. 5.1.2a, is acceptable (the parameters of the output signals of the scintillation detectors are studied in Section 5.5.2).

When ionizing radiation passes through the detector, each event will generate a similar pulse, the amplitude and duration (or width) of which will depend on its energy[1]. For this reason, the current in the outer circuit will have a discrete (pulse) character. Nevertheless, the output signals can be **discrete** or **analog**, depending on the parameters of the outer electrical circuit. The

[1] This analysis is carried out assuming that the radiation flux is low enough to neglect the dead time of the detector (see Section 5.1.5).

detector mode of operation in the first case is called the **pulse mode**, and in the second – the **current mode**. When operating in the pulse mode, the radiation parameters can be transformed into signal amplitude, signal shape, mean frequency (count rate), or moment of generation, while in the current mode, they can only be transformed into an instantaneous-, or a mean value of the output current.

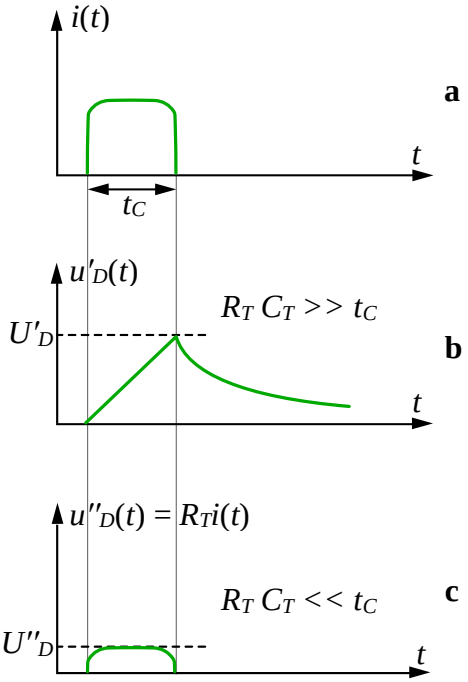

Fig. 5.1.2. Amplitude and form of the detector signal

Typically, each detector is connected to a preamplifier (see Part 7) with an input resistance of R_{IN} and an input capacitance of C_{IN}. In such a case, the processes of detector signal generation depend on the total resistance $R_T = R_D R_{IN}/(R_D + R_{IN})$ and the total capacitance $C_T = C_D + C_{IN}$ (instead of only on R_D and C_D).

A. Pulse mode of operation

For this mode of operation, the capacitance has to be as small as possible (determined by the circuit), and the time constant of the circuit depends only on the total resistance R_T. Normally, one of two time constants is used:

- **Large time constant ($R_T C_T >> t_C$)**
  In this case, the current passing through the resistor R_T can be neglected, and the full charge Q_D is transferred to the capacitance C_T. Therefore (Fig. 5.1.2b), the amplitude of the voltage signal will be the maximal possible:

$$U_D' = \frac{Q_D}{C_T} = 2q_e k_D E/\varepsilon C_T, \qquad (5.1.4)$$

using equation (5.1.2).

When the current has finished passing through the detector, the capacitance C_T discharges very slowly through the resistor R_T:

$$u_D' = \frac{Q_D}{C_T} e^{-\frac{t-t_C}{R_T C_T}}. \qquad (5.1.5)$$

Should a new particle or photon pass through the detector during this pulse, its proper signal amplitude will be changed, and a false magnitude will be measured. This harmful process, called the **pile-up effect**, can be limited by differentiating the signals in one of the following electronic stages.

The relation (5.1.4) shows that the amplitude of the signal is proportional to the energy of the particle or photon if the detector is **linear** – the gain k_D and the capacitance C_D are constant and do not depend on the particle's energy. For this reason, a mode with a large time constant will have extensive applications for measuring the energy distribution of radiation – the so-called **radiation spectroscopy**. It is also preferred for radiation flux measurements (called **radiometry**) because of its relatively high signal amplitude.

- **Small time constant ($R_T C_T << t_C$)**
  In this case, practically the entire current passes through the total resistor R_T and

$$u_D''(t) = R_T i(t), \qquad (5.1.6)$$

i.e. the signal has the form and width of the detector current pulse (see Fig. 5.1.2c). *The signal amplitude is very small, but the pulse duration is minimal.*

Despite problems identifying and separating the signals from the noise, this mode is used when the purpose of the measurement is to find the time distribution of the signals or when very large radiation fluxes have to be measured.

B. Current mode of operation

To operate in this mode, it is necessary to use a preamplifier with low input resistance (i.e. a current-sensitive preamplifier) as well as a supplementary capacitance in order to provide a high time constant of the detector output

circuit. In this way, the current through the R_{IN}, which is measured, will be proportional to the mean detector current:

$$I_{IN} = nQ_D = 2nq_e k_D E/\varepsilon, \qquad (5.1.7)$$

where n is the count rate (the mean number of events in the detector during a unit of time).

The current mode of operation is preferred when the amplitude of the detector's signals is low, as it is in the ionization chambers (see Section 5.2.2). The advantage of this mode is that the mean noise current is zero (because of the random distribution of the noise signals), and the noise does not influence the measurement.

5.1.3. Energy resolution

The dependence of the number of ions (i.e. the total charge) created in the detector on the incident radiation energy allows for the measurement of the energy distribution of the radiation particles or photons. This measurement process is called **radiation energy spectroscopy** and is widely used in scientific nuclear investigations and their applications.

The **energy spectrum** is the differential number of particles or photons dN/dE as a function of their energy E. However, in the detector, the radiation energy is transformed into the number of generated ions L_0 (see eq. (5.1.1)), i.e. into the output pulses' amplitude U_D. Respectively, the energy spectrum is presented by the so-called **energy response function** of the detector 0, which is the differential number of output pulses $n = dN/dU_D$ as a function of their amplitude U_D (Fig. 5.1.3).

When the radiation is mono-energetic (with an energy E_1), then ideally, all detector pulses should have equal amplitudes (U_{D1}) so that the peak will be only one spike above U_{D1}, corresponding to the mathematical delta function. However, due to the random character of the interactions between the radiation and detector material, the number of generated ions L_1 and the output pulses' amplitude varies. As a result, the peak expands. Two typical cases are shown in Fig. 5.1.3a – with high and low energy resolutions, respectively. If the same total number of pulses are recorded, the surfaces under each peak will be equal. The difference between both resolutions is due to the different fluctuations of the signal amplitudes in both cases.

When the fluctuations are smaller, the peak will be narrower, and the amplitude (i.e. the radiation energy) can be determined more precisely. For this reason, the energy resolution R_E is evaluated by the ratio of the full peak width at half of its maximum $\Delta U_1(\Delta E_1)$ (usually abbreviated as **FWHM** –

Full **W**idth at **H**alf **M**aximum) to the amplitude (or the energy) corresponding to its maximum (see Fig. 5.1.3b):

$$R_E = \Delta U_1/U_1 = \Delta E_1/E_1. \qquad (5.1.8)$$

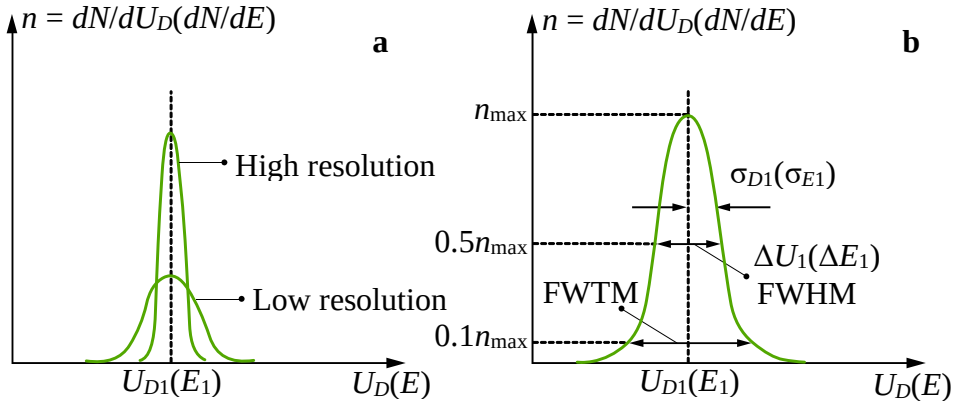

Fig. 5.1.3. Radiation energy spectrum and its parameters

The fluctuations in the number of ions generated by each particle correspond to a Poisson distribution. However, because of their relatively high values (L_0 >> 1), the peak can be approximated by a Normal (Gauss) distribution. Since the radiation energy is proportional to L_0, the fluctuations of its measured values will have a Gauss distribution too:

$$G(E) = \frac{E}{\sigma_E\sqrt{2\pi}}\exp\left(-\frac{(E-E_1)^2}{2\sigma_E^2}\right), \qquad (5.1.9)$$

whose standard deviation σ_E is connected with **FWHM** by the relation:

$$\text{FWHM} = \Delta E_1 \approx 2.355\sigma_E \text{ [eV]}. \qquad (5.1.9a)$$

The following equation is used for the energy resolution:

$$R_E = \Delta E_1/E_1 = 2.355\sigma_E/E_1 = 2.355\delta_E \text{ [\%]}, \qquad (5.1.8a)$$

where $\delta_E = \sigma_E/E_1$ is the relative standard deviation of the energy.

Recently, some detector manufacturers have begun using the quantity **FWTM** (**F**ull **W**idth at one-**T**enth of the **M**aximum) to evaluate the energy resolution (see Fig. 5.1.3b). For an absolute normal distribution, the ratio between **FWTM** and **FWHM** is approximately 1.85.

Due to the fact that the random distribution of the number of events L_0, which are created by the mono-energetic radiation in the detector volume, follows a Poisson distribution, its variance $Var(L_0)$ will be equal to the mean value of the number $\bar{L}_0$ [3]:

$$Var(L_0) = \bar{L}_0 \approx L_0. \quad (5.1.10)$$

However, experiments have shown that the actual variance is smaller. The reason is that the process, giving rise to each individual charge carrier, is not independent since the discrete electron shells limit the number of ways an atom may be ionized. The net result is a better energy resolution than predicted by purely statistical consideration. Its influence can be recognized by introducing into the corresponding equation a correction factor *F*, called the **Fano factor**. Thus the actual variance will be:

$$Var(L_0) = FL_0. \quad (5.1.11)$$

The Fano factor is determined experimentally and has values from 0 to 1 depending on the specific interactions in each detector. For example, for gas proportional counters, $F \approx 0.05–0.2$, and for semiconductor detectors, $F \approx 0.05–0.15$. For scintillation detectors, $F = 1$, which corresponds to an exact Poisson distribution.

For detectors without intrinsic amplification ($k_D = 1$), the radiation energy measured by the number of ions can be calculated through equation (5.1.1):

$$Var(E) = \varepsilon^2 Var(L_0) = \varepsilon^2 FL_0 = \varepsilon FE \quad (5.1.12)$$

(taking into account that the variance of the product of a random quantity with a constant is equal to the variance of the random quantity multiplied by the square of the constant).

Therefore, the standard deviation will be:

$$\sigma_E = \sqrt{Var(E)} = \sqrt{\varepsilon FE}, \quad (5.1.12a)$$

and then the relative standard deviation will be:

$$\delta_E = \sqrt{\frac{\sigma_E}{E}} = \sqrt{\frac{\varepsilon F}{E}}. \quad (5.1.12b)$$

For detectors with intrinsic amplification, k_D is also a random quantity, the statistical distribution of which depends on the particular type of detector. Thus, the problem has to be analyzed in conjunction with the description of the relevant detector.

Another reason for fluctuations in the signal amplitude is the electrical noise in the detector and the electronic devices following it. The noise voltage has a random character and modulates the signal amplitudes, thus broadening the peak and worsening the energy resolution.

5.1.4. Counting characteristic

Detectors are very often used to measure the radiation flux, and thereby, the radiation source's activity. In such a case, it is necessary to measure the counting rate – the number of the detector's signals n with an amplitude higher than a certain threshold U_{th}, which are received in a fixed time interval. (There is always such a threshold in order to eliminate a large segment of the noise signals.) It can be seen that the precision of the measurement depends not only on the threshold stability but also on the stability of the detector signals' amplitude.

In turn, the operation of the detector depends on its supply voltage. For this reason, it is important to know the relation between the registered number of signals and the detector supply voltage, which is called the **counting characteristic** of the detector. In Fig. 5.1.4, the counting characteristic of a Geiger-Müller counter is shown. It is evident that it has an almost horizontal plateau between the supply voltages U_1 and U_2, which provides good operating stability and high measuring precision. The counting characteristic has this form because the Geiger-Müller counter is strongly nonlinear, and the amplitude of the pulses do not depend on the particle energy (see Section 5.2.4).

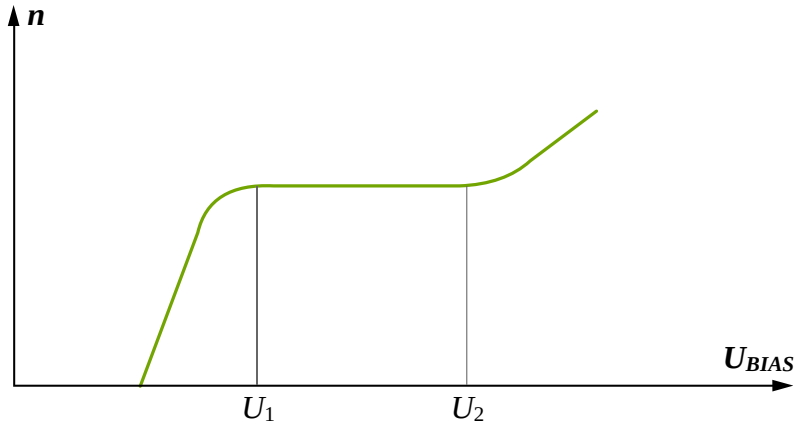

Fig. 5.1.4. Typical counting characteristic of a Geiger-Müller detector

The counting characteristic of mono-energetic radiation is important for linear detectors. Their plateau begins at a supply voltage at which the amplitudes of all signals created by the radiation are greater than the threshold voltage. The slope of this plateau depends on the background radiation and on the rate of false signals generated by the detector (see Section 5.2.3).

5.1.5. Time resolution

The time resolution of detectors is characterized by the so-called **dead time**. The dead time of any electronic device is the minimum time interval between

two input signals at which they will be accepted as two separated events. For detectors, it is the minimum time interval after the passing of one particle or photon through the detector volume (an interaction event), at the end of which the detector can record a new event. Because the time intervals between the radioactive decays are randomly distributed, and the shorter intervals are more probable (see Section 2.5.4), there will always be signal losses. For these reasons, dead time is one of the most important detector parameters.

The detector dead time depends on the processes in the detector and, first and foremost, on the mobility of the ions created in its volume. Based on these dependencies, two different models are used to describe the detector's reaction to very short intervals between the radiation particles – a **paralyzable** and **non-paralyzable** 0 response.

Fig. 5.1.5a represents a sequence of different moments with the presumption that a particle passes through the detector at each moment. Fig. 5.1.5b shows a paralyzable detector response, which causes an extendable dead time: in this case, each particle passing through the detector prolongs the dead time with the time of its delay, adding it to the previous event. As a result, the input sequence of six events will generate only three output signals. Fig. 5.1.5c shows the generated output pulses of a detector with a non-paralyzable response. As can be seen, the dead time is constant in this case – after the end of each signal, the detector is ready to generate a new signal regardless of whether a new event took place during the pulse duration or not. Therefore, from the same input sequence of six events, four output signals will be generated by the detector.

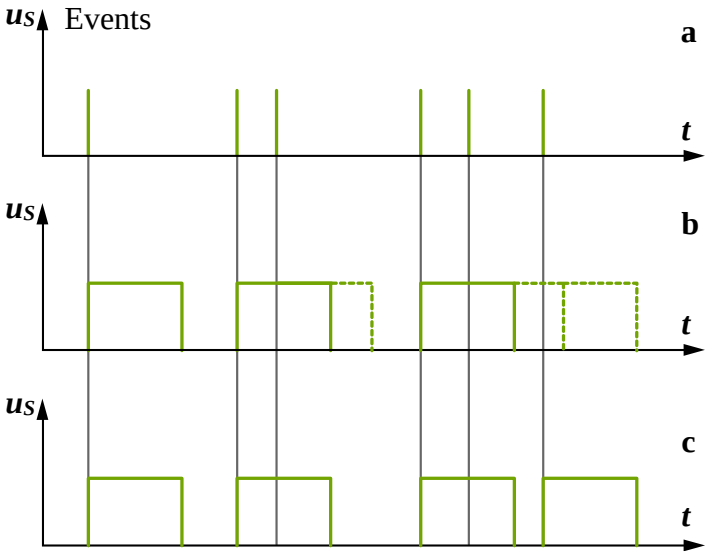

Fig. 5.1.5. Types of detector dead time

These two kinds of detector operations are slightly idealized. Actual detectors often display behavior in between these two extremes. Nevertheless, the response of most of them is exactly, or close to, the paralyzable model.

The dead time of a measuring system not only depends on the detector parameters but also on the delay introduced by the electronic devices that process and record the signals. In the commonly used counting systems, however, the detector sets the dead time of the instrument.

5.1.6. Efficiency

Generally, efficiency is a parameter showing how many of the particles or photons emitted by the radioactive source will produce detector signals that the electronic measuring device will record. Some authors 0 call this efficiency **absolute**, other [4] – **total**, and it can be defined as:

$$\eta = n_R/n_S. \tag{5.1.13}$$

Here, n_S is the number of all emitted particles per unit of time by the source, and n_R is the number of signals recorded by the electronic device.

Realistically, absolute efficiency consists of two components. The first (η_G), shows how many of all emitted particles per unit of time (n_S) enter the operating volume of the detector (n_D):

$$\eta_G = n_D/n_S \tag{5.1.14}$$

and is called the **geometrical efficiency**. It is defined by the solid angle Ω between the source and the detector:

$$\eta_G = \Omega/4\pi. \tag{5.1.15}$$

For a radioactive point source, Ω can be calculated [5] by:

$$\Omega = 2\pi\left(1 - \frac{d}{\sqrt{d^2 + r^2}}\right), \tag{5.1.16}$$

where *d* and *r* are shown in Fig. 5.1.6. The sample should be placed inside the detector to provide a geometrical efficiency of 100 %.

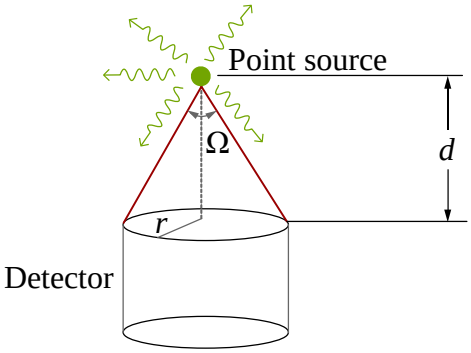

Fig. 5.1.6. Determination of the detector's solid angle

The second component is called **intrinsic** detector efficiency (η_I) and it shows how many of the particles, which entered the operating detector volume in a unit of time (n_D), produced electrical signals recorded by an electronic device (n_R):

$$\eta_I = n_R/n_D. \tag{5.1.17}$$

The processes in the detector define the intrinsic efficiency. There are many reasons for one particle not to produce a recordable detector signal: a loss of energy in the detector envelope, which is typical for alpha particles; not enough energy to produce a signal with an amplitude higher than the following electronic device's threshold, which is typical for beta particles because of their continuous energy spectrum; passing through the detector without any interaction is typical for gamma photons. The intrinsic efficiency also takes into account the signal losses due to the dead time.

Obviously, the absolute efficiency is the product of these two components – the geometric and intrinsic efficiencies:

$$\eta = \eta_G \eta_I. \tag{5.1.18}$$

References

[1] *Sion, N*. Neutron Flux Detector Diagnostic Methodology. http://irpa11.irpa.net/pdfs/3h67.pdf

[2] *Knoll, G.F*. Radiation detection and measurement. Third ed. John Valley & Sons Inc., New York, 2000. https://phyusdb.files.wordpress.com/2013/03/radiationdetectionandmeasurementbyknoll.pdf

[3] *V.I. Goldansky, A.V. Kutsenko, M.I. Podgoretsky*. Counting statistics of nuclear particles. Delhi: Hindustan Pub. Corp., 1962.

[4] *Ahmed, S.N*. Physics and Engineering of Radiation Detectors. Academic Press Inc., Elsevier, 2007. https://www.elsevier.com/books/physics-and-engineering-of-radiation-detection/ahmed/978-0-12-045581-2

[5] Solid angle. https://en.wikipedia.org/wiki/Solid_angle

5.2. Gas-filled detectors

5.2.1. Gas discharge under the influence of ionizing radiation

Gas-filled detectors belong to the so-called ionization detectors group, which transforms the radiation parameters into parameters of electrical signals through the creation of ions in the detector volume. Liquid filled detectors, as well as semiconductor detectors, are also included in this group. In this course, only gas-filled and semiconductor detectors are discussed.

In general, a gas-filled detector is a closed volume filled with gas in which two electrodes are placed to create an electric field (Fig. 5.2.1). When there is no supply voltage, the **electric field strength**[1] (or **intensity**) is $\mathscr{E} = 0$, but the detector is irradiated, and ion pairs are formed on the path of each particle or gamma quantum. These charges, created by the incident radiation, are called **primary charges** (or **primary ions**) to distinguish them from those that are produced later during the drift of the primary electrons to the anode (i.e. not directly by the radiation).

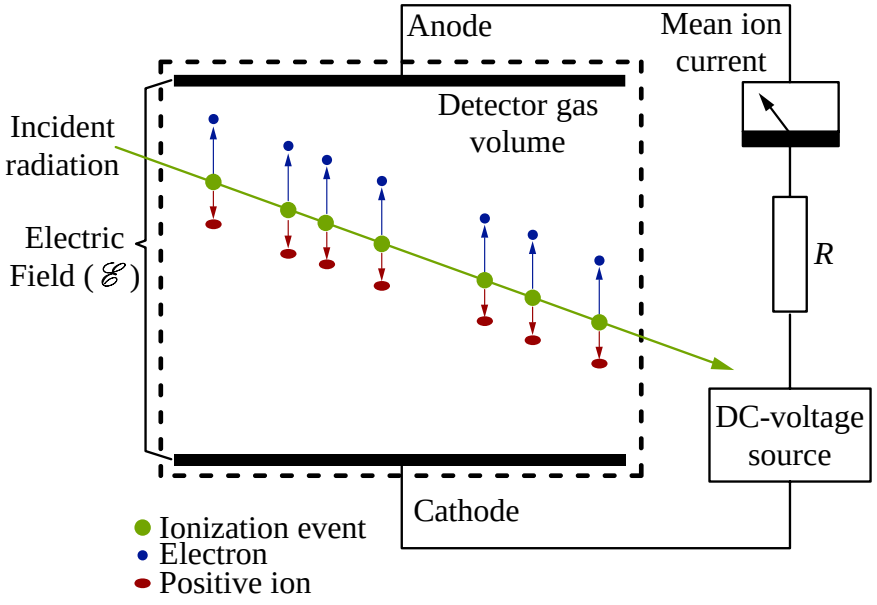

Fig. 5.2.1. A typical gas-filled detector

Depending on the nature of the gas, the ion pairs can be one of two types:

[1] The electric field strength is a vector quantity. In our course, however, we shall always bear its magnitude $\mathscr{E}$ in mind.

- **One electron and one heavy positive ion**: they are typical for so-called **electropositive** gases – helium, argon, neon, nitrogen, etc., whose atoms have an outer shell filled, or almost filled, by electrons.
- **One electron and one heavy negative ion**: they are characteristic of **electronegative** gases (oxygen, water vapors, nitrogen oxides, halogen gases, carbon oxides etc.) – their atoms have incomplete electronic outer shells. For this reason, one free electron captured by an atom creates a heavy negative ion. In most cases, electronegative gases aggravate the characteristics of the detector, and therefore, measures are taken to purify the basic gas and thus remove them.

The number of primary ion pairs L_0 can be calculated using equation (5.1.1). Here, E is the energy deposited by the radiation in the detector volume. However, it should be noted that the **mean energy** ε spent to produce one pair of ions is significantly higher than the first ionization potential i_P (or energy) of the gas atoms. The reason is that a big part of the radiation energy is spent on **exciting** the gas atoms (see Section 4.2.4). Equation (5.1.1) shows that the number of primary ions will be proportionate to the radiation energy.

The basic parameters of the most often-used gases are given in Table 5.2.1 [1].

Gas	***Z***	**Density** $\times 10^{-4}$ **g/cm**^{3}	i_p **eV**	**ε eV/pair**	***dE/dx*** **keV/cm**
H_2	2	0.9	15.4	37	0.34
He	2	1.8	24.6	41	0.32
N_2	14	12.5	15.5	35	1.96
O_2	16	14.3	1.2	31	2.26
Ne	10	9.0	21.6	36	1.41
Ar	18	17.8	15.8	26	2.44
Kr	36	37.5	14.0	24	4.60
Xe	54	58.9	12.1	22	6.76
CO_2	22	19.8	13.7	33	3.01
CH_4	10	7.1	10.8	28	1.48

Table 5.2.1. Basic parameters of the most often-used gases

Z indicates the number of protons in the corresponding atom or molecule. The information about the stopping power (*dE*/*dx*) makes it possible to calculate the size of the detector so that the radiation deposits all of its energy into the detector's volume. However, it should be noted that its value depends on the gas pressure in the detector (the data in Table 5.2.1 are for atmospheric gas pressure).

Without an electric field, primary ions diffuse into the volume of the detector (from areas with a higher concentration to those with a lower one), and after a while they are evenly distributed throughout the volume. During their dispersion, there are also collisions between electrons and positive ions, resulting in numerous **recombinations** – a restoration of the original neutral atom. The number of recombinations increases with the increase in the ion density, and at constant radiation intensity, a dynamic equilibrium is reached – the number of recombinant ions equals that of the newly created.

When voltage is applied to electrodes, an ion's drift begins, leading to a gradual decrease in diffusion and chaotic motion. The electrons move to the positive electrode (anode) and, because of their small mass, they receive considerable acceleration, which determines their active role in the gas discharge processes. Positive ions move much more slowly to the cathode than the electrons.

The processes in the gas can best be studied by the so-called **current-voltage characteristic** – the dependence of the current moving through the detector on the applied voltage. It can be divided into different regions corresponding to the specifics of the processes in the gas (Fig. 5.2.2).

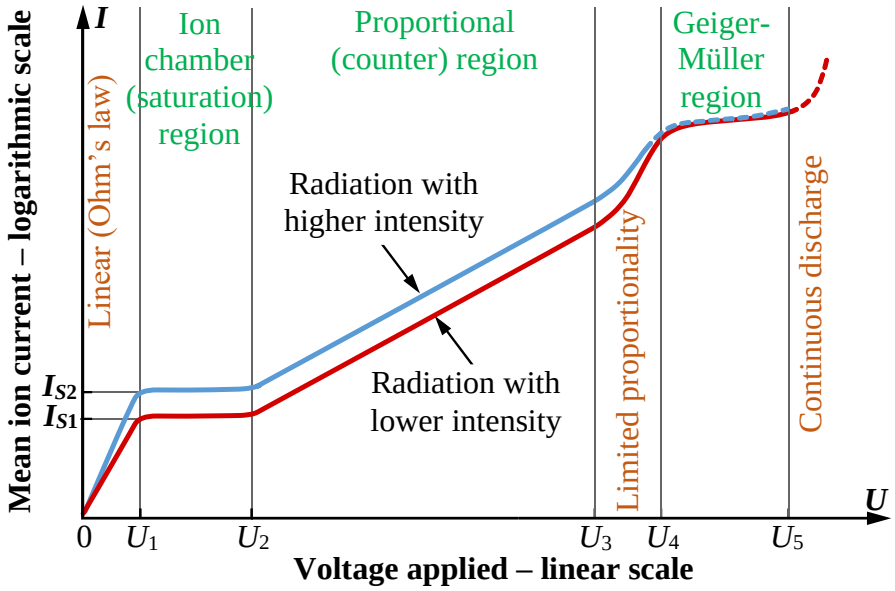

Fig. 5.2.2. Typical current-voltage characteristics

1. Voltage $U = 0 \div U_1$

In this region, the dependence is almost linear, and therefore it is called **linear** or is referred to as the **Om's law** region. In it, the electric field strength is still small, the speed of the ions is low, and some of them recombine before reaching the respective electrode. As the voltage increases, their speed increases and more ions reach the electrodes before they recombine; thus, the current also increases. When the voltage grows high enough ($U = U_1$) that all ions generated per unit of time reach the electrodes without recombining, the current stops depending on the voltage.

2. Voltage $U = U_1 \div U_2$

In the so-called **saturation region**, the increase in the voltage causes practically no change in the ion current – it reaches its **saturated value** when all primary ions have reached the electrodes (without any recombination). The specific value of the current depends on the number of primary ions generated per unit of time by the radiation in the detector volume, i.e. on the flux and the radiation energy. With higher flux and higher energy (i.e. at a higher radiation intensity), the current is greater at the same voltage (see Fig. 5.2.2). Gas-filled detectors operating in this region of the current-voltage characteristic are called **ionization chambers**.

3. Voltage $U = U_2 \div U_3$

When $U = U_2$, the kinetic energy of some of the electrons increases to a level at which they can ionize the neutral atoms of the gas when colliding with them. This process (Fig. 5.2.3) is called **impact (secondary) ionization** or the **Townsend discharge**[1] (also referred to as the **Townsend avalanche**) [2]. Thus, it causes the supplementary generation of **secondary ions** in the detector volume, resulting in an increase in the current called **gas amplification** (also referred to as **gas multiplication**). In this region, each primary ion produces only a single ion avalanche, and thus the amplitude of the current pulse is proportional to the radiation energy. Respectively, by increasing the voltage, the mean ion current increases (Fig. 5.2.3) but remains proportional to the number of primary ions, i.e. to its saturated value (I_S):

$$I = k_D I_S = k_G I_S. \qquad (5.2.1)$$

Here, k_D is called **gas gain** (or the **gas multiplication factor**) and is marked by k_G. It grows with the increase in the voltage U, but for each fixed value of U, k_G is constant. That is why this region is called **proportional**, and the

[1] The Townsend discharge is named after **John Sealy Townsend** who discovered this fundamental ionization mechanism between 1897 and 1901.

detectors working in it are referred to as **proportional gas detectors** (**proportional counters**).

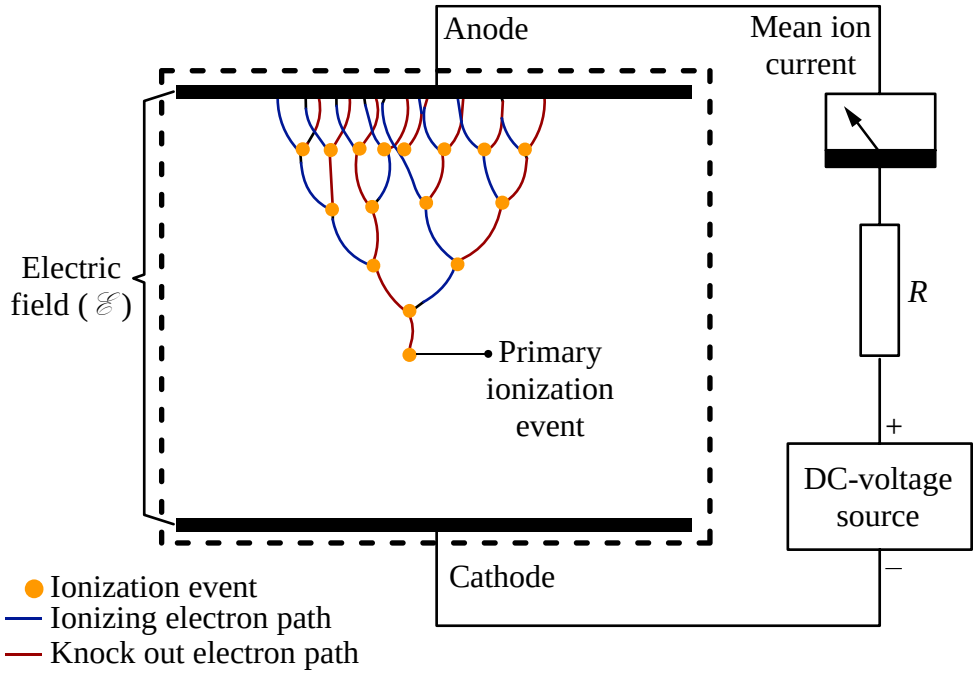

Fig. 5.2.3. Impact ionization in a gas-filled detector

4. Voltage $U = U_3 \div U_4$

This is the so-called region of **limited proportionality**. In it, impact ionization becomes very strong and positive ions form a **space charge** that shields the cathode, lowering the electrical field strength therein. This influences the process of impact ionization and disturbs the strict proportionality between the ion current and the number of primary ions produced by the radiation (k_G ceases to be constant).

5. Voltage $U = U_4 \div U_5$

A further increase in the voltage results in an operation mode in which only the ionization impact processes determine the ion current. One pair of ions arising in the volume is sufficient to create the first avalanche, causing the discharge to spread throughout the entire detector volume mainly because of the generated UV photons. Its value is limited only by the space charge of the positive ions and by the resistor R of the outer circuit. This region is called the **Geiger-Müller** region; detectors operating in it bear the same name.

It is important to note that the gas discharge in all mentioned regions is convertible – when the ionizing source is removed, the discharge is interrupted without any change in the voltage U. However, at voltage $U > U_5$,

the discharge becomes **continuous** – it does not cease when the radiation is removed as it is maintained by the secondary electrons emitted from the cathode. This type of discharge quickly damages the detector and **should be avoided at all times**.

Under certain conditions, a detector current at a continuous discharge can be greatly limited to ensure the safety of the detector. Such a mode of operation is called a **corona discharge**, and the corresponding detectors are referred to as **corona counters** (see Section 5.2.5).

5.2.2. Ionization chambers

Ionization chambers operate in the region of ion current saturation (see Fig. 5.2.2). The lack of gas amplification results in a relatively low ion current value (it is determined only by the primary ions as generated by radiation) and a very small pulse amplitude. Therefore, most of the ionization chambers operate in a current mode (see Section 5.1.2) with a saturation current of $I_S = 2nq_eE/\varepsilon$ (according to Eq. (5.1.7) at $k_D = 1$). The measurement of this current makes it possible to determine:

- The count rate of the radiation particles interacting with the gas in the chamber – $n = I_S\varepsilon/2q_eE$, if the radiation is mono-energetic (E = const).
- The energy deposited by the radiation in the detector gas – $nE = I_S\varepsilon/2q_e$, i.e. the dose absorbed by the detector gas.

In all cases, the currents are too small. For example, when irradiating an argon-filled ionization chamber (ε = 26 eV) with alpha particles with energy E = 5.5 MeV at a count rate of n = 1000 s^{-1} (for the whole chamber), the current will be

$$I_S = 2\cdot1000\cdot1.6\cdot10^{-19}\cdot5.5\cdot10^{6}/26 = 67.69\cdot10^{-12}\ \text{A} \approx 68\ \text{pA}.$$

The low current moving through the chambers puts specific requirements on their construction as well as on the materials used to provide small leakage currents. Special electronic devices are also used to amplify such low currents.

The amplitude of the output pulses is also very low. Using the data of the above example and taking a typical value of 75 pF for the chamber capacitance C, we receive

$$U_D = Q/C = 2L_0q_e/C = 2Eq_e/\varepsilon C = 2\cdot5.5\cdot10^{6}\cdot1.6\cdot10^{-19}/26\cdot75\cdot10^{-12} =$$
$$= 0.9\cdot10^{-3}\ \text{V} = 0.9\ \text{mV}$$

as the amplitude of the signal. Beta particles and gamma quanta generate pulses with a much smaller amplitude.

In Fig. 5.2.4, the currents for three different radiation intensities are shown. The problem is that with the increase in the radiation intensity (the flux, the

energy or both), the number of primary ions also increases. For this reason, a higher voltage (U_1) is needed to finish their recombination, and the current saturation region (i.e. the ion chamber's operating region) becomes narrower.

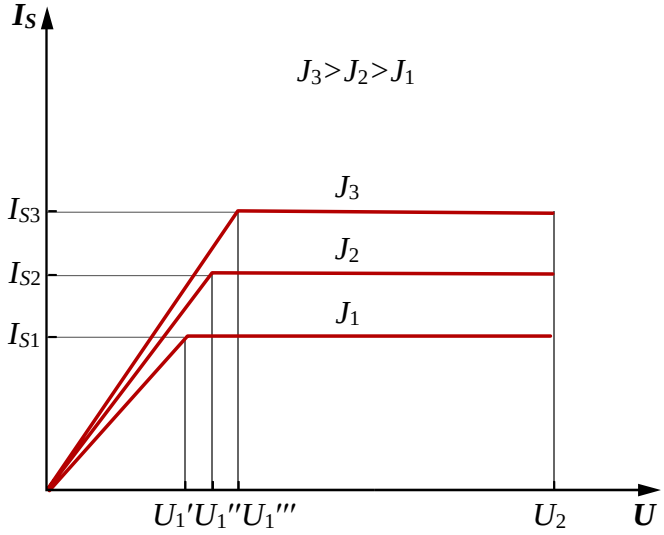

Fig. 5.2.4. The saturation current for three different radiation intensities

Depending on the purpose, ionization chambers with different designs – with flat, cylindrical or spherical forms – are produced. Cylindrical chambers are mainly used for the measurement of nuclear radiation, while large-volume spherical chambers are used for the measurement of cosmic rays.

The construction of a cylindrical ionization chamber is shown in Fig. 5.2.5. It consists of an outer metal cylinder (1), also serving as a cathode, an internal electrode (2) as an anode, insulating rings (3) and a conducting safety ring (4). The supply voltage is fed between electrodes 1 and 2. The quality of the camera depends heavily on the insulation properties of the material between the two electrodes. For example, at $U = 100$ V with a resistance of the insulator $R_I = 10^{12}$ Ω, a leakage current of $I_L = U/R_I = 100/10^{12} = 10^{-10}$ A would flow between the electrodes. This current is equal to or exceeds the minimum currents flowing through the ionization chambers many times over, which may be in the range of 10^{-12}–10^{-15} A. Therefore, very high-quality insulators such as quartz, amber, ceramics, etc., are used. The best results are obtained with the insertion of an additional electrode –such as the ring (4) in Fig. 5.2.5. In this case, all leakage current passes between cathode 1 and this electrode and does not flow through the current measuring device. At the same time, the voltage between electrode 4 and anode 2, and the leakage current between them, are negligible.

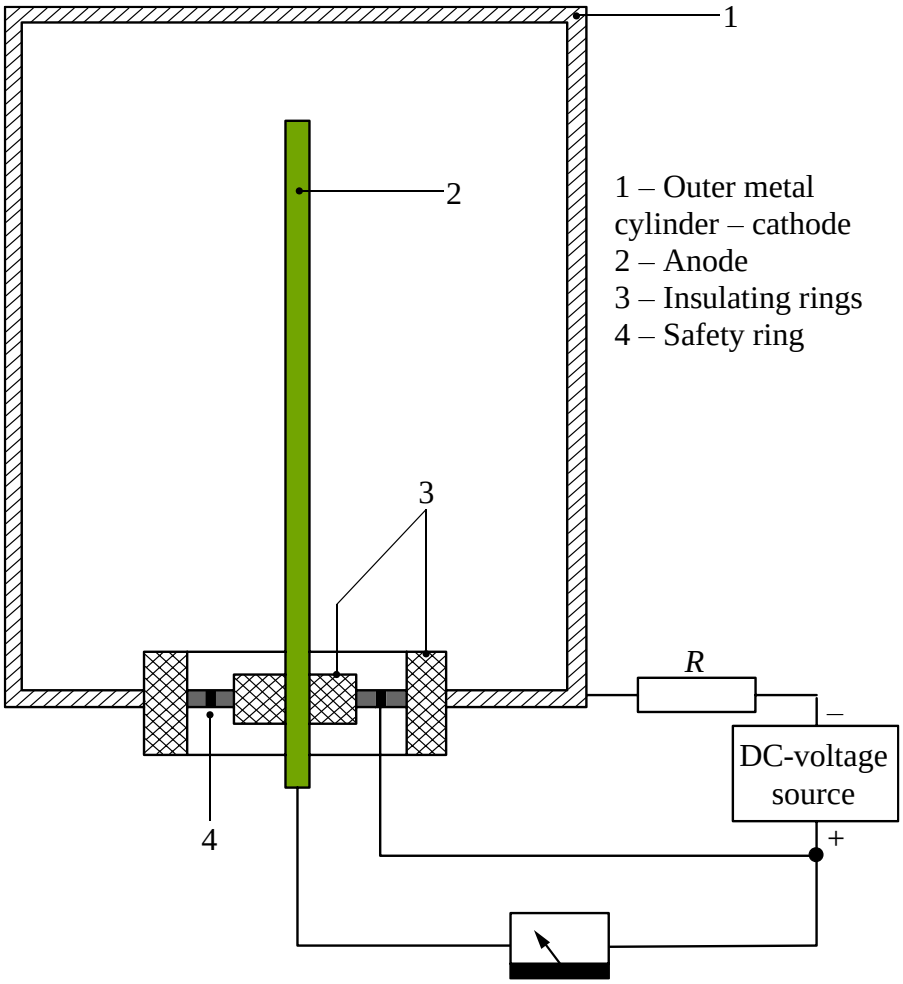

Fig. 5.2.5. Construction of a cylindrical ionization chamber

Cylindrical chambers have many advantages over flat (parallel plate) ones. Firstly, they have a much higher charge collection efficiency due to the non-uniform electric field strength in their active volume as well as the large ion-collection area of their cathode.

Secondly, the alpha-particle chambers have a window covered by a very thin (a few microns thick) plastic film. Furthermore, the alpha source is placed inside the chamber. In order to measure the total energy of the alpha particles, the chamber size should be greater than the particle range in the gas used (see Section 4.2.6). For example, at $E_\alpha = 10$ MeV, the required volume of a chamber filled with argon at a pressure of 10 atmospheres is about 1 liter.

Beta particles have a higher particle range, but their energy spectrum is continuous. In order to register as many beta particles as possible, the same

type of chambers that are used for the registration of alpha particles is also used for beta particles.

Gamma quanta interact very poorly with the gas atoms in the chamber, and their registration efficiency is very low. However, this increases as a result of interaction with the walls of the chamber – the electrons produced during the interaction enter the volume of the detector and are recorded.

The neutrons do not cause ionization. Therefore, for their registration, the chambers must contain a suitable substance, which, interacting with the neutrons, releases charged particles. Depending on the type of substance utilized, several types of chambers are available:

1. **The outer wall of the chamber is covered on the inside by the boron-10 ($^{10}_{3}$B) isotope** (Fig. 5.2.6).

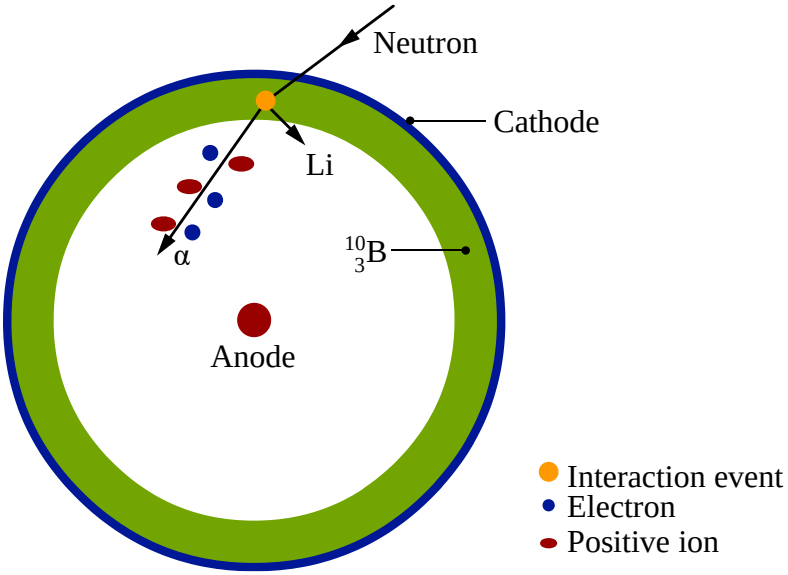

Fig. 5.2.6. A chamber of neutrons using boron-10 as a covering inside

Then, the neutrons enter the following reaction with the boron atoms:

$$^{1}_{0}n + {}^{10}_{5}\mathrm{B} \rightarrow {}^{7}_{3}\mathrm{Li} + {}^{4}_{2}\alpha + W, \qquad (5.2.2)$$

where W is the heat output. Alpha particles thus emitted ionize the gas and generate a pulse sequence that can be counted or measured by the mean ion current.

These chambers are widely used to record neutrons. Another possibility is to use BF_3 gas to fill the chamber. Unfortunately, there are problems with the purification of this gas.

2. **Using helium-3 ($^3_2$He) for working gas in the chamber.** In this situation, the neutrons are involved in the reaction:

$$^3_2\mathrm{He} + {}^1_0n \rightarrow {}^1_1p + {}^3_1\mathrm{T} + W. \qquad (5.2.3)$$

Recording occurs through the protons (p) and tritium nuclei ($^3_1$T), which ionize the chamber gas.

3. **Using fissile material.** Boron and helium cameras cannot be used for neutron measurements in nuclear reactors due to the rapid exhaustion of the boron or helium atoms after the high neutron flux irradiation. The chambers that are the most suitable for such conditions are the ones containing fissile material – uranium-233, uranium-235, plutonium-239 or others. When a neutron passes through this material, it interacts with a heavy nucleus, causing a fission reaction and the generation of two lighter nuclei. They have much higher masses and energy and cause a much stronger ionization of the gas than the alpha particles or protons. Therefore, the sensitivity of these chambers is considerably higher, and they can measure neutron fluxes even in the presence of background gamma radiation, as is the case in nuclear reactors. (The interaction of the gamma rays with the heavy nucleus produces mainly electrons, the very low mass of which is the reason that the generated pulses have a negligible amplitude compared to the pulses produced by the fission fragments).

The construction of a camera of this type is shown in Fig. 5.2.7.

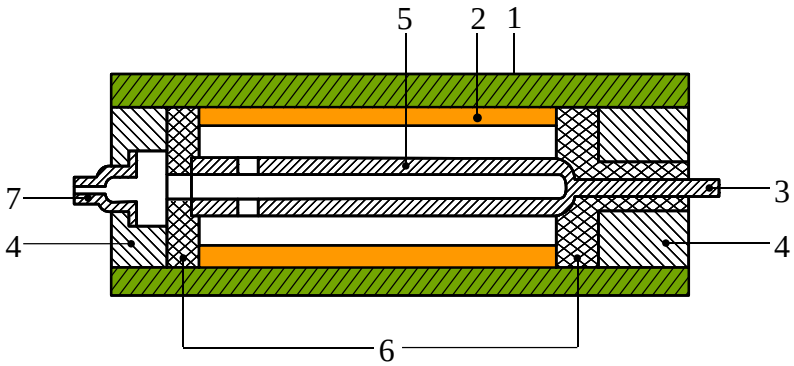

Fig. 5.2.7. A chamber of neutrons using a fissile material as an inside covering

It has a cylindrical shape, and the outer case of the chamber (1) serves as a cathode. The fissile material (2) is placed inside this cylinder. Uranium-235 alloy in combination with a light metal (for e.g., aluminum), or pure uranium-235, is commonly used for this purpose. The material is applied electrolytically. The internal electrode (5) is embedded in the isolators (6) and is led out through the terminal (3). The chamber is hermetically sealed on both sides by means of sleeves (4). A tube (7) passes through one of

them. It is designed to evacuate the chamber and fill it with the necessary gas, after which the tube is closed. The electrodes are usually made of stainless steel, and the distance between them must be as small as possible – this provides a higher electric field strength while the camera can operate at a lower supply voltage. However, for technological reasons, this distance cannot be reduced to less than 1 mm. The external diameter of these chambers is 5–10 mm, and the length is 50–200 mm.

4. **Gamma-compensated ionization chambers.** When it is necessary to measure the neutron flux in an intense gamma field, the difference in the sensitivity of fissile chambers to neutrons and gamma rays may be insufficient to provide the necessary accuracy of the neutron measurements. In this case, a gamma-compensated ionization chamber is used. This chamber (Fig. 5.2.8) consists of two chambers that are identical in shape and size (1 and 2) and are combined in a common construction. They differ only in that the electrodes of one (1) are covered with neutron-interacting material (3), and the other (2) are free of such a coating.

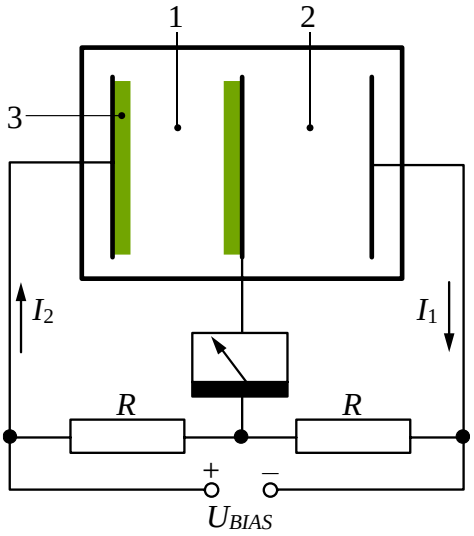

Fig. 5.2.8. A gamma compensated neutron chamber

The chambers share a common electrode, and the ionization current meter is also connected to it. The second electrode of the first chamber (1) receives a positive supply voltage, while the same electrode of the second chamber (2) – negative. Thus, the current meter measures the difference between the two ionization currents:

$$I = I_1 - I_2. \qquad (5.2.4)$$

The current of chamber 1 has two components – generated by neutrons and gamma-quanta:

$$I_1 = I_n + I_{\gamma 1}, \tag{5.2.5}$$

while that of chamber 2 is generated only by the gamma-ray flux:

$$I_2 = I_{\gamma 2}. \tag{5.2.6}$$

The result for the measured current can be obtained by replacing the values of the two currents in equation (5.2.4):

$$I = I_n + I_{\gamma 1} - I_{\gamma 2}. \tag{5.2.7}$$

The two chambers are identical and are located close enough to each other that the gamma-ray flux moving through them is almost the same. Therefore, it can be assumed that $I_{\gamma 1} = I_{\gamma 2}$, i.e. that

$$I = I_n. \tag{5.2.8}$$

It is difficult to fully compensate for the gamma-background impact, but using a compensated chamber highly reduces the gamma background influence.

The pulse mode of the ionization chamber operation has a very limited application – mainly when radiation of heavy particles such as alpha and fission fragments are measured – because they can generate output signals with greater amplitude, of the order of a few millivolts.

5.2.3. Proportional counters

Proportional counters operate in the linear region of the impact ionization in the gas discharge (see Fig. 5.2.2). Therefore, the ion current is greater than the saturation current (see Eq. (5.2.1)), and the amplitude of the output pulses is higher.

Suppose a chamber with flat electrodes (see Fig. 5.2.1) is placed in a proportional mode of operation, the number of secondary pairs of ions created by each electron will depend on the length of its path to the anode, i.e. on the place of its creation in the detector volume and on the trajectory of the charged particle, or quantum, through the detector. For this reason, there will be an inadmissible dependence of the gas gain on the particle- or quantum trajectory, which will break the proportionality between the radiation energy and the amplitude of the generated output pulses.

Proportional counters are constructed differently (Fig. 5.2.9) to avoid this problem.

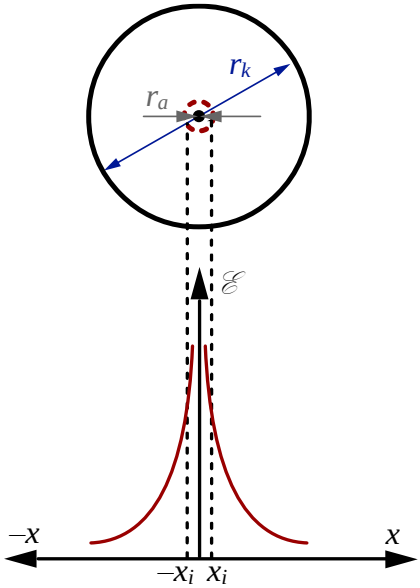

Fig. 5.2.9. Electrical field strength distribution in a proportional counter

In a proportional counter, the cathode is a cylinder, on the axis of which a very thin metal filament (acting as an anode) is stretched. The electric field strength $\mathscr{E}$ in such a detector configuration is very irregular:

$$\mathscr{E}(x) = U/x\ln(r_k/r_a), \tag{5.2.9}$$

where U is the supplying voltage, and r_k and r_a are the radii of the cathode cylinder and the anode wire, respectively. Thus, the impact ionization is possible only in a small region around the anode – in a radius of $r \leq |x_i|$ (see Fig. 5.2.9) where the field strength $\mathscr{E}$ is sufficiently high.

Under such conditions, each electron, regardless of where it is created in the detector volume, initially moves to this region without causing ionization. By only passing through this zone, it creates an avalanche of secondary pairs of ions. In this way, all electrons generate secondary ions passing practically the same distance, which ensures the stability of the gas gain k_G and the strong proportionality between the radiation energy and the output signals' amplitude.

However, the gas amplification in proportional counters, except for the impact ionization caused by the primary electrons, is also due to some other reasons:

- Electrons moving to the anode produce not only pairs of ions but also cause the excitation of many gas molecules. When returning to their normal state, these molecules emit light quanta – photons with a wavelength in and around the ultraviolet region of the spectrum. Their

energy is higher than the ionization energy [3] of the metals commonly used as proportional counter's cathodes. Hence, when an ultraviolet photon strikes the cathode wall, it may knock out an electron from the metal (a process well known as the **photoelectric effect**). Usually, this electron enters the gas and, accelerated by the electrical field, produces a new avalanche of secondary electrons.

- Due to the slow movement of positive ions, a space charge of these ions is formed near the cathode. These ions attract free electrons from the surface of the metallic cathode and recombine with them to form neutral atoms. The neutralized atoms are in excited states due to the excess energy of the ions. The transition to the ground state is accomplished through the emission of a photon, which may also induce a secondary electron emission from the cathode. Furthermore, since there are many positive ions attracting electrons from the cathode, more electrons can be freed than is required for the neutralization. All of these electrons can also produce new impact avalanches.

All of these processes are referred to as **secondary** processes. Evidently, they cause a supplementary increase in the gas gain, which can be evaluated in the following manner. Because of the N_0 of primary ion pairs generated by the radiation, the anode and cathode reach $N = k_G N_0$ electrons or heavy positive ions, respectively. The interactions of the photons (emitted by the excited gas molecule) and heavy ions with the cathode produces $N_k = \zeta N = \zeta k_G N_0$ new electrons from the cathode (ζ is the so-called **factor of the secondary processes**). The new electrons, in turn, produce new avalanches and, as a result, $N' = k_G N_k = \zeta k_G^2 N_0$ new electrons and positive ions reach the anode and cathode, respectively. The latter causes a new emission of $N_k' = \zeta N' = \zeta^2 k_G^2 N_0$ electrons from the cathode and the generation of $N'' = \zeta^2 k_G^3 N_0$ new pairs of ions reaching the anode and the cathode, respectively, and so on.

Ultimately, the total number of electrons that will reach the anode can be calculated by:

$$\begin{aligned} N_T &= N + N' + N'' + \cdots = \\ &= k_G N_0 + \zeta k_G^2 N_0 + \zeta^2 k_G^3 N_0 + \cdots = \\ &= k_G N_0 (1 + \zeta k_G + \zeta^2 k_G^2 + \cdots). \end{aligned} \tag{5.2.10}$$

For $\zeta k_G < 1$, the expression in parenthesis represents an infinitely decreasing geometric progression, the sum of which is $1/(1 - \zeta k_G)$ [4]. Then, the total number of electrons that will reach the anode will be:

$$N_T = \frac{k_G N_0}{1 - \zeta k_G}. \tag{5.2.11}$$

The quantity

$$k_T = k_G/(1 - \zeta k_G) \qquad (5.2.12)$$

is called the **total gas gain**. In the case of $\zeta k_G = 1$, the total gas gain is $k_T = \infty$, which means that the gas discharge becomes continuous (self-sustaining), i.e. it should not stop after the passing of an ionizing particle or quantum through the detector. In practice, this effect leads to the appearance of multiple impact avalanches after each initial one (caused by the radiation) and to the generation of false output signals. Thus, the counter ceases to perform its function. For this reason, the supply voltage, on which the gas gain factor k_G depends, must be kept low enough so as not to violate the condition $\zeta k_G < 1$.

The only way to increase the gas gain (and the amplitude of the output pulses, respectively) while observing this condition is to reduce the factor of the secondary processes ζ. That can be achieved by adding an agent with a high absorption coefficient for photons in the ultraviolet region to the base gas. For this purpose, gases with polyatomic molecules such as methane (CH_4), ethylene (C_2H_4), vapor of methyl alcohol (CH_3OH), and so forth, are used. They are called **quenching** gases, or **quenchers**, derived from the term **quenching** since they decrease the probability of secondary discharges. A quencher effectively reduces secondary processes in two ways:

- the polyatomic gases have a number of closely spaced vibrational and rotational energy levels and, after the absorption of a photon, their molecules generally dissociate to radicals without emitting photons;
- the positive ions of the base gas that are moving to the cathode are neutralized by charge transfers when colliding with the quenching gas molecules, but since the de-excitation processes of the quencher molecules are mostly non-radiative (they dissociate into radicals), the emission of electrons from the cathode is drastically decreased.

Quenching gases are not commonly used in detectors as a base gas because they require a very high operating voltage. Preference is given to mixtures of a noble gas (up to about 90 %) with a quencher agent (up to 10 %).

Although the use of polyatomic gases has obvious advantages, their application creates some negative effects on the counter's operation. There are two important problems caused by their use: the formation of polymers on anode and cathode surfaces; the shortening of the lifespan of the counter. Both problems have the same cause – the dissociation or polymerization of quenching molecules during the process of their de-excitation. The degradation of the electrodes over time is a serious problem because it may change the properties of the counter. The decrease in the detector's lifespan

is a big problem for sealed counters. It can be avoided if the gas flows continuously through the detector.

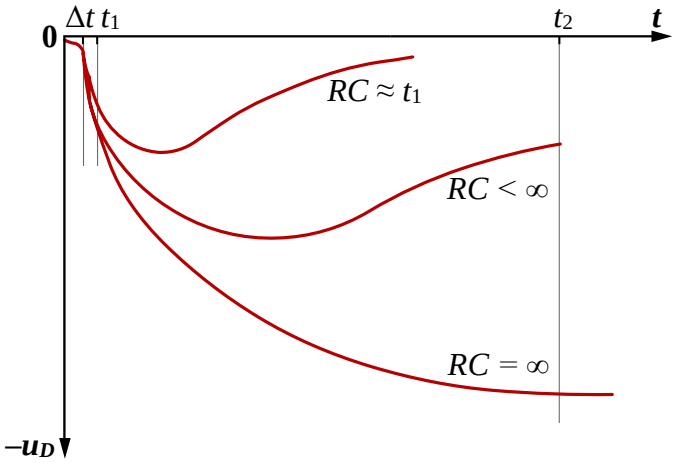

Fig. 5.2.10. Signal generation in a proportional counter

The signal formation in the proportional counter passes as follows (Fig. 5.2.10). Initially, there is a slight delay ($\Delta t \approx 0.1$μs) between the moment of the particle or the quantum passing through the detector and the start of the pulse. During this time, the electrons move from the point of origin to the zone of impact ionization. Thereafter, the electrons move to the anode very quickly ($t_1 - \Delta t \approx 0.01$ μs), but because of the short distance covered, they induce a small proportion of the total charge – 10–15 %; the main contribution to the induced charge is by the positive ions, which are collected at a much slower rate – over a period of $t_2 \approx 100$ μs. The amplitude and the duration of the signals are dependent on the time constant of the detector output circuit (as was discussed in Section 5.1.2).

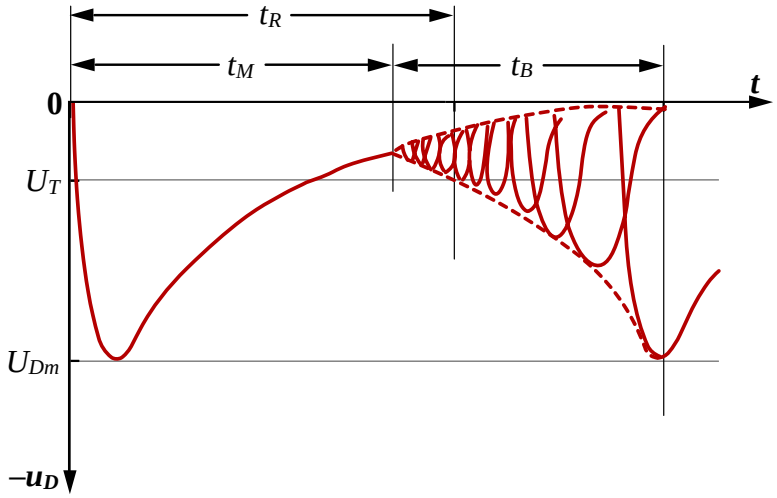

Fig. 5.2.11. Detector signals at a high radiation rate

Fig. 5.2.11 shows the generation of signals in a proportional counter irradiated with ionizing radiation at a very high flux. Upon completion of one discharge, the positive ions slowly move to the cathode, creating a space charge. The latter compensates for the electric field around the anode and prevents the occurrence of impact ionization. After a certain interval t_M, usually considered as detector dead time, the positive ions have moved sufficiently away from the anode and impact ionization can occur. Initially, the electrical field strength is small, and the gas gain is low, so the pulses are very small in amplitude. The more time passes, the more the space charge decreases, and when all positive ions are neutralized, the amplitude of the pulses reaches its normal value. The actual resolution time t_R of the counter is as long as the time during which the output pulses' amplitude reaches the threshold U_T of the electronic device connected to the detector. The time from the end of t_M to the moment the pulses reach their normal amplitude U_{Dm} is called **the detector recovery time** (t_B). For proportional counters, this usually amounts to $t_M \approx t_B \approx$ 10–100 µs.

Because of the primary and secondary gas amplification processes, the precise analytical estimation of the energy resolution is difficult. After some simplifications, the following dependence is recommended [5] for mono-energetic radiation flux to determine the relative standard deviation of the energy resolution, which can be calculated by:

$$\delta_E = \sqrt{\varepsilon(F + b)/E}, \qquad (5.2.13)$$

where ε, F and E are as stipulated in Section 5.1.3, and b is a parameter considering the fluctuations in the gas amplification factor k_G, which is a result of the random character of Townsend ionization. For most gases, $b \approx$ 0.4–0.5.

For example, for argon (Ar) with a quenching additive of 0.5 % ethylene (C_2H_4), ε = 20.3 eV, F = 0.075, and b = 0.43. With a radiation energy of 5.9 keV (X-radiation of ^{55}Fe), $\delta_E \approx$ 4.17 % and the energy resolution is $R_E \approx$ 9.8 % (see Eq. (5.1.8a)). For E = 136.5 keV (γ-energy of ^{57}Co), $\delta_E \approx$ 0.87 % and $R_E \approx$ 2 %.

The counting characteristic of proportional gas detectors for **mono-energetic** radiation is as shown in Fig. 5.1.4. The boundary voltage of the plateau depends on the type of counter, the base gas used and the radiation energy.

Proportional counters are mainly used for spectrometry of low-energy beta and gamma rays. They are also utilized to register neutrons by adding boron trifluoride (BF_3) to the gas or by covering the inner surface of the cathode

with pure boron-10 (see Eq. (5.2.2)). Proportional neutron counters filled with helium-3 (see Eq. (5.2.3)) are also produced for neutron spectrometry.

Proportional counters' operational time is limited by the quenching gas used due to the rate of dissociation of its molecules into radicals. The decomposition of all gas molecules occurs after 10^8–10^9 events, after which the detector ceases to operate normally. For this reason, counters with free-flowing gas are often used. For this purpose, the pressure of the gas entering the counter has to be a little higher than the atmospheric pressure.

5.2.4. Geiger-Müller counters

Geiger-Müller counters (GM-counters) operate in the region of the current-voltage characteristic bearing the same name (see Fig. 5.2.2). The gas gain k_G increases with the rise of the supply voltage and, at a certain value $U_{BIAS} = U_4$ (see Fig. 5.2.2), the condition $\zeta k_G = 1$ is fulfilled. The total gas gain (k_T) increases drastically but cannot become infinitely large (as should be possible according to equation (5.2.11)) because of a large space charge of positive ions, which decreases the electrical field strength and limits the k_T value.

When an ionizing particle or quantum passes through the detector, the discharge first occurs around its trajectory. Due to the very high total gas gain, however, the discharge spreads very quickly over the whole length of the anode at a speed of about 10^4 m/s. Therefore, the amplitude of the output pulses does not depend on particle or photon energy – only one pair of primary ions in the counter is enough to produce a discharge throughout the entire detector volume.

The amplitude and duration of the output pulses of the GM-detectors depend on the applied voltage and on the parameters of the external circuit *R* and *C* (Fig. 5.2.12).

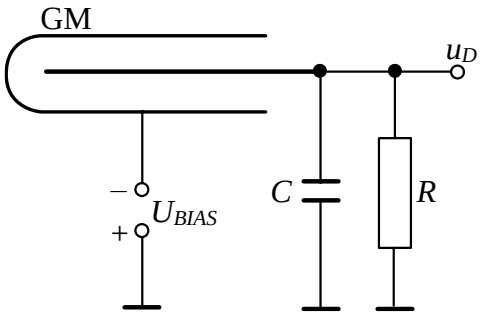

Fig. 5.2.12. A typical GM-detector's circuit

If the resistance *R* is infinite ($RC = \infty$), the entire ion current flows through capacity *C* and charges it. The pulse, as with proportional counters, begins with a certain delay (Fig. 5.2.13).

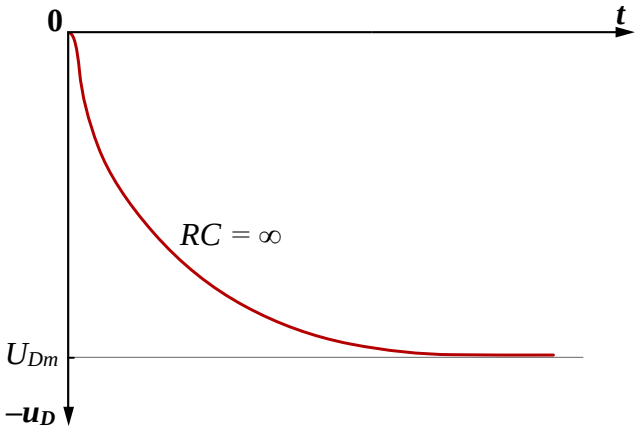

Fig. 5.2.13. The GM-counter output signal at RC = ∞

Apart from the time needed by the electrons to reach the area of impact ionization, it also includes the time for the discharge to propagate throughout the entire volume of the detector. However, the latter is too short – about 0.1 μs. Again, the first part of the leading edge (induced by the electrons) is steep but with a smaller contribution to the amplitude U_{Dm} due to the short distance covered by the electrons to reach the anode. The prolonged movement of the heavy positive ions to the cathode generates the main portion of the pulse amplitude. The discharge is terminated when the voltage on the counter $u_{GM} = U_{BIAS} - u_D$ becomes lower than U_4, as in Fig. 5.2.2. Therefore, the amplitude of the signal is

$$U_{Dm} \approx U_{BIAS} - U_4. \qquad (5.2.14)$$

It must be mentioned that the amplitude of GM-counter's output pulses is the largest of all gas detectors – in the order of tens of volts.

A GM-detector's dead time strongly depends on the resistance R. Due to its smaller size, capacity C will be discharged faster, and the counter's operating voltage will be restored more quickly. However, R cannot be set lower in order to decrease the dead time. The problem is that, at the moment when the voltage of the detector reaches its operating value ($u_{GM} \geq U_4$), the electron's neutralization at the anode should be finished. Otherwise, only one free electron is enough to start a new discharge in the counter volume, which will create a false output pulse (not caused by an ionizing particle or photon). Therefore, for GM-counters containing only a working gas (without a quenching agent), R has to be in the order of 10^9 Ω, which results in the dead time becoming enormous.

For this reason, only GM-counters with quenchers are currently being used. As with proportional detectors, polyatomic gases such as methane (CH_4), ethylene (C_2H_4), vapors of ethyl alcohol (C_2H_5OH), boron trifluoride (BF_3),

etc. are added for quenching. Their disadvantage of having a limited working time is of the utmost importance for GM-counters because the number of electrons and positive ions in each discharge is much larger. They also require relatively high working voltages – over 800 V.

The so-called **halogen GM-counters** have significantly better features in which halogen gases such as chlorine, bromine or iodine are used as a quencher. Their quenching action is similar to that of organic gases. Their molecules, after photon absorption, or their positive ions after neutralization, dissociate into atoms. However, when these atoms collide with each other, they bind again into molecules. Therefore, the dissociation is reversible, and the detector's operating time is much longer. Since the halogen elements have a higher atomic number than hydrogen and carbon, they absorb photons more efficiently. For this reason, only small amounts of the quenching gas (0.1–1 %) have to be added to the basic one. The most widely used gas is bromine because it has the lowest chemical activity.

Another advantage of halogen GM-counters is the lower operating voltage – 350–500 V, which is due to the unique process of ionization in the gas mixture. Due to the small concentration of quenching gas, the electrons, when moving to the anode, collide exclusively with the primary gas atoms and excite them. Their excited state is metastable – with a duration of 10^{-4}–10^{-2} seconds. During this relatively long time interval, the excited atoms undergo a large number of heat collisions with other atoms, including atoms of the halogen gas. Since the ionization energy of the halogen gas atoms (for e.g., bromine has $\varepsilon = 12.8$ eV) is lower than that of the primary gas (e.g., 16.9 eV for neon), these interactions lead to the ionization of the halogen gas. Their electrons are accelerated, and thus the impact ionization and the avalanche process of gas discharge occur at a significantly lower voltage.

The dead time of quenching GM-counters is in the order of several tens of microseconds. It can be further reduced (up to 5–10 μs) by using electronic devices that reduce the supply voltage immediately after the occurrence of the gas discharge and thus stops them.

An important advantage of Geiger-Müller counters is that the voltages limiting the plateau of their counting characteristic (see Fig. 5.1.4) do not depend on the radiation energy (since the amplitude of the pulses is independent of the energy). The length of the plateau is from 100 to 200 V, and the slope is 2 to 5 % at 100 V. It is mainly due to false pulses that sometimes occur despite the quenching agent. They increase in number as per the detector's operating time, especially when organic quenchers are used.

The relatively small slope of the counting characteristic provides these detectors with highly stable measurement results without taking extra

measures to stabilize the electronic device's supply voltage and the threshold. Therefore, these counters have extensive applications in radiometric and radioisotope devices, which is further supported by their simple construction and relatively small dimensions.

The efficiency of GM-counters for the recording of alpha and beta particles is very high while it is too low for gamma quanta – 1–2 %, which is strongly dependent on the thickness of the detector wall. In the case of a very thin wall, interaction of the gamma rays with the wall are rare and very few electrons are emitted, whereas, with too thick a wall, most of the produced electrons are absorbed by it. Thus, the optimum wall thickness is in the order of the beta-particle radiation length (see Section 4.3.4).

GM-counters are usually made in a cylindrical shape; most commonly, the tube is metallic – made of copper, aluminum or stainless steel, and serves as a cathode for the detector. Its thickness for alpha- and beta-ray detectors is minimal to limit energy loss when particles pass through it. GM-detectors with glass housings, covered inside with a suitable conductive material, are also used, mainly for gamma radiation. The covering materials must have high ionization energy to reduce their electron emission. Examples of such materials are copper, graphite, tungsten, etc.

The anode is made of a thin metal filament of either tungsten or stainless steel with a thickness of 0.01–0.05 mm. It should be well polished to avoid an auto-electronic emission, which could possibly stop the discharge spread – this would result in output pulses of varying amplitude. The dimensions of GM-counters vary depending on their design – diameter 10–30 mm, length 10–100 cm.

For alpha and low energy beta particles, **end-window** GM-counters are used (Fig. 5.2.14).

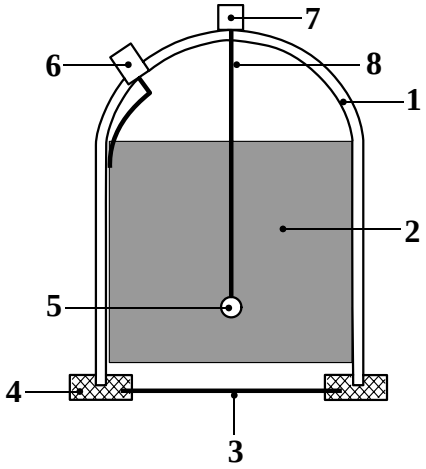

Fig. 5.2.14. Typical construction of an end-widow GM-counter

Their casing (1) is made of glass and is coated on the inside with a conductive material (2), which serves as a cathode. It is connected to a metal electrode on the outside of the housing (6). The window is closed with a thin foil of mica or plastic (3) held in the holders (4). The measured radiation passes through it without significant energy and flux losses. The anode (8) is a wire ending with an insulating ball (5) to avoid an auto-electronic emission from its end. It also has a metal terminal (7). Because the wire is not stretched, it needs to be thicker. This reduces the electrical field strength, and therefore these detectors operate at a higher bias voltage.

5.2.5. Corona counters

Under suitable conditions – a strong, non-uniform electric field (which is achieved with an extremely thin anode filament) and high gas pressure – a corona discharge – may occur. It is a variation of the continuous discharge, but the gas is conductive only in a very thin volume around the anode, and the ion current is limited by the low conductivity of the remaining discharge region. With a gradual increase in the bias voltage, the counter is initially operating as proportional, and then, at a specific voltage, a corona discharge starts to run a weak current (about 0.1 μA) without any external radiation. This current is due to multiple micro discharges in the gas, which have a statistical distribution, and the output signal has a noise character (Fig. 5.2.15). When an ionizing particle passes through the sensitive volume of the detector, it produces many electrons, each of which, while moving to the anode, creates a Townsend avalanche. As a result, an output pulse with an amplitude significantly exceeding the noise signals is generated, and its amplitude is proportional to the energy of the ionizing particle.

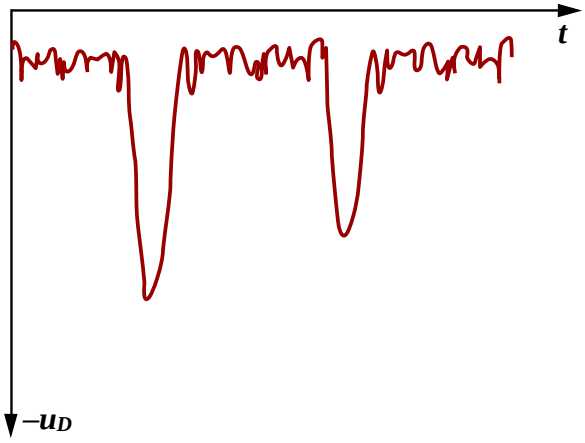

Fig. 5.2.15. The corona counter output signals

Corona counters are widely used, but mainly for the detection of particles causing strong ionization – alpha particles and especially neutrons (with so-

called **boron counters** – the primary gas is supplemented with BF_3 while **helium counters** are filled with helium-3). The nuclear reactions of neutrons with boron-10 or helium-3 atoms produce alpha particles generating output signals with a high amplitude (see Fig. 5.2.15). This amplitude is proportional to the neutron energy, which enables neutron spectrometry.

References

[1] *Ahmed, S.N*. Physics and Engineering of Radiation Detectors. Academic Press Inc., Elsevier, 2007. https://www.elsevier.com/books/physics-and-engineering-of-radiation-detection/ahmed/978-0-12-045581-2

[2] *Townsend, J. S.* The theory of ionization of gases by collision. Constable and Co, London, 1910. https://en.wikipedia.org/wiki/Townsend_discharge

[3] Ionization energy. https://en.wikipedia.org/wiki/Ionization_energy

[4] Geometric progression. https://en.wikipedia.org/wiki/Geometric_progression

[5] *V.I. Goldansky, A.V. Kutsenko, M.I. Podgoretsky*. Counting statistics of nuclear particles. Delhi: Hindustan Pub. Corp., 1962.

5.3. Semiconductor detectors

5.3.1. Radiation interaction with semiconductor material

It is well known that semiconductors have a crystalline structure in which atoms are held together by covalent bonds. These bonds are created when the valence electrons of each atom include an adjacent atom in their orbits. For example, in germanium and silicon, which have four valence electrons, each electron begins to circle around one of the four adjacent atoms, and one electron from each adjacent atom moves around the atom under consideration. Fig. 5.3.1 shows the trajectories of all valence electrons going around the central atom (in red) and only some of those circling the other atoms (in blue).

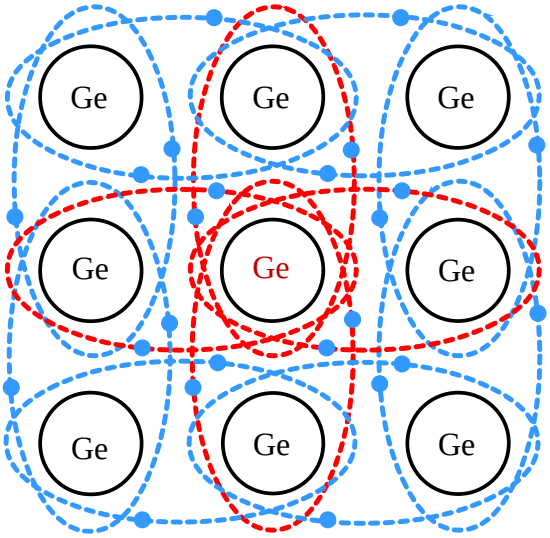

Fig. 5.3.1. The crystalline structure of pure germanium

Under the laws of quantum mechanics [1], electrons of the same atom shells in the crystal structure are confined to several **bands of energy** and are **forbidden** from other regions. The highest energy band (Fig. 5.3.2) is called a **conduction** band because the electrons in it have broken the covalent bonds and can move freely when an external electric field is applied. The next lower energy band, called **valence**, is formed by the electrons of the outer atomic shell, which determine the valence of each atom.

The **energy gap** between these two bands ΔE_F is called the **forbidden gap**, or **band gap**, and it determines the electrical conductivity of the solids. For the metals, $\Delta E_F \approx 0$ and both bands overlap. Thus, the electrons are located in the conduction band, and the conductivity is very high. The insulators have a large band gap – $\Delta E_F > 4$ eV – and there are no electrons in the conduction

band. Only with strong external influences such as high temperature or radiation flux can some electrons reach a high enough energy level to jump into the conduction zone. Because of this, insulators could be used for detectors, but for various reasons, no large scale-applications have been made.

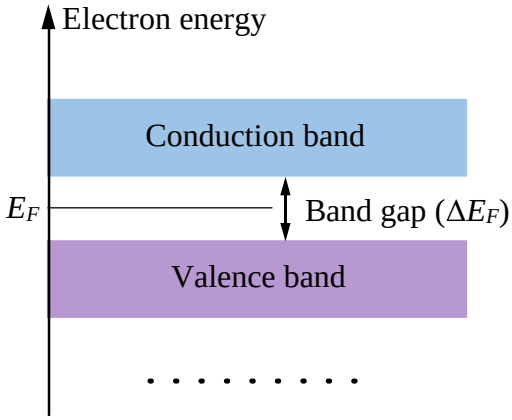

Fig. 5.3.2. Electron energy bands in a solid material

Semiconductors have a relatively narrow band gap. For example, at room temperature (~300 K), the germanium band gap is $\Delta E_F = 0.66$ eV and for silicon – $\Delta E_F = 1.11$ eV. As a result, there are excited electrons whose heat energy is greater than ΔE_F, and they jump into the conduction band. In their vacated place in the valence band, there is a shortage of one electron that can be considered as a positively charged particle and is called a **hole**. When an external voltage is applied, two directed movements begin: the electrons move toward the positive electrode, and the holes move toward the negative one. However, the holes have lower mobility since their current consists of a series of electron jumps (of the covalent bonds) from atom to atom in the direction of the positive electrode.

In a pure semiconductor, the number of excited electrons and created holes are equal, and the **Fermi energy** [2] corresponds to the middle of the band gap (E_F, Fig. 5.3.2). Its conductivity is called **intrinsic**, and, frequently, these semiconductors are called **intrinsic semiconductors**. They could be used as radiation detectors because the radiation will increase the number of electrons jumping into the conduction band and the current. For this purpose, however, their impurities must be extremely low in order to decrease the **dark** current (the current in the absence of radiation). Furthermore, these detectors are cooled by liquid nitrogen (to a temperature of 77 K) to reduce the number of heat-excited electrons (see Section 5.3.3).

Used more frequently in practice are the semiconductors whose electrical conductivity are drastically changed by adding tiny amounts of impurities,

a process known as **doping**. During this process, another element with a different number of electrons in its outer atomic shell than that of the semiconductor atom is added in a very small quantity to the bulk of the material. Two types of elements are used for this purpose, called **donors** and **acceptors**.

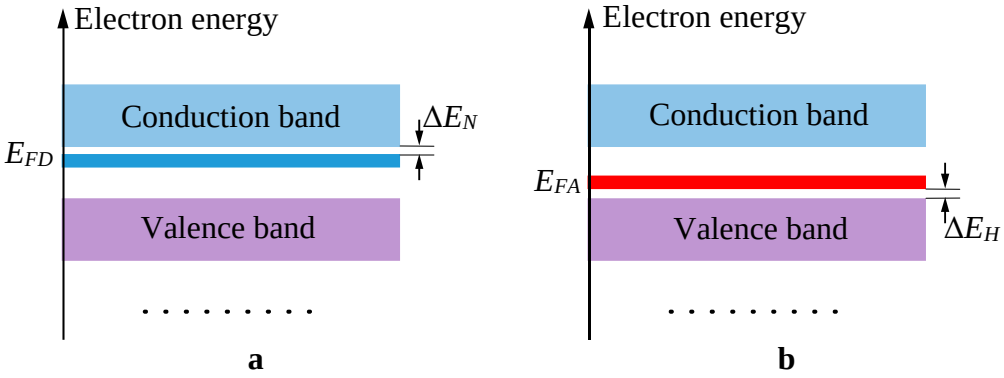

Fig. 5.3.3. Energy band distribution in semiconductors with: a) electronic (n-type) conductivity; b) hole (p-type) conductivity

1. **Five-valence elements such as phosphorus, bismuth, antimony, and others are used as donors**. Since germanium and silicon are four-valence elements, each donor's atom replaces one atom of the semiconductor, thereby forming four covalent bonds while one electron remains free. The effect of donor impurity addition is the shifting of Fermi energy towards the conduction band (E_{FD}, Fig. 5.3.3a), which confirms the surplus of free negative charges. The energy of these free electrons forms a band very close to the conduction band – $\Delta E_N \approx 0.01$ eV. Therefore, even at room temperature, many electrons can be found in the conduction band. They determine the conductivity of this type of semiconductor, which is called **electronic** or **n-type**.
2. **Three-valence elements are used as acceptors**, such as boron, gallium, indium, etc. When a three-valence atom replaces one four-valence atom in the primary material, a covalent bond remains unbuilt – so a hole "is created". The Fermi energy is shifted closer to the valence band (E_{FA}, Fig. 5.3.3b) and the energy band of these holes is very close to the valency band – $\Delta E_H \approx 0.08$ eV. As a result, the electrons in the valency band easily recombine with the holes, simultaneously creating new holes. Thus, there is a surplus of positive charges in the valence band, which determines the conductivity of these types of semiconductors, called **hole-type** or **p-type**.

Realistically, there are impurities in every semiconductor. Therefore, all three types of conductivity – intrinsic, electronic and hole-type – exist in each actual semiconductor. In the case of main donor impurities, the electronic one

is predominant, i.e. the **electrons are the majority charge carriers**, and the **holes are the minority charge carriers**. In the case of acceptor impurities, the **basic charge carriers are the holes**. Most importantly, when placed under the influence of an externally applied electrical field, both types of carriers begin to move in opposite directions by creating their own current.

Notably, both types of semiconductors are not suitable for radiation detectors because their dark current is very high. However, the so-called **pn-junction** occurring at the boundary between two semiconductor materials with the opposite types of conductivity has very different properties.

It is known that when p- and n-type semiconductors are brought together, a diffusion of charges immediately starts to compensate for the imbalance in charge concentrations across the junction. The free electrons, which makes up the majority of charge carriers in the n-type semiconductor, move towards the p-type material. There, they recombine with the holes, i.e. they rebuild the missing covalent bonds (because of the trivalent acceptor). At the same time, the departure of the electrons from the n-type region corresponds to the diffusion of the holes, which compensates for the negative charges of the electrons. This process continues until the Fermi energies in the boundary regions of the two materials become equal ($E_{FD} = E_{FH} = E_F$, see Fig. 5.3.2 and 5.3.3). As a result, the boundary region of the p-type semiconductor is charged negatively, and an equivalent positive charge is created in the n-type semiconductor (Fig. 5.3.4). Both charges create an electric field, $\mathscr{E}$, which finally stops their diffusion.

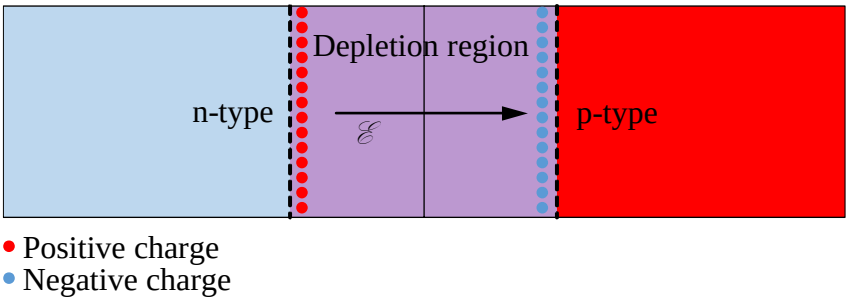

Fig. 5.3.4. Charge distribution in a pn-junction

An important property of this boundary region is the complete absence of free charge carriers, which gave rise to the name the **depletion region**. Hypothetically, in a situation where a positive voltage is applied to the n-type material and a negative voltage to the p-type material (the junction is said to be **reverse biased**), the electrons will be "pulled farther away" from the junction by the positive voltage on the n-type material, thus creating a much thicker depletion region around the pn-junction. The exact width (thickness) of the depletion region, d, can be determined by

$$d \propto (\rho U)^2. \qquad (5.3.1)$$

Here, ρ is the electrical resistivity of the material, and U is the magnitude of the applied reverse bias voltage. Note that the width of the depletion region **can be altered by changing the bias voltage applied to the junction**.

Such a depletion region (a reverse biased pn-junction) is very suitable for a radiation detector. The interactions of the radiation with the semiconductor material will create charge carriers in the depletion region. Then, the electron will migrate to the positive electrode, and the holes will move to the negative. Thus, a current will start to flow that can be measured in the external electrical chain. Even without an external bias, such a current will flow due to the created barrier voltage. However, this possibility is not really used because of the very low time and energy resolution in such a mode of operation.

5.3.2. Basic parameters of semiconductor detectors

1. Amplitude of a signal

It is known that the amplitude of a signal is determined by the total electrical charge generated in the detector volume and by the number of created primary charge carriers $L_0 = E/\varepsilon$ (see Eq. (5.1.1)). Table 5.3.1 shows that the energies needed to create an electron-hole pair (ε) in the most commonly used semiconductor materials are of the order of a few eV, i.e. about 8–10 times smaller than that of the detector gases (for argon ε ≈ 25 eV, and for neon ε ≈36 eV (see Table 5.2.1)).

Material	**Atomic number, Z**	**Density, g/cm³**	**Bandgap (ΔE_F), eV**		**Ionization energy (ε), eV**	
			300 K	**77 K**	**300 K**	**77 K**
Germanium	32	5.33	0.66	0.73	2.80	2.96
Silicon	14	2.33	1.11	1.16	3.62	3.72
Gallium Arsenide		5.32	1.43	1.50	4.10	4.80

Table 5.3.1. Basic parameters of some semiconductor materials

For this reason, the number of charge carriers generated by the radiation and, respectively, the amplitude of the output signal of the semiconductor detectors is nearly one order of magnitude greater than that of the ionization chambers' signals. Nevertheless, because most of the semiconductor detectors have no intrinsic amplification ($k_D = 1$), the amplitude of their signals is relatively small – between several hundred microvolts and a few millivolts.

Thus, these detectors need special low-noise preamplifiers.

2. Time resolution

The mobility of the holes in the semiconductor detectors is about three orders of magnitude higher than that of the positive heavy ions in gas detectors. Therefore, their time resolution is much higher:

- In thin silicon detectors (width of 10–500 μm), the so-called **charge collecting time** (the time during which the full charge reaches the outer electrodes) is from 100 ps – 50 ns. Some delay is caused by the transitioning of the charge carriers through the semiconductor material outside of the pn-junction. There, the electrons and holes move diffusively (the bias voltage is applied almost entirely to the pn-junction). Therefore, the design of the detectors provides a maximum extension of the pn-junction to the electrodes. (As we have seen, the thickness of the depletion region can be enlarged by increasing the bias voltage. However, its maximum value depends on the electrical resistivity of the basic semiconductor, i.e. on the purification from impurities other than the dopants).
- In large germanium and silicon spectroscopy detectors, the charge collection time is from 1 to 10 μs. Because the total charge collection is obligatory for a high energy resolution, the time parameters of the preamplifier should be matched to the detector's characteristics.

3. Energy resolution

Semiconductor detectors have the highest energy resolution for two reasons:

- The initially created charge carriers in the semiconductor are about ten times more than in gas-filled detectors (at equal radiation flux and energy).
- When interacting with a semiconductor material, the radiation spends its energy not only on ionization. A portion of the energy creates vibrations in the crystal lattice (the so-called phonon). The loss of energy during such an interaction is very small – in the order of millielectronvolts – and so the number of interactions is very large. Because these numerous interactions are not statistically independent, Fano's factor is very low – $F = 0.05–0.15$. Thus, for a high purity germanium detector ($\varepsilon = 2.96$[1] eV and $F \approx 0.1$), the energy resolution R_E is between 1.5 % and 0.1 %, depending on the radiation energy and the detector type.

[1] At the temperature of liquid nitrogen – 77 K, which is the typical operation temperature of the germanium spectrometric detectors (see next Section).

In order to keep this high energy resolution, it is necessary to use an electronic device with very low noise as well as to collect all of the generated charge carriers. Incomplete charge collection, called a **ballistic deficit**, is mainly due to the temporary capture of some holes and electrons in semiconductor traps.

4. Dark current

This is the current flow through the detector when the bias voltage is fed into it while there is no incident radiation. It is mainly due to the drift current of the minority charge carriers in the semiconductors, and the dark current increases rapidly with a rise in temperature. This current is higher in germanium detectors whose band gap (0.66 eV) is much lower than that of silicon detectors (1.1 eV).

The dark current is another factor that may reduce the energy resolution. It has a random character and increases the fluctuations in the amplitude of the output signals. For this reason, and in most cases, semiconductor detectors (especially the germanium ones) must be cooled to the temperature of liquid nitrogen (77 K) during the measurement taking process.

An additional ingredient of the dark current may be the leakage current present between the detector's electrodes. The influence of this current can be eliminated by the placement of a protective electrode (PE, Fig. 5.3.5), similar to that used in ionization chambers (see Fig. 5.2.5). As a result, the leakage current cannot flow through the load resistor R_D, and therefore cannot affect the output signal.

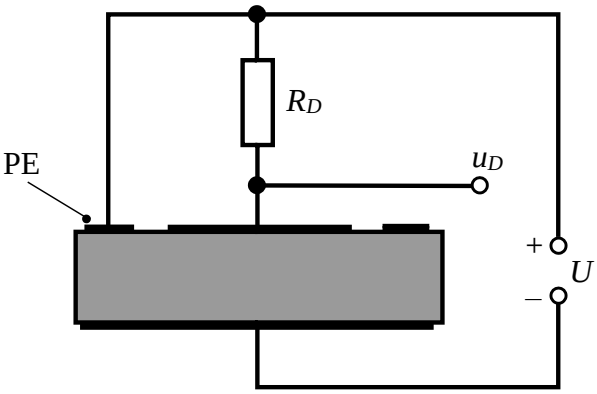

Fig. 5.3.5. A typical semiconductor detector's circuit with a protective electrode, PE

5. Efficiency

For detectors of equal volume, efficiency depends on the density, i.e. on the atomic number of the material used. Due to the differences in densities, the efficiency of semiconductors is about three times higher than that of gases. In addition, when the energy distribution has to be measured, the particles or

photons must spend all their energy in the detector volume. Since germanium has a significantly higher atomic number ($Z_{GE} = 32$) than silicon ($Z_{SI} = 14$), and its density is more than two times higher (see Table 5.3.1), germanium detectors are exclusively used for gamma-rays- and high-energy particle spectroscopy.

5.3.3. Types of semiconductor detectors

Until now, only two basic materials have been used for semiconductor detector production – silicon and germanium. Many attempts have been made to use gallium arsenide, but they have been unsuccessful. The choice between silicon and germanium detectors depends on the type of radiation and its measurement parameters.

The main advantages of silicon are the relatively low price and its larger band gap – an average of 1.1 eV versus 0.66 eV of germanium. This allows silicon detectors to operate without cooling, or with minimal cooling, to between –10 and –20 °C, usually provided by a Peltier Cooler [3]. At the same time, the silicon density is twice as low as that of germanium, and the radiation particle range thereof is larger. Conversely, germanium has a higher density and the best energy resolution. Additionally, high volume germanium detectors are much easier to produce than silicon ones. However, these detectors are only able to operate at a temperature of 77 K due to their small band gap. At higher temperatures, too many electrons jump from the valence band into the conduction one, creating a very large dark current. The latter increases the noise and decreases the measurement precision, especially the energy resolution. Therefore, a silicon detector should be used whenever the volume of the silicon detector is sufficient to cover the radiation particle range, or the radiation energy is not being measured. In addition, the lower density of silicon, compared to that of germanium, reduces radiation backscatter.

A. Silicon detectors

Silicon detectors can be divided into three general categories – **surface barrier devices**, **PIN diodes**, and **Si(Li)** (pronounced "**silly**") detectors.

1. **Silicon surface-barrier detectors**. These devices consist of a thin disc of high resistivity (10^3 ohm · cm) pure low-doped n-type silicon (Fig. 5.3.6).

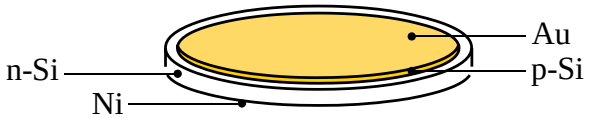

Fig. 5.3.6. A typical silicon surface-barrier detector

After the pre-grinding and etching of both surfaces, a very thin layer (about $20 \cdot 10^{-9}$ mm) of gold (Au) is applied to one by evaporation in a

vacuum. After that, the detector is exposed to dry air at atmospheric pressure, and a diffusion of oxygen occurs through the thin gold electrode. As a result, the silicon surface is oxidized under the gold and yields p-type conductivity, creating the pn-junction. The second electrode is formed on the other side of the disc where chemical precipitation of nickel (Ni) is applied, forming an ohmic contact with the n-type silicon.

The very thin gold electrode and oxide layers allow the incident particles to reach the working detector volume without loss of energy. However, the gold layer is sensitive to physical wear. During use, the detector must be shielded from visible light as electron-hole pairs can be created by photons that enter the detector volume through the thin gold layer.

The thickness of the detector's working volume (i.e. the depletion region of the pn-junction) can be changed by regulating the bias voltage. It can reach up to 0.5 mm. These detectors are only used for radiometry or spectroscopy of charged particles such as alpha particles, fission fragments, and protons with small energies because of their relatively small thickness.

Surface-barrier detectors are also used to record neutrons. For this purpose, a thin layer of lithium 6 is applied instead of a gold electrode. The reaction is

$$^{6}_{3}\mathrm{Li} + {}^{1}_{0}\mathrm{n} \rightarrow {}^{4}_{2}\mathrm{He} + {}^{3}_{1}\mathrm{H} + 4.78\ \mathrm{MeV}, \qquad (5.3.2)$$

and the emitted alpha particles and tritium nuclei trigger the detector. For the detection of fast neutrons, a thin polyethylene film is placed on the gold electrode, which releases protons when interacting with the neutrons.

In some of the most modern detectors [4], both the entrance and the back contact are ion-implanted. The entrance contact is an extremely thin ($\sim$500 Å) boron implantation. The distance between the silicon surface and the top of the mounting is < 1 mm to provide maximum geometric efficiency. The front contact can easily be cleaned with a solvent-moistened cotton swab. A wide range of detectors with an active area of 25 to 3000 mm^2 is available, and all of them operate at room temperature.

2. **Silicon PIN diodes**. They are a more recent class of detectors, which have become available due to advancements in semiconductor technology utilized in electronics. Each detector is a p-i-n sandwich, which is made up of a p-type layer (p-Si, Fig. 5.3.7) that is formed on one side of an intrinsic silicon wafer (i-region) and an n-type layer – on the other side (n-Si).

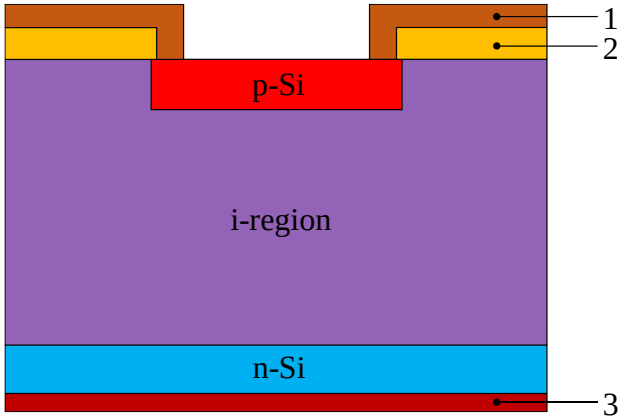

Fig. 5.3.7. A silicon PIN diode detector

Terminals 1 and 3 are connected with the p- and n- regions, respectively. 2 is an isolating layer. Terminal 3 is a thin metal layer also serving as a radiation entrance window.

PIN diode detectors are produced in a large range of shapes and sizes. Moreover, position-sensitive (coordinate) detectors (see Part 12) can easily be created by forming mutually perpendicular strips of p- and n-electrodes on both sides of the silicon wafer (Fig. 5.3.8).

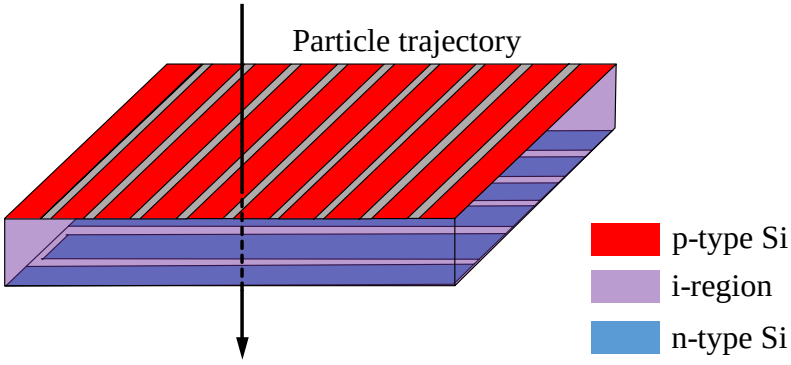

Fig. 5.3.8. A silicon PIN coordinate detector

The coinciding of the signals coming from the strips that are the closest to the trajectory of the passed particles will pinpoint its coordinates within the detector space.

Similar technology is used in the building of special detectors for the spectroscopy of X- and low-energy gamma rays [5]. A strip structure and a directing electric field are combined in its design. For this purpose, a pn-junction is formed across the entire lower surface of a thin wafer of n-silicon (Base, Fig. 5.3.9).

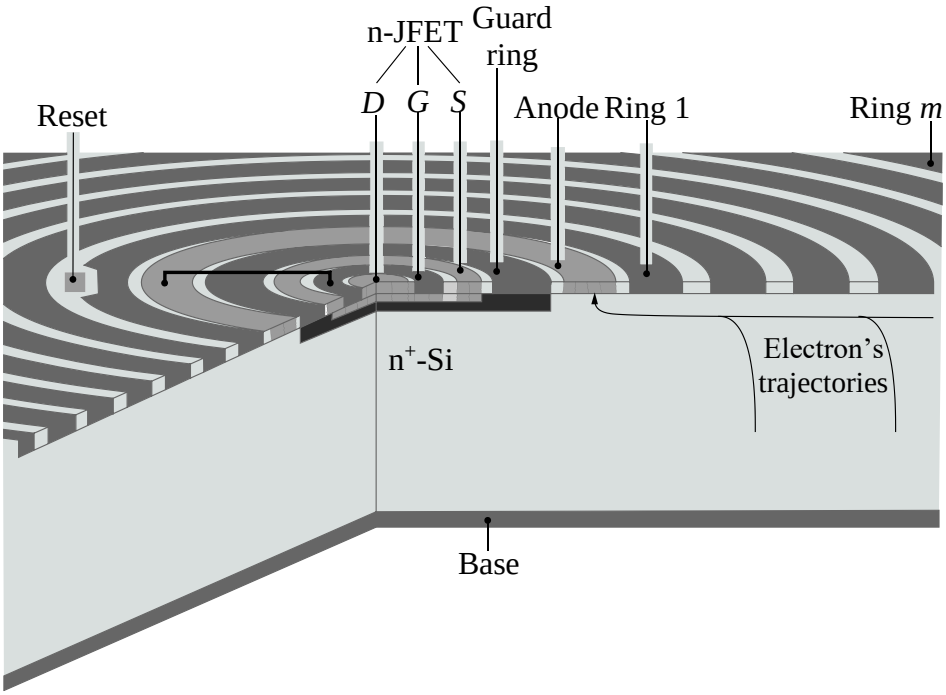

Fig. 5.3.9. A silicon detector for spectroscopy of X- and low-energy gamma rays

It serves as a thin entry window for the radiation. The electric field is created by a series of concentric p^+-silicon electrodes deposited on the other side of the wafer (Anode, and Ring 1 to Ring m). They all receive a positive voltage that is lowest for the outermost electrode (m) and highest for the innermost (anode). Intermediate rings receive voltage from a resistor voltage divider built into the structure. Thus, the electrons generated in the pn-junction by the incident radiation are pointed to the anode and are collected on it. An n-type field effect junction transistor (JFET) is built in the center of the detector, the gate (G) of which is connected to the Anode.

These detectors have several significant advantages:

- A very low initial current (1 nA/cm^2 at room temperature) – at a temperature of –10 ℃, it generates an equivalent noise charge of 9 electrons, which is similar to that of a detector of ultra-pure germanium cooled to 77 K.
- Very high performance – the electric field provides directional rather than a diffuse movement of the electrons, and the full charge collection is carried out for around 100 ns (about two orders of magnitude faster than in the germanium-lithium detectors). Therefore, these detectors are particularly suitable for very high radiation flux

measurements – there is no shift in the positions of the recorded peaks up to a signal rate of 10^5 s^{-1}.

- Greater amplitude of signals as a consequence of the minimum input capacity of the built-in JFET.
- Large area detectors are easily manufactured – the production technology allows many detectors of this type to be created on a joint base (wafer); such a design will increase the recordable radiation flux rate as well.

The disadvantage of these detectors is their relatively small working thickness, and therefore they cannot be used for gamma-rays with higher energy.

3. **Lithium-drifted silicon detectors**. They are usually called **Si(Li)** (pronounced as "silly") detectors and have been developed for the measurement of beta particles. Beta radiation is more penetrating than heavier charged particles. The larger thickness of these devices is obtained by combining the diffusion and drift of lithium atoms in a p-type silicon bulk. The lithium donor is applied through evaporation in a vacuum on one of the bases of this bulk (the upper base in Fig. 5.3.10).

Fig. 5.3.10. Structure of a lithium-drifted silicon detector

Then, at a temperature of about 400 ℃, the lithium diffuses to a relatively large depth as its diffusion coefficient is over 10^7 times that of phosphorus and arsenic. In this manner, a wide pn-junction is formed. There, the lithium atoms readily donate one electron to the silicon lattice, neutralizing the existing holes and becoming positive ions. Thus, when a reverse bias voltage is applied, it causes a drift of the positive lithium ions from the n-side of the junction to the p-side, where they compensate for the acceptor's influence in the p-material. As such, the impact of the donor and acceptor atoms are mutually compensated in a large region of up to 5 mm in length, and its conductivity is close to that of the intrinsic one. The lithium atoms retain their high mobility in the lattice, even without a bias voltage. Therefore, the detectors need a small, retainable bias voltage when they are stored for a long time at room temperature.

Si(Li) detectors are favored for β-particle spectroscopy because of their low gamma sensitivity and lower backscattering. Their energy resolution

(FWHM) for electrons is about 1000–2000 eV up to an electron's energy level of 1 MeV. These compelling results can be obtained by operating at a temperature between –10 and –20 ℃ to decrease the thermal noise.

Si(Li) detectors with an active area of up to 80 mm^2 and 5 mm thickness [6] are also used for X-ray spectroscopy. For this purpose, they operate at a temperature of 77 K (in a cryostat, Fig. 5.3.11), providing a very good energy resolution – FWHM is 160 eV at 5.9 keV ($R_E \approx 2.5$ %).

Fig. 5.3.11. A cryostat with the Si(Li) detector

All semiconductor detectors are damaged by long-term exposure to charged particles. The particles generally come to rest in the silicon and stay there, disrupting and poisoning the lattice. If the particles are mono-energetic, then they will stop in a very narrow region of the detector and can create a dead layer inside the silicon. This degradation becomes observable over a threshold dose that is dependent on the radiation intensity (in particle/cm^2): 10^8 for fission fragments, 10^9 for α-particles, 10^{10} for fast neutrons and 10^{13} for electrons.

B. Germanium detectors

Germanium detectors have the highest energy resolution of any ionization device without proper amplification. This is due to germanium's small band gap of 0.73 eV (at 77 K) and its effective ionization potential of 2.95 eV, which allows the generation of the largest number of ions at a given radiation intensity. The amplitude of the output signal is also higher compared with that of silicon devices. The relative difference is equal to the inverse ratio of their ionization potentials (3.76/2.95 ≈ 1.27).

The only disadvantage of germanium detectors is their higher thermal noise (due to the small band gap), which is about five times greater than that of silicon devices. Nonetheless, germanium devices are almost exclusively used for gamma radiation detection. The reasons are:

- The higher density of germanium decreases the stopping power of the photons and, thereby, their penetration depth.
- The probability of a photoelectric interaction with an atom, which contributes significantly to the absorption of the full energy of photons, increases in proportion to Z^5; thus, germanium with $Z = 32$ is a much more effective absorber of photons.
- Technology has been developed to produce very high purity germanium crystals that are much larger than silicon crystals.

There are two main types of germanium detectors, those that use lithium compensated material, called Ge(Li) (pronounced like "jelly"), and more recently, those using intrinsic germanium, called **high purity germanium detectors** (**HPGe**).

1. **Ge(Li) detectors**. The production technology of Ge(Li) detectors is similar to that used for Si(Li) devices. Because their efficiency is more dependent on the volume size of the working region than on its length, a coaxial design is preferred. Lithium is applied to the outer surface of a cylindrical ingot consisting of p-type germanium (Fig. 5.3.12).

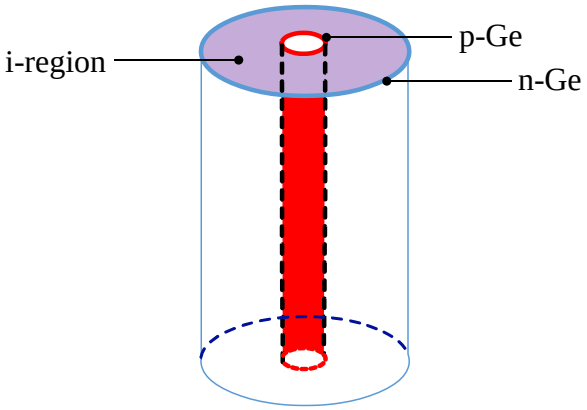

Fig. 5.3.12. Structure of a Ge(Li) coaxial detector

Subsequently, some lithium atoms diffuse into the germanium lattice, donating their electrons, and the lithium ions drift through the bulk material. The mobility of the lithium ions is much higher in germanium than in silicon, which allows very effective compensation for the p-conductivity. During this process, the lithium contact produces an n-type region on the surface of the crystal, the bulk becomes intrinsic through

compensation, and a small p-type region is left un-drifted around the central axial well. Thus, a PIN-diode structure with a very large working volume (up to 1 liter) is created.

However, the high mobility of lithium ions necessitates that Ge(Li) detectors be kept at liquid nitrogen temperature throughout their entire useful lifetime. The reason is that the number of lithium atoms introduced by the drift in germanium is significantly higher than the quantity corresponding to the equilibrium state. Therefore, at room temperature, they emerge on the surface of the germanium, destroying the i-region and thereby damaging the detector. This problem, along with the incredibly rapid development of germanium purification technology, led to the suspension of the production of new Ge(Li) detectors.

At present, these detectors are no longer available from companies manufacturing nuclear measuring equipment, probably due to the requirement to store them at 77 K and a reduction in the price of HPGe devices. At the same time, the production of Si(Li) detectors has increased.

2. **High-purity germanium (HPGe) detectors**. Technological advances have made it possible to produce the so-called high-purity germanium bulk, in which the concentration of electrically active impurity atoms is less than 10^{10} cm^{-3}. Depending on the type of these impurity atoms, the material may be of p- or n-type. However, the impurity quantities are so low that the material actually has an intrinsic conductivity and can be used as a working region of the detector.

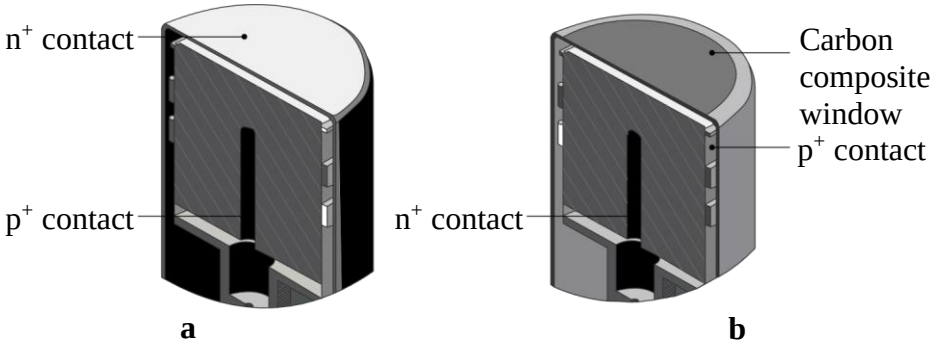

Fig. 5.3.13. High purity germanium detectors produced in the industry: a) standard electrode location; b) reverse electrode location

Once again, the coaxial design is used. In Fig. 5.3.13a, the structure of an actual HPGe detector, as produced by CANBERRA Industries [7], is shown.

As can be seen, an n^+-layer with a thickness of about 0.5 mm is created by lithium diffusion, not only on the outer surface of the cylinder but on

the top end cap too. For this reason, the central cylindrical hole does not pass through the whole crystal but becomes a well. On its surface, a much thinner p^+ layer (about 0.3 μm) is formed by boron ion implantation. The detector is housed in a vacuum case, through which it is in contact with the cooling agent. The end cap of the case is covered by 0.5 mm thick aluminum that serves as the entry point for gamma-rays.

This electrode location is referred to as the **standard**, and these detectors (**SEGe**) have a decent efficiency for photons with an energy level above 40 keV up to a few MeV. Their energy resolution is very good – R_E is 0.67 % at 122 keV and 0.13 % at 1.33 MeV on an end cap diameter of 76 mm. Similar detectors with different end cap diameters of up to 108 mm are also available.

A reverse electrode location is used in **REGe** detectors to increase the efficiency at low-energy radiation (Fig. 5.3.13b). Here, the very thin p-type electrode (0.3 μm ion-implanted boron) is on the outside, and the n-type contact (diffused with lithium) is on the inside. The end cap case is normally made of a thin carbon composite window, which is robust and provides excellent transmission to photons. Thus, a high detector efficiency for photons with an energy level as low as 10 keV is provided. A beryllium end cap window is available for measuring even lower energy levels (down to 3 keV). Another advantage of this type of detector is the increased radiation damage resistance. It has been found that radiation damage, principally due to neutrons or charged particles, causes hole trapping in germanium. Unlike the case of the standard coaxial detector, holes are collected by the outside electrode of the REGe detector. Since a much greater portion of the detector's active volume is situated within a given distance ΔR of the outside contact than of the inside contact (Volume $\approx R^2$), it follows that, on average, holes have less distance to travel if they are attracted to the outside contact than if they are attracted to the inside contact. With less distance to travel, they are less likely to be trapped in radiation-damaged material. Experimental tests suggest that the REGe detector could be up to 10 times as resistant to damage as SEGe detectors.

Many other variants of HPGe detectors are available on the professional market [7, 8].

Usually, the bias voltage of HPGe detectors is in the order of several hundred volts. As it increases, the amount of time required for the total charge collection decreases. However, its maximum value is limited by the increase of the dark current and the corresponding thermal noise. For

crystals purified to 10^{10} cm^{-3} impurity atoms, the maximum supply voltage is 600 V.

Cooling of the HPGe detectors is provided by different types of cryostats. Most often, the so-called flange cryostat is used. The detector occupies a vacuum chamber with a dipstick-like tail, which is inserted into the neck tube of a Dewar full of liquid nitrogen (Fig. 5.3.14a).

a **b** **c**

Fig. 5.3.14. Methods of HPGe detector cooling: a) by liquid nitrogen; b) by an electro-mechanical cooler; c) by a combination of liquid nitrogen cooling and electromechanical cooler

Lastly, electromechanical coolers are also available. They use the so-called Stirling Cooler based on the cycle of Stirling [9], which provides temperatures of around 80 K without any open liquid or gas agent (Fig. 5.3.14b). The system [10, 11] incorporates a hardened cryostat for superior operational performance. This feature allows instant recovery after a loss of power, eliminating the need to fully thermal cycle the detector in the event of a partial warm-up. The cooler is designed to virtually eliminate vibrational and audible noise levels. This provides a resolution performance comparable to systems cooled by liquid nitrogen.

A combination of both systems is also available [12, 13]. In it (Fig. 5.3.14c), the cooling of the detector is done with liquid nitrogen, which itself is cooled by an electro-mechanic cooler. Such a system can work without adding new liquid nitrogen for a period of up to one year.

References

[1] Pauli exclusion principle. https://en.wikipedia.org/wiki/Pauli_exclusion_principle

[2] Fermi energy. https://en.wikipedia.org/wiki/Fermi_energy

[3] Thermoelectric cooling. https://en.wikipedia.org/wiki/Thermoelectric_cooling

[4] Ion-implanted silicon charged particle detectors. http://www.ortec-online.com/-/media/ametekortec/brochures/ultra_ultra-as-a4.pdf

[5] *Dongliang, Yao, Li Shenghui*. Ultra high-resolution radiation detector (UHRD) and method for fabrication thereof. USA Patent, IPC8 Class: AH01L310352FI, USPC Class: 257465. http://www.faqs.org/patents/app/20090026569#ixzz0dAU86ODe

[6] Silicon-Lithium detector for X-ray spectroscopy. https://mirion.s3.amazonaws.com/cms4_mirion/files/pdf/spec-sheets/c40120_sili_det_for_x-ray_spect_ss_2.pdf?1562601347

[7] Germanium detectors. https://www.mirion.com/products/germanium-detectors

[8] High purity germanium (HPGe) radiation detectors. http://www.ortec-online.com/products/radiation-detectors/germanium-hpge-radiation-detectors

[9] Stirling cycle. https://en.wikipedia.org/wiki/Stirling_cycle

[10] ICS integrated cryocooling system. http://www.ortec-online.com/products/radiation-detectors/germanium-hpge-radiation-detectors/detector-cooling/ics

[11] Electrically refrigerated cryostat. https://www.mirion.com/products/cryo-pulse-5-plus-electrically-refrigerated-cryostat

[12] Mobius recycler condensing liquid nitrogen cooling system. http://www.ortec-online.com/products/radiation-detectors/germanium-hpge-radiation-detectors/detector-cooling/mobius

[13] Hybrid cryostat. https://www.mirion.com/products/cryo-cycle-ii-hybrid-cryostat

5.4. Thermoluminescent detectors

As we have already seen, impurities in semiconductors create traps for electrons in the band gap and interfere with the normal operation of semiconductor detectors. Their presence in some crystals creates intermediary energy levels in the band gap (the forbidden band), allowing the crystals to be used as radiation detectors. Some of the impurities form an energy level near the conduction band, while others do so near the valence band. When the crystal is exposed to ionizing radiation, electrons are liberated from the lattice and captured by the impurity traps near the conduction band. There, they can remain for a very long period of time (even years). When the crystal is heated, the energy of the electrons increases; they are then released from the traps and jump into the conduction band, after which they can fall into the impurity level near the valence band, emitting a photon during this process [1].

The number of captured electrons is proportional to the radiation energy deposited in the crystal, i.e. to the radiation dose absorbed by the crystal. Therefore, by measuring the total light flux emitted by the crystal during the heating, we can determine the absorbed radiation dose. Due to this fact, these devices are called thermoluminescent dosimeters (TLD). Prof. Farrington Daniels of the University of Wisconsin-Madison invented TDLs in 1954.

Fig. 5.4.1 shows an example of the process described above.

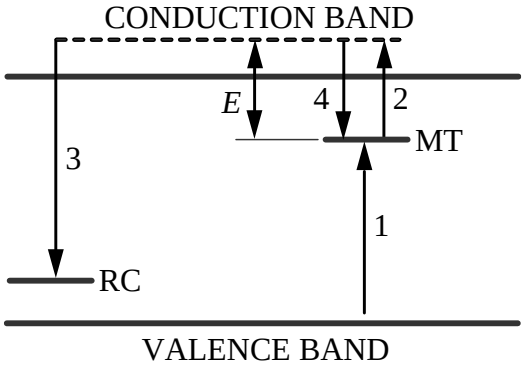

Fig. 5.4.1. Typical processes in a TLD

The crystal is one of the most used TLD materials – lithium fluoride doped with magnesium and titanium (LiF: Mg, Ti). The magnesium atoms create traps at an energy level near the conducting band (MT), while the titanium atoms do the same near the valence band. After receiving energy from radiation, the electrons jump from the valence band to the conducting one and are captured by the magnesium traps MT (transition 1). At the same time, the holes created in the titanium by the impurities form the so-called

recombination centers (RC). If the energy E required to release the electrons from the trap (called trap depth) is high enough (around or above 1 eV), the electrons remain in the traps for a long time. Only when an external impact is applied (in our case, heat) do they get enough energy to escape from the traps and reach the conduction zone (transition 2). Losing some of their energy into it (due to thermal movement), they either recombine with a hole in a recombination center (transition 3) and emit a light quantum (photon), or they fall into another impurity trap (transition 4).

A photomultiplier is used to measure the light flux emitted during the heating of the crystal to determine the crystal's absorbed dose. The photomultiplier (see Section 5.5.2) is connected to a specialized electronic device.

Different types of crystals are used in TLDs. The most suitable materials are fluorides – calcium fluoride (CaF_2) and lithium fluoride (LiF) – activated with manganese (Mn) and titanium (Ti). Advantages of LiF are: its density is almost equivalent to that of human tissue, i.e. it can measure the radiation dose absorbed by people; it can also measure the dose of neutrons since it has been enriched with Li-6 (see Eq. (5.3.1)).

Sulfates are also widely used in detection devices – primarily calcium sulphate ($CaSO_4$) doped with thulium (Tm), dysprosium (Dy) or (LiF). It is mainly used for personal radiation dose monitoring devices because of its higher sensitivity to lower doses. For this purpose, several calcium sulphate pellets are placed in a plastic plate (Fig. 5.4.2a).

a **b**

Fig. 5.4.2. TLDs using calcium sulphate: a) plates with TLD pellets; b) personal dosimeter badge

This plate is then installed inside a personal badge (Fig. 5.4.2b). The purpose of each individual pellet can be modified by placing an appropriate radiation filter in front of it. This allows the simultaneous measurement of doses of different types of radiation – e.g. beta ray can be stopped with an aluminum

plate and low-energy gamma-rays with a lead plate. Dosimeters of different materials can also be placed on such a dosimeter plate.

Some producers [2] make so-called extremity TLDs designed as a ring (Fig. 5.4.3a) or a bracelet (Fig. 5.4.3b), the readings of which are done by laser.

a **b**

Fig. 5.4.3. Extremity TLDs designed as: a) rings; b) bracelets

They are designed to measure beta radiation at a depth equivalent to that of the sensitive basal layer of the skin (about 3 mm). The TLD material is LiF sealed in a plastic holder. The holder shields the TLD from lower energy betas (under 70 keV), which cannot penetrate the basal layer.

Personal TLD dosimeters have a precision of approximately 15 % for low doses. This precision improves to approximately 3 % for high doses. The advantages of a TLD over other personnel dose monitors are its linear response to the dose, its relative energy independence, and its sensitivity to low doses. It is also reusable, which is an advantage over film badges.

Nowadays, special dosimeters of optical glass fibre cables are produced [3]. They are very small (Fig. 5.4.4) – with a diameter between 150 and 450 μm and a length between 3 and 5 mm.

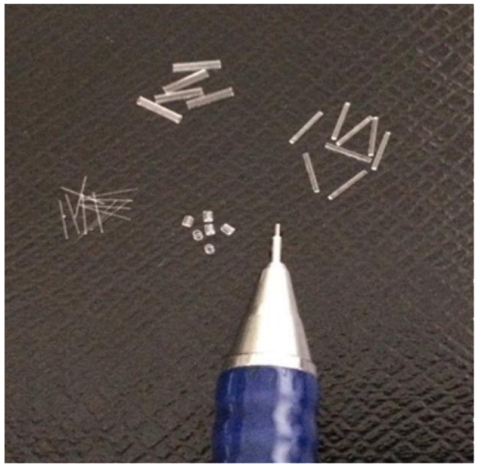

Fig. 5.4.4. Miniature glass TLDs

Their technical parameters are similar to the other TLDs, and all standard TLD readers can read them. Applications for this TLD are found mainly in medical studies, and it can even be placed in the human body for irradiation control in cancer treatment.

Apart from applications in personal radiation control and medical treatments, TLDs find applications in many other spheres of human activity. For example: determining the absorbed dose in the radiation-hardness testing of electronic devices; measuring the dose around detectors in high-energy physics studies; dose control during space expeditions.

Advantages of thermoluminescent dosimeters are the very wide range of measurable doses – from 10^{-5} to 10^{4} Gy – their simple structure, easy production, low cost, safe operation, and small size and weight. Their drawbacks are the low precision – up to $\pm$30 %, the fading effect (gradual reduction of the accumulated dose during its storage before reading), and difficulty obtaining the same parameters in serial production.

References

[1] *Furetta, Cl.* Handbook of thermoluminescence. http://www.fulviofrisone.com/attachments/article/466/Handbook%20of%20Thermoluminescence.pdf

[2] *Al-Gafri, F.* TLD. https://www.slideshare.net/fatmaMSG/tld-47009931

[3] Radiation dosimeters. https://www.flexilicate.com/products/dosimeter?gclid=Cj0KCQjwm6HaBRCbARIsAFDNK-hHs9lNWmb-AwBN0wbEhs3cV7iiKEYdU3ePPp-SMk6f23dUREdomJUaAipGEALw_wcB

5.5. Scintillation detectors

Scintillation detectors are the most commonly used type of radioluminescent detectors. Within these detectors, the radiation energy is first transformed into light energy, which is then transformed into an electrical signal. For this purpose, scintillation detectors consist of two parts:

- **Scintillator** – converts the energy of ionizing radiation into light energy.
- **Photodetector** – converting the light pulse parameters into parameters of an electrical signal.

5.5.1. Scintillators

A **scintillator** is a material that emits light photons when its atoms or molecules are excited by ionizing radiation. It absorbs the energy of each incoming particle or γ-quantum (photon) and then releases it in the form of a light pulse.

Scintillators are subject to a number of requirements in order to perform the function of detectors: they have to convert the energy of radiation into light with high efficiency; this transformation has to be linear; the transformation processes have to be fast; the scintillators have to be transparent to the light quanta emitted, and so on. Therefore, different parameters are used to evaluate their properties, the most important of which are given below.

A. Basic parameters of scintillators

1. **Density**. The high density of the scintillator is important because it reduces the material size for full absorption of high-energy γ-quanta and electrons.

2. **Light yield**. It is estimated by the so-called **quantum (conversion) efficiency** – the ratio of the energy of the generated light photons to the energy delivered by the ionizing particle or γ-quantum in the scintillator:

$$\kappa = L_{PH} h\nu_{PH} / E, \qquad (5.5.1)$$

where

L_{PH} is the average number of photons,

$h\nu_{PH}$ – the average energy of one photon,

E – the energy deposited by the radiation particles or γ-quanta.

The higher the quantum efficiency, the lower the energy radiation levels that can be measured. For photons from the visible region, $h\nu_{PH}$ is about

3 eV and κ reaches several tens of percent. For the same scintillator, κ depends on the type of radiation.

Lately, scintillator manufacturers prefer to indicate the number of light quanta emitted (instead of quantum efficiency) when irradiating a scintillator with radiation at a specified energy level – 1 keV or 1 MeV.

Quantum efficiency does not take into account the transparency of the scintillator. Therefore, the so-called **technical efficiency (technical light output)** is also used. It shows the ratio of the light energy emitted outside the scintillator to the energy delivered by the particle or γ-quantum in the scintillator.

3. **Spectral characteristic of the scintillator**. It shows the dependence of the quantum efficiency on the wavelength λ of the light emitted (Fig. 5.5.1).

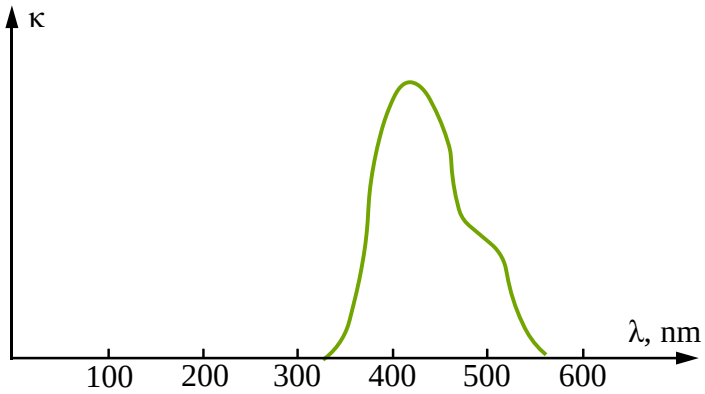

Fig. 5.5.1. The typical spectral characteristic of a scintillator

It is better for the maximum to be in the region of visible light in order to pass through the windows of the photodetectors, which is most often made of glass. The maximum overlap of the spectral characteristic of the scintillator with that of the photodetector must also be provided.

4. **Form and duration of the scintillation**. Most of the scintillators emit a light signal with a simple exponential decay (Fig. 5.5.2). However, for some of them, the signal may be a sum of two exponents – fast and slow, which is used to identify the radiation type (see Part 11). For the majority of scintillators, it can be assumed that the scintillation rise time is much shorter than its decay time. Therefore, the scintillation duration is most often evaluated by the time constant of its exponential decay τ_D, for which the light flux decreases *e* times. For different scintillators, this time constant varies within a wide range – $\tau_D = 10^{-9} \div 10^{-6}$ s (see Tables 5.5.1, 5.5.2 and 5.5.3). It is only necessary to take into account the scintillation rise time (see Table 5.5.4) for the fastest scintillators.

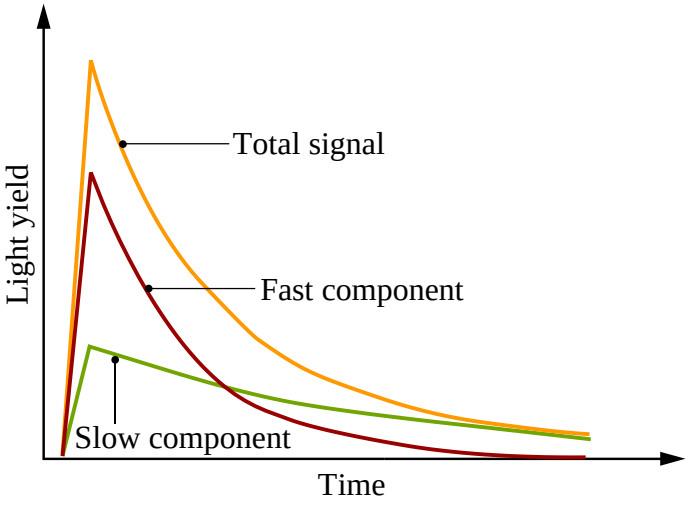

Fig. 5.5.2. Forms of scintillator light signals

B. Types of scintillators

The scintillation mechanisms in different materials vary, so the scintillators are divided into groups according to their aggregate state and their chemical composition.

1. **Inorganic scintillators**. Only crystals of a limited number of compounds are used as inorganic scintillators. In order to increase their quantum efficiency, a small amount (up to 10 %) of another substance, called an **activator**, is added. The activator greatly increases the number of visible light photons.

   Table 5.5.1 depicts the most commonly used inorganic scintillators and their basic parameters. The first row shows a zinc sulphide scintillator activated with silver – $ZnS(Ag)$, which was the first scintillator ever to be used. Its very high light yield allows one to observe the scintillation through a microscope in a darkened room when it is irradiated by alpha particles. A flaw of this scintillator is that it cannot form large crystals. Therefore, zinc sulphide scintillators are prepared as a thin layer of microcrystals applied on a transparent base, usually a glass disc (Fig. 5.5.3), which makes contact with the photodetector.

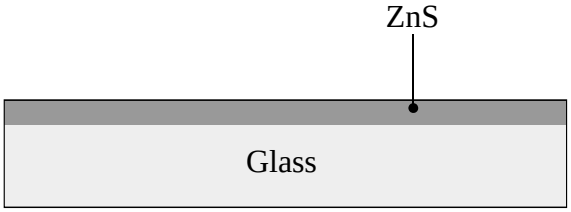

Fig. 5.5.3. A scintillator of $ZnS(Ag)$

Scintillator	Light yield		Maximum light yield at λ, nm	Time const. τ_D, ns	Density g/cm^3
	κ, %	Phot./keV			
ZnS(Ag)	28[1]	88[1]	450	110	4.09
$LaBr_3$(Ce)	18	63	380	16	5.29
NaI(Tl)	12	38	415	250	3.67
CsI(Tl)	17	54	550	1000	4.51
CsI(Na)	13	41	420	630	4.51
CaF_2(Eu)	6.5	19	435	940	3.19
BaF_2		1.8	220	0.6-0.8	4.88
		10	310	630	
$Bi_4Ge_3O_{12}$	2.8	9	480	300	7.13
$PbWO_4$	1.3	0.2	440-530	6-30	8.30
LYSO(Ce)		33	420	36	7.1
^{6}Li(Eu)	4.5	11	470-485	1400	4.08
^{6}Li-glass	1.3	3.8	395	75	2.50

Table 5.5.1. Inorganic scintillators

The next seven scintillators are monocrystalline and are mainly used for gamma-ray spectrometry. Cerium-activated lanthanum bromide – $LaBr_3$(Ce) – was created in the year 2000, and it has very good properties: very high light yield, large linearity over a wide range of gamma-quanta energy variation, relatively high density ensuring full absorption of a large portion of the gamma-radiation, low-temperature dependence and high performance. Its high efficiency and high density are the cause of its

[1] For alpha particles

record high energy resolution for gamma quanta of over 100 keV: 2.9 % at 662 keV gamma quanta energy (γ-line of ^{137}Cs) compared to the 7 % for sodium iodide (Fig. 5.5.4).

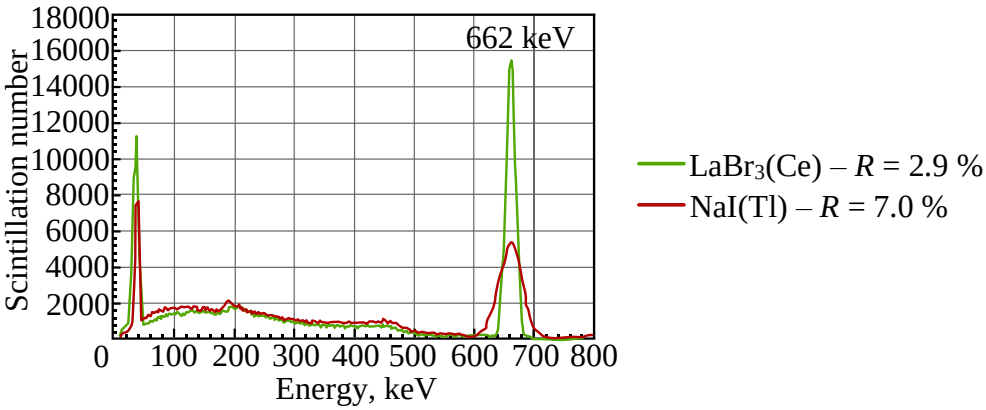

Fig. 5.5.4. Energy spectra obtained by $LaBr_3$ and NaI scintillators

Some disadvantages are its lower resolution for energies below 100 keV and its own background radiation due to the natural radioactive isotopes lanthanum-158 (^{158}La) and actinium-227 (^{227}Ac), which will always cause some trace contamination.

In Table 5.5.2, the energy resolution of both scintillation detectors is compared with the same parameter of an HPGe detector. Regardless of the apparent superiority of the HPGe detectors, scintillators are always preferred when lower cost and smaller sizes are essential.

Detector Type	**Resolution at 662 keV, %**
$LaBr_3$(Ce)	2.8-4.0
NaI(Tl)	7
HPGe	0.2 (1.3 keV)

Table 5.5.2. Comparison of energy resolution

A common disadvantage of both scintillators is that they are very hygroscopic – when coming into contact with the air, they absorb moisture and become opaque, resulting in a loss of their qualities. They are therefore hermetically sealed in a metal housing, one base being transparent in order to make contact with the photodetector. The surface of the scintillator in the housing is covered with a diffuse reflector layer, consisting of, for example magnesium oxide (MgO), to increase their light

output. Actual encapsulated scintillators of different shapes and sizes consisting of lanthanum bromide are shown in Fig. 5.5.5a and of sodium iodide – in Fig. 5.5.5b.

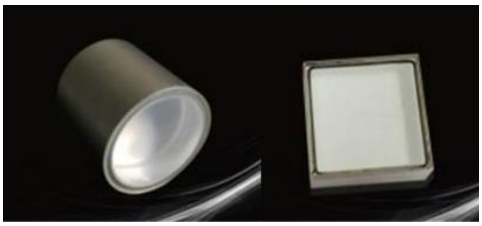

Fig. 5.5.5a. Scintillators of $LaBr_3(Ce)$

Fig. 5.5.5b. Scintillators of NaI(Tl)

Cesium iodide monocrystals, activated by thallium – CsI(Tl), have a lower light yield and energy resolution with a greater time constant but are not hygroscopic. This allows them to be used without any form of housing and to measure both alpha and beta radiation. Besides being non-hygroscopic, the scintillators of calcium fluoride, activated by europium – $CaF_2(Eu)$ – has high mechanical strength and are therefore used in portable radiation spectrometers.

Scintillators of barium fluoride (BaF_2) have two components in their scintillation. One of them is very fast (time constant – $\tau_{D1} < 1$ ns) and makes it very suitable for timing measurements or measuring radiation with very high flux density.

The highest density scintillators are made of bismuth germanate ($Bi_4Ge_3O_{12}$) and lead tungstate ($PbWO_4$). Despite their lower quantum efficiency, they are widely used to register high-energy gamma quanta in current particle physics experiments. For example, the Electromagnetic Calorimeter (ECAL) of the CMS detector at the Large Hadron Collider (LHC) in CERN contains 75,848 crystals of ($PbWO_4$). Several such scintillators are shown in Fig. 5.5.6.

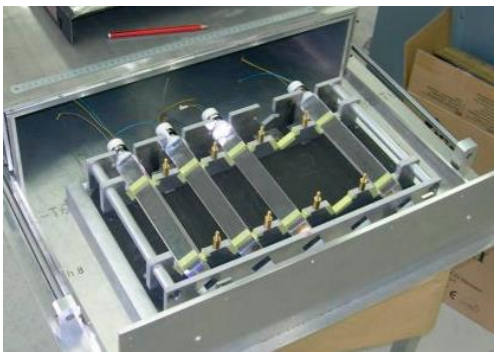

Fig. 5.5.6. Four scintillators of lead tungstate in a test box

The next two scintillators in the table are synthetic crystals: LSO is a cerium doped lutetium oxyorthosilicate and LYSO – a cerium doped lutetium-yttrium oxyorthosilicate. Their high density and good light yield are the reason for their widespread use in particle physics detectors and in PET (positron-electron tomography).

A lithium-6 scintillator, activated by europium – ^{6}Li(Eu) – as well as lithium glasses, are mainly used for the detection of slow neutrons by way of the (n, α) reaction (see Eq. (5.3.1)).

2. **Organic scintillators**. The mechanism of scintillation in organic scintillators differs in principle from that in inorganic crystals: the energy obtained at each interaction with radiation leads to the excitation of a single molecule. Whereas in the case of inorganic scintillators, the processes of excitation, ionization and neutralization occur within the entire crystalline grid and are not limited to one molecule. For this reason, organic scintillators retain their properties even when changing their aggregate state, for example, in polymerization, dissolution, and the like.

   Three different types of organic scintillators are generally used.

   a. **Organic crystals**. The most commonly used (Table 5.5.3) are pure crystals of **anthracene** ($C_{14}H_{10}$), **stilbene** ($C_{14}H_{12}$) and **naphthalene** ($C_{10}H_{8}$) [1]. Their use is relatively limited because they are brittle, and it is difficult to produce crystals larger than a few cubic centimeters. However, they have a special feature. When they interact with heavy particle radiation (for example, alpha particles), their molecules are mostly ionized. Then, the light quanta generation is exclusively due to the recombination of these ions. For this reason, these scintillations are slower, i.e. their decay time constant for heavy particles is much larger – in the order of hundreds of nanoseconds. This phenomenon is used to separate the signals caused by light and heavy particles (e.g. gamma photons and neutrons) irradiating the detector at the same time. A specific method, known as the **pulse shape discrimination technique**, is used for this purpose (see Part 11).
   b. **Organic liquids**. They contain three ingredients:
      - **solvent** – the main substance of which the detector is made (also called the **base**);
      - **activator** – the substance that scintillates (also called the **fluor**);
      - **spectrum shifter** – a substance that alters the scintillations' light wavelength to the visible spectrum where the photodetectors have maximum efficiency.

Scintillator	Light yield		Maximum light yield at λ, nm	Decay const., ns		Density g/cm^3	Features	Application
	κ, %	Phot./keV		τ_R	τ_D			
Anthracene	4	16	447	–	30	1.25	Crystal	α, β, γ
Stilbene	2	8	410	–	4.7	1.16	Crystal	γ, fast neutrons
Naphthalene	2	8	348	–	100	1.025	Crystal	γ, fast neutrons
BC400	2.6	10.4	423	0.9	2.4	1.023	~NE102	Generic purpose
BC404	2.7	10.9	408	0.7	1.8	1.023	Fast	Timing meas.
BC408	2.6	10.4	425	0.9	2.1	1.023	Large surface	TOF[1]
BC412	2.4	9.6	434	1.0	3.3	1.023	Most transp.	Generic purpose
BC416	1.5	6.1	434	–	4.0	1.023	Cheapest	Generic purpose
BC422Q	0.8	3.0	370	0.1	0.7	1.023	Very fast	Timing meas.
BC436	2.1	8.3	430	–	2.2	1.130	With deuterium	Fast neutrons
BC454	2.0	7.7	425	–	2.2	1.026	With boron-10	Slow Neutrons

Table 5.5.3. Organic scintillators

Ionizing particles or quanta give their energy to the solvent, exciting its molecules without causing them to scintillate. The bulk of the energy of these molecules is transferred to the activator molecules via the process of thermal movement within the solution. The fluor molecules go into an excited state and then scintillate while returning to normal. The scintillation intensity depends on the amount of activator in the solution, with the optimal concentration being about 1-2 %.

The spectrum of activator scintillations is located in the field of ultra-violet rays. That requires the addition of a third component – a light

wavelength shifter. For this purpose, substances that absorb the light quanta as the activator releases it are excited and, in turn, scintillate by emitting photons of a greater wavelength, which fall within the visible light spectrum. The most often used solvents are **toluene**, **xylene** and **benzene**. Activators include **p-terphenyl** ($C_{18}H_{14}$), **2-phenyl-5-(4-biphenylyl)-1,3,4-oxadiazole** (**PBD** –$C_{20}H_{14}N_2O$), and **butyl PBD** ($C_{24}H_{22}N_2O$), **2,5-diphenyloxazole** (**PPO** –$C_{15}H_{12}NO$). Most often, **1,4-di-(5-phenyloxazol-2-yl) benzene** (**POPOP** – $C_{24}H_{16}N_2O$) is used for spectrum shifting.

Scintillator	Light yield		Maximum light yield at λ, nm	Decay const, ns	Density g/cm^3	Features/ Purpose	Application
	κ, %	Phot. /keV					
BC501A	3.1	12.5	425	3.2	0.874	n - spectrometry	γ, fast n[1]
BC505	3.2	12.8	425	2.5	0.877	Maximal κ	γ, fast n
BC517H	2.1	8.3	425	2	0.860	General purpose	α , β, γ, fast n
BC517P	1.1	4.5	425	2.2	0.850	Cheapest	α , β, γ, fast n
BC517S	2.6	10.6	425	2	0.870	Petroleum based	α , β, γ, fast n
BC519	2.4	9.6	425	4	0.870	$n-\gamma$ separation	γ, fast n
BC521	2.4	9.6	425	4	1.310	With 1 % gadolinium	n- spectrometry
BC523A	2.6	10.4	425	3.7	0.916	With 5% boron-10	Slow n- spectr.

Table 5.5.4. Liquid scintillators

Table 5.5.4 contains the most typical organic liquid scintillators produced by Saint-Gobain Crystals&Detectors (USA), one of the world's largest detector producers [2].

They have relatively good light yield and very short scintillations. As can be seen, they have different features corresponding to the various applications. There are also a few special liquid scintillators being produced: BC517S – petroleum-based, for oil-soluble samples; BC519 – also using mineral oil, but providing $n-\gamma$ separation based

on pulse form discrimination (fast and slow scintillation components); BC521 – with added gadolinium for neutron measurement by (n, γ) reaction; BC523A – with added boron-10 for spectrometry of slow neutrons (using the (n, α) reaction of equation (5.5.20)).

An important feature of liquid scintillators is that they can have the desired volume and shape according to the shape of the container in which they are poured. It is also very easy to add different components (such as a wavelength shifter, an additive to increase neutron cross-Section and so on). Another important advantage is that the measured samples can be placed in direct contact with the detector by dissolving or mixing it mechanically in the scintillator. Thus, 100 % geometrical efficiency is provided – all the particles or quanta of the sample pass through the scintillator, avoiding any absorption or backscattering before they reach the detector. This is the reason why liquid scintillators can measure particles and quanta with very low energy, which is particularly important for the studies with labeled atoms in biology and carbon-14 in archeology. Very often, researchers prepare liquid scintillators themselves by mixing the necessary components together.

Another useful property of liquid organic scintillators is that in them, as in the case of organic crystals, the shape of the pulse depends on the type of radiation (see Part 11).

c. Plastic scintillators. They are produced through the polymerization of suitable liquid scintillation solutions. Most often, the bases are polymers with aromatic rings, such as polyvinyltoluene and polystyrene. They have a very low light yield and negligible transparency to their own emissions, but they let the activator's photons pass. **Polymethylmethacrylate** (**PMMA**), which is being utilized in a wide variety of applications, carries two advantages over other bases: high ultra-violet- and visible light transparency and good mechanical properties for machining.

Organic compounds such as **stilbene**, **n-terphenyl**, **p-terphenyl** and the like are used as activators. The spectrum can be shifted by **POPOP**, **PPO** and others.

The second part of Table 5.5.3 contains plastic scintillators with different properties and applications, as trademarked by Saint-Gobain Crystals [2]. BC400, BC412, and BC416 scintillators are for general applications. BC412 has very high transparency that allows large-scale scintillators to be produced (Fig. 5.5.7). BC416 has a lower light

yield and low cost. In terms of speed, BC404 and BC422Q are very fast-acting. The decay time constant (τ_D) of the latter is further reduced by adding 0.5 % benzophenone. BC-400 and BC-404 are largely used as thin sheets (Fig. 5.5.8) for alpha and beta detection.

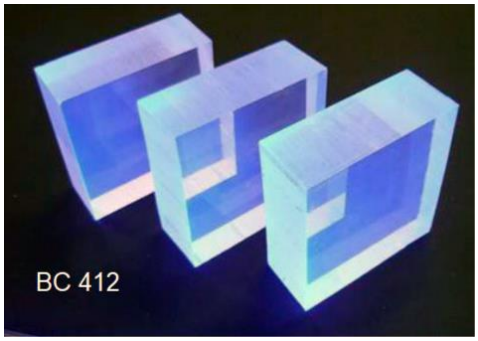

Fig. 5.5.7. Typical large plastic scintillators of BC412 material

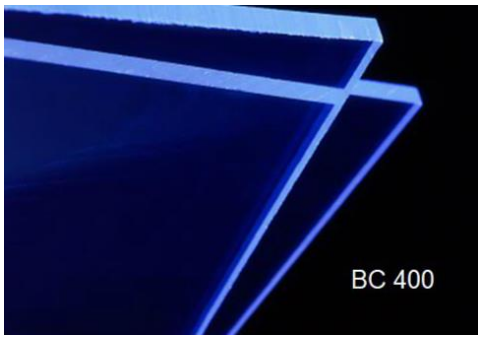

Fig. 5.5.8. Typical thin sheet scintillators of BC400 material

Generally, all organic scintillators can measure fast neutrons because they contain many hydrogen atoms (about 50 %): as noted in Section 4.5.1, neutrons primarily interact elastically with hydrogen nuclei (protons), giving them much of their kinetic energy; these recoil protons then cause the excitation of the plastic material molecules. Nevertheless, scintillator BC436 is enriched with deuterium, which increases its efficiency for fast neutrons. To better measure slow neutrons, BC454 contains 5 % boron-10.

Recently, a new type of plastic material has become available – **polyethylene naphthalate** [3] – that scintillates itself and is transparent to the photons emitted. Because of its important advantages, such as a high light yield of 10.5 Phot/keV, photon emission in the visible light range (maximal light yield at $\lambda = 425$ nm), and low price, it could replace other plastic scintillators in the near future.

The extremely widespread use of plastic scintillators is warranted due to their many valuable qualities: simple technology for production; excellent mechanical properties and easy machining by metal cutting machines; high transparency, allowing large-scale scintillators with a diameter of up to 0.5 m and a length of up to 1 m; high performance; low price. However, they are mainly used for radio-metric purposes: on the one hand, due to the complex transformation processes of radiation energy into light, their energy resolution is too low, but on the other hand – they are the fastest radiation detectors and can

measure very high fluxes of particles or quanta. Plastic scintillators are also widely used in radioisotope equipment for industry.

Plastic scintillators are subject to aging, which diminishes their light yield. Exposure to solvent, vapors, high temperatures, mechanical flexing, irradiation, or rough handling will aggravate the process. A particularly fragile region is the surface, which can craze, i.e. develop micro-cracks, which rapidly destroy the capability of plastic scintillators to transmit light, increasing the total internal reflection. Crazing is particularly likely where oils, solvents, or fingerprints have made contact with the surface.

3. **Gas scintillators**. The best gas scintillators are **noble gases – helium, argon, krypton, xenon** – the heavier gases having higher light yields. The gas mixture with the highest light yield consists of as high as 90 % helium and 10 % xenon. The scintillation mechanism in noble gases is a purely atomic process, and therefore they are very fast – $\tau_D \leq 1$ ns. Their scintillations are in the ultraviolet light area, so a spectrum shifter is needed. The highest light yield provides the use of **diphenylstyrene**. The inner surface of the gas chamber and the glass window to which the photodetector adheres are covered with a thin layer of the shifter.

   Gas scintillators are mainly used for the measurement and spectrometry of heavy particles, fragments of fission, and so forth. They are indispensable when such measurements have to be carried out in the presence of a gamma background due to their negligible gamma-ray efficiency.

4. **Cherenkov's detectors**. In these detectors, the production of light is due to the Cherenkov Effect (see Section 3.3.7). Their main advantage is their high-speed action. It results from the fact that light is emitted only during the time in which the particle is slowing down. However, in contrast with the isotropically emitted scintillation light, Cherenkov light is emitted along the surface of a forward-directed cone centered on the particle velocity vector. The wavelength of the light is preferentially shifted toward the short-wavelength (blue) end of the spectrum. The total intensity of Cherenkov light is much weaker than the light emitted from equivalent energy loss in a good scintillator and may be only a few hundred photons or less for an electron with an energy of 1 MeV.

   Different materials (called radiators) are used as Cherenkov detectors [4]:

   - solid state radiators, most often made of quartz;
   - liquid radiators – very often made of water;
   - gas radiators – usually incorporating helium (He) or Nitrogen (N_2).

In some experiments, even the atmosphere or the ocean are used as radiators.

All these detectors are normally used with the same type of light sensors employed in scintillation detectors (see the next section). They are most often photomultipliers to which lenses and mirror direct the light.

5.5.2. Photodetectors

The purpose of **photodetectors** is to accept the light pulse from the scintillator and transform its parameters (amplitude, form, and frequency) into relevant parameters of a single (or numerous) electrical signal. There are many types of photodetectors, but the most commonly used ones in scintillation detectors are **photomultiplier tubes** (**PMT**), **avalanche photodiodes** (**APD**), **silicon photomultipliers** (**SiPM**), **hybrid photodetectors** (**HPD**) and a few others.

A. Photomultiplier tubes

1. Principle of operation

A photomultiplier tube (usually called **photomultiplier** or **PMT**) is typically constructed with an empty cylindrical glass bulb (Fig. 5.5.9). In the most commonly used PMT, a thin layer of vapor-deposited material with a photoelectric effect, called a photocathode, covers the frontal base inside the bulb. Following the photocathode along the PMT, a focusing electrode and a series of electrodes called **dynodes** are installed, only the latter being an anode. Each dynode is held at a higher positive voltage (about 100 V) than the preceding one, which causes an acceleration of the electrons when moving between the dynodes.

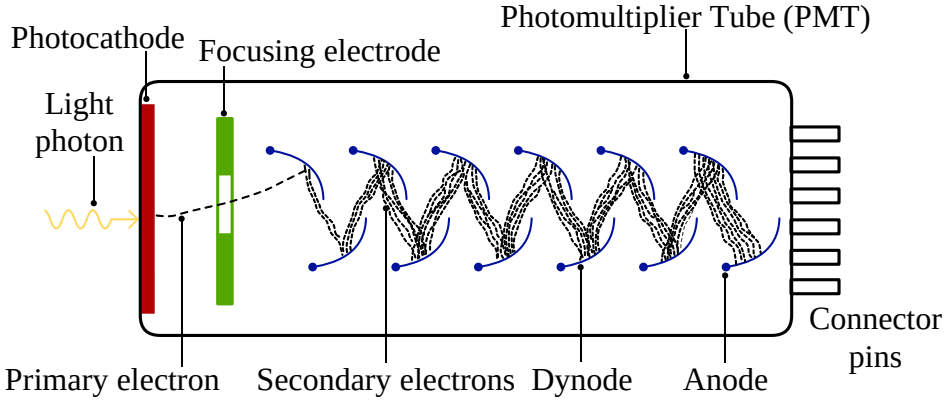

Fig. 5.5.9. Construction of a photomultiplier

When one scintillation light photon enters the PMT photocathode, a primary electron is emitted. Its initial energy is equal to the incident photon's energy (about 3 eV for the so-called blue photons) minus the

work function[1] of the photocathode. In the same way, the photons of one scintillation cause the emission of a group of electrons, the amount of which corresponds to the scintillation intensity. These electrons are accelerated (because of the positive voltage of the focusing electrode and the first dynode) and focused on the first dynode. A material of high impact electron emission covers each dynode. For this reason, when the primary electrons strike the first dynode with an energy of about 100 eV, more low energy electrons are emitted, and these electrons are in turn accelerated toward the second dynode. The geometry of the dynode chain is such that a cascade occurs with an exponentially increasing number of electrons being produced at each stage. The coefficient of the dynodes' impact emission depends on the energy of the electrons that strike them, i.e. on the voltage of each respective dynode. For example, if at each stage an average of 5 new electrons is produced for each incoming electron, and if there are 11 dynode stages, then the number of electrons that will reach the anode (generated by one primary electron) will be about $5^{11} \approx 5 \cdot 10^7$. This number corresponds to the actual gain of the PMTs (see below).

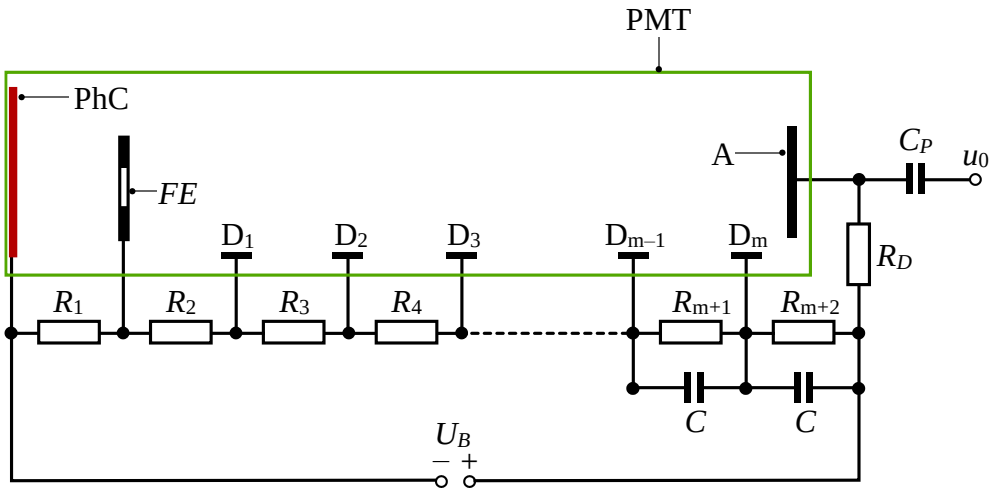

Fig. 5.5.10. A voltage divider supplying the dynodes chain

A resistor voltage divider ($R_1 - R_{m+2}$, Fig. 5.5.10) creates the necessary distribution of voltage along the focusing electrode (FE) as well as the dynode chain ($D_1 - D_m$). In this way, the PMT gain can be regulated by varying only the bias voltage U_B. The current running through the divider must be at least 10 times higher than the maximum current pulses of the

[1] In solid-state physics, the work function is the minimum thermodynamic work (i.e. energy) needed to remove an electron from a solid to a point in the vacuum immediately outside the solid surface.

PMT. The capacitors marked C are connected in parallel to the last resistors, providing energy during the current pulses moving through the PMT and thus stabilizing the voltage of the last dynodes.

One important question is which terminal of the bias voltage should be grounded? Commonly, the positive terminal is grounded, and the cathode receives a high negative voltage. This allows the usage of a low voltage capacitor C_P or the removal thereof. In some cases, however, the high negative voltage of the cathode can cause problems: for example, when the PMT shell is metallic, it must be grounded, but then it will attract most of the electrons emitted from the cathode. A similar effect occurs when the PMT is placed in a metal shield – the attracted electrons bombard the PMT glass wall, and the emitted light pulses increase the dark current (see the point about dark current below).

2. Photomultipliers – basic characteristics

There are many parameters characterizing the functional possibilities of a PMT:

- **Quantum efficiency**. It shows the number of electrons separated from the cathode when one photon is absorbed and can be calculated thus:

$$k_Q = n_E/n_{PH}, \tag{5.5.2}$$

  where n_E is the number of emitted electrons from the cathode when it is illuminated by n_{PH} photons.

- **Integral cathode sensitivity**. It indicates the current of the photocathode electrons when a light flux from one lumen enters it and is measured in μA/lm. Recently, Hamamatsu also defined it as the current obtained by the incident radiant flux at a given wavelength – in A/W [5].

- **Spectral sensitivity**. It shows the dependency of quantum efficiency or integral photocathode sensitivity on the wavelength of light falling on the photocathode. In the most common PMTs, **bialkali** (antimony-potassium-cesium – SbK_2Cs) and **multialkali** (antimony-sodium-potassium-cesium – $SbNa_2KCs$) photocathodes are used. Fig. 5.5.11 presents the spectral sensitivities of all photocathodes currently in use [5]. It shows that the bialkali photocathode corresponds well to the light spectra of most scintillators. The multialkali is similar but has extended sensitivity to the infrared region. In PMTs with an ordinary (borosilicate) glass window located at the device's front end, these

dependencies are limited to 300 nm. Special PMTs with quartz or synthetic silica glass windows are also produced, which retain their sensitivity in the ultraviolet light region.

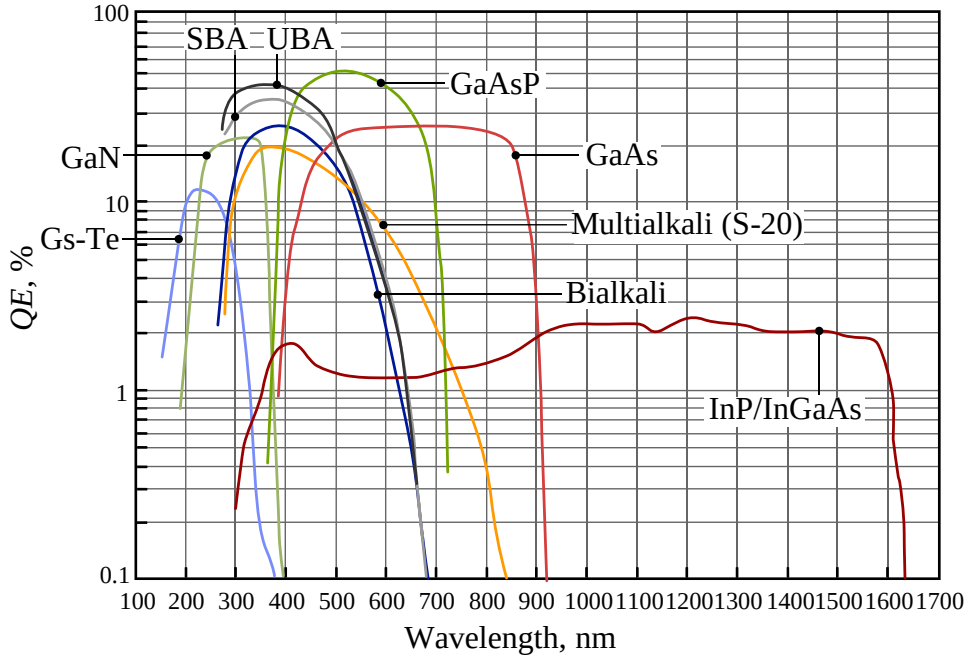

Fig. 5.5.11. Spectral sensitivities of currently used photocathodes

- **Gain**. It is determined by the ratio between the number of electrons that reaches the anode and the number of electrons emitted by the cathode:

$$K_{PMT} = \eta\theta^{M}, \tag{5.5.3}$$

where

$\eta = 0 \div 1$ is a factor accounting for the incomplete collection of cathode-emitted electrons by the first dynode,

θ – the factor of impact emission of the dynodes,

M – the number of dynodes.

Since θ depends on the velocity of electrons falling on each dynode, the gain depends heavily on the PMT power supply voltage. Depending on this voltage and the number of dynodes, the PMT gain can be 10^6–10^9.

- **Integral anode sensitivity**. It shows the value of the anode current by illuminating the cathode with one lumen light. It is given in A/lm for a specific anode voltage.

- **The maximum allowable current and voltage of the anode**. The maximum permissible current is usually in the range of microamperes, but there are also special PMTs that allow currents of up to several milliamps. The maximum voltage varies between 1500–3000 V.

- **Dark current**. This is the current flowing through the anode circuit when the cathode is completely in the dark. There are several reasons for this:
  - **thermo-electron emission** from the photocathode and the first dynode;
  - **auto-electron emission** from the photocathode and the first dynode; this occurs at very high anode voltage;
  - **glass scintillation from the PMT stem**; they can be caused by the electrons emitted from the photocathode striking the wall of the glass bulb; this may happen, for example, when the cathode is not grounded and receives a high negative voltage while the PMT is installed in a grounded metal cylinder; to avoid this effect, PMTs are produced with a glass bulb coated on the outside with conductive paint, creating the same electrical potential as the cathode (the so-called HA Treatment – Fig. 5.5.12 [6]);

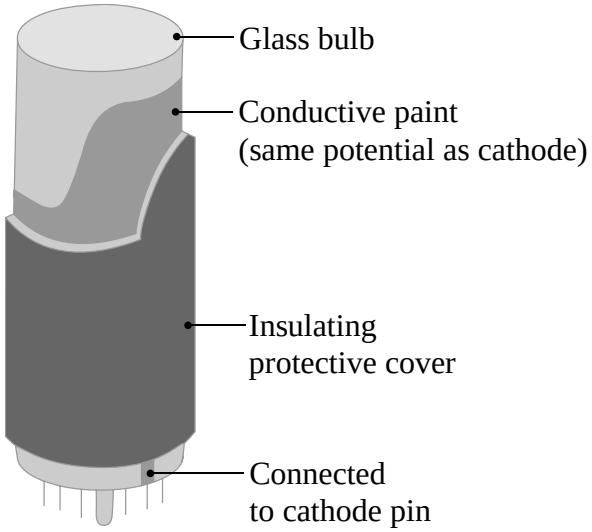

Fig. 5.5.12. HA Coating of a PMT

  - **luminescence of the residual gas** in the volume of the PMT.

The dark current has a discrete nature – noise pulses with arbitrary amplitude and frequency, which increases the measurable background. PMT cooling, lower supply voltage and other methods are used to counter this effect. In modern PMTs, the dark current is in

the range of 2 to 10 nA at an anode sensitivity of 2000 A/lm. It is important to point out that the dark current is considerably higher than its nominal value after the bias voltage is turned on and reaches this value after about 30 minutes.

A very low dark current combined with a very high gain is the most important advantage of PMTs – they provide an excellent signal-to-noise ratio.

- **Amplitude resolution**. It is limited by the statistical nature of photocathode emissions and the electron impact emissions from the dynodes. It can be improved by increasing the intensity of the scintillation (or radiation energy) as the relative fluctuations decrease (see Eq. (5.1.8)). At low energy levels of the particles and γ-quanta, the resolution is in the order of several percent.
- **Time resolution**. It is evaluated by two parameters: **the transit time** – the time interval between the arrival of a very short light pulse at the photocathode and the instant when the anode output pulse reaches its peak amplitude; **the rise time of the anode output pulse** (see below for details). The transit time depends strongly on the applied bias voltage. The transit time of all-purpose PMTs is in the order of several tenths of a nanosecond, and the output rise time – of 1-2 nanoseconds. Special fast PMTs are also produced with a transit time of a few nanoseconds.
- **The activity of the material of the PMT tube**. For ordinary PMTs, the tube is made of potassium glass containing the natural radioactive isotope potassium-40 (^{40}K), and its activity is quite high. Therefore, low-activity measurements should be made using special head-on or end-on type PMTs with a glass bulb window of sodium glass, quartz glass or synthetic silica glass (the last two being transparent for ultraviolet light).
- **Photocathode form and size**. The wide variety of research carried out with scintillation detectors requires the use of scintillators of different shapes and sizes. Therefore, PMTs are also produced with a round photocathode (diameters of 10 to 250 mm) and in a variety of other forms (see below).

3. PMT output signal shape and duration

The circuit depicted in Fig. 5.5.13 must be taken into account when analyzing a PMT output signal formation. Here, R_D and C_D represent the anode load resistor of the PMT and the total capacitance of the detector output circuit (the PMT anode circuit), respectively.

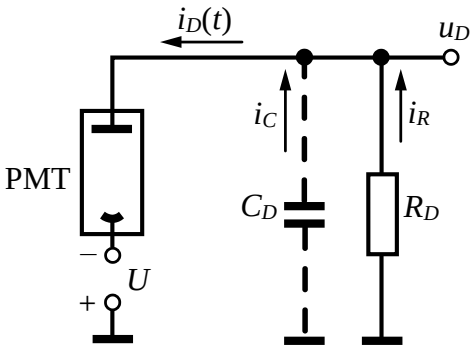

Fig. 5.5.13. An equivalent schematic of the PMT output circuit

The shape and duration of the PMT output (anode) current pulses are determined by the shape and the duration of each incoming scintillation. As noted above, for most scintillators, the scintillation rise time can be neglected, and its duration is evaluated by the decay time constant τ_D. Therefore, the following equation is valid for the PMT output current:

$$i_D(t) = I_D e^{-t/\tau_D}, \qquad (5.5.4)$$

where I_D is the current pulse amplitude (Fig. 5.5.14a).

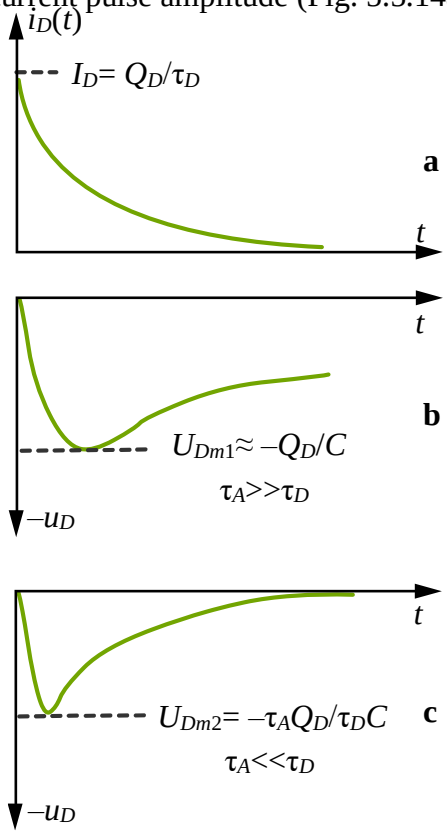

Fig. 5.5.14. PMT signal shapes

The total charge Q_D created by this current is

$$Q_D = \int_0^\infty i_D(t)dt = I_D \int_0^\infty e^{-t/\tau_D} dt = I_D \tau_D, \qquad (5.5.5)$$

from where $I_D = Q_D/\tau_D$, and by replacing it in equation (5.5.4), we obtain

$$i_D(t) = \frac{Q_D}{\tau_D} e^{-t/\tau_D}. \qquad (5.5.6)$$

This current (Fig. 5.5.13) flows into the parallel RC circuit at the output of the PMT, i.e. $i(t) = i_C + i_R$, or

$$C_D \frac{du_D}{dt} + \frac{u_D}{R_D} = \frac{Q_D}{\tau_D} e^{-t/\tau_D}. \qquad (5.5.7)$$

Here, u_D is the PMT output voltage signal. The solution to this inhomogeneous linear differential equation is [7]

$$u_D = -\frac{\tau_A}{\tau_A - \tau_D} \frac{Q_D}{C_D} (e^{-t/\tau_A} - e^{-t/\tau_D}), \qquad (5.5.8)$$

where $\tau_A = R_D C_D$ is the time constant of the anode circuit.

Typically, one of the two extreme magnitudes of this time constant are selected during actual operation:

1. $\boldsymbol{\tau_A >> \tau_D}$. In this case, τ_D in (5.5.8) can be neglected and $u_D = -\frac{Q_D}{C_D}(e^{-t/\tau_A} - e^{-t/\tau_D})$, where the first exponent in the brackets fades much slower than the second one. Thus, for the very short rise time, it can be assumed that $e^{-t/\tau_A} \approx 1$, and the signal increases according to the dependence $u_D = -\frac{Q_D}{C_D}(1 - e^{-t/\tau_D})$, reaching its amplitude $U_{Dm1} \approx -Q_D/C_D$. Then it decreases according to $u_D = -\frac{Q_D}{C_D} e^{-t/\tau_A}$ (Fig. 5.5.14b), because $e^{-t/\tau_D} \approx 0$.
2. $\boldsymbol{\tau_A << \tau_D}$. Now, $u_D = -\frac{Q_D}{C_D}\frac{\tau_A}{\tau_D}(e^{-t/\tau_D} - e^{-t/\tau_A})$ and again, the first exponent fades much slower than the second one. Therefore, the signal (Fig. 5.5.14c) increases exponentially faster with the time constant τ_A (which is much smaller than τ_D) and decreases faster with the time constant τ_D. In this case, although the signal is very short, its amplitude is considerably smaller – $U_{Dm2} \approx -\tau_A Q_D/\tau_D C_D = (\tau_A/\tau_D)U_{Dm1}$.

In order to provide maximum amplitude, C_D is always left minimal, and the mode of operation is selected according to the resistance of the resistor

R_D. In most cases, the mode $\tau_A >> \tau_D$ is used to obtain the maximum amplitude of the signal and a better signal-to-noise ratio. However, when very fast action is required – at a high count rate of the light pulses or during timing measurements – the mode $\tau_A << \tau_D$ has to be selected.

4. PMT Disadvantages

The PMTs have two important disadvantages:

- they cannot operate in a magnetic field: the magnetic field deflects the photoelectrons, and they may not reach the first dynode;
- the PMT photocathode should be protected from external light; if light falls on the photocathode when the bias voltage is turned on, it would be destroyed immediately.

5. Types of Photomultipliers

a. Head-on PMTs

Because of the very wide use of head-on PMTs for a variety of tasks, they are produced in a great number of different shapes and sizes (Fig. 5.5.15).

Fig. 5.5.15. A variety of head-on photomultipliers produced by Hamamatsu

Fig. 5.5.16. Hamamatsu R669 PMT (Φ 51)

A typical PMT (Hamamatsu[1], type R669) is shown in Fig. 5.5.16.Its main parameters include: diameter – 51 mm (photocathode diameter – 46 mm); wavelength of maximum response – 600 nm (the photocathode has increased red sensitivity); cathode window material – borosilicate glass; cathode sensitivity – 230 μA/lm; the number of dynodes – 10; gain – $5.3 \cdot 10^5$ with anode sensitivity of 75 A/lm at 1000 V of bias voltage; anode dark current – 7 nA.

[1] One of the biggest optical sensor producers in the world.

b. Side-on PMTs

Side-on is another modification of a PMT whose photocathode is installed to receive the incident light through the side of the glass bulb (Fig. 5.5.17). The electron multiplier system ($D_1 - D_9$ in Fig. 5.5.17) is of the circular-cage type, which is very compact and has a fast response and a high gain obtained at relatively low supply voltage.

A typical side-on type PMT (Hamamatsu R928) is shown in Fig. 5.5.18.

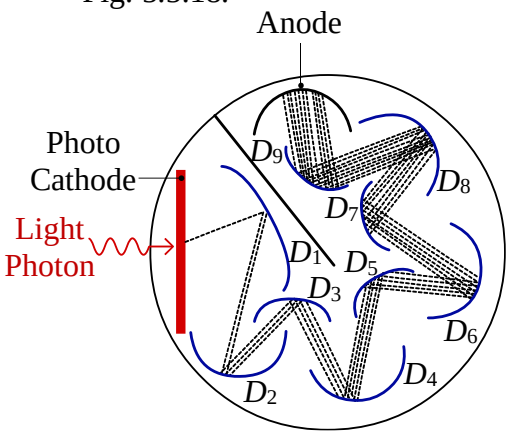

Fig. 5.5.17. Cross-section of a side-on PMT

Fig. 5.5.18. A side-on PMT – Hamamatsu R928

Its basic technical characteristics are: glass bulb diameter of 28 mm; photocathode surface of 8 × 24 mm; a spectral response of 185–900 nm; wavelength of maximum response – 400 nm; cathode sensitivity of 250 μA/lm; the number of dynodes – 9; gain – 1.0×10^5 with anode sensitivity of 2500 A/lm, both at 1000 V bias voltage; anode dark current – 3 nA; anode pulse rise/transit time – 2.2/22 ns. These values confirm the high photosensitivity, high gain and fast response time of this type of PMT.

Side-on PMTs are widely used for spectrophotometers and general photometric systems in biofluorescence detection and environmental monitoring. However, they have very limited application in nuclear and high-energy physics experiments because of their difficult coupling with the scintillators in use.

c. Multiple anode PMTs

Another type of PMT is the so-called multiple anode PMT. They use a common photocathode (divided into sectors) and individual electron multipliers and anodes. By doing so, they can replace many PMTs in

a multichannel measuring system, taking up much less space and allowing for significant savings in terms of volume and financial means. Usually, they have a metal housing and a square shape wherein the anodes (with the electron multipliers) are installed in a matrix form – 2 × 2, 4 × 4, and so on. Fig. 5.5.19 depicts a PMT with 64 anodes, creating a quadratic photocathode (49 × 49 mm). Another version is where anodes are installed linearly, forming PMTs that are suitable for some medical and biological research. Fig. 5.5.20 shows a 32-anode PMT (Hamamatsu H7260) with a rectangular photocathode (10 × 35 mm).

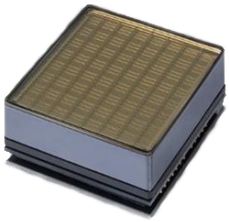

Fig. 5.5.19. A multiple anode PMT containing 8×8= 64 anodes

Fig. 5.5.20. A PMT with 32 anodes installed in a single line

The gain for all multiple anode PMTs is about 10^6 (with 9-stage electron multipliers), which is enough for most applications. They have a relatively fast response time – the rise time is less than 1ns with a transit time spread of around 0.5 ns.

d. Photomultipliers based on a microchannel plate (MCP)

A modern microchannel plate (MCP) is a slab made from a highly resistive material of typically 2 mm thickness with a regular array of tiny tubes or slots (microchannels) leading from one surface right through to the opposite (Fig. 5.5.21a).

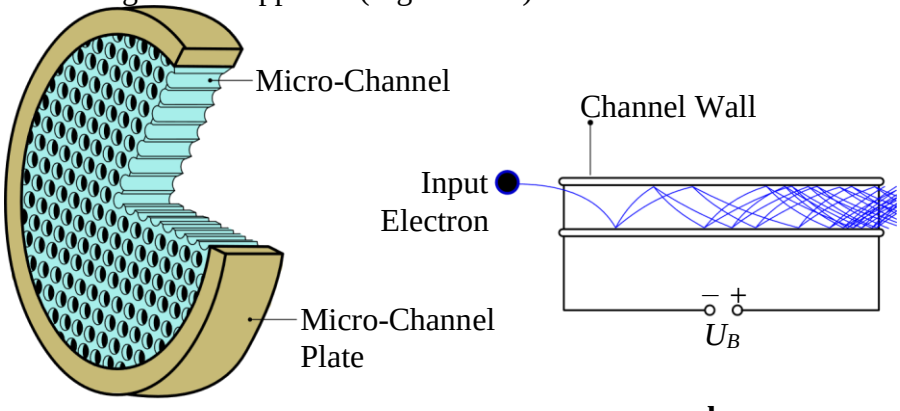

Fig. 5.5.21. Structure of a microchannel plate (a) and of a channel (b)

The microchannels have a diameter of several micrometers and are densely distributed (spaced apart at around 10 μm) over the entire surface. They are parallel to each other and often enter the plate at a slight angle to the surface (∼8°). The wall of each channel is covered on the inside with a substance that has a high electron impact emission coefficient. A high voltage (1–2 kV) is applied to both sides of the MCP, which reaches all channels (U_B, Fig. 5.5.21b). Thereby, an accelerating electrical field is created inside all of the channels (for the electrons at the shown voltage polarity). Thus, when an electron enters any one of the channels, it is accelerated and strikes the wall (because of the 8° angle), producing a few new electrons. They are accelerated in turn, hit the wall on the opposite side, and generate new electrons. As depicted, the channel is a kind of electron multiplier – something like a continuous dynode system. An anode collects the electrons as they exit the channel. The gain depends on the bias voltage and can reach up to 10^4. It can be increased significantly if two such MCPs with angled channels are mounted sequentially and rotated 180° from each other – the so-called Chevron MCP.

A photocathode is coupled with an MCP in a vacuum tube for it to be used as a PMT. Fig. 5.5.20 shows a typical modern MCP PMT (Hamamatsu R3809U-50 [6]), which has the following characteristics: photocathode diameter – 11 mm; 2 MCPs; MCP channel diameter – 6 μm; output pulse rise time – 160 ps; transit time spread – 55 ps; operating bias voltage – 3400 V. The very low transit time spread is due to the equal trajectory of all of the electron avalanches, which is fixed by the equal longitude of the channels.

Fig. 5.5.22. An MCP PMT

Besides the special PMTs, MCP detectors have many other applications [8]. Because they have many separate channels, they can, for example, reproduce spatial images.

B. Avalanche photodiodes

An **avalanche photodiode** (**APD**) – as depicted in Fig. 5.5.23 – is a highly sensitive electronic semiconductor device that exploits the photoelectric effect to convert light pulses into electric signals. An important feature of an APD is that, besides this transformation, it amplifies the created electric signal through avalanche multiplication.

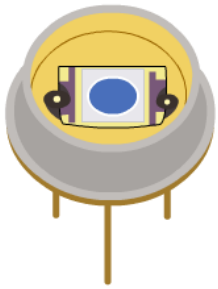

Fig. 5.5.23. A typical APD

From a functional standpoint, they can be regarded as the semiconductor analog of photomultipliers. Avalanche photodiodes operate at high reverse bias voltages (typically 100–200 V). It creates a strong electric field in the depletion region, which accelerates the electrons through the silicon crystal lattice and produces electrons through impact ionization. The avalanche process is similar to the impact ionization in proportional counters (see Section 5.2.3). This electron avalanche can produce gain factors of up to several hundred.

Some diodes that utilize specialized manufacturing processes enable much higher bias voltages of up to 1500 V. As the avalanche amplification increases when higher voltage is applied, the gain of these APDs can rise to 1000. This can provide a distinct advantage where sensitivity is of paramount importance, but this is obviously at the expense of all the additional circuitry and safety features needed in order to operate safely at such high voltages.

APDs are used when light signals are too high for photomultiplier tubes and too low for conventional photodiodes. Their most important advantages are low noise, high speed, slight influence from the magnetic field, and being small in size. These qualities make them very suitable for multichannel scintillation detectors used in particle physics experiments where there is very often a high magnetic field. For example, specially designed APDs are used in the electromagnetic calorimeter (ECAL) of the CMS detector at CERN, operating in a magnetic field of around 4 Tesla. They are coupled together with lead tungsten crystal scintillators ($PbWO_4$) – Fig. 5.5.24. The total number of channels is more than 75000.

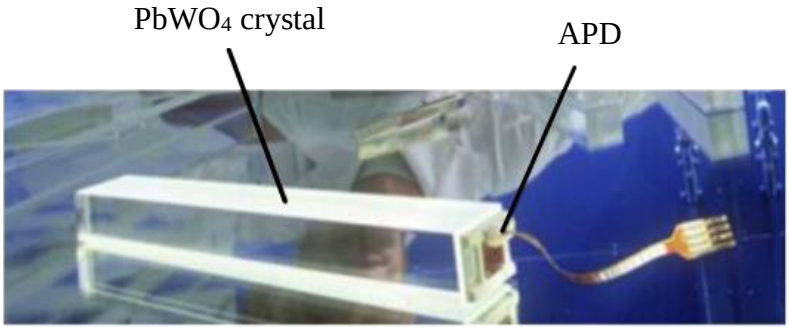

Fig. 5.5.24. One CMS ECAL scintillation detector composed of a $PbWO_4$ crystal and an APD

Typically, APDs work in a linear mode – the amplitude of the output signal is proportional to the incident light (optical) flux. However, they can operate in another mode too. It occurs when the applied reverse bias voltage is higher than the diode breakdown voltage U_{BD}.

In this mode of operation, the gain becomes very high (about 10^5), and the presence of only one electron-hole pair in the APD depletion zone is enough to break down the diode. To avoid damaging the APD, the current moving through it should be limited. For this purpose, a quenching resistor must be connected serially with the APD (R_Q in Fig. 5.5.25a).

This mode of operation is called the **Geiger mode** because the processes are similar to those of the Geiger-Müller gas counters (see Section 5.2.4) – only **a single incident photon** is enough to start an avalanche finishing with a temporary APD breakdown. For this reason, APDs operating in the Geiger mode are also called **Single Photon Avalanche Diodes** (**SPADs**[1]).

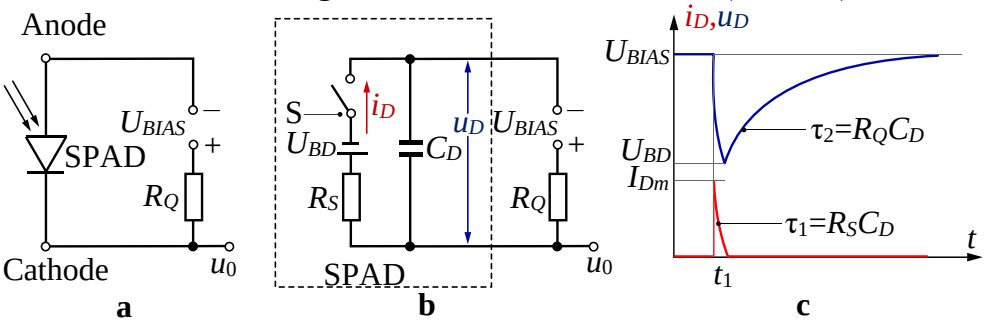

Fig. 5.5.25. a) Operational circuit of an APD in Geiger-mode (SPAD); b) Equivalent circuit of a SPAD; c) Shapes of the current and voltage pulses in the SPADs circuit

[1] Hamamatsu (one of the biggest optical device makers in the world) came up with the name **Geiger APDs** (**GAPDs**) [9].

The processes in this mode can be analyzed using the SPAD equivalent circuit shown in Fig. 5.5.25b [9]. In it, the SPAD is represented by its own resistance R_S and capacitance C_D, the brake-down voltage drop U_{BD} and the switch S. C_D is initially biased at U_{BIAS} – while the switch S is open. When an electron-hole pair is generated (at the moment of t_1 – Fig. 5.5.25c) within the depletion layer (whether thermally or by a photoelectric effect), the switch S closes. Then the C_D begins to discharge through the SPAD's resistance R_S. The small value of R_S (diminished by the avalanching charge carriers) provides for a short current pulse through the SPAD with an amplitude of $I_{Dm} = (U_{BIAS} - U_{BD})/R_S$. During the pulse, the C_D voltage (u_D, Fig. 5.5.25c) decreases exponentially to U_{BD} and, if $R_Q >> R_S$, the avalanche in the SPAD is quenched when $U_C = U_{BD}$, which corresponds to turning off the switch S. The condition $R_Q >> R_S$ is very important, because when $U_D \approx U_{BD}$, only a current of $I_D = (U_{BIAS} - U_{BD})/R_Q$ could flow through the SPAD, and this current must be small enough not to sustain the avalanche process. Then, the current flowing through R_Q will only charge C_D until $U_C = U_{BIAS}$, after which the SPAD will be ready to record any new incident light photon. The negative pulse, which formed on C_D (u_D, Fig. 5.5.25) is commonly used as an output signal.

As can be seen, the SPAD generates only one output signal with a fixed amplitude $U_{Dm} = U_{BIAS} - U_{BD}$, regardless of the number of light photons falling simultaneously on its photocathode. For this reason, it cannot measure the light flux and, respectively, the radiation energy.

Consequently, individual SPADs have limited applications.

C. Silicon photomultipliers

1. Principle of operation

Silicon photomultipliers (often called SiPM[1]) are an extremely promising practical application of SPADs. They consist of many SPADs implemented on one common silicon substrate. The diameter of every single SPAD can vary from 10 to 100 μm, and their density can be up to 1000 per square millimeter. Each of these SPADs has its own quenching resistor (R_1 to R_M in Fig. 5.5.26).

The combination of each SPAD with its quenching resistor is referred to as a microcell or pixel. Each microcell detects photons identically and independently. Its current is the same regardless of the number of incident photons that entered simultaneously. However, the photocurrents of all these individual microcells combine and pass through the anode and

[1] Hamamatsu produce these devices under the name **Multi Pixel Photon Counter** (**MPPC**).

cathode outputs. When a load resistor (R_L) is connected between one of the SiPM outputs (in our case, the cathode) and the corresponding output of the bias power supply (in our case, $+U_B$), a quasi-analog output signal is formed thereupon, which is proportional to the sum of all the individual microcells' currents:

$$u_0 = R_L \sum_{1}^{M} I_i. \tag{5.5.9}$$

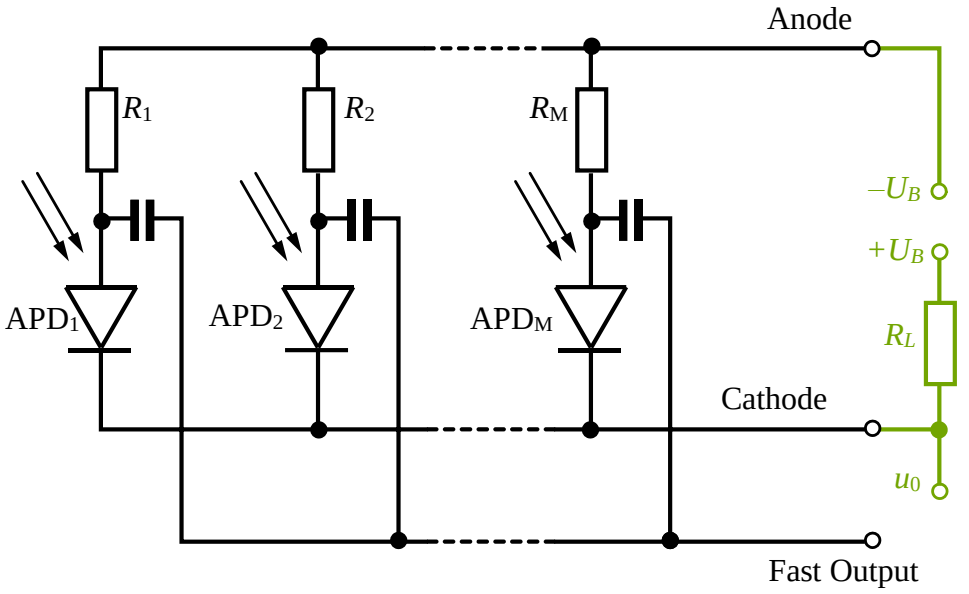

Fig. 5.5.26. Electrical diagram of a SiPM

Thus, the SiPM can provide information about the magnitude of an incident photon flux and respectively about the radiation energy. It is useful to ground this bias power supply terminal to which the load resistor is connected because then there will be no DC voltage component in the output signal (u_0).

The output signal is quasi-analog because it is proportional to a sum of discrete currents. They are equal in number to the number of microcells, each of which receives one photon at the same time. Fig. 5.5.27 [10] shows a typical oscilloscope graph of the SiPM output signals when illuminated by brief pulses of low-level light – they have only amplitudes corresponding to the number of activated microcells (respectively to the number of incident photons) – 1, 2, 3 or 4. The same is confirmed by the amplitude spectrum of these pulses shown in Fig. 5.5.28.

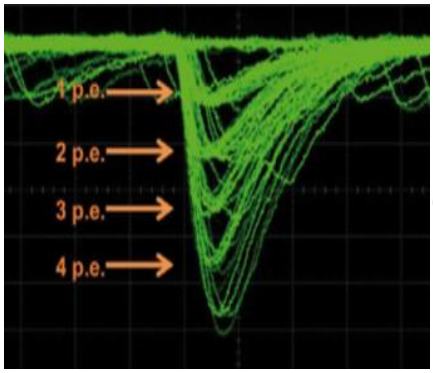

Fig. 5.5.27. Typical oscilloscope graph of the SiPM's output signals

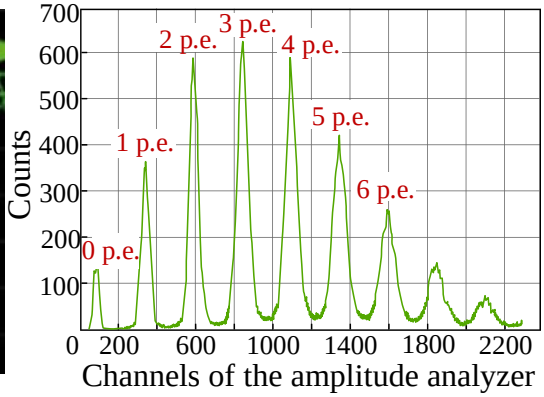

Fig. 5.5.28. Amplitude spectrum of the SiPM's output signals

Some manufacturers [11] produce SiPMs with a fast output, to which the individual output of all microcells are connected (see Fig. 5.5.26). The fast output signal is also formed from the sum of all activated microcell signals, and thus information on the magnitude of the photon flux can be obtained in addition to timing information. A typical fast output pulse is shown in Fig. 5.5.29. This signal can be used to make ultra-fast timing measurements, enabling the ability to clearly distinguish the arrival time of the first photon in the pulse.

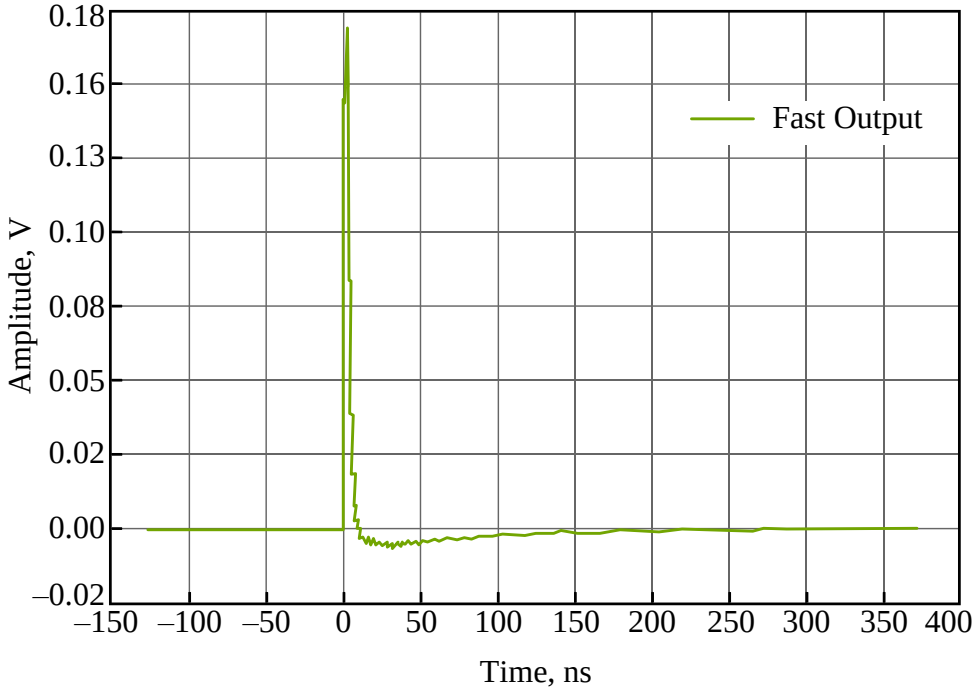

Fig. 5.5.29. A fast output signal

SiPMs are manufactured in different sizes with either a square (from 1 × 1 to 6 × 6 mm) or round shape (diameter 1–3 mm). The number of microcells varies depending on their pitch, which is between 10 and 50 μm. Fig. 5.5.30 depicts two types of SiPM – rectangular (a) and round (b), as produced by Hamamatsu [12]. The photosensitive area of the first is 1.3 × 1.3 mm, consisting of 1668 microcells (with a pixel size of 25 μm). The same area of the second SiPM has a diameter of 1.5 mm and consists of 2876 microcells (with the same pixel size). Matrices of SiPMs are also produced when larger photosensitive areas are needed (Fig. 5.5.31).

a **b**

Fig. 5.5.30. Two types of SiPM constructions

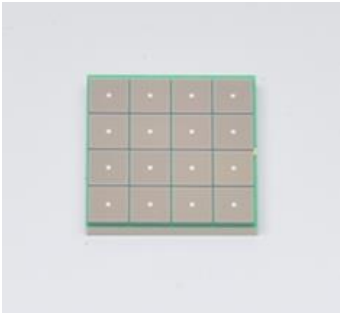

Fig. 5.5.31. A matrix of 16 SiPMs

2. Performance parameters of a silicon photomultiplier[1]

- **Breakdown voltage and overvoltage**. The breakdown voltage (U_{BR}) is the bias point at which the electric field strength generated in the depletion region is sufficient to create a Geiger discharge. The U_{BR} point is clearly identified on the SiPM current-voltage characteristic by a sudden increase of the current as in Fig. 5.5.32 [11]. The figure shows that the larger microcells have a steeper increase in the current after the breakdown.

  SiPMs are operated at a bias point that is typically 10-25 % higher than the U_{BR}. The difference between the U_{BR} and the bias point is referred to as the overvoltage (ΔU). Normally, the U_{BR} and the recommended ΔU range are provided as part of the SiPM production information. These values make it possible to calculate the necessary bias voltage U_{BIAS}:

$$U_{BIAS} = U_{BR} + \Delta U. \qquad (5.5.10)$$

[1] Thanks to the company **SensL** – this section is mainly based on its Technical note: An Introduction to the Silicon Photomultiplier [11].

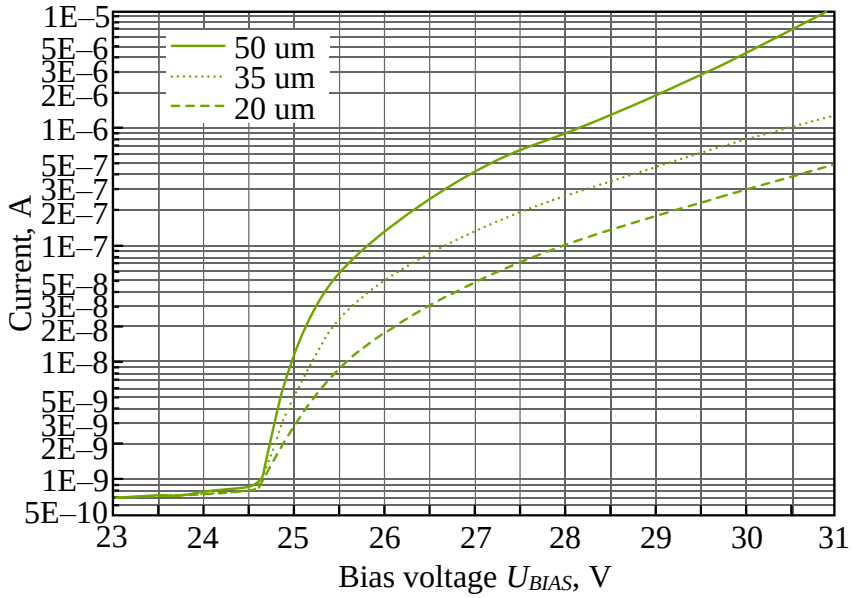

Fig. 5.5.32. SiPM's current vs U_{BIAS} for different microcell sizes

SiPMs made by different producers often have different breakdown voltages, thereby requiring different bias voltages. For example, the SiPMs produced by SensL need bias voltages of around 30 V, while those made by Hamamatsu – around 70 V. However, in all cases, the bias voltage is below 100 V.

- **Gain.** The gain of a SiPM is estimated by the amount of charge created for each detected photon and is a function of overvoltage and microcell size. Each microcell in the SiPM generates a highly uniform and quantized amount of charge ($Q_{MC} = C_{MC}\Delta U$) every time an avalanche is generated by an absorbed photon in the active volume. Here, C_{MC} is the microcell capacitance and ΔU – the overvoltage. The gain of a microcell (and hence of the SiPM) is then defined as **the ratio of the charge created by an activated microcell to that of an electron q_e**:

$$G = C_{MC}\Delta U/q_e. \qquad (5.5.11)$$

Fig. 5.5.33 [11] shows the gain as a function of the overvoltage for four microcells of different sizes. As can be expected, the largest microcells have the highest gain because of their larger capacitance. In all cases, the figure shows that the SiPMs have a very high gain – in the order of 10^5–10^7.

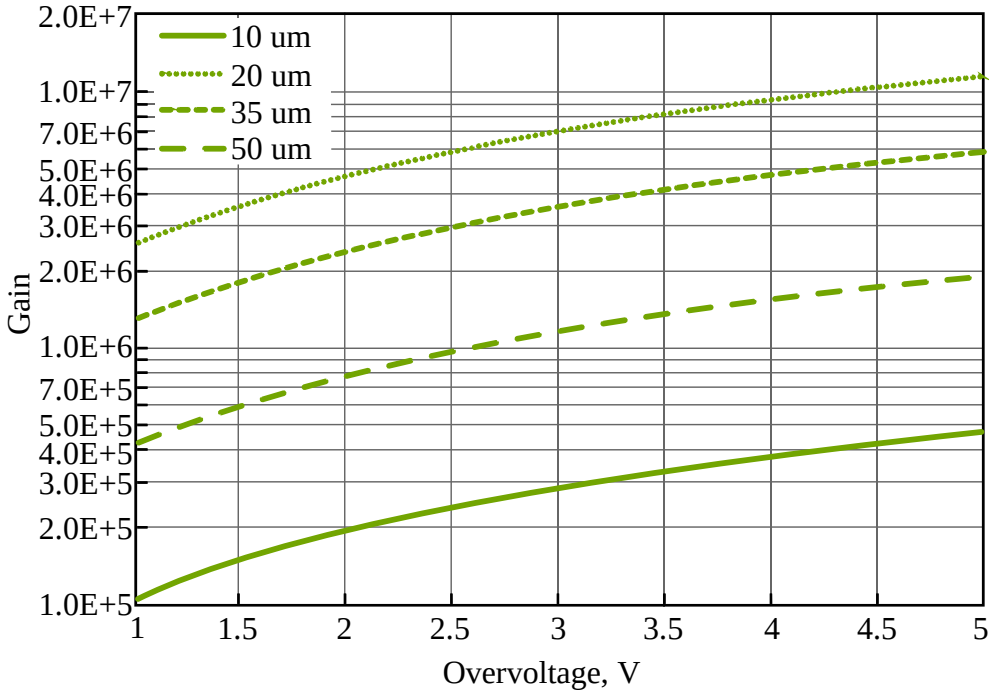

Fig. 5.5.33. Gain versus overvoltage ΔU for different microcell sizes

- **Photon Detection Efficiency.** The photon detection efficiency (PDE) is a measure of the sensitivity of a SiPM and depends on the incident light wavelength, the applied overvoltage, and the microcell fill factor. The PDE corresponds to the quantum efficiency (QE) that is quoted for a PMT or APD but is slightly different due to the microcell structure of the SiPM. The PDE shows the probability of an incident photon interacting with a microcell and producing an avalanche. It is defined as:

$$PDE = k_{SI}(\lambda)\varepsilon(\Delta U)F, \qquad (5.5.12)$$

where

$k_{SI}(\lambda)$ is the quantum efficiency of the silicon,

$\varepsilon(\Delta U)$ – the avalanche initiation probability,

F – the fill factor of the device.

The quantum efficiency presents the probability of an incident photon creating an electron-hole pair in the sensitive volume of the sensor. The avalanche initiation probability reflects the fact that not all charge carriers in the microcell's active volume will initiate an avalanche. The fill factor is the ratio between the active- and inactive area on the

SiPM due to the dead space between the microcells (see the next point), and therefore depends on their respective size.

The dependence of the PDE on the wavelength of two overvoltage values – 2.5 and 5 volts – is shown in Fig. 5.5.34.

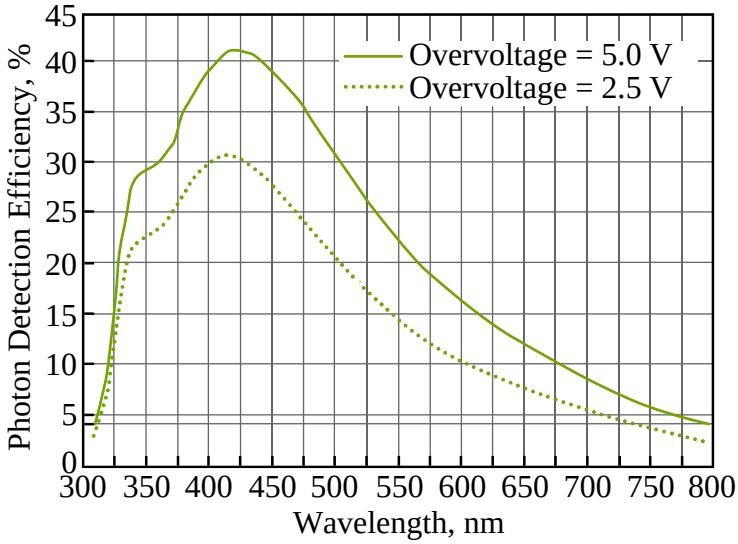

Fig. 5.5.34. PDE versus wavelength

As can be seen, the PDE's maximum value is between 400 and 425 nm, which corresponds to the wavelength of most of the scintillators. In Fig. 5.5.35, the PDE dependence on the overvoltage is given at a wavelength of 420 nm. It shows that there is some saturation at ΔU over 4–5 volts where the PDE increases very slowly.

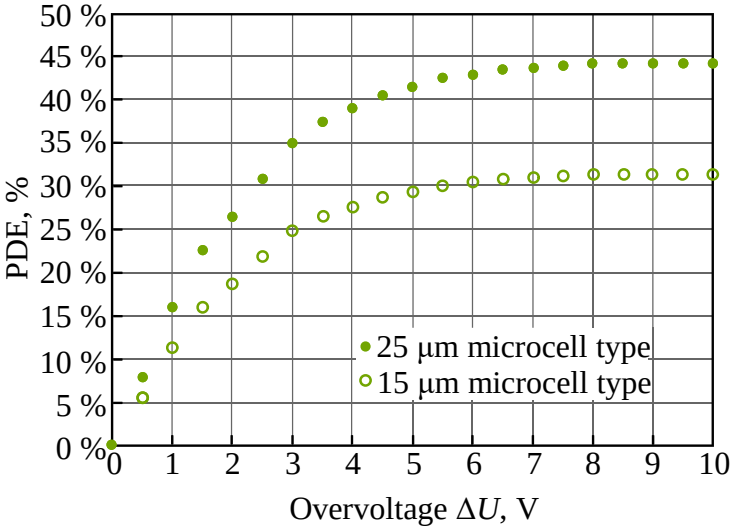

Fig. 5.5.35. PDE versus overvoltage

- **Fill Factor.** The fill factor F is the ratio between the light-sensitive SiPM surface area and the total device surface area expressed as a percentage. Due to the structure of the SiPM, each microcell needs to be separated from its neighbor for optical and electrical isolation purposes. In addition, some surface area is required for the quench resistor and signal tracks. All of these considerations result in a "dead space" around each microcell. The space required for microcell separation, the quench resistor and signal tracking is relatively constant, regardless of the microcell size. Therefore, larger microcells result in a higher percentage of active surface area.

  It should be noted, however, that a higher fill factor (larger microcells) results in higher PDE and gain, but also in higher capacitances, longer recovery times and a lower dynamic range. A lower fill factor (smaller microcells) results in lower PDE and gain, but also in lower capacitances, shorter recovery times and a higher dynamic range.

  Exemplary values of F for different microcell sizes are given in Table 5.5.5. It is clear that the differences between them are significant. This calls for careful selection of SiPMs in accordance with the requirements of the particular measurement.

Microcell size, μm	**Fit factor, %**
10	28
20	48
35	64
50	72

Table 5.5.5. The fill factor for different microcell sizes

- **Dark count rate.** The main component of the noise in a SiPM is the dark count rate (DCR), which is primarily due to thermal electrons generated in the active volume initiating avalanches in the depletion region. The signals resulting from the breakdown of the microcell due to either photon-generated- or thermally generated electrons are identical. Therefore, these thermal electrons are a source of noise at the single-photon level. For this reason, the number of false pulses due to thermal electrons can be limited by setting the discrimination threshold above the

amplitude of the single-photon signals. However, the number of measured signals will decrease because of the exclusion of the useful one-photon pulses.

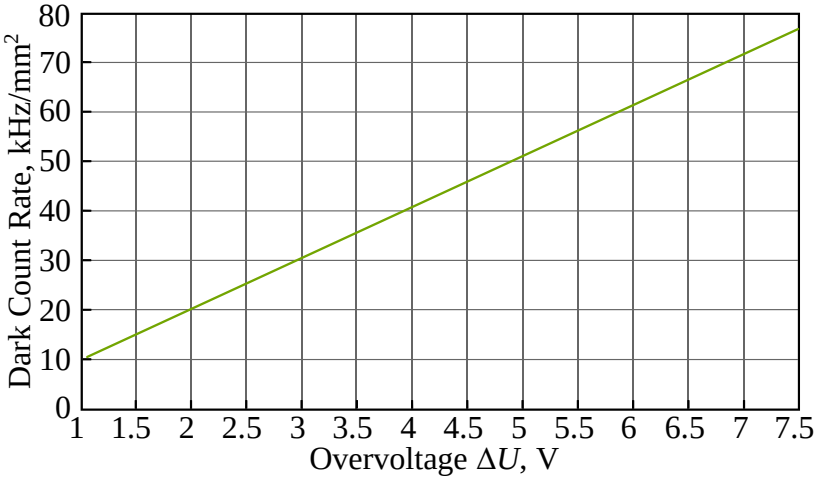

Fig. 5.5.36. Dark Count Rate versus overvoltage

The DCR magnitude is commonly quoted as a pulse rate (kHz) or pulse rate per unit area (kHz/mm^2). For current integration measurements (see Part 10), it is more convenient to consider the DCR contribution as a dark current, which is also provided in the producer's datasheets.

The DCR depends on the overvoltage, active area size and temperature. Fig. 5.5.36 illustrates its linear increase in relation to the overvoltage. Its dependence on temperature is particularly strong – for every 10℃ reduction in the device temperature, there is a 50 % decrease in the dark count rate. Therefore, actively cooling a SiPM significantly reduces the DCR.

- **Dynamic range and linearity**. The dynamic range of a SiPM can be defined as the incident optical signal range over which the amplitude of the output signal remains proportional to the input one. The relationship between the number of incident photons N_{IN} (corresponding to the amplitude of the incident optical signal) and the number of fired (illuminated by light) microcells N_F (determining the output signal) is given as

$$N_F = M\left[1 - \exp\left(1 - \frac{PDE.N_{IN}}{M}\right)\right], \qquad (5.5.13)$$

where M is the total number of microcells in the SiPM. Because the PDE is a function of the overvoltage and wavelength, the dynamic

range also depends thereupon. However, the most important factor is the total number of microcells M.

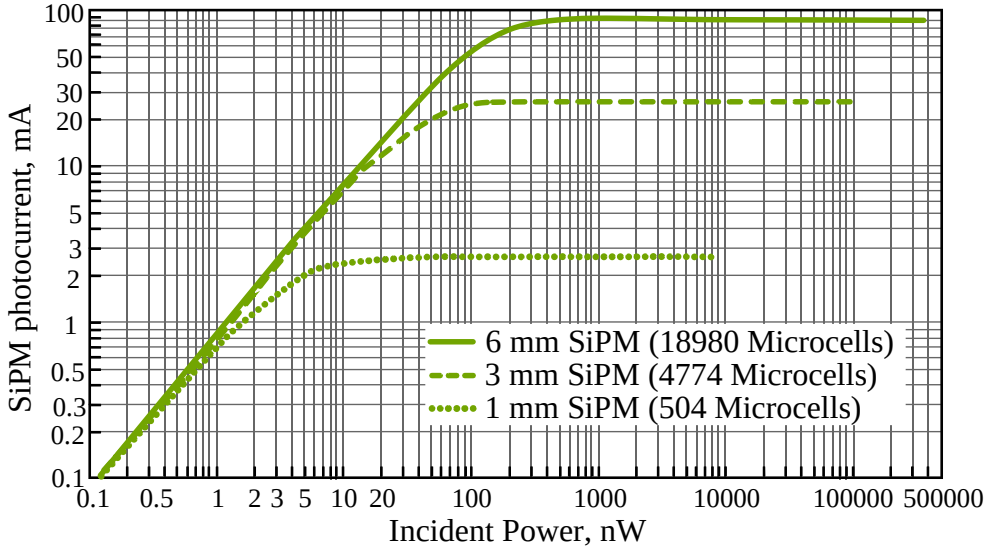

Fig. 5.5.37. Linear range due to the number of microcells

Fig. 5.5.37 illustrates this dependence graphically (the SiPM photocurrent is proportional to the N_F, and the incident power to the N_{IN}) for three different SiPM diameters (i.e. M). Evidently, the linearity of this dependence is preserved by an unspecified upper limit of the increasing input signal, after which it is broken, and, after a nonlinear transition, saturation is reached. At the same time, this limiting value increases with the increase of the SiPM's size, i.e. with an increase in the number of microcells. In practice, the linearity can be regarded as being preserved up to about 70 % of the saturated value.

- **Temperature dependence**. Temperature alterations directly change the SiPM's breakdown voltage and the dark count rate. The changes in the breakdown voltage directly alter the effective overvoltage, the gain, and PDE, respectively, which are the basic parameters of a SiPM. The breakdown voltage increases linearly as a function of temperature, decreasing the overvoltage and the gain. All manufacturers are making great efforts to reduce this dependence. The best results have been obtained by Hamamatsu – 0.73 %/℃ for a SiPM of 1 mm^2 with cells of 10 μm. A similar value was provided by SensL [11] – 0.86 %/℃ (Fig. 5.5.38).

  These values are relatively small, and so, in many applications, temperature compensation may not be required. However, for stable operation in the presence of significant temperature fluctuations,

either bias compensation or thermal regulation should be considered. Bias compensation is the simpler of the two methods – ready-made devices are available on the market for this purpose. They automatically adjust the bias to ensure a constant overvoltage.

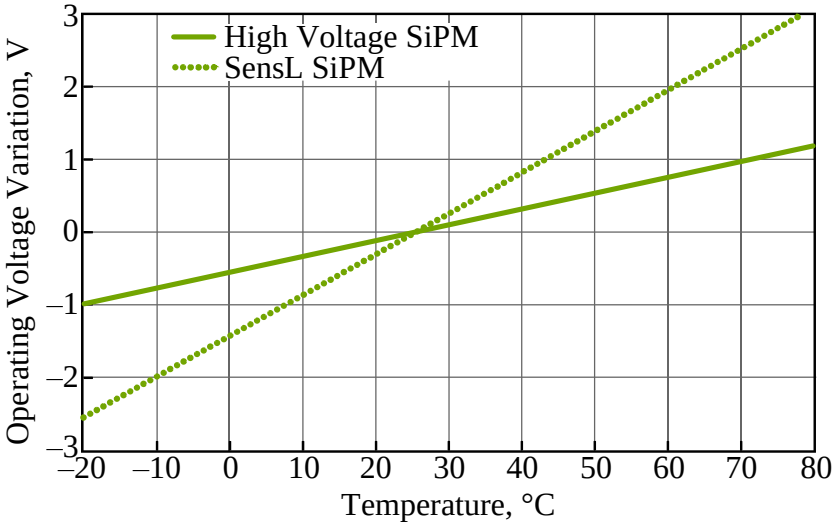

Fig. 5.5.38. Operating voltage (i.e. overvoltage) variation versus temperature

Most SiPM's parameters, such as gain, PDE and timing, remain the same with a constant overvoltage. Only the DCR will change with the temperature variation due to the change in the generation rate of thermal electrons in the sensitive volume. Thus, the dark current increases as the temperature increases.

- **Optical crosstalk**. During each avalanche, accelerated carriers in the depletion region emit photons that can initiate a secondary avalanche in a neighboring microcell. This process is called **optical crosstalk**, and it creates an additional component of SiPM noise. These secondary photons are in the near-infrared region and can travel

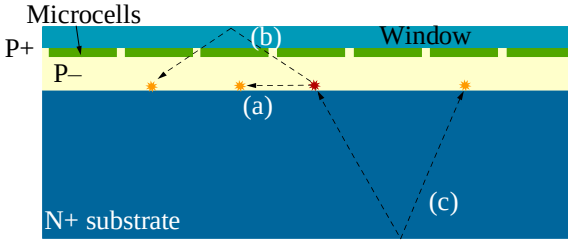

Fig. 5.5.39. Different routes of secondary photons to neighboring microcells

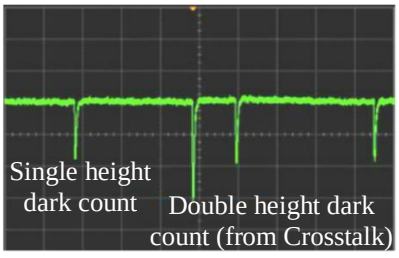

Fig. 5.5.40. SiPM output in the dark

substantial distances through silicon. Fig. 5.5.39 shows their different routes to neighboring microcells: (a) directly to a neighboring microcell, (b) reflected from the window material on the top of the sensor (usually epoxy or glass), or (c) reflected from the bottom of the silicon.

The crosstalk is estimated by the probability that an avalanching microcell will cause an avalanche in a second microcell. All secondary avalanches happen simultaneously with the original one, and in this way, a single incident photon may occasionally generate signals equivalent to 2 or 3 photons, or even higher. This effect is illustrated in Fig. 5.5.40 [11], which shows the output of a SiPM in the dark. Thus, all of the signal pulses are due to dark counts. The central dark count pulse has double the amplitude of the other dark counts, which are at the single-photon level, and so it will be due to a crosstalk event.

Optical crosstalk is a function of overvoltage and is also affected by the fill factor of the SiPM. Fig. 5.5.41 [11] shows the crosstalk increasing with overvoltage for a 3 mm SiPM with 35 μm microcells. The reason is the increased number of carriers crossing the junction at a higher gain.

The relationship between PDE and crosstalk is shown in Fig. 5.5.42. It is evident that an increase in PDE leads to an increase in the crosstalk because the former is achieved by increasing the overvoltage. This figure also shows that the SiPM with larger microcells has a more advantageous ratio between the PDE and the crosstalk.

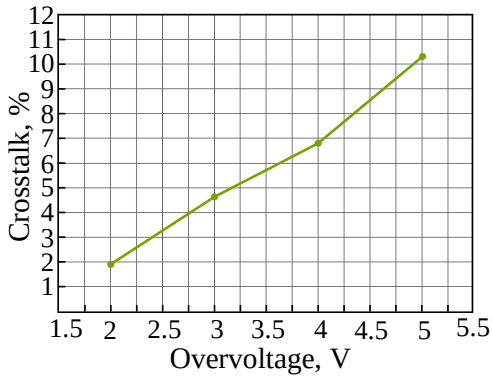

Fig. 5.5.41. Crosstalk versus overvoltage

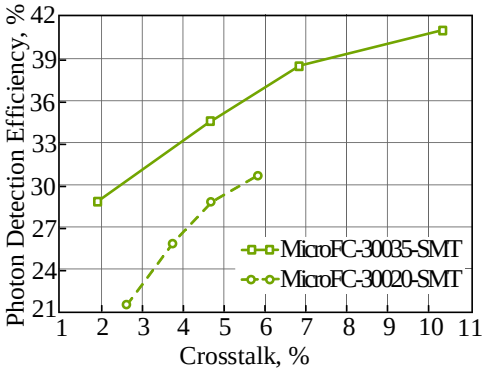

Fig. 5.5.42. Dependence between PDE and the crosstalk

- **Afterpulsing**. During breakdown, some carriers may be trapped in defects in the silicon. After a delay of up to several ns, such carriers are released, potentially initiating an avalanche and creating an

afterpulse in the same microcell. Afterpulses with a short delay (that occur during the microcell recovery time) have a negligible impact since the microcell is not fully charged. However, longer delayed afterpulses (Fig. 5.5.43) can affect measurements with the SiPM if the rate is high. Afterpulse probability increases in parallel with the overvoltage (due to increased avalanche initiation probability).

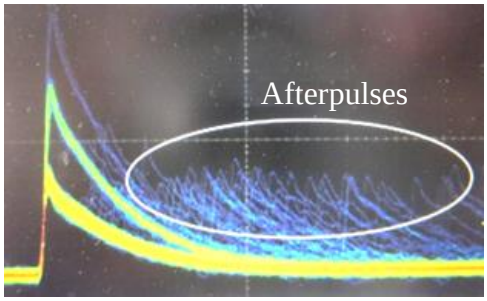

Fig. 5.5.43. Afterpulsing of earlier SiPMs

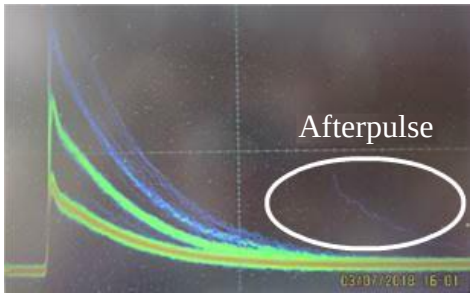

Fig. 5.5.44. Afterpulsing of modern SiPMs

Modern devices have particularly low afterpulsing due to the use of improved materials with minimum defects and wafer process technologies. Fig. 5.5.44 depicts the afterpulses of a Hamamatsu SiPM 3 × 3 mm with 10000/mm^2 microcells [13]. The reduction of afterpulses provides a better signal to noise ratio, a wider operating voltage range, and an improved time resolution.

3. Comparison between SiPM and PMT

In-depth knowledge of the basic parameters of a SiPM allows an objective comparison between the qualities of silicon- and vacuum photomultipliers used as photodetectors in scintillation counters. The primary advantages of SiPMs are:

- Single-photon resolution.
- A higher photon detection efficiency than that of a PMT – up to 40 %.
- High gain – 10^5–10^7.
- Short recovery time – a few nanoseconds.
- High signal to noise ratio.
- Low bias voltage –30–80 V.
- Very compact devices – a few square millimeters.
- Insensitive to magnetic fields.
- Not damaged by daylight.
- Relatively low cost.

Fundamental SiPM disadvantages were the temperature dependence of some important parameters (gain, DPE, DCR and others) and the higher noise. However, in recent devices, both effects have drastically been reduced. In addition, effective methods to compensate for temperature changes through suitable regulation of the bias voltage or temperature stabilization have been developed.

4. Digital SiPM

In recent years, the continuous development of SiPMs has led to the creation of a qualitatively new type of photodetectors – the digital SiPM.

In principle, one of the most important features of a SiPM is the separate registration of each photon, as it has been noted that each cell can register only one photon. In analog SiPMs discussed above, the total number of photons in each scintillation (i.e. the scintillation intensity) is measured analogously: the currents of all activated pixels are summed into the load resistor (R_L, Fig. 5.5.26) and the voltage thereupon determines the total number of photons.

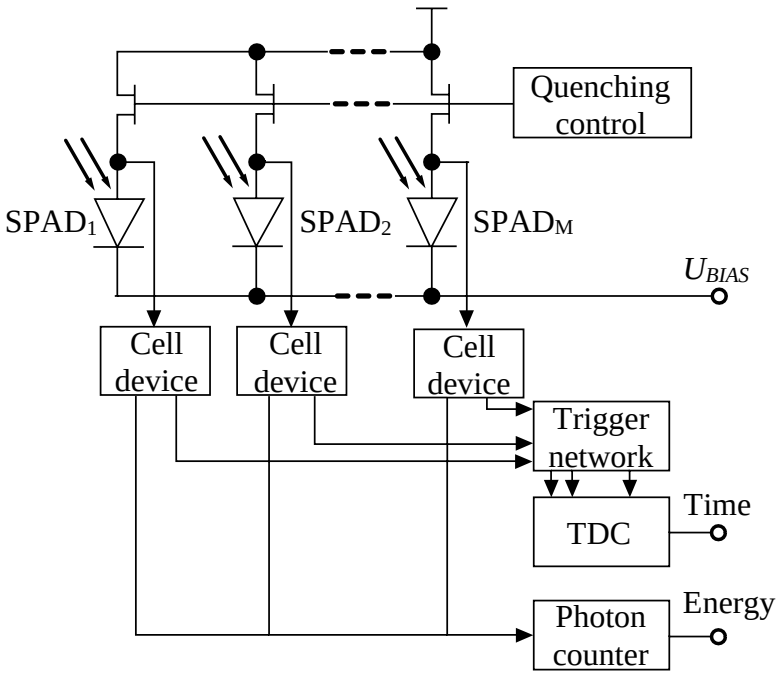

Fig. 5.5.45. Structure diagram of a digital counting SiPM

But in fact, the information contained in a light-irradiated SiPM is digital: each cell is either activated or not, which corresponds to a single-digit binary number. This particular feature of the SiPM was used in the first generation of digital devices called **Digital Counting Silicon Photomultiplier** (**d-SiPM**).

For this purpose, on-chip electronic devices are added to analog SiPMs [14, 15] (Fig. 5.5.45). Photons are detected directly by sensing the voltage at the SPAD anode using a dedicated electronic cell device next to each diode. They are then counted as digital signals and recorded in the photon counter, providing direct digital information about the scintillation amplitude and respectively about the particle energy. Thus, the sensors are less susceptible to temperature variations and electronic noise. In addition, a balanced trigger network coupled with a **Time-to-Digital Convertor – TDC** provides an accurate determination of the photon detection time – relative to a precise clock generator. At the same time, the quenching system has significantly been improved – quenching resistors have been replaced with controllable transistors, which substantially reduces the recharge time and the power consumption. Each cell is also provided with a one-bit memory, allowing the selective inhibition of detector cells (with the highest dark count rate, for example).

The Digital Counting SiPM is a crucial step in the further development of SiPM structures. Using the intrinsically digital nature of sensor microcells, they present the detector information directly in digital form. This creates an opportunity for the detector signals to be digitally processed even further, avoiding the most complicated and power-consuming front-end analogue electronics.

D. Hybrid photodiodes

The **hybrid photodiode** (**HPD**) is a relatively new device. It was developed around 1980 for High Energy Physics (HEP) experiments where photodetectors with positive characteristics, like that of a PMT, were needed; however, they must retain these characteristics when working in a strong magnetic field.

The HPD structure is similar, yet different, from a conventional PMT. Like PMTs, the HPD is a vacuum tube with a photocathode that detects light, plus an electron multiplier that multiplies electrons. However, unlike PMTs, which use a long chain of dynodes such as electron multipliers, the HPD uses a silicon avalanche diode (AD) instead (Fig. 5.5.46).

This AD is composed of three semiconductor layers:

- A thin layer of heavily doped p-region that faces the photocathode and serves as an anode of the AD. It is connected to the output terminal and, by means of a load resistor (R_L) – to the earth (0 V).
- A much thicker silicon substrate, which is in the middle.
- A pn-junction connected to the bias terminal.

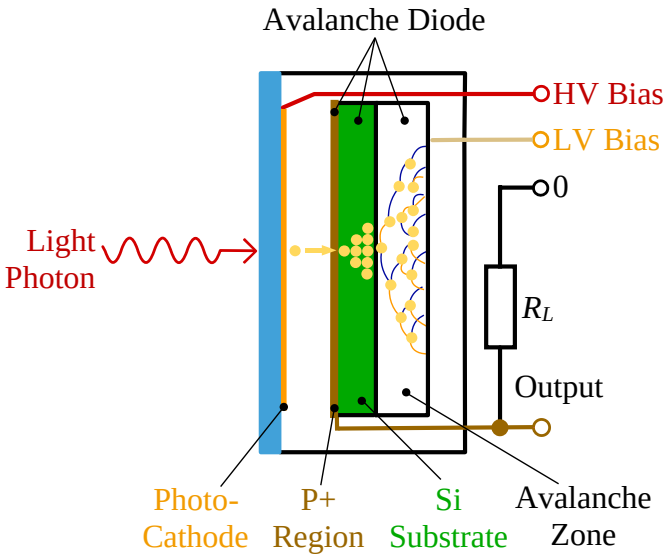

Fig. 5.5.46. The structure of an HPD

The electron multiplication takes place in two stages:

- In the AD silicon substrate, each electron deposits its kinetic energy and produces many electron-hole pairs. The gain generated in this step depends on the voltage applied to the photocathode (at the HV bias terminal, Fig. 5.5.46), which is between –8 and –12 kV. For example, at a voltage of –8 kV (when the photoelectrons enter the AD with an energy of 8 keV), the gain is about 1600.
- The electrons generated in the first stage drift to the AD pn-junction where they arouse an avalanche. The gain of this step depends on the reverse voltage applied to the AD (at the LV Bias terminal, Fig. 5.5.46). This voltage is usually several tens of volts resulting in a gain of between 10 and 100.

The total gain of the HPD is the product of the electron bombardment and avalanche gains and can be greater than 10^5. Fig. 5.5.47 shows a typical HPD (production by Photonis [16]).

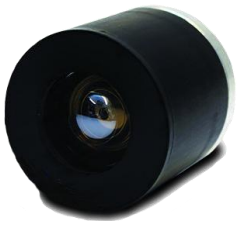

Fig. 5.5.47. A typical HPD

Although the gain of the HPD is lower than the gain of PMTs, the HPD offers other useful characteristics. Their main advantages include better signal-to-

noise ratio and pulse height resolution, fast time response, excellent time resolution, very low to no after-pulses, and no sensitivity to magnetic fields. The latter is due to the very short distance between the photocathode and the AD (1–2 mm), which does not allow the electrons to deviate.

The better pulse-height resolution of HPDs than that of PMTs is due to its very high gain in the first stage. In HPDs, one photoelectron produces over 1500 electrons, while in PMTs, the first dynode liberates typically only 5–6 electrons. For this reason, HPDs have a much better signal-to-noise ratio and the ability to count multiple photons (photoelectrons). Fig. 5.5.48 illustrates the much better radiation energy resolution of the HPD.

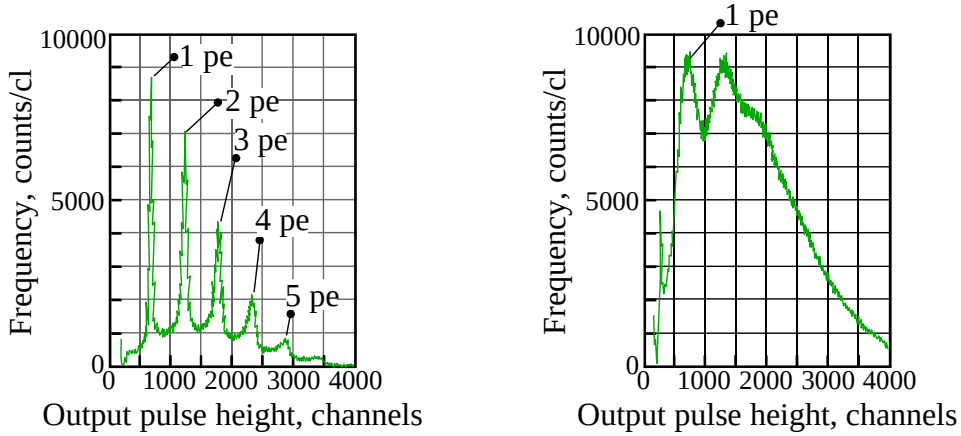

Fig. 5.5.48. Comparison between the pulse heights spectra of an HPD (left) and a PMT (right)

Due to the short distance between the photocathode and the AD, the HPD has an excellent time response and time resolution. The rise and fall times for a high-speed model are less than 400 ps, and the time resolution for a single photoelectron was about 50 ps.

Another important advantage of the HPD is the possibility to separate the photocathode into several independent sectors, each one with proper ADs, i.e. to create a multichannel device. In Fig. 5.5.49, a 144-channel HPD is shown.

Fig. 5.5.49. A 144-channel HPD

These positive characteristics are the reason for a wide range of applications of HPDs, such as LIDAR (LIght Detection And Ranging), TCSPC (Time-Correlated Single Photon Counting) and especially in HEP experiments. For example, in the Hadron Calorimeter of the detector CMS (Compact Muon Solenoid) operating at the LHC (Large Hadron Collider) at CERN, more than 400 HPDs consisting of either 19 or 73 channels were used.

One significant drawback of the HPD is the need for a very high supply voltage, which is relatively expensive and requires meticulous work. For this reason, there has recently been a tendency to replace HPDs with SIPMs [17].

5.5.3. Scintillation detector assemblies

Scintillation detector assemblies, often called scintillation counters, represent a combination of a scintillator and a photodetector assembled into a suitable construction.

A. Scintillation counters with photomultipliers

These scintillation counters are mostly mounted in a metal housing ((1) in Fig. 5.5.50), which, in addition to mechanical protection, also protects them from external light penetration.

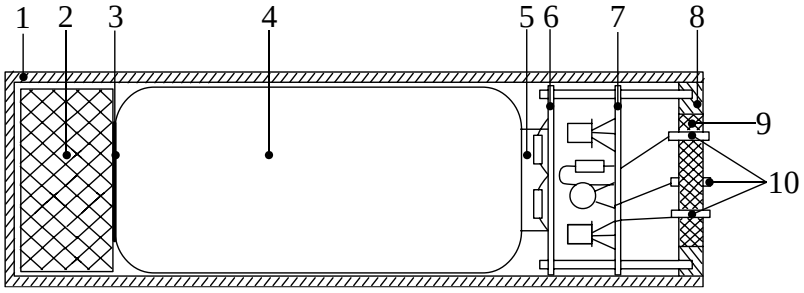

Fig. 5.5.50. Typical construction of a PMT scintillation counter

The scintillator (2) and the PMT (4) are installed, and a special paste (3) is added in-between them to improve the optical contact. The resistor divider supplying the dynodes is mounted on a common PCB (Printed Circuit Board – 6) with a PMT socket (5). The preamplifier (7) provides sufficient power for the output signal to be transmitted by cable. The light impermeability of the casing is very important because the photocathode has high sensitivity, and the slightest penetration of light unacceptably increases its dark current. Therefore, the housing is closed with a metal screw cap (8) holding the printed circuit boards and PMT. A disc (9) of opaque insulating material is installed in the middle of the cap, through which pins (10) pass the feeds of the PMT's and electronic device's bias voltages as well as the output signal.

When measuring gamma radiation, the thickness of the casing around the scintillator is not essential. However, to record beta and alpha particles, the

front-end cap of the casing is replaced with a thin foil of metal or of metallized plastic that is opaque.

Fig. 5.5.51 depicts two typical scintillation counters using scintillators of NaI (13 and 30 mm in diameter with a thickness of 1–5 mm) and corresponding PMTs, as produced by FMB Oxford [18].

Fig. 5.5.51. Scintillation counter with Phi 30 and Phi 13 mm NaI(Tl) crystals

They have only two feeding lines (wires) – one for the PMT high voltage and the second – for the preamplifier output. For this purpose, the load resistor of the preamplifier's end-stage is installed at the other end of the cable, close to the power supply of the basic electronic measuring device.

Very often, there is a difference between the size and shape of the scintillator and the PMT used. In such a case, a light guide should be utilized. In the simplest case of a cylindrical scintillator of a larger diameter than that of the PMT, introducing a truncated cone of transparent material between them is sufficient (Fig. 5.5.52).

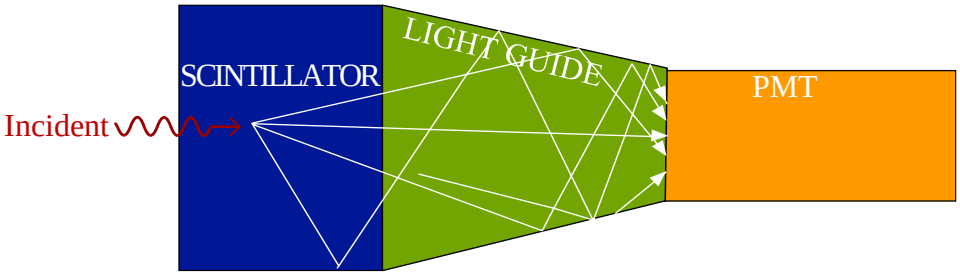

Fig. 5.5.52. Delivery of the light signals from the scintillator to the PMT using a truncated cone as a light guide

In the case of a large difference in the scintillator's form to that of the PMT, light guides with more sophisticated forms should be used [19]. For example, a light guide (called a Fishtail) is used to connect a thin sheet scintillator to a cylindrical PMT (Fig. 5.5.53).

Fig. 5.5.53. A "Fishtail" light guide

In HEP detectors, where many thin sheet scintillators are often used, the connection between them and the photodetectors is made by optical fibers.

B. Scintillation counters with other photodetectors

SiPM manufacturers offer ready-made modules mainly for optical measurements. They do not offer any scintillation counters to measure ionizing radiation parameters. Nonetheless, the HPDs and the SiPMs are widely used in nuclear research and high energy physics. Because of the specific features of each experiment, researchers often create the necessary scintillation measuring systems themselves.

References

[1] *Maddalena, F*. et al. Inorganic, organic, and perovskite halides with nanotechnology for high–light yield X- and γ-ray scintillators. https://www.mdpi.com/2073-4352/9/2/88/htm

[2] Solid plastic and liquid scintillation materials. https://www.crystals.saint-gobain.com/products/organic-scintillation-materials

[3] *Nakamura, H, Y. Shirakawa, S. Takahashi, H. Shimizu*. Evidence of deep-blue photon emission at high efficiency by common plastic. Europhysics Letters, **95**, No 2, 2011.

[4] *Easo, S.* Particle identification. Science & Technology Facilities Council, 2011. https://warwick.ac.uk/fac/sci/physics/staff/academic/gershon/gradteaching/warwickweek/material/detectors/Warwick_week_Pid_Lecture_2011_pdf.pdf

[5] Hamamatsu. Photomultiplier tubes. https://www.hamamatsu.com/resources/pdf/etd/PMT_handbook_v3aE.pdf

[6] Hamamatsu, Photomultipliers tube. http://staff.ustc.edu.cn/~sunday/detector/Hamamatsu-PMT.pdf

[7] *Bronshtein, I.N., K.A. Semendyayev, G. Musiol, H. Muehlig*. Handbook of Mathematics. 6th ed., 2015, Springer Verlag.

[8] Micro-channel plate detector. https://en.wikipedia.org/wiki/Microchannel_plate_detector

[9] *Ghassemi, A., K. Sato, K. Kobayashi*. MPPC. Hamamatsu Technical Note.

https://hub.hamamatsu.com/sp/hc/resources/TN0014/mppc_kapd9005e.pdf

[10] Introduction to silicon photomultiplier (SiPM). Techn. Doc. AND9770/D AND9770 - Introduction to the Silicon Photomultiplier (SiPM) https://www.onsemi.com/pub/collateral/and9770-d.pdf

[11] An Introduction to the Silicon Photomultiplier. Techn. Note of SensL. https://www.sensl.com/downloads/ds/TN%20-%20Intro%20to%20SPM%20Tech.pdf

[12] Hamamatsu. MPPCs/SiPMs. https://www.hamamatsu.com/eu/en/product/optical-sensors/mppc/index.html

[13] Multi-pixel photon counter MPPC. https://www.hamamatsu.com/resources/pdf/ssd/s12572-010_etc_kapd1045e.pdf

[14] *Frach, T., G. Prescher, C. Degenhardt, R. de Gruyter, A. Schmitz and R. Ballizany.* The digital silicon photomultiplier — principle of operation and intrinsic detector performance. IEEE Nuclear Science Symposium Conference Record (NSS/MIC), Orlando, FL, 2009, p.p. 1959-1965.

[15] *D'Ascenzo, N., V. Saveliev, Q. Xie, L. Wang*. The digital silicon photomultiplier. https://www.intechopen.com/books/optoelectronics-materials-and-devices/the-digital-silicon-photomultiplier

[16] Hybrid photo diodes. https://www.photonis.com/product/hybrid-photo-diodes

[17] *Strobbe, N.* on behalf of the CMS collaboration. The upgrade of the CMS hadron calorimeter with silicon photomultipliers. https://inspirehep.net/files/73a40b504d55dba583cb83bd02b93232

[18] Scintillation Detectors. https://www.fmb-oxford.com/wp-content/uploads/2014/12/Scintillation-Detectors_2012.pdf

[19] Zmescal, J. Detectors and detectors systems for particle and nuclear physics I. Part 2. https://www.oeaw.ac.at/fileadmin/subsites/etc/Institute/SMI/PDF/Detectors_WS2014-15_A2.pdf

5.6. Applications of radiation detectors

This section looks at the methods and apparatus for measuring only the basic parameters and characteristics of ionizing radiation and their sources, such as energy, source activity, flux, dose and some parameters describing the time relation between radioactive events. These studies can be combined into the following groups:

5.6.1. Radiation energy measurements

In these measurements (see Part 8), also known as spectroscopic measurements, the task is to determine the energy of the particles and quanta emitted by the radioactive source. Since detectors regularly convert the energy of a particle or quantum into the amplitude of a generated signal, this task aims to find the amplitude distribution of these signals. At the same time, it is necessary to measure the number of signals (or the count rate) corresponding to each isotope in order to determine the amount of each isotope in the studied sample.

The type of detector used for energy measurement is largely determined by the type of particles or quanta as well as their energy levels.

1. **Gamma-ray spectroscopy** is mainly performed with semiconductor detectors (see Section 5.3), germanium-lithium or high purity germanium, as they provide the highest energy resolution and efficiency. Their disadvantages are the high cost and the need to be cooled down to the temperature of liquid nitrogen. Therefore scintillation detectors are sometimes used for this purpose since they are cheaper and easier to operate – even more so after the creation of a new lanthanum bromide ($LaBr_3(Ce)$) scintillator with very good energy resolution (see Section 5.5).
2. **In spectroscopy of X-rays** and **low-energy gamma quanta**, silicon PIN-diode detectors have increasingly been used to provide good resolution at room temperature or with minimal cooling to around –10°C. In some cases, proportional counters are also applied.
3. **For the measurement of alpha particles' energy**, surface barrier silicon detectors are used. Appropriate proportional counters are also utilized.
4. **Neutron energy** is measured mainly by scintillation detectors using special neutron sensitive scintillators such as ^{6}Li glass, stilbene and others (see Section 5.5.1).

5.6.2. Timing measurements

In timing measurements (see Part 9), the information is included in the timing parameters of the detector signals. Very fast detectors (with minimal dead

time) are necessary for two types of timing measurements: selection and recording of simultaneously occurring signals in two or more detectors; measuring of time intervals between signals**.** Three types of detectors are commonly used for timing measurements.

1. **Plastic scintillators coupled with very fast PMTs** provide the shortest dead time. The best time resolution ensured by them is in the order of hundreds of picoseconds.
2. **Silicon surface-barrier and PIN-diode detectors** also have a good time resolution. They are very suitable when radiation energy and their respective time parameters must be measured simultaneously. Particularly good results are obtained when these detectors are coupled to a silicon photomultiplier.
3. **Micro-channel plates (MCPs)** are used as ultra-fast photodetectors.

5.6.3. Radiation activity and flux measurements

All measurements of the activity of radioactive sources, or that of the radiation flux, refer to the so-called **radiometric studies**. In order to **directly** measure the activity of a radioactive source, it is necessary **to count all the particles or quanta emitted by the radioactive source per unit of time**. This can only be done with so-called 4π-detectors (see Section 5.1.6), where the source is placed inside the volume of the detector, and thus all events of radioactive decay are recorded. Only gas proportional counters (Section 5.2.3) and liquid scintillators (Section 5.5.1) provide such capabilities.

In practice, during radiometric studies, the radiation flux is measured by determining the number of detector signals recorded per unit of time, i.e. the so-called **count rate**. Then, from the result obtained, the activity of the source can be calculated by considering the efficiency of the detector (see Section 5.1.6).

Determining the radioisotope's half-life $T_{1/2}$ (or the constant λ of its radioactive decay) is also a radiometric task. It requires multiple sequential measurements of the radiation flux. From the obtained results, it is necessary to determine the constant λ of the exponent $e^{-\lambda t}$ by which the measured flux decreases over time (see Eq. (2.5.2)).

The choice of detector for radiometric surveys depends on the type of radiation and the activity of the source.

1. **Geiger-Muller counters** (see Section 5.2.4) are widely used to measure beta and gamma radiation at relatively low count rates – up to around 1000 s^{-1} – due to their low cost and high amplitude of output pulses. Thus, simple and cheap radiometers are built using this type of counter.

2. **Scintillation detectors** (see Section 5.5.1), with either solid or liquid scintillators, are used to measure high activity samples of beta and gamma radiation. Solid plastic scintillators are ordinarily used in these tasks because of their low cost and the fact that they can easily be obtained in the required shape and size. An advantage of liquid scintillators is that the test substance can be dissolved in the scintillator. This allows not only a 4π solid angle of measurement but also direct contact of the sample with the detector. Thereby, the particles avoid passing through the intermediate medium and transmit all of their energy to the detector instead, which is particularly important for alpha and low-energy beta radiation.
3. **Scintillation detectors** with spectrometric scintillators, such as **NaI(Tl)** or **$LaBr_3$(Ce)**, are suitable for combined measurements when the fluxes of different isotopes have to be measured simultaneously.
4. **Scintillation detectors** are also preferred for measuring **low activity samples** as they are more easily shielded from a cosmic ray background by a protective detector and an anti-coincidence circuit.
5. **Proportional**-(see Section 5.2.3) or **corona counters** (see Section 5.2.5) filled with boron trifluoride (BF_3) or helium-3 (^3He) are widely used to measure neutron fluxes. **Ionization chambers** with fissile materials (see Section 5.2.2), as well as **plastic scintillators** with suitable additives, are also used at high fluxes.

5.6.4. Dose measurements

The task of these measurements is to determine the dose absorbed by different objects (**internal dosimetry**) or the dose rate in a particular area (**dosimetry of the environment**), including environmental radioactive contamination control. They are mandatory when working with radioactive isotopes as well as inside or near nuclear power plants and experimental nuclear facilities, such as reactors and accelerators.

1. **Miniature Geiger-Muller counters** are used to measure the gamma-rays' **equivalent dose rate**. Special steps (such as sophisticated shielding) are taken to eliminate the energy dependency of the results. A dosimeter of this type [3] covers a range of gamma energies, from 60 keV to 1.3 MeV, as well as an equivalent dose rate range of 0.1 μSv/hour to 10 mSv/h with an error of less than $\pm$10 %. The dose rate range can be expanded to 1 Sv/h using a probe with two GM counters of a similar type.
2. **Probes with scintillation detectors** are most often used for **dose rate** measurements of alpha or beta particles.
3. **Current ionization chambers** (see Section 5.2.2) are generally used in portable dosimeters since the average current flowing through them is

proportional to the radiation flux intensity that determines the absorbed dose.

4. **Thermoluminescent dosimeters** of different types (see section 5.4) are predominantly applied for individually equivalent dose control (in humans and objects). In recent years, their accuracy and the stability of their results have become quite satisfactory.
5. **Miniature plastic scintillators with silicon photomultipliers** have recently been introduced in radiotherapy to control the dose absorbed by patients.

5.6.5. Radioisotope methods application

In these methods, the variation of the ionizing radiation parameters, after its interaction with a substance or object, serves to measure its physical, mechanical or chemical characteristics. Radiometric and spectrometric methods are mainly applied to these measurements, and the results are further processed to determine the significance of the measured quantity.

The detector type used for these measurements is mainly determined by the type of radiation used. An additional consideration is the type of measurement.

1. **Scintillation detectors with plastic scintillators** are the most commonly used sensors for measuring gamma-ray parameters in radioisotope devices. Their important advantages include the high efficiency and availability of these scintillators in various shapes and sizes. For **gamma-spectroscopy**, the most frequently employed scintillators are NaI and KI because of their relatively low price.
2. **Different types of GM-counters** are also used. Long cylindrical counters are installed in parallel to create a large area for gamma radiation measurements. Thin-walled GM counters are employed to record beta particles [4].
3. **Neutron fluxes**, used to determine an object's moisture level, are usually measured by **^{3}He corona counters** [5].

References

[1] *Kamburov, Ch., I. Vankov, S. Avramov*. 4π-scintillation system for low beta-activity counting. Nucl. Instr. and Meth. **143**, 1977, p.p. 537-542. https://www.sciencedirect.com/science/article/abs/pii/0029554X77902439

[2] Gamma detectors. https//www.distrelec.de/Web/Downloads/r_/en/wyMullard_Geiger-Mueller-Zaehlrohr_EN.pdf

[3] Automess. Productfamily 6150AD. https://www.automess.de/produkte/produktfamilie-6150ad

[4] *Batchvarov, N.S., I.D. Vankov, L.P. Dimitrov, Ch.D. Shukov, P.A. Pavlov*. Betareflektometer SR 77. Isotopenpraxis, **19**, No 9, 1983, p. 312.

[5] *Бочваров, Н. С., И. Д. Ванков, Л. П. Димитров, П. А. Павлов, Х. Д. Шуков*. Нейтронный влагомер для почв типа НВП-79 (Soil moisture meter type NVP-79). Новости ИАИ, вып. 1, 1981, с. 27.

INDEX

Учебное издание

VANKOV Ivan
KAMANIN Dmitry
PANEBRATTSEV Yury

INTRODUCTION TO EXPERIMENTAL NUCLEAR PHYSICS AND NUCLEAR ELECTRONICS

Volume 1: Introduction to Experimental Nuclear Physics

УНЦ-2021-62

Отпечатано с файлов, предоставленных авторами.

Подписано в печать 9.11.2021
Формат 70×100/16. Печать цифровая
Усл. печ. л. 25,35. Уч.-изд. л. 24,34. Тираж 185 экз. Заказ № 60300

Издательский отдел Объединенного института ядерных исследований
141980, г. Дубна, Московская обл., ул. Жолио-Кюри, 6.
E-mail: publish@jinr.ru
www.jinr.ru/publish/

VOLUME 1

Introduction to Experimental Nuclear Physics

“An experiment is a question which science poses to Nature and a measurement is the recording of Nature's answer.”

– Max Planck –